UNIVERSITY OF LIVERPOOL

Bonding of Small Molecules on Metal Surfaces

Thesis submitted in accordance with the requirements of the University of Liverpool for the degree of Doctor in Philosophy by:

Christine McMahon

Supervised by:

Dr. George Darling

and

Prof. Andrew Hodgson

June 2017

Abstract

At metal surfaces, water structures are determined by a competition between optimizing the bonding of molecules to the surface and optimizing the hydrogen bonding within the layer. Density Functional Theory calculations will be used to examine how the hydrogen bonding or water-metal bonds change the structure of the water overlayer. This work compliments experimental studies on the same systems, that employ the standard surface science tools of LEED, to provide accurate starting points for the calculations. From the work studied it is possible to narrow down the ratio of water to hydroxyl on the Rh(111) surface.

Water is a by product of many industrial reactions so a better understanding is important. This aims to increase understanding of surface alloys and the trends across a series. Density functional theory is once again used to provide an understanding of the adsorption sites and energies of intact and dissociated water molecules on four different alloy surfaces, AgSn, PdSn, PtSn and RhSn.

Density Functional Theory has once again been used to provide a good understanding of carbon monoxide and oxygen binding to Cu(110). It has also been used to provide a better understanding of CO oxidation on the Cu(110) added row oxide surface, although it is clear there are significant energy barriers to be overcome for this to happen.

Acknowledgements

First I would like to thank my supervisor Dr. George Darling for his guidance and patience during the last four years and also to my secondary supervisor Prof. Andrew Hodgson. I would like to thank Dr. Chris Collins, Dr. Matthew Dyer and Dr. John Sharp for their invaluable help when I was beginning to use VASP a program quite different to those I had used before and Dr. Alan Massey for the experimental work he performed.

I would like to thank everyone in the surface science research centre for making the time during my PhD enjoyable (especially the tea breaks), a special note to Dr. Fiona McBride and Dr. Chris Collins for keeping my spirits up until the very end.

I'd also like to thank family for putting up with me over the last four years, especially my parents for allowing me to move back home rather than waste my money on rent. To my friends for all the games nights or escaping to the mountains with me whenever I needed a release or providing me with a free B and B when I missed the train home from Liverpool; I thank you and one day I may be able to repay you.

Contents

List of Figures

List of Tables

Chapter 1

Introduction

It is now possible to predict the atomic and electronic structures of adsorbed atoms and molecules on surfaces with reasonable accuracy. This thesis looks at trying to gain an understanding of how some adsorbates bond on different transition metals in model systems. Including looking at the sites of adsorption, geometries and how they interact with other molecules on the surface, whether they form complete overlayers or cause catalytic reactions to occur. The discussions in this thesis focus on density functional theory (DFT) calculations performed over the course of this PhD.

1.1 Catalysts

Catalysts are used to increase the rate of a reaction by decreasing the activation required for a reaction to occur, by providing a different reaction route or by lowering the barriers through a change in local bonding. Heterogeneous catalysts

are in a different phase to the reactants and are studied in this thesis. Catalysts are not used up by the reactions they are increasing the rate of, however they can become poisoned or ruined by secondary processes occurring in the reactions. Transition metals are important in electrocatalysis and can be important for such things as redox reactions in fuel cells.

Fuel cells are being studied as alternatives to the power sources already available however CO is formed in the combustion reactions and needs to be removed before it can poison the catalyst by bonding to the active sites.[11, 12] Catalytic oxidation of carbon monoxide on some surfaces is believed to proceed via a Langmuir-Hinshelwood process at higher CO coverage, as shown in Equation 1.1.[13]

$$CO_{(ad)} + O_{(ad)} \rightarrow CO_{2(g)} \tag{1.1}$$

CO_2 reduction can occur by the mechanism shown in Equation 1.2. The water produced in such reactions binds with surfaces and this water can deactivate the catalysts.[14] CO_2 produced in combustion reactions has been shown to enhance the greenhouse effect, contributing to global warming. Therefore reducing the amounts of CO_2 emitted to the atmosphere in industrial processes is important.[15, 16]

$$CO_2 + 2H^+ + 2e^- \rightarrow CO + H_2O \tag{1.2}$$

Electrochemical reactions use electrocatalysts at the electrode surface or as

electrodes to increase the rate of reactions. They have been used for water formation from hydrogen and oxygen working in a similar way to fuel cells. The solid-liquid interface, between an electrode and a solution, is where important reaction steps take place in electocatalytic processes.[17]

1.2 Water

Water is one of the most abundant molecules in the universe, and is readily available in all three states of matter. Water is one of the only liquids that get less dense as it freezes, causing ice to float on water- this is due to the formation of hydrogen bonds. Each water atom has two lone pairs of electrons causing it to be a good electron donor; this in turn results in water binding to most metal surfaces. The remaining four valence electrons make up covalent bonds between the O and H atoms.

There is a dipole moment on the water molecules resulting in a strong polarisation in the direction of the electronegative oxygen. This increases the ability of the H atom to be a hydrogen bond donor to the oxygen acceptor, hence hydrogen bonding occurs.[2] Once the hydrogen has donated to oxygen, there is a further redistribution of electron density towards the oxygen on the donor molecule; this causes it to become a better acceptor. It is due to this cooperative effect that H-bonded water clusters occur so readily in the gas phase and on surfaces at both low and higher temperatures. Water molecules can have two H bonds donating and two H-bonds accepting, shown in Figure 1.1. Due to water's dipole moment

changing with each new bond, the ability of water to accept and donate H-bonds increases causing stronger bonding within the network.[18]

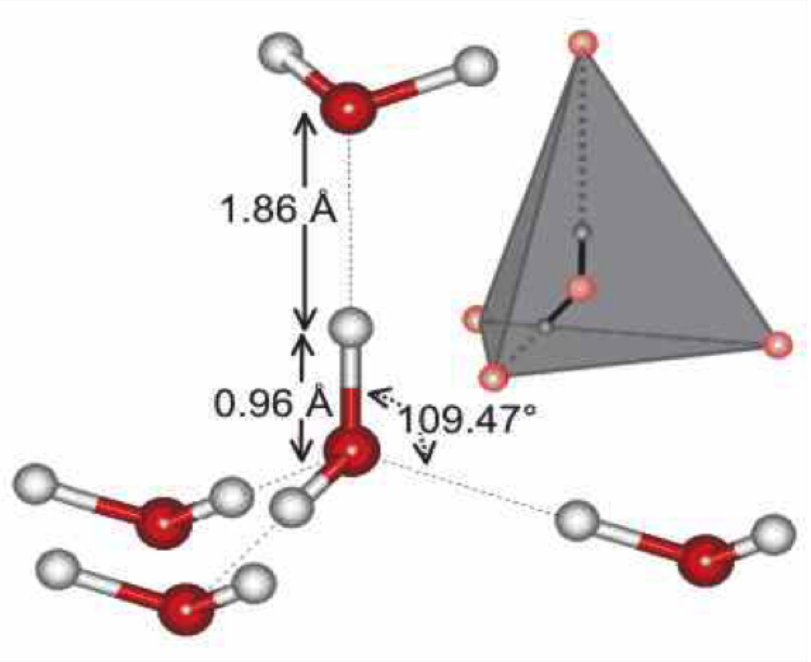

FIGURE 1.1: The four possible H bonds a water molecule can form, showing two H-bond donating and two H-bond accepting.

Water's highest occupied molecular orbital (HOMO), is highly localized on the oxygen atom and is non-bonding, as shown in $1b_1$, shown in Figure 1.2 and 1.3. $2a_1$ can be thought of as non-bonding also, due to the lobe pointing in the opposite direction from the two hydrogens. $1a_1$ and $1b_2$ show Oxygen takes a large proportion of the electron density compared to the two hydrogens.

1.2.1 Ice

Ice has many known phases with two of the most common being ice I_h (hexagonal ice) and ice I_c (cubic ice). Ice I_h has a hexagonal unit cell with an ABAB stacking sequence whereas ice I_c has a cubic unit cell with an ABCABC stacking sequence.[19, 20] The ice structure has water bonding in hexagonal rings and

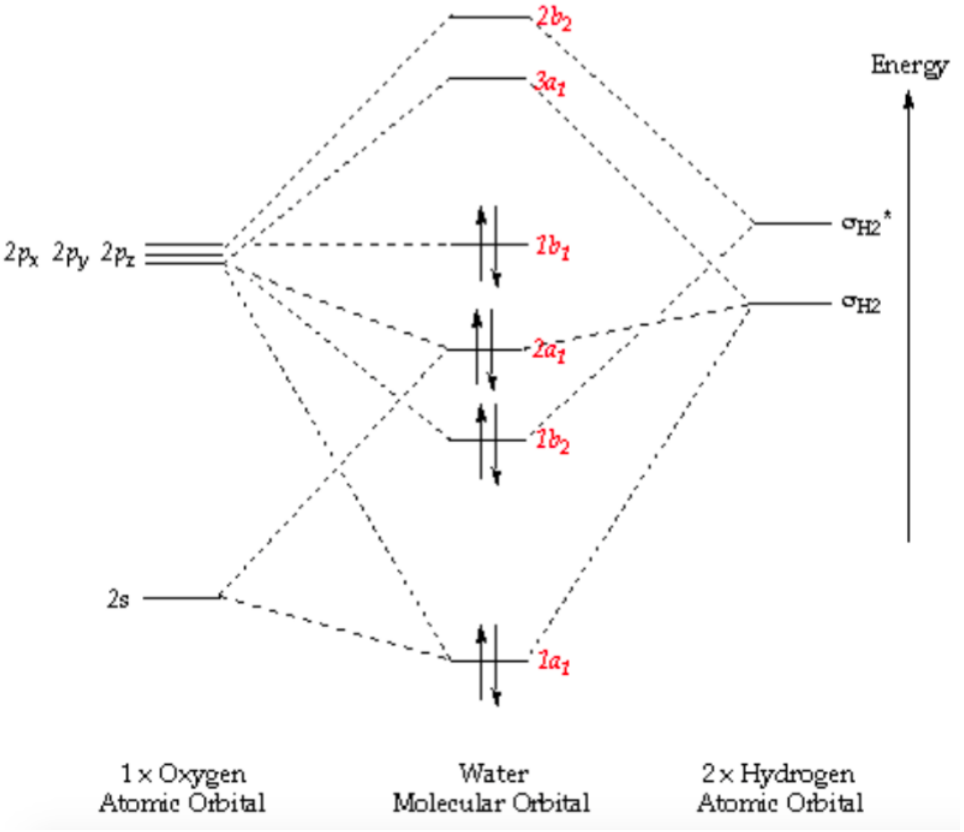

FIGURE 1.2: A molecular orbital diagram for water.

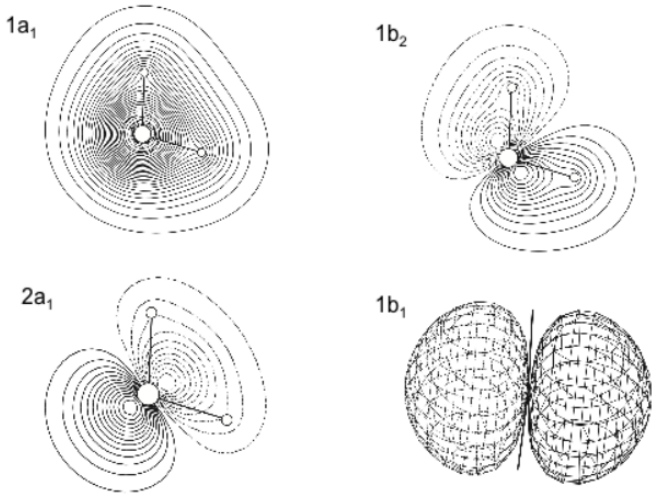

FIGURE 1.3: A molecular diagrams of the different occupied orbitals for water.

to achieve the tetrahedral bonding environment that is observed, it has half of the water molecules bond higher than the other three resulting in the "bilayer" structure, shown in Figure 1.4.

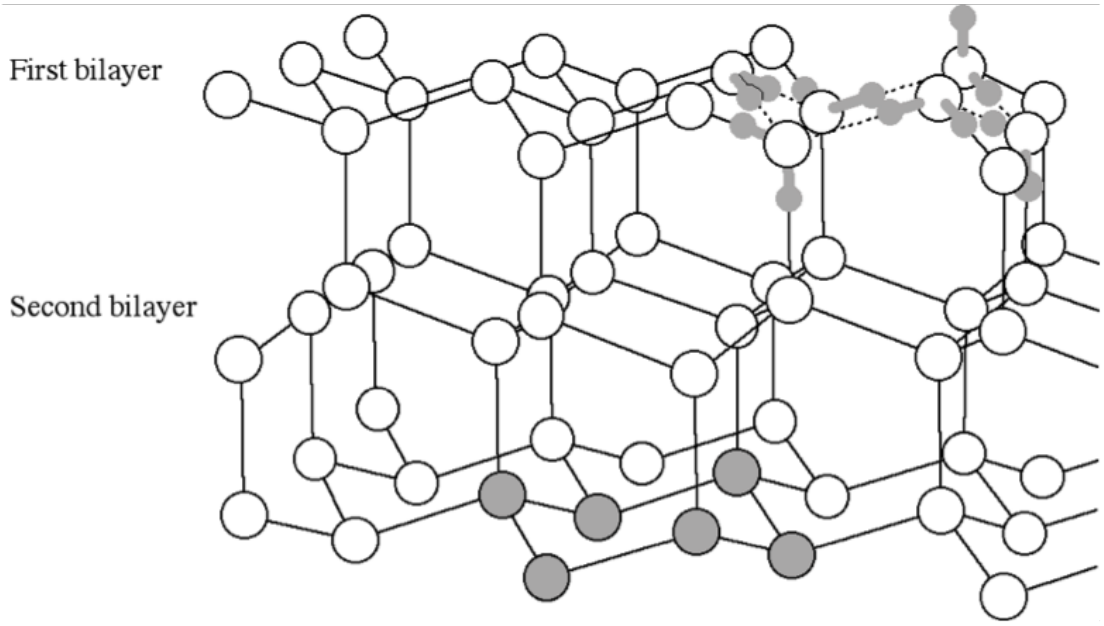

FIGURE 1.4: Bulk ice I_h showing the hexagonal network (circles) and the proton ordering (H atoms shown in grey). Bilayer shown in one of the hexagonal rings(shaded grey circles). Adapted from Doering and Madey [1]

Atoms in water arrange in very specific ways these are often referred to as the ice rules and these are as follows.

1. Each water molecule is oriented such that its two hydrogen atoms are directed toward two of the four surrounding oxygen atoms (arranged almost in a tetrahedron this was shown in Figure 1.1)

2. Only one hydrogen atom is present between each oxygen-oxygen linkage

3. Each oxygen atom has two nearest neighboring hydrogen atoms such that the water molecule structure is preserved

Violations of these rules lead to structural defects in ice.

1.2.2 Surfaces

This thesis looks at water binding on two bulk metals that possess the *fcc*, or face centered cubic structure as is common in many metals favoured in catalysis. In both cases they were looked at with a (111) surface by cutting each of the x, y & z axis at the same point in the *fcc* metal, as shown by Figure 1.5.

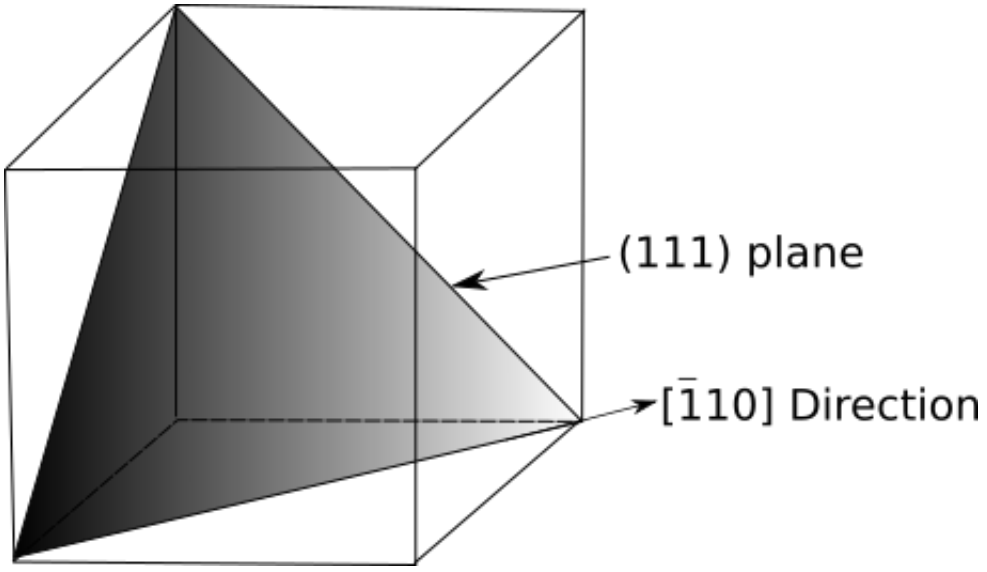

FIGURE 1.5: (111) plane of *fcc* crystals

For Rh(111) the smallest unit cell size looked at is shown in Figure 1.6, this is a (3 x 3) unit cell. A unit cell that was double in one direction was also looked at, a (3 x 6) unit cell size and one which doubled in both directions, a (6 x 6) unit cell size. Although the (6 x 6) unit cell size was the main size examined, with some smaller sizes studied as they were less computationally expensive.

Some surface alloys were also looked at with Sn substituted into the surface as shown in Figure 1.7. M shows either Ag, Pd, Pt or Rh which is what the rest of the bulk consists of. A $(2\sqrt{3} \times 2\sqrt{3})$R30° unit cell is shown as this is the size looked at on these surfaces.

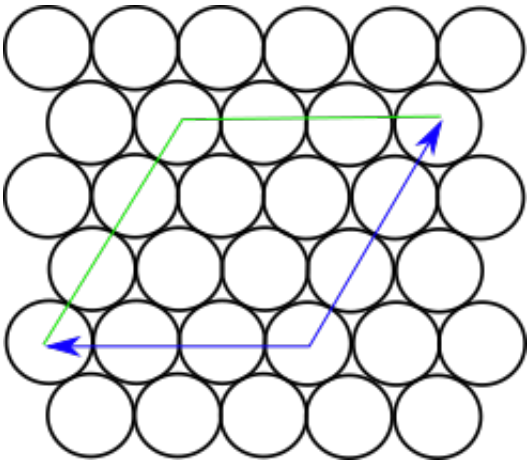

FIGURE 1.6: (111) surface with a (3 x 3) unit cell shown

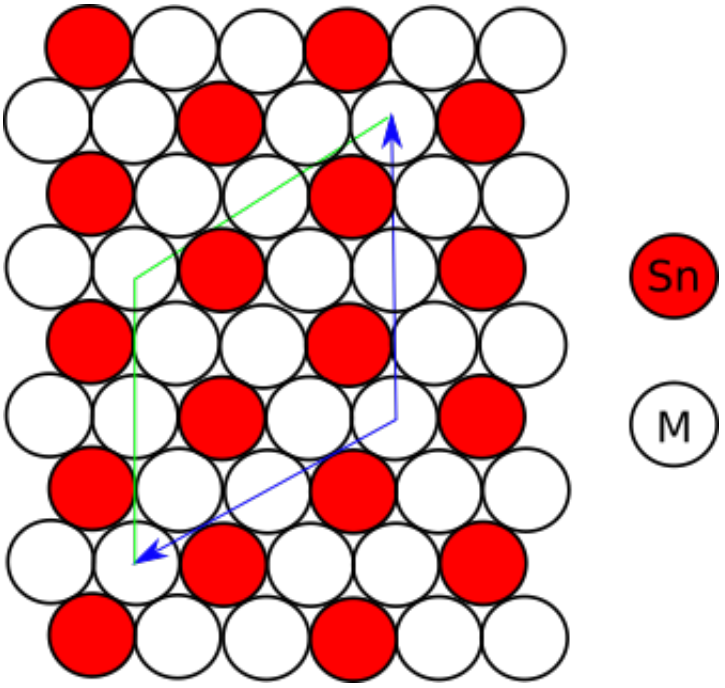

FIGURE 1.7: (111) surface with a $(2\sqrt{3} \times 2\sqrt{3})$R30° unit cell shown. M shows either Ag, Pd, Pt or Rh.

1.2.3 Water on Surfaces

Under ambient conditions water covers most solids but unfortunately the adsorption on metal surfaces is still not fully understood.[21] Knowledge of the wetting behaviour is important, as this could lead to a better understanding in many areas of scientific research such as corrosion, electrochemical interfaces and catalytic

surface reactions.[4, 22, 23] The overlayers created on metals are a balance between the optimisation of the water-water hydrogen bonding and the water-metal interaction and it is in understanding these interactions at a molecular level where the problem arises.[24–26] On many transition metals these interactions have a similar bond strength; Ru(0001) is however an exception to this rule as the water is bound stronger to the surface and this results in an irreversible reaction at higher temperatures.[1, 27]

A list of generalisations for water monomers binding to metal surfaces has been created by Thiel and Madey [19] based upon theoretical and experimental studies;

1. Water bonds to the surface through the oxygens atom $1b_1$ orbital.The surface rarely bonds directly to the Hydrogen atoms.

2. Net charge transfer to the surface occurs when bonding takes place, with the water therefore acting as a Lewis base. The work function decreases upon adsorption due to the charge transfer to the surface.

3. The internal bond angle, bond lengths and vibrational frequencies of the water molecule are only slightly perturbed from the gas phase values by interaction with the surface.

4. Formation of hydrogen-bonded clusters is common even at very low coverages as hydrogen bonding between two or more H_2O molecules is often energetically competitive with the molecule-substrate bond.

Many theoretical and experimental studies have dedicated to understanding the optimal binding geometry and position for a water monomer [2, 28]. Experimental findings most commonly find that water favours binding directly atop a metal site on close packed *fcc* (100), (110) and (111) metals. DFT calculations are in agreement with this and also predict that H_2O monomers favour a virtually flat lying orientation. This can be understood by studying the interaction between the metal and the two highest occupied molecular orbitals of water, the $3a_1$ and $1b_1$ O "lone pair" orbitals. These orbitals are perpendicular to each other, so an upright water molecule would interact through the $3a_1$ orbital, whereas a parallel geometry would demand interaction through the $1b_1$ orbital. The $1b_1$ orbital is closer to the Fermi level.

It is not easy to achieve the understanding necessary for the disordered nature of water on some metal surfaces, therefore this leads to many challenges. Surface interactions can change the orientation of the water molecules, so a combination of experimental data with theoretical models is used to try and gain a clearer picture of what is going on at these interfaces.[29]

There are different types of water overlayers that can be formed on metal surfaces, such as partially dissociated or intact water adsorption. The traditional model on inert transition metal surfaces has water bonding in a multilayer, non-wetting, ice cluster structure, this leaves the metal surface exposed.[3, 30–33] With more chemically active metals this however does not seem to be the case, the overlayers appear to be more likely to form a stable first layer by optimising the water-metal interaction, this leads to surface specific overlayers that can affect the

ability to form other multilayers. [30, 34] There are many structures that water is believed to bond in above the metal, whether it be through the creation of a bilayer or by hydroxyl co-adsorption. Dissociation of water to hydroxyl molecules has been studied to look at the barriers that are needed to overcome for hydroxyl formation.[35]

1.2.4 Ice-like Bilayer on metal surfaces

The "ice-like" bilayer is a suggested structure of water at the metal surface, with only weak water-metal interactions [3]. It consists of a buckled hexagonal network of water molecules and is called a bilayer as there are two distinct heights of the water above the surface.[22, 36] The water molecules in the lower section of the bilayer are almost parallel to the surface and are the ones that bond with the surface.[31] The higher water molecules are hydrogen bonded to the lower level of the bilayer and do not have any interaction with the surface.[23] Each water molecule in the lower layer has three hydrogen bonds, two are proton donors and one is a proton acceptor.[37, 38] The water molecules in the upper part of the bilayer have one uncoordinated H atom which can either be directed toward, H-down, or away from the metal surface, H-up.[34, 39]

Although the bilayer model was once thought of as the standard model increasing evidence leads to the belief it may not be stable on flat transition metal surfaces.[3] It does not fit recent data for the close packed Ru(0001) surface as bulk ice has a higher binding energy compared to the bilayer so would be more

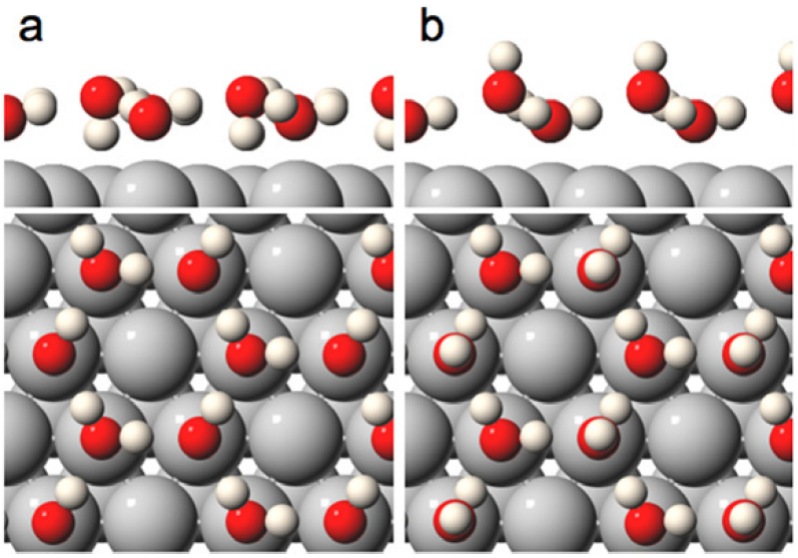

FIGURE 1.8: Idealised water bilayer adsorbed in $(\sqrt{3}\times\sqrt{3})$R30° arrangement on close packed metal surface with water in (a) an H-down geometry (b) an H-up geometry.[2]

likely to form.[40] Also using Density Functional Theory with generalised gradient approximations the bilayer structures are almost always less stable than ice showing their formation to be unlikely.[21]

To force water into this bilayer structure at a metal surface, this has occurred by creating an alloy template of SnPt(111), shown in Figure 1.9. The surface itself was modified by pre-adsorbing Sn onto Pt(111).[3, 24] The Sn displaces every second Pt from the flat terraces on the surface producing a $(\sqrt{3} \times \sqrt{3})$ patterned surface exactly matching the bilayer structure which was shown to form by quantitative LEED. It is stabilised by corrugation, and likely the charge transfer from Sn to Pt, so the oxygen of the flat water molecule prefers the Sn site.

1.2.5 Other Overlayers

Although partially dissociated structures are probably the lowest in energy other types of wetting layers are also able to form. For instance a flat water and H-down

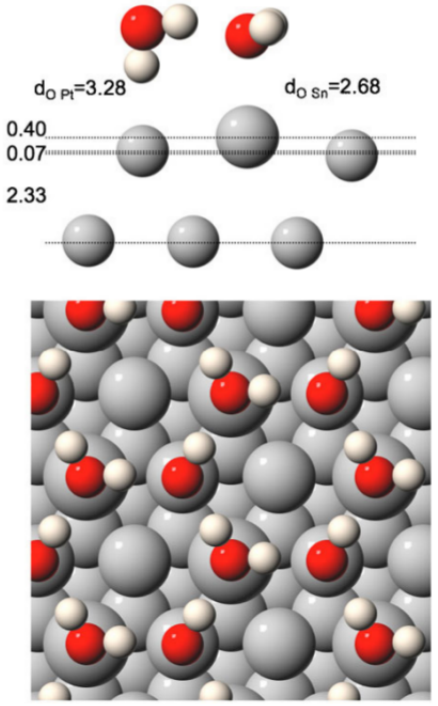

FIGURE 1.9: 0.67 ML water layer on $\sqrt{3}$ SnPt(111).[3]

chain structure has been proposed for Ru(0001) in a hexagonal network, shown in Figure 1.10. This results in a greater binding energy than the bilayer structure, enough to wet the surface, when van der Waals interactions are accounted for.[4, 21]

Another proposed wetting layer for Pt(111) has flat lying water molecules in hexagons surrounded by 5 and 7 member rings. This wetting layer has H-down water molecules in the 5 and 7 member rings to complete the structure. The energy gained by the full amount of H bonds and the fact some of the water molecules are very close to the surface leads to the lower energies of this structure in comparison to the bilayer.[5]

Studies have also been done to look at multilayer growth of water, the initial layer is clearly strongly influenced by the surface structure it is bonding to, the

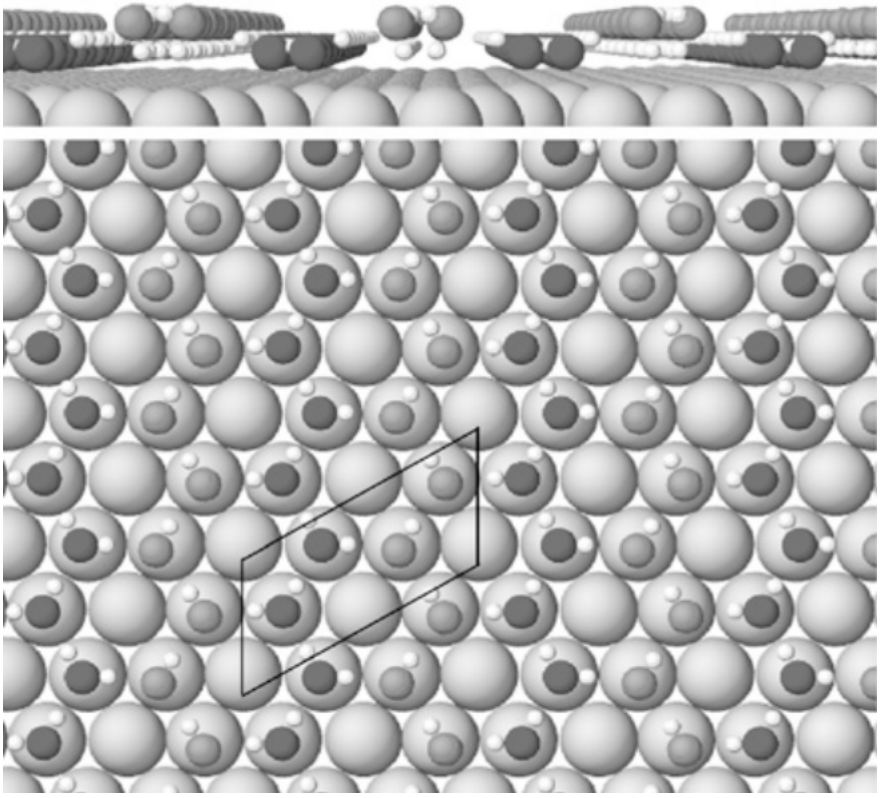

FIGURE 1.10: Chains of flat and H-down water on Ru(0001).[4]

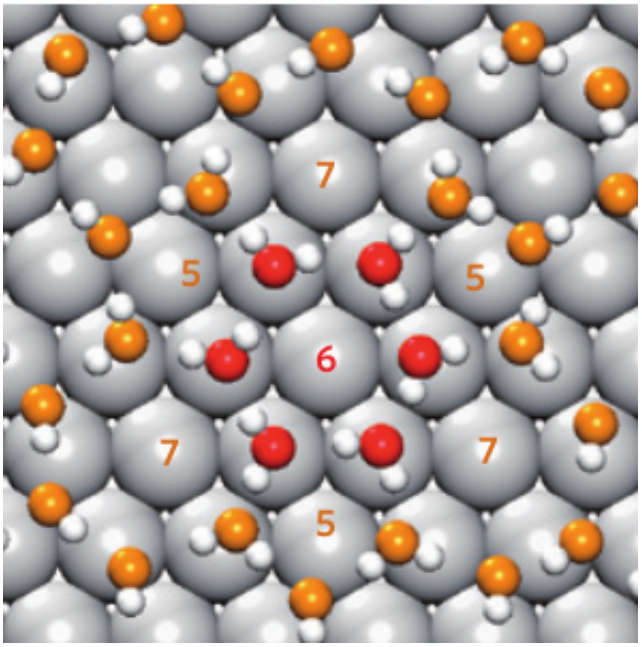

FIGURE 1.11: The structural model consists of five, six and seven-membered rings with the water molecules at various heights above the surface. The water molecules in the six-membered rings that bind to the surface most strongly are indicated with red oxygen atoms.[5]

following layers are however purely dependent on water- water interactions. These multilayers have been studied on Pt(111) using scanning tunneling microscopes (STM) and it has been shown that both ice I_h (hexagonal ice) and ice I_c (cubic ice) are present in the proceeding layers.[41] Both Pt(111) and Pd(111) are not good at growing layer by layer smooth ice films.[42]

Chapter 2

Theory and Computational Methods

This thesis focuses on how small molecules interact at different surfaces, working alongside experimentalists to gain a better understanding of the overlayers formed. These structures that include both molecules on the surface forming an overlayer and the substrate itself consist of hundreds of atoms therefore any calculations performed offer a significant challenge. Density Functional Theory (DFT) can be used to make these calculations achievable, this chapter will look at the computational and theoretical methods that this work uses, in particular at the aspects of DFT that were used for the study of the structures in this thesis. The specific code used was the Vienna Ab initio Simulation Package (VASP) that also allows inclusion of Van der Waals interactions necessary for accurate determination of the stability of the overlayers.

2.1 Density Functional Theory

2.1.1 Schrödinger Equation and the Born-Oppenheimer Approximation

Most quantum chemistry calculations start from an approximation of the many-body time-independent Schrödinger equation in order to calculate the ground state for a many electron system. The many-body time independent Schrödinger equation for a many electon sytem in atomic units is.[43–45]

$$\left\{ -\frac{1}{2}\sum_{i=1}^{N}\nabla_i^2 + \frac{1}{2}\sum_{i\neq j}^{N}\frac{1}{|\vec{r}_i - \vec{r}_j|} + \sum_{j=1}^{N} v_{ext}(\vec{r}_j) \right\} \psi(\vec{x}_1, \vec{x}_2, ..., \vec{x}_N) = E\psi(\vec{x}_1, \vec{x}_2, ..., \vec{x}_N) \tag{2.1}$$

In this equation $\psi(\vec{x}_1, \vec{x}_2, ..., \vec{x}_N)$ is the many-body wavefuntion, which is subject to the Pauli exclusion principle, i.e. two electrons cannot occupy the same quantum state simultaneously. $\vec{x}_i$ takes into account the position and spin index, while $\vec{r}_i$ is the position vector of the ith electron, E is the energy of the system and v_{ext} is the external potential experienced by the electrons from interactions with the nuclei :

$$v_{ext} = -\sum_{I}\frac{Z_I}{|r_i - R_I|} \tag{2.2}$$

Z_I is the nuclear charge and R_I is the position vector of the Ith nucleus.

The wave functions represent the possible quantum states of the system. To make the Schrödinger equation easier to solve, the nuclear and electronic degrees of freedom are separated. This can be done with the assumption the electrons are travelling fast relative to the nuclei due to the fact the nuclei are so heavy in comparison. The nuclei are then considered as fixed, while the electrons are still free to move, this is the Born-Oppenheimer approximation. The dimension of the wavefunction grows with $3N$ electrons, where N = the number of electrons, causing the computational costs to be large even for small systems.[46]

2.1.2 Hohenberg-Kohn Theorems

Hohenberg and Kohn proved that all properties can be determined by the electron density, $n(\vec{r})$, rather than the many-body wavefunction ψ, and the ground-state energy written as a functional of $n(\vec{r})$, where the ground state electron density is unknown. The first Hohenberg-Kohn theorem states that the ground state density is uniquely determined by v_{ext}. The Hohenberg-Kohn theorems give no clue towards the nature of the density functional or how to find it.[47] The ground state energy of a system is therefore obtained by the minimisation of:

$$E = F[n(\vec{r})] + \int v_{ext}(\vec{r}) n(\vec{r}) d^3\vec{r} \tag{2.3}$$

For all electron systems the Hohenberg-Kohn functional $F[n(\vec{r})]$ will work without adjustment. Equation 2.3 gives the exact ground state density and energy,

however $F[n(\vec{r})]$ is unknown therefore further steps need to be taken to calculate these properties.

2.1.3 Kohn-Sham Equations

The Hohenberg-Kohn theorem shows a one to one relationship between the external potential v_{ext} and the electron density $n(\vec{r})$. Thomas and Fermi produced the first 'DFT' by trying to obtain the ground state energy from a functional of the density, however it was hindered by self interaction of the electrons in the Hartree potential and not knowing $T[n(\vec{r})]$, the kinetic energy functional.[48]The solution is to map this problem onto non-interacting wave functions in an effective potential, dependent on $n(\vec{r})$.[49]

$$n(\vec{r}) \rightarrow \hat{H} \rightarrow \phi_i \rightarrow all\ properties \tag{2.4}$$

$\hat{\mathrm{H}}$ is the Hamiltonian operator, and ϕ_i is the Kohn-Sham orbital. Equation 2.4 shows how from this theorem the ground state electron density $n(\vec{r})$ can serve as an understanding of the system. Although the Kohn-Sham orbitals manage to yield a good appoximation of the electron density and energy, this is not necessarily the case with the wave function. The minimisation of these orbitals leads to the Kohn-Sham equation for non-interacting wave-functions using atomic units as follows

$$\left[-\frac{1}{2}\nabla^2 + V_{\text{ext}}(\vec{r}) + \int \frac{n(\vec{r})}{|\vec{r}-\vec{r'}|} d^3\vec{r'} + v_{xc}[n(\vec{r})] \right] \phi_i(\vec{r}) = \epsilon_i \phi_i(\vec{r}) \tag{2.5}$$

$-\frac{1}{2}\nabla^2$ is the kinetic operator which works on the wave functions of the non-interacting single electrons. This does not take into account the electron correlation but this is taken into account in the exchange correlation functional v_{xc}. v_{ext} is the external potential, including the ionic potentials that the electrons are moving in. $\int \frac{n(\vec{r})}{|\vec{r}-\vec{r'}|} d^3\vec{r'}$ is the mean field approximation of the Hartree potential, it gives an approximation of the electron- electron Coulomb interaction. It does not however take into account the many body effects of exchange and correlation, these once again should be taken into account in v_{xc}. ϵ_i represents the eigenvalues and energies of the various Kohn-Sham orbitals.

A flow chart of the iteration scheme needed to solve the Kohn-Sham equation is shown in Figure 2.1. An initial start for the electron density is assumed, which is required for the calculation of $v_{eff}(\vec{r})$ and the subsequent evaluation of $n(\vec{r})$ along with E_{tot}. Until the convergence criteria is fulfilled the loop will continue to run, using the new $n(\vec{r})$ in place of the previous. Once it has reached the correct $n(\vec{r})$ the outputs are given and the calculation is terminated.

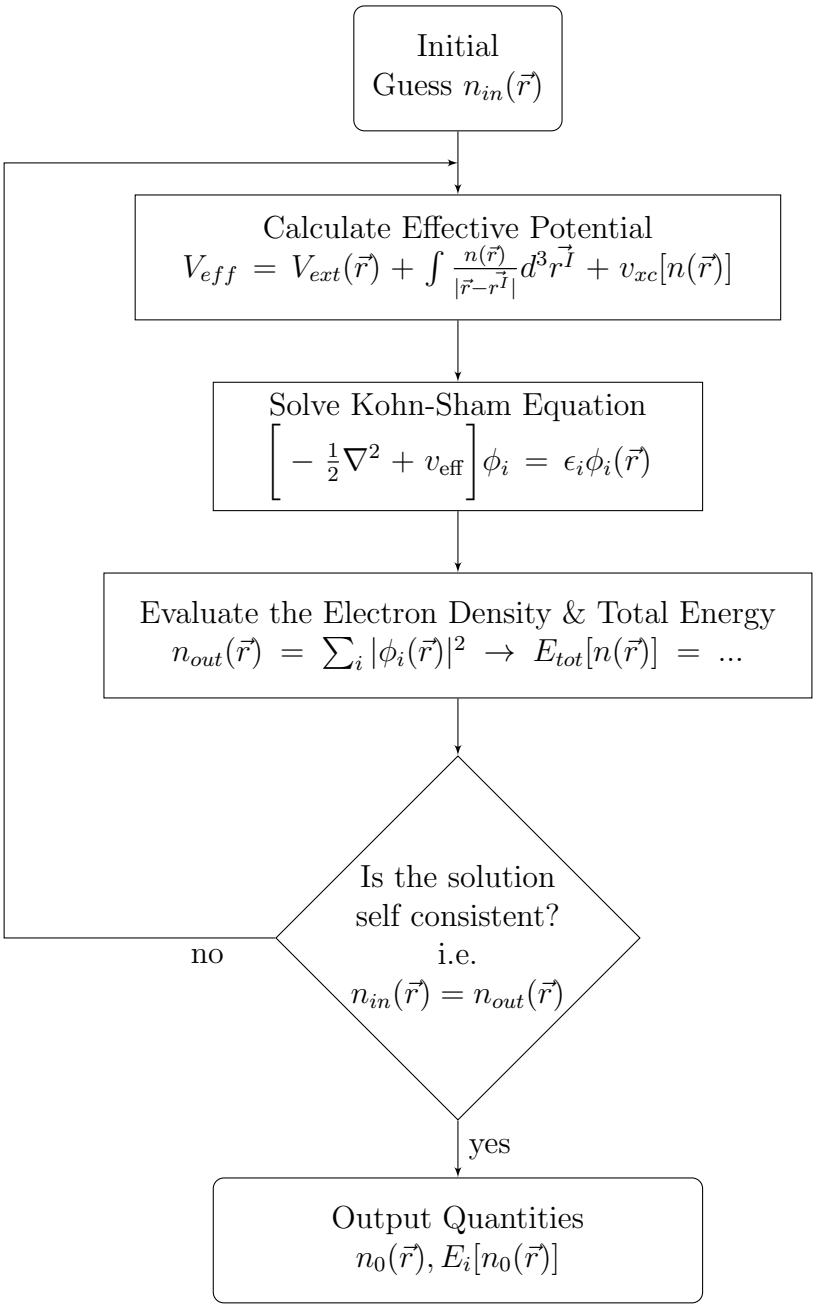

FIGURE 2.1: Flow chart of how to reach self-consistency in Kohn-Sham equation

2.1.4 The Exchange-Correlation Functional

The exchange correlation functional, E_{xc}, is what causes approximations to enter Density Functional Theory. Various approximations to E_{xc} will be discussed here.

2.1.4.1 The Local Density Approximation

In the Local Density Approximation (LDA) E_{xc} is split into separate exchange and correlation parts:

$$E_{xc}[n(\vec{r}) = E_x[n(\vec{r})] + E_c[n(\vec{r})] \tag{2.6}$$

E_x for a homogenous electron gas can be calculated exactly using:

$$E_x[n(\vec{r})] = C_{ex} \int n(\vec{r})^{4/3} d^3\vec{r} \tag{2.7}$$

For E_c there is no formula that can directly calculate this, instead the correlation energy per electron, ϵ_c, can be used to obtain E_c using the following equation:

$$E_c[n(\vec{r})] = \int d^3\vec{r} n(\vec{r}) \epsilon_c(n(\vec{r})) \tag{2.8}$$

Although the Local Density Approximation is quite a simplification it provides good results. The LDA assumes the nature of the electron gas in the system varies slowly across space.[50] This method of working out E_{xc} is exact when electrons move within a uniform positive background within a uniform electron gas.

2.1.4.2 The Generalised Gradient Approximation

The Generalised Gradient Approximation uses the LDA plus an extra term which adds in variation in the electron density for the system as shown:

$$E_{xc}[n(\vec{r})] = \int d^3\vec{r}(\epsilon_{xc}(n(\vec{r})))F_{xc}(s(\vec{r})) \tag{2.9}$$

where ϵ_{xc} is the exchange correlation energy per electron in a homogeneous gas with the electron density $n(\vec{r})$ and s is the gradient of the electron density.[51, 52] Implementations of GGA are numerous with the most commonly used being the Perdew-Wang 91(PW91)[53] and Perdew-Burke-Ernzerhofer (PBE).[54]

2.1.4.3 The van der Waals Density Functional

DFT is known to struggle to describe intermolecular interactions, especially van der Waals interactions (vdW interactions). LDA and GGA alike do not take vdW interactions into account, there are therefore some corrections to be added in to include these. However these interactions are important for the work done in this thesis so have been included.[51, 55, 56]

The method used only modifies the correlation functional therefore once again only the electron density is being used to describe the vdW interactions, this is done by:

$$E_{xc,vdW} = E_{c,LDA} + E_{x,GGA} + E_{c,nl} \tag{2.10}$$

The exchange is still given by the GGA functional, $E_{x,GGA}$, however the correlation functional instead is given by the LDA approximation, $E_{c,LDA}$ to take the local correlation into account. A new functional $E_{c,nl}$ is used for the long range correlation.

Klimeš et al.[52] created the functional optB86b that is used in this thesis. It has been proven to give good results over a large amount of materials. Even with hard solids it was found to improve the predictions for many properties of materials.[52] It approximately accounts for dispersion interactions and reduces the overestimation of the binding distances observed in many systems. In VASP (Vienna Ab initio Simulation Package) the method is implemented using the algorithm of Roman-Perez and Soler which transforms the double real space integral to reciprocal space and reduces the computational effort. [57] A study has also been done on different popular density functionals that include van der Waals and it was found that most vdW functionals increased the adsoption energies compares to PBE but predicted the same adsorption sites, therefore the choice of which vdW functional to use is not too important.[58]

2.1.5 Plane Wave Basis Sets

Plane waves are good for surface calculations as they work well in periodic conditions. The structures in this thesis are set up to be periodic in the xy-plane so are especially well described by a plane-wave basis set, as shown in Figure 2.2. The z- direction is set up with a slab followed by a large enough vacuum that no interaction will occur with the periodic image of the cell in this direction. The

slab in this thesis consists of a small number of layers with the bottom few layers constrained.

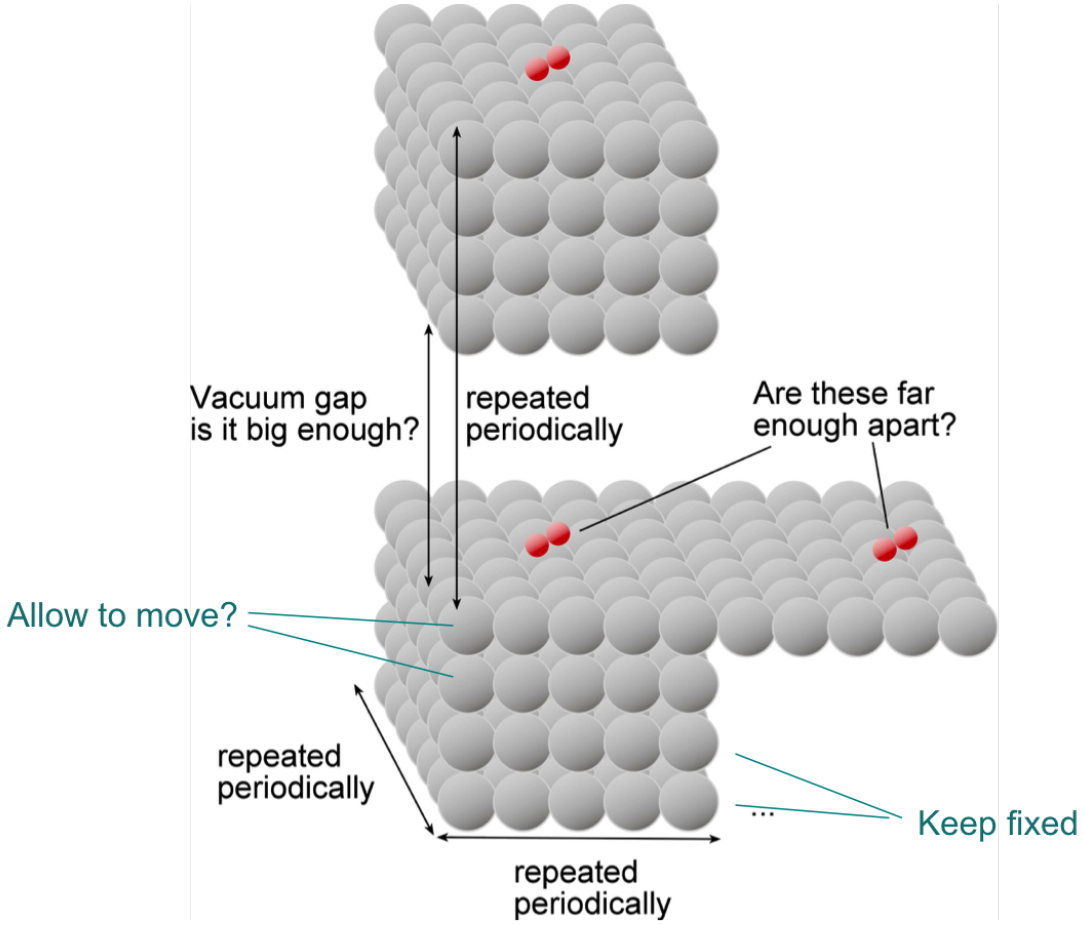

FIGURE 2.2: Diagram explaining periodic boundary conditions

The wavefunctions follow Bloch's theorem as observables of the system must remain unchanged upon translation along the lattice vectors.[59] A wavefunction for a system like this is a product of a periodic function $u_k(\vec{r})$ and of a plane wave, $e^{i\vec{k}\vec{r}}$ where k is the wavevector

$$\psi_k(\vec{r}) = e^{i\vec{k}\cdot\vec{r}} u_k(\vec{r}) \tag{2.11}$$

Applying periodicity:

$$\psi_k(\vec{r}+\vec{R}) = e^{i\vec{k}\cdot(\vec{r}+\vec{R})}u_k(\vec{r}) \tag{2.12}$$

The first Brillouin zone contains $\vec{k}$ which is a wave vector in this primitive unit cell in reciprocal space. Vienna *ab-initio* Simulation Package (VASP) solves plane wave DFT calculations and this was used in this thesis. These plane waves have a kinetic energy cutoff that needs to be stated. Ideally an infinite number of plane waves is required but this is obviously not computationally feasible. However the plane waves with small kinetic energies are more important than those with large kinetic energies. Therefore the plane wave basis set can have a cutoff introduced at a larger energy. The cutoff energy should be increased until the calculated total energy converges within the required tolerance. The number of k-points in k-space need to be specified also, in this thesis the Monkhorst-Pack scheme for k-points was used.[60]

2.1.6 Pseudopotential Approximation

Pseudopotential approximations can be used to lighten the computational load when the number of atoms are increased or atoms with a large number of electrons such as transistion metals are included in the system.

Due to the large quantity of oscillating wavefunctions of electrons in the core region the plane wave basis set is a bad method to expand the electronic wavefunctions.[61] As most of the physical properties of solids are dependent on valence electrons and core electrons do not change very much due to the external

potential, pseudopotential approximations can be introduced. These are defined to smooth out the valence electrons' wave functions in the core regions, while leaving the behaviour of the wave functions unchanged outside those regions. There are two main assumptions for these approximations, that the core electrons are treated as a frozen core and minimal interaction with the surroundings are ignored and that it is the valence electrons that interact with the environment. The Projector Augmented Wave method (PAW) is implemented in VASP and that is therefore the method used in this thesis.[62, 63]

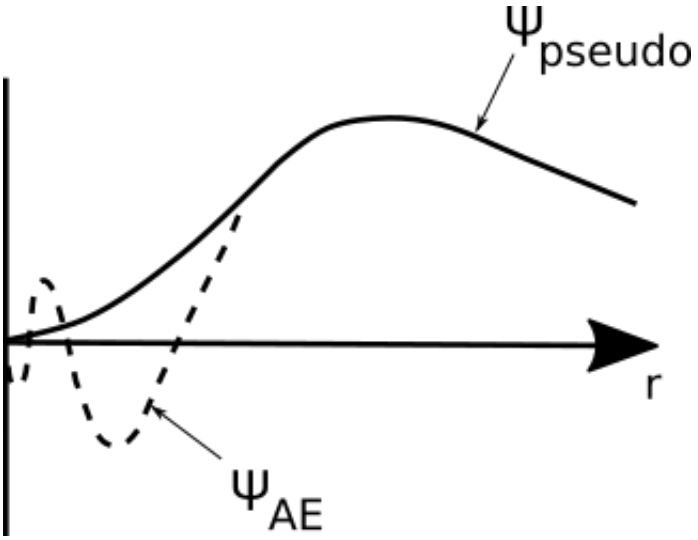

FIGURE 2.3: The all-electronic wavefunction (AE) (dotted line) plotted against distance, r, from the atomic nucleus. The pseudo wavefunction is also shown (solid line). Adapted from [6].

2.2 Vienna Ab initio Simulation Package (VASP)

In computational chemistry the term "relaxing a structure" is often used, this is referring to the optimization of the structures to the most stable, lowest energy structure. In VASP this is done by minimising the forces between the atoms of the structure. However a structure that has been relaxed in VASP may be different

to an experimental structure, as the materials are based on a description of its potentials and these vary based on which level of theory has been used to produce them. The aim is to relax the structure to the global minimum, that is the lowest energy structure. However there are also local minima present, these are lower energy structures than the surrounding possible structures but are not the lowest energy structure available. When relaxing the structure these local minima will be found and energy will need to be put into the system to get out of these wells in the potential energy surface. At the saddle point between two minima the computational program will take the steepest descent, as this may be more likely to reach the global minimum. Once the calculations are relaxed to within a certain defined threshold, say 0.01 eVÅ^{-1}, then the calculation will end and the most stable lowest energy structures should have been found.

Chapter 3

OH/H_2O overlayers on Rh(111)

3.1 Introduction

In this chapter the co-adsorption of H_2O and OH on the close packed surface of Rh is investigated. The overlayers are formed experimentally by predosing the surface with O and subsequently dosing H_2O which partially dissociates to give OH. The experimental LEED pattern that prompted these cpmputational studies, shows a clear pattern of a (6x6) overlayer, however the ratio of H_2O/OH is not precisely known, although desorption studies indicate it is likely either 2:1 or 3:1. Our aim here is to use DFT to attempt to determine the ratio computationally, to see if we can predict the optimum structure, and to study the bonding within the overlayer to see if it conforms to a normal H bonding network, or if the ice rules are broken in the formation of Bjerrum defects.

3.1.1 Partially Dissociated H_2O/OH Overlayers

Adsorbed OH is present in many environments and could be an intermediate in reactions such as steam reforming, and the water gas shift reaction.[25, 64, 65] The adsorption properties of OH alone are difficult to study, however on transition metals OH can form highly ordered overlayers with H_2O. The hydrogen bonding network is hexagonal and fulfilled in one layer with a 1:1 H_2O/OH ratio, as unlike with the "ice-like" bilayer there is no uncoordinated H atom, instead the OH is bonded to the surface and the H_2O and OH are almost coplanar.[2, 66] Studies on different metals have found different ratios of H_2O/OH. Some of these H_2O/OH have formed on surfaces that would preferentially have full water overlayers but have been precoated with oxygen causing dissociation to occur, as shown in Equation 3.1.[67–69]

$$O + H_2O \rightarrow 2OH \tag{3.1}$$

Pt(111) is an example where an overlayer is formed, in a $1H_2O$:1OH ratio, this structure is shown in Figure 3.1. It is produced by either the reaction between H_2 and O_2 or by the co-adsorption of H_2O and oxygen [2, 7]. Both of these overlayers form OH when the surface is heated.[2, 70] There is a substantial energy barrier for the dissociation of water which needs to be overcome for partially dissociated H_2O/OH to form without desorption taking place.[38] These overlayers form a hexagonal honeycomb pattern with the OH or H_2O being bonded in the atop site and the overlayer is almost coplanar.[30] The chemisorption energy for water

on Pt(111) is higher than the barrier for reaction of O and water therefore the formation of OH is expected.[30, 71]

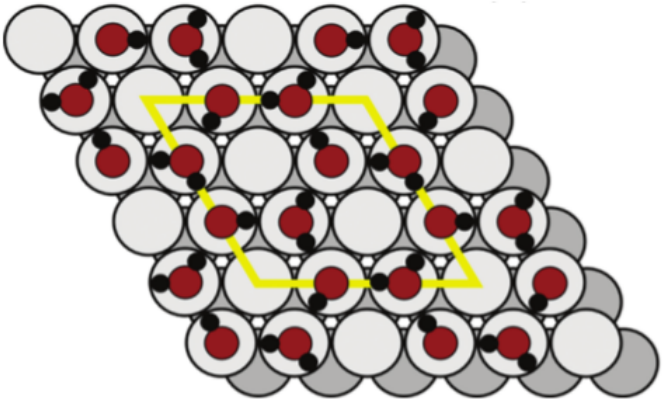

FIGURE 3.1: Idealised water bilayer in 3 x 3 arrangement on close packed metal surface with water in a partially dissociated structure with equal quantities of OH and water.[7]

Another overlayer structure observed is a $2H_2O$-OH network. Cu(110) has been shown to form a 2:1 H_2O/OH overlayer which stabilises by the formation of Bjerrum defects. In this network it can be observed that hydroxyl groups form Bjerrum defects, situations where the hydrogen atoms of two hydroxyl groups face towards each other.[8] This breaks the ice rules that only one H atom may be between any two O atoms, this is shown in Figure 3.2.[27] The Bjerrum defects also play a key role in multi layer growth as it is more preferential for water adsorption on top of these sites, which also takes place before the surface is completely covered.[8] The energetically more favourable structure is to have this partially dissociated monolayer, with the hydroxyl oxygens and water molecules almost coplanar.[66]

Calculations have been done which show the wetting layer on Ru(0001) can not be formed in an ice-like bilayer structure instead it forms Bjerrum defects. DFT calculations have shown a large concentration of broken H-bonds on Ru(0001),

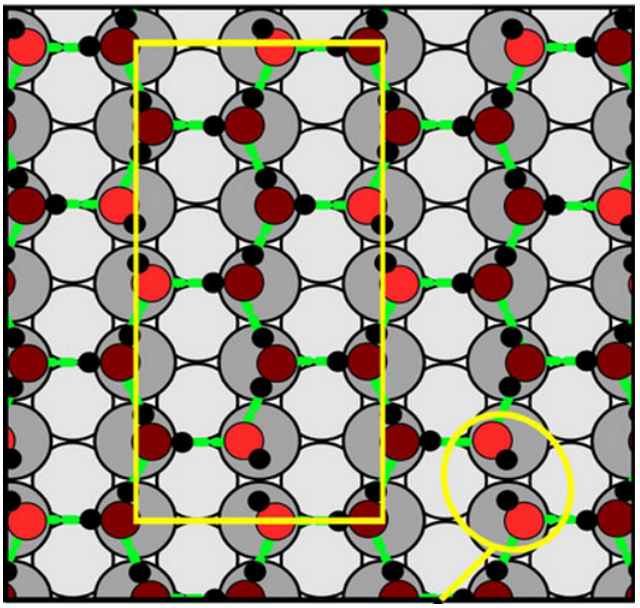

FIGURE 3.2: Structure showing $2H_2O$:OH p(2 x 6) PDO-2 overlayers on Cu(110), with two defects (yellow ellipse) in the unit cell (rectangle).[8]

the stronger O-Ru bonds are still present.[40, 66] The lengths of the remaining H-bonds are relaxed to make up for these broken H-bonds. As more H bonds are broken to form Bjerrum defects the energy gained from strain relaxation decreases, so the more Bjerrum defects there are the less likely it is for more to occur. The OH group acts as a strong H bond acceptor to the water molecules,[23, 27] this suggests that the hydroxyl group is a poor H bond donor considering this is the most stable configuration for some metal surfaces.[8]

The understanding of the different ratios of H_2O/OH overlayers already observed on different metals, formed the basis for the starting point when looking at what ratios of H_2O/OH were most favoured on Rh(111). Theory is needed to answer some important questions about the structure of the H_2O/OH overlayers formed on Rh(111), because the only experimental information available is that the H_2O/OH ratios is most probably 2:1 or 3:1 and a LEED pattern consistent with a (6x6) supercell has been observed.

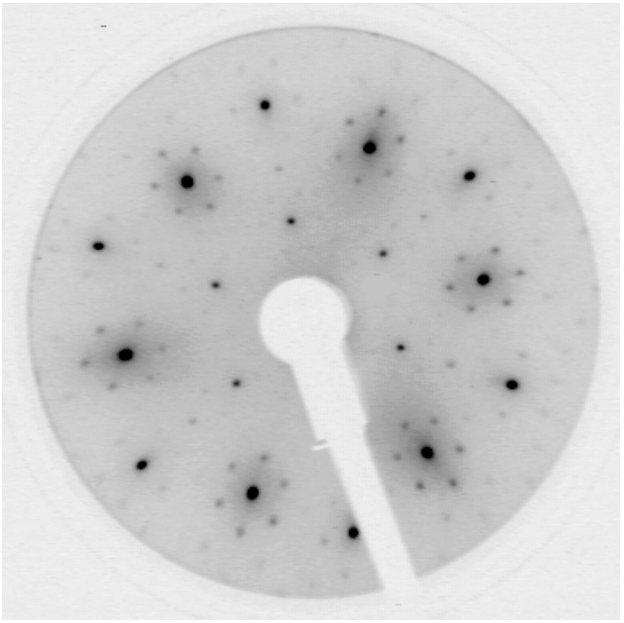

FIGURE 3.3: LEED pattern for water doped onto oxygen precovered Rh(111) surface (120K)

3.2 Method

3.2.1 Calculation Details

The DFT calculations were carried out using Vienna *ab-initio* Simulation Package (VASP), discussed in chapter 2. This current work first used Perdew-Burke-Ernzerhof (PBE) exchange correlation functional with the projector augmented wave (PAW) method. Once these calculations were completed the more stable structures were re-optimised with the optB86b van der Waals functional.[52] VASP is known to work well for metals and it is also known to give a satisfactory agreement with experimental work. It uses plane wave basis sets to expand the Kohn-Sham wave equations. A cut off energy of 400 eV was used with a Monkhorst-Pack grid of 3 x 3 x 1 for the k-point sampling of the Brillouin zone in the (6 x 6) unit cell, this was scaled appropriately for the other unit cell sizes. Due to this being a

high density of k-points for the size of the unit cell this k-point grid was not tested as there would have been more than enough. Also other papers with similar sized unit cells have used similar amounts of k-points.[3, 24]

The simulations were performed using a 4-layer Rh(111) slab and one adlayer of OH/H2O adsorbates. This size represents a compromise between the thickness needed to give an approximate bulk region and the large number of metal atoms in a 6 x 6 supercell. The top 2 layers of the metal in each system are allowed to relax while the other layers are constrained. Each unit cell has a 12Å vacuum to try and reduce any interaction due to the periodicity of the cell.

The overlayer structures were made in either (3 x 3), (3 x 6) or (6 x 6) unit cell sizes. With 1:1, 2:1, 3:1 and 5:1 H_2O:OH ratios with and without Bjerrum defects. This variation in unit cell sizes and ratios was done to make sure that more stable structures with different unit cell sizes were not left out based on what the experimentalists had predicted and to try to better understand the bonding.

3.2.2 Test of method

In order to confirm the method being used was reliable at providing the correct structures and adsorption energies, a test was carried out using the structures in a paper on Cu(110).[8] A 1:1 and 2:1 H_2O:OH structure were used as can be seen in Figures 3.4 and 3.5.

When the structures were optimised with the setup from the paper, a larger 12 x 12 x 1 k-point grid, compared to that used in this work (which has a larger

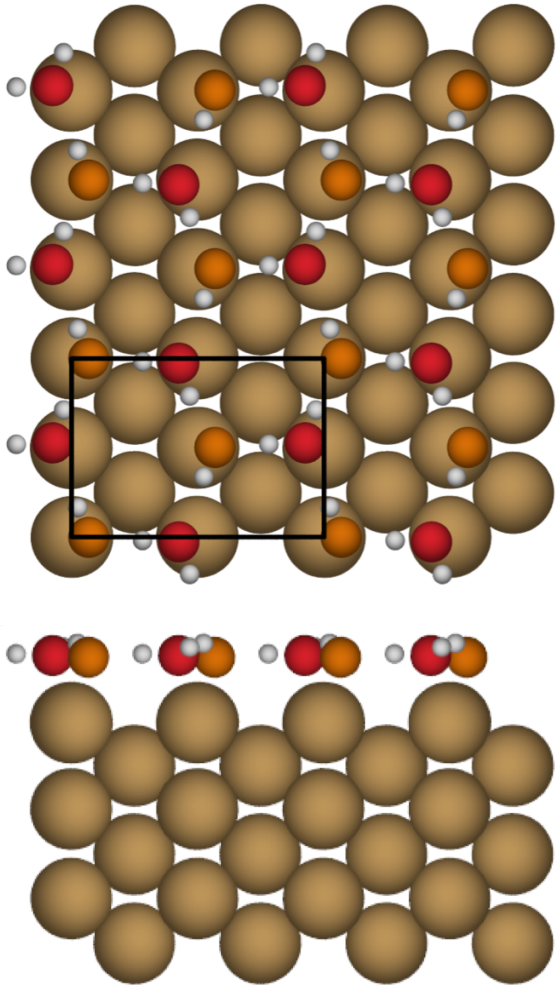

FIGURE 3.4: $1H_2O$:1OH structure on Cu(110), p(2 x 2) [8]

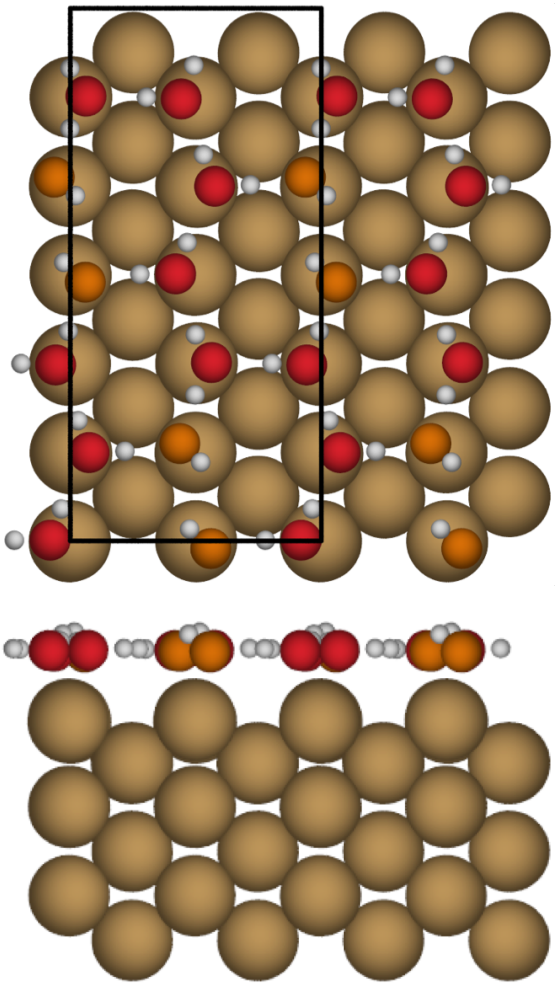

FIGURE 3.5: $2H_2O$:1OH structure on Cu(110), p(2 x 6) [8]

unit cell size), the same overlayer structure and very similar total energies were found, shown in Table 3.1. These results show that for the structures I would be running the setup was accurate enough.

TABLE 3.1: Total energies of 1:1 and 2:1 on Cu(110)structures with my method and a method taken from paper [8]

Ratio	Present calculations (eV)	Published method (eV)
1:1	−58.908	−58.939
2:1	−183.981	−183.970

3.2.3 Adsorption Energies

The adsorption energies were calculated using equation 3.2. Due to the inclusion of the oxygen preadsorbed on the surface this method of calculating the adsorption energies causes it to be comparable to the experiments.

$$E_{\text{ads}} = \frac{1}{n}\Bigg(E(Total) - E(Rh) - n(water) \times E(water) - n(OH) \times \frac{E(water) + E(O/Rh) - E(Rh)}{2}\Bigg) \tag{3.2}$$

Where E(Total) is the total energy of the relaxed complete overlayer of H_2O and OH on rhodium, E(Rh) is the total energy of the clean Rh(111) surface, n(water) is the number of water molecules present in the overlayer and E(water) is the total energy of a water molecule in the gas-phase. The final term accounts for the OH molecules. These are formed in pairs from a H_2O and an adsorbed oxygen. The energies are divided by n, the total number of H_2O and OH molecules in the overlayer structure, so that we can compare structures with different unit cell sizes. For pure water overlayers, n(OH) = 0.

It is possible to compute binding energies for the mixed H_2O/OH overlayers that could be formed by partial dissociation of pure water on clean Rh(111), i.e. not in reference to adsorbed O, as shown in 3.3 and 3.4. In 3.3 the excess H goes to the gas phase, while in 3.4 it stays on the surface. Neither of these methods is representative of the experiments we are modeling. As shown later in 3.3.3 the exothermic chemisorption of the H on the surface favours a partially dissociated overlayer.

$$E_{\text{ads}} = \frac{1}{n}\Bigg(E(Total) - E(Rh) - n(water) \times E(water) \\ - n(OH) \times \left(E(water) - \frac{E(H_2)}{2}\right)\Bigg) \tag{3.3}$$

With E(Total), E(Rh), n(water), E(water), and n(OH) as defined above. E(H_2) is the energy of H_2 in the gas phase.

$$E_{\text{ads}} = \frac{1}{n}\Bigg(E(Total) - E(Rh) - n(water) \times E(water) \\ - n(OH) \times \left(E(water) - E(H_{ads}) - E(Rh)\right)\Bigg) \tag{3.4}$$

With E(Total), E(Rh), n(water), E(water) and n(OH) as defined above. E(H_{ads}) is the energy of one hydrogen molecule adsorbed onto the Rh(111) surface.

Zero point energies have not been taken into account although these would affect the energies slightly.[27] They can show an increase or decrease in the stability of a specific adsorption site on a surface. Including this may have made the calculations more accurate.[72]

3.2.4 Convex hull calculations

The adsorption energies were calculated with the same method; however, different H_2O:OH ratios are composed of different numbers of H and O atoms, therefore the energies are not directly comparable across different compositions. To take this into account, we have to compare the energy of each composition with the

energies obtained for combinations of the competing compositions that would yield the same numbers of each atom type.

For instance, a 1:1 structure is composed of 36 H atoms and 24 O atoms. This composition can also be achieved with part (9/10) of the surface covered by a 2:1 structure (having 40 H's and 24 O's) and the remainder (1/10) with only adsorbed O on the surface. The energy of the 1:1 ratio can then be compared with $0.9\ E_{2:1} + 0.1\ E_O$, where E_O is the energy of a surface covered with O atoms only.

If the energy of the single phase structure is lower, it will likely form, whereas if the energy of multiple competing compositions is lower then it is likely that the surface will segregate into patches of these competing phases. The set of the lowest energy combinations found for all possible compositions is said to form the "convex hull". This needs to be done for each ratio with each combination, this is discussed more within the results.

3.2.5 Measurements

During this and the following chapters there are dicussions about the height of some of the molecules above the metal surface. In every case in this chapter this has been calculated by measuring from the centre of the metal Rh atom that the molecule is bound above, to the centre of the O present in the water or hydroxyl molecule. This is due to the oxygen atom being the point the surface binds to as opposed to the hydrogen atoms that do not bind readily with the surface in either hydroxyl or water molecules. This is demonstrated in Figure 3.6.

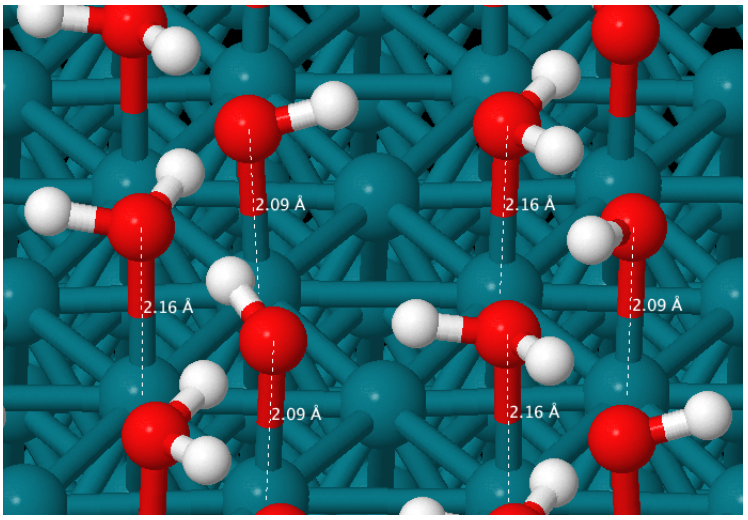

FIGURE 3.6: Height of molecules above surface

Also commented on are distance between some of the molecules which are binding together above the metal surface. These distances are measured from the centre of one oxygen atom to the centre of another oxygen atom, as shown in Figure 3.7.

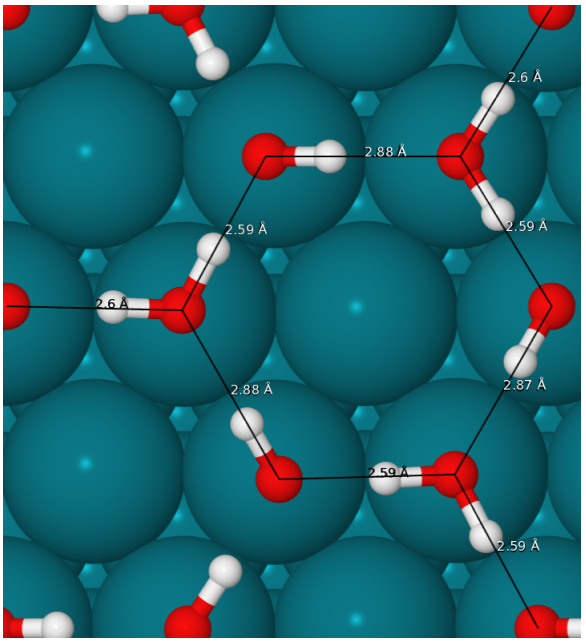

FIGURE 3.7: Distance of molecules measured from oxygen atom to oxygen atom

The angles of some of the hydroxyl molecules are also discussed, these have been calculated by measuring the angle between the centre of the surface atom,

to the centre of the oxygen atom above that surface atom, to the centre of the hydrogen atom. This is shown in Figure 3.8.

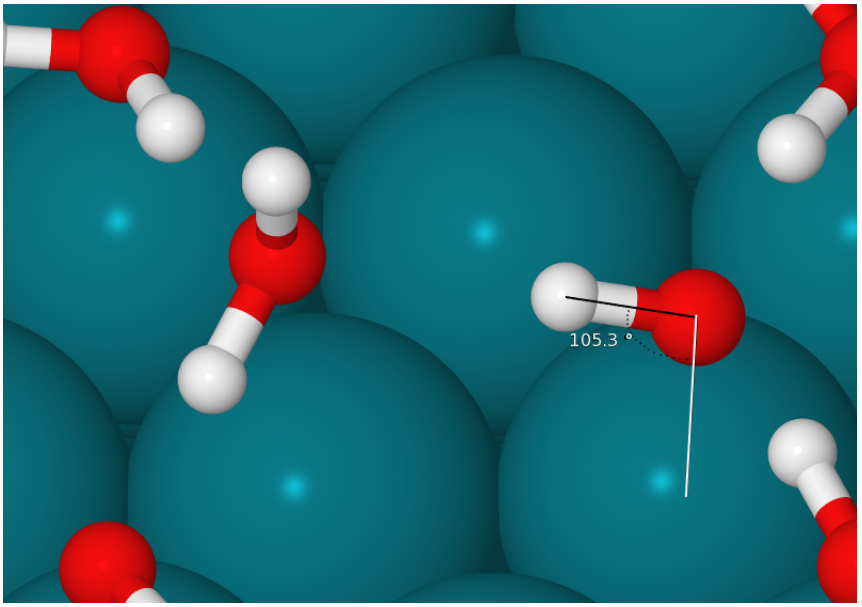

FIGURE 3.8: Distance of molecules measured from oxygen atom to oxygen atom

3.3 Results

DFT calculations on many different structures have been performed to try and predict the ideal composition of the molecules in the overlayer. Due to the way the experiments were conducted with an oxygen precovered surface the most likely arrangement is for H_2O:OH mixed overlayers to form, i.e. some dissociation occurs, or the surface is covered by separated islands of pure water and pure adsorbed O. From geometry optimised structures different aspects such as the ratio H_2O:OH, the unit cell size and whether the water molecules with excess H-bonds will bond H-up or H-down can be looked at from the binding energies and trends. The oxygen of the water or hydroxyl binds in the atop position in all of the structures.

The energy barrier for the dissociation of water needs to be overcome for partially dissociated OH/H2O overlayers to form. Two calculations were run with one water molecule and one O atom adsorbed on the surface, the total energies can be seen in Table 3.2, similar studies have been done previously.[73, 74] One had a water molecule far away enough from this oxygen so there was no rearrangement of atoms between the two and it is just bound to the surface in the atop position. The other had the water close enough to interact with the oxygen atom and in this case it chose to dissociate forming 2 hydroxyl species. Interestingly when both of the hydroxyls are started in the atop position on rhodium atoms one will still move to bind in the bridge site. The two relaxed structures are shown below in Figures 3.9 and 3.11. These calculations show that in the initial dosing of water on the O covered surface, we should expect to find dissociation.

TABLE 3.2: Total energies of O + H_2O and 2OH on Rh(111)

Picture	Type	Total Energy (eV)
Picture 3.9	O + H_2O	−186.165
Picture 3.11	2 OH	−186.752

The structure with the water and oxygen molecules present on the surface has the water bonding to the surface at 2.26Å. The structure with two hydroxyl molecules had the hydroxyl in the atop position binding to the surface at 2.03Å. This trend of water binding further from the surface is seen across the results.

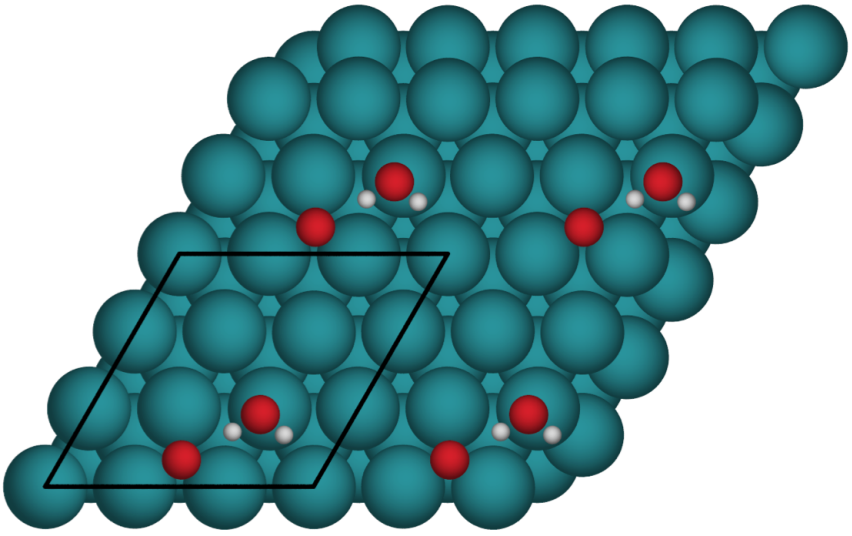

FIGURE 3.9: No interaction between preadsorbed oxygen and the water molecule seen

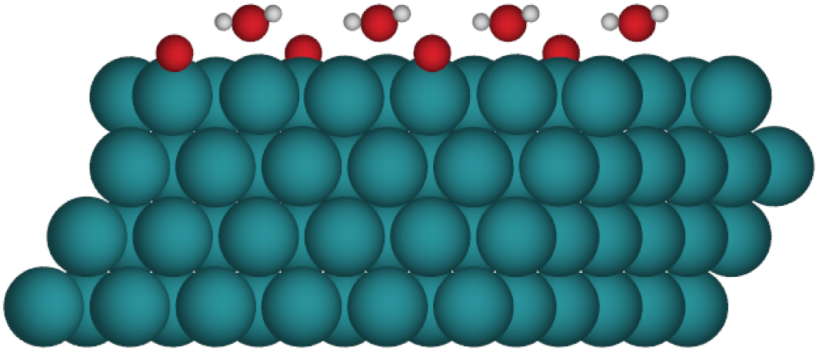

FIGURE 3.10: No interaction between preadsorbed oxygen and the water molecule seen, side view

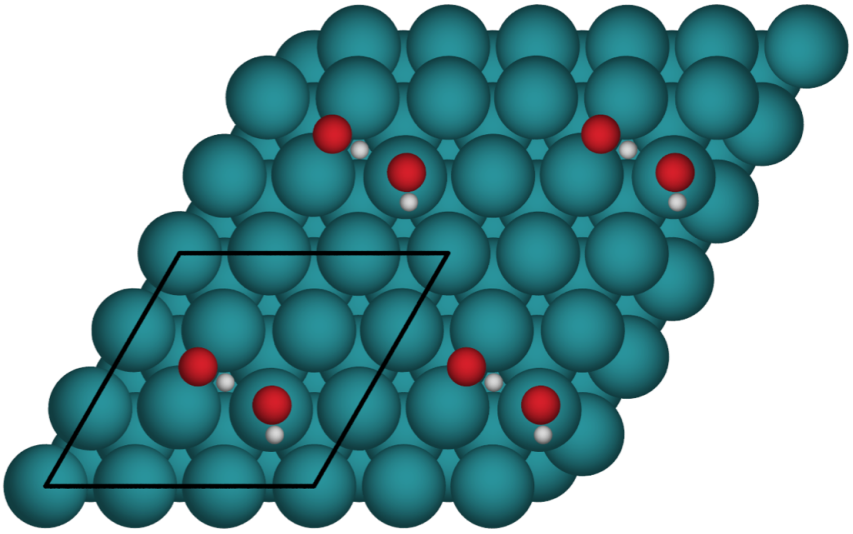

FIGURE 3.11: Dissociation between the preadsorbed oxygen and the water molecule forming two hydroxyl molecules

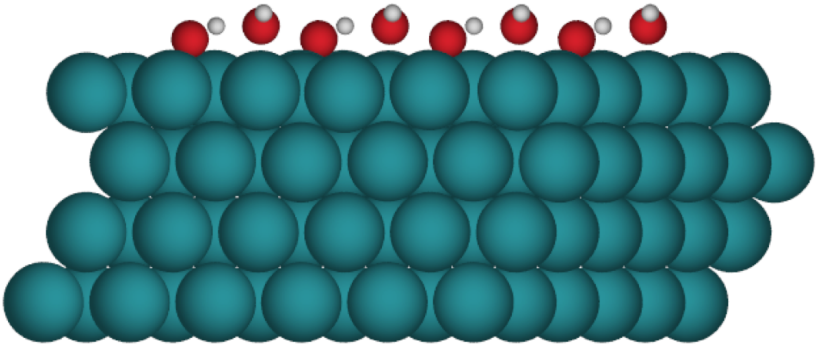

FIGURE 3.12: Dissociation between the preadsorbed oxygen and the water molecule forming two hydroxyl molecules, side view

3.3.1 Perdew-Burke-Ernzerhof exchange correlation

The initial calculations were performed with the PBE exchange correlation functional. When we began running these calculations the focus was on (6x6) unit cell size with either a 2:1 or 3:1 H_2O:OH ratio. Due to this many structures were made fulfilling these requirements, then the adsorption energies were compared to get an idea of what made the most stable structures. In total 41 structures were relaxed with PBE exchange correlation functionals and 12 of these formed the basis of the search with the van der Waals calculations. Each of these structures are shown in

Appendix A and the adsorption energies are listed. The following two figures show how the same trend in adsorption energies is seen when calculations are performed with PBE and vdW, 3.13 and 3.14.

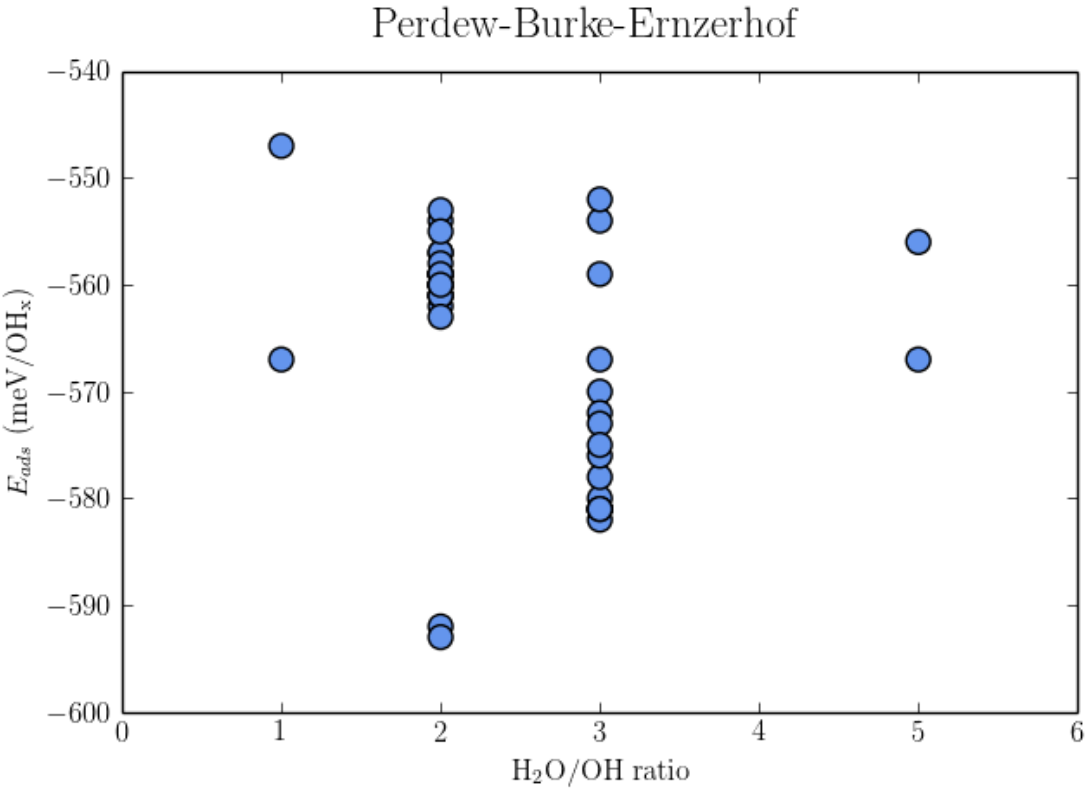

FIGURE 3.13: Perdew-Burke-Ernzerhof calculations adsorption energys vs ratio H_2O:OH. 21 points for 2:1 and 16 points for 3:1 structures.

From trends observed from the PBE calculations it was possible to create new overlayer structures that were likely to be very stable. As these new structures were made when the van der Waals calculations were being run they were not run with only the PBE exchange correlation functionals. As previously stated 12 structures from the PBE results formed the basis of the search with the van der Waals calculations, a further 6 structures were created, resulting in 18 different H_2O:OH structures being studied in total with the van der Waals corrections.

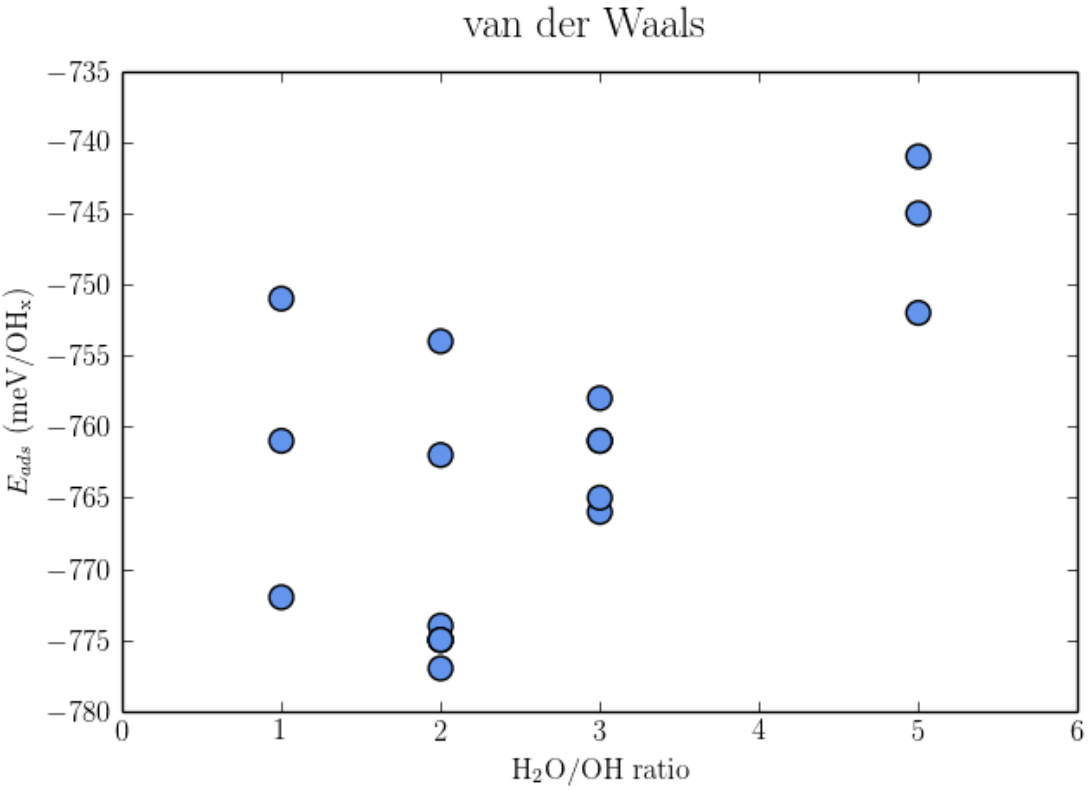

FIGURE 3.14: Van der Waals calculations adsorption energys vs ratio H_2O:OH. 7 points for 2:1 and 5 points for 3:1.

The correlation between the sets of calculations has been shown in Figure 3.15. The blue dots represent the 1:1 ratio structures, the grey dots represent the 2:1 ratio structures, the red dots represent the 3:1 ratio structures and the green dots represent the 5:1 ratio structures. As can be seen although there is some variation there is a general trend.

The only clear difference with the overlayer structures when relaxed with PBE or van der Waals is that the molecules are bound very slightly closer to the surface in the van der Waals structures than the PBE. This is shown in Figure 3.16 and 3.17. The O-Rh distance for an OH decreases from 2.11Å with PBE to 2.09Å with van der Waals, similarly the O-Rh distance for an H_2O decreases from 2.18Å to 2.16Å. Figure 3.15 shows that the correction is slightly greater for a larger

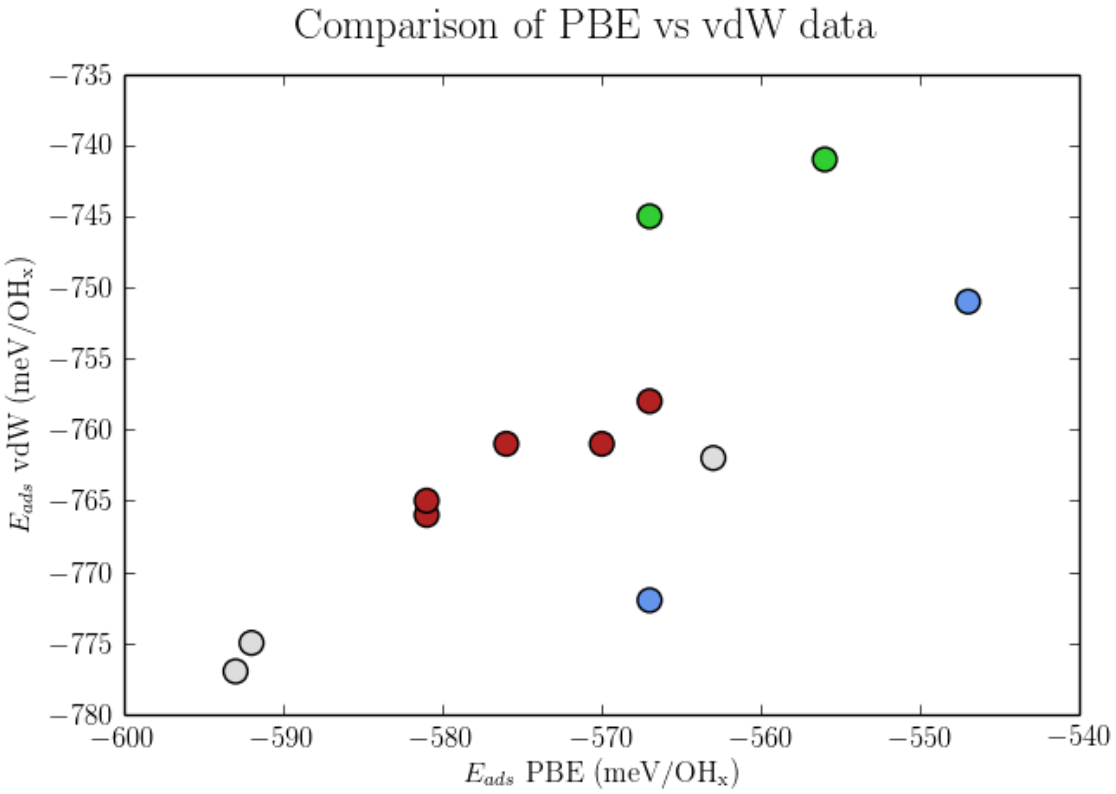

FIGURE 3.15: Perdew-Burke-Ernzerhof adsorption energies vs Van der Waals adsorption energys

percentage of OH in the structure as these are overall closer and more strongly bound by the metal.

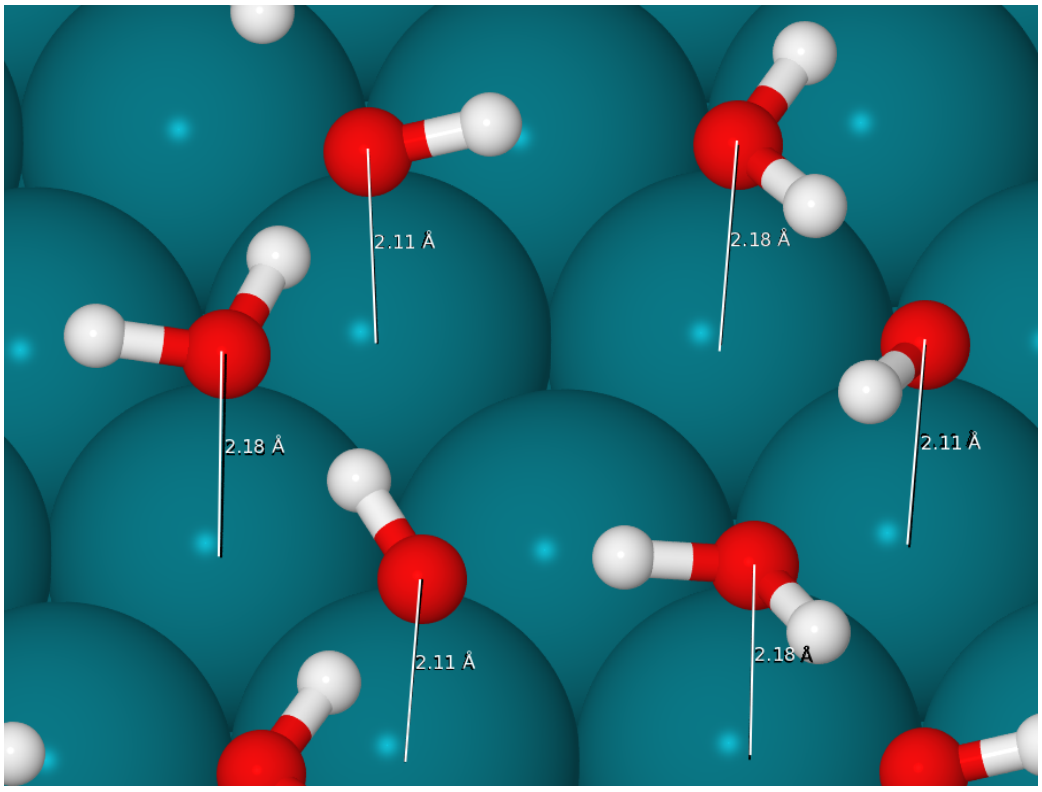

FIGURE 3.16: Height of water and hydroxyl molecules with PBE claculations

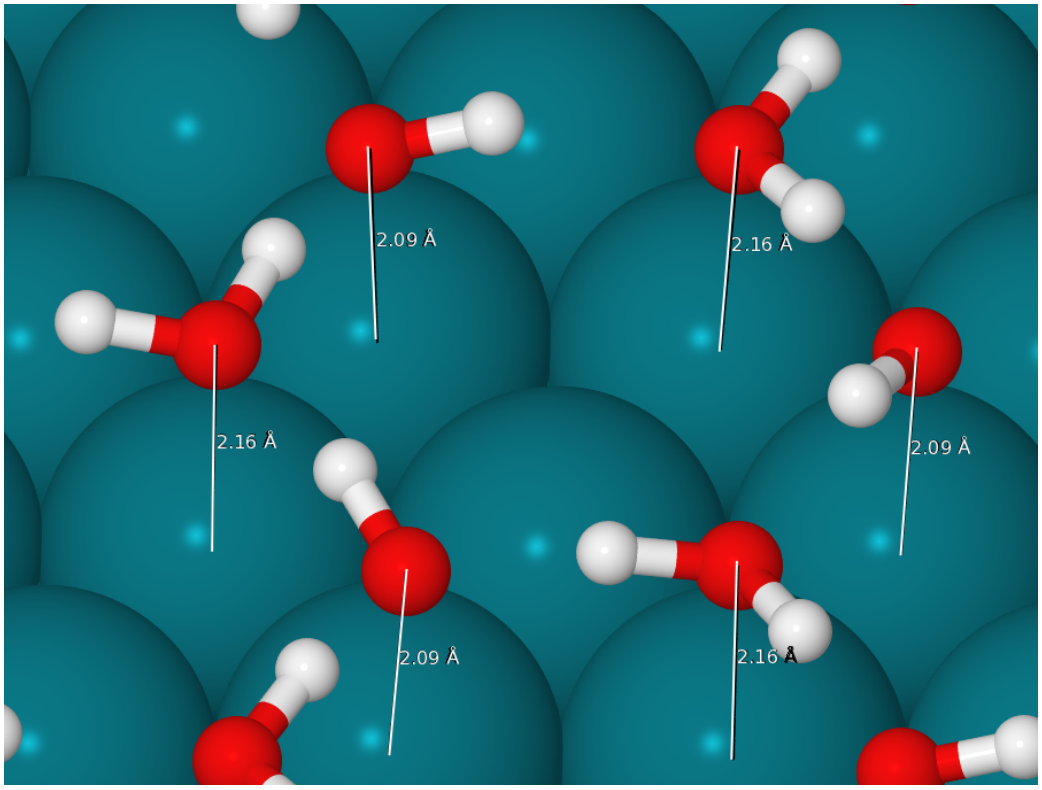

FIGURE 3.17: Height of water and hydroxyl molecules with vdW calculations

3.3.2 Van der Waals calculations

In the following we discuss overlayer structures relaxed with the optB86b van der Waals functional. There were many differing possible adsorption geometries of the water and hydroxyl in the overlayers. Along with varying the ratios the structures were made with Bjerrum defects, chains of hydroxyl molecules bonding to each other and hydroxyl molecules separate and not bonding to other hydroxyl molecules. Varying unit cell size allows different numbers of OH configurations allowing us to test if Bjerrum defects are important.

3.3.2.1 1:1 H_2O:OH

For the 1:1 H_2O:OH the adsorption energies are shown in Table 3.3, the most stable structure had strictly alternating hydroxyl and water molecules, as can be seen in Figure 3.18.

The thermal energy, kT at 120K, a typical temperature for the experiments, is equal to 10.35meV. For the 2:1, 3:1 and 5:1 structures that follow most have energies within kT of the lowest energy structure showing that they are likely all present on the surface. For the 1:1 structures, as can be seen in Table 3.3, this is not the case, indicating that only the alternating OH-H_2O structure should be present. For these calculations the assumption has been made that due to the similar bonding, the vibrational entropy would be similar in all of the structures and therefore does not need to be taken into account, as it would have the same effect on each structure. In a similar study it has been found that even up to

high temperatures inclusion of vibrational contributions has little effect. [75] The configurational entropy would be difficult to take into account as there would be a lot of disorder within the structures since many lie within kT of the minimum. This proton disorder would not have shown in the LEED data as that is only sensitive to the O atom locations. Helium atom scattering, which was not used, would have shown this disorder more.[24]

TABLE 3.3: Calculated adsorption energies of different 1:1 H_2O:OH structures on Rh(111)

Figure	Type	Adsorption Energy (meV)
Figure 3.18	Alternating water and hydroxyl (3x3)	−772
Figure 3.22	Interrupted chains of water and hydroxyl (3x3)	−751
Figure 3.25	Alternating and chains of water (6x6)	−761

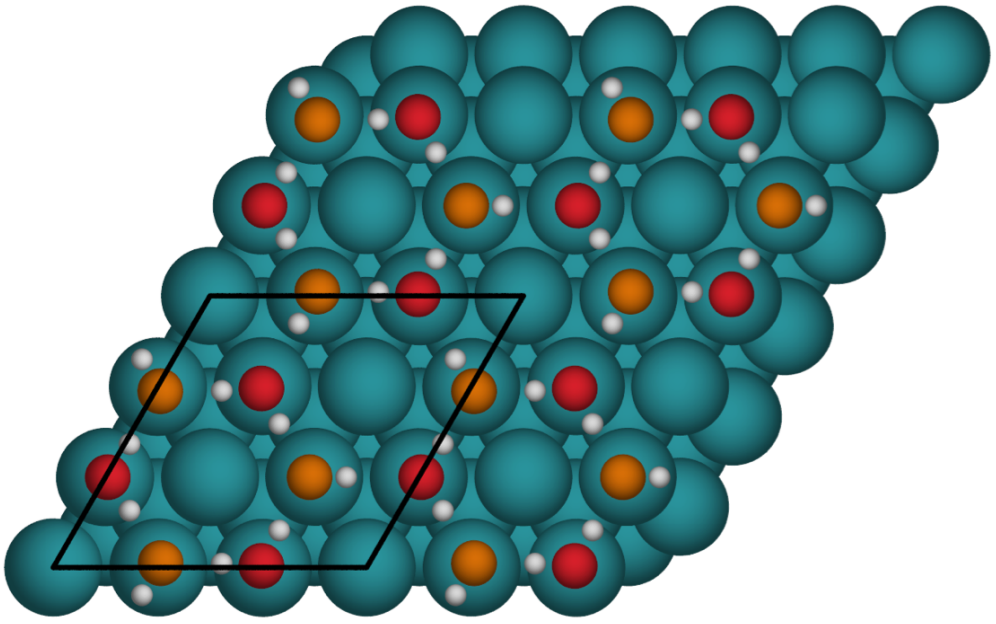

FIGURE 3.18: Most stable 1:1 structure with alternating water(red) and hydroxyl(orange) molecules, top view

The structure has all of the hydroxyl molecules bound at a height of 2.09Å, this height was calculated by measuring the distance between the oxygen molecules in the hydroxyl to the rhodium atom that the hydroxyl molecule was in the atop

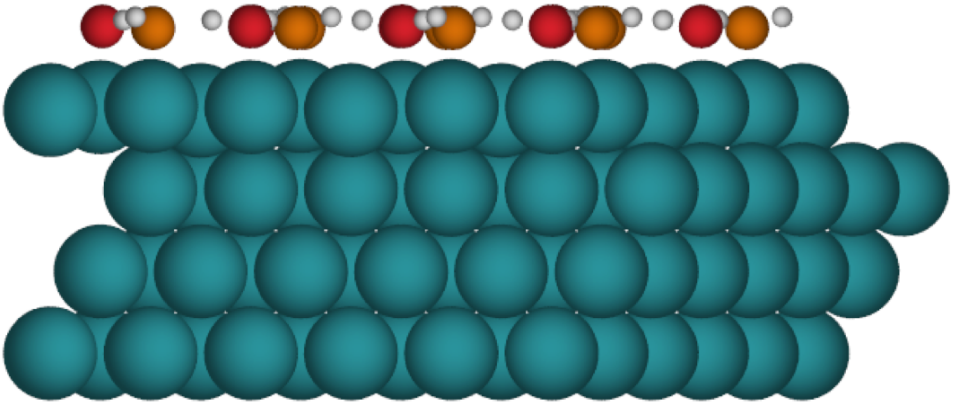

FIGURE 3.19: Most stable 1:1 structure with alternating water(red) and hydroxyl(orange) molecules, side view

position above and all of the water molecules bound at 2.16Å, this is shown in Figure 3.20.

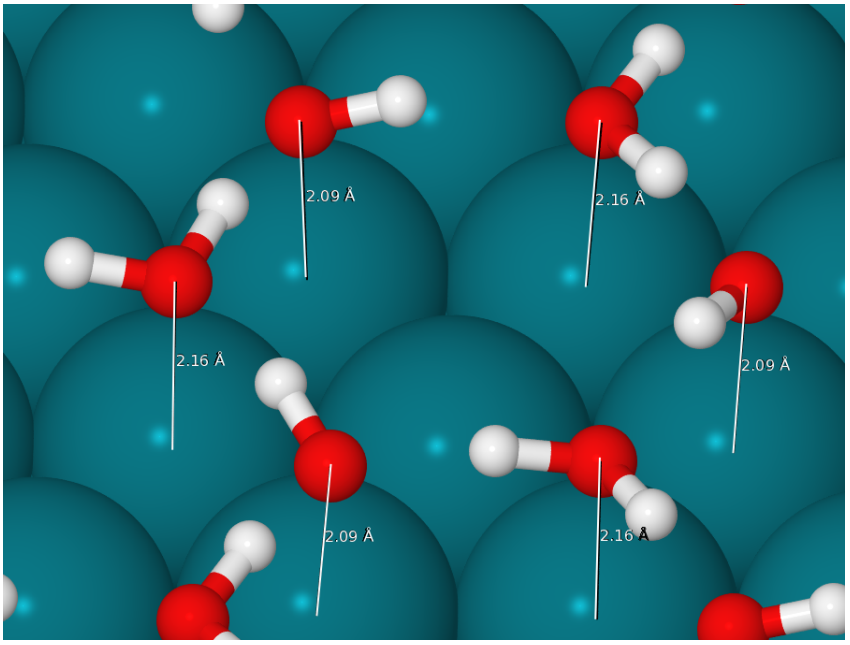

FIGURE 3.20: Height of oxygen in water or hydroxyl molecule above surface atom for most stable 1:1 structure

Figure 3.21 shows that when a hydroxyl molecule is being a hydrogen bond donor to a water molecule the O-O bonding distance is 2.88Å ± 0.1Å and when a water is donating to a hydroxyl molecule the O-O distance is 2.59Å ± 0.1Å. These were calculated by measuring the distance from the centre of one O atom

to the centre of the other O atom. This overlayer shows that at least for the 1:1 structures there is a definite preferred height and bonding distance as all of the molecules have relaxed into very similar positions.

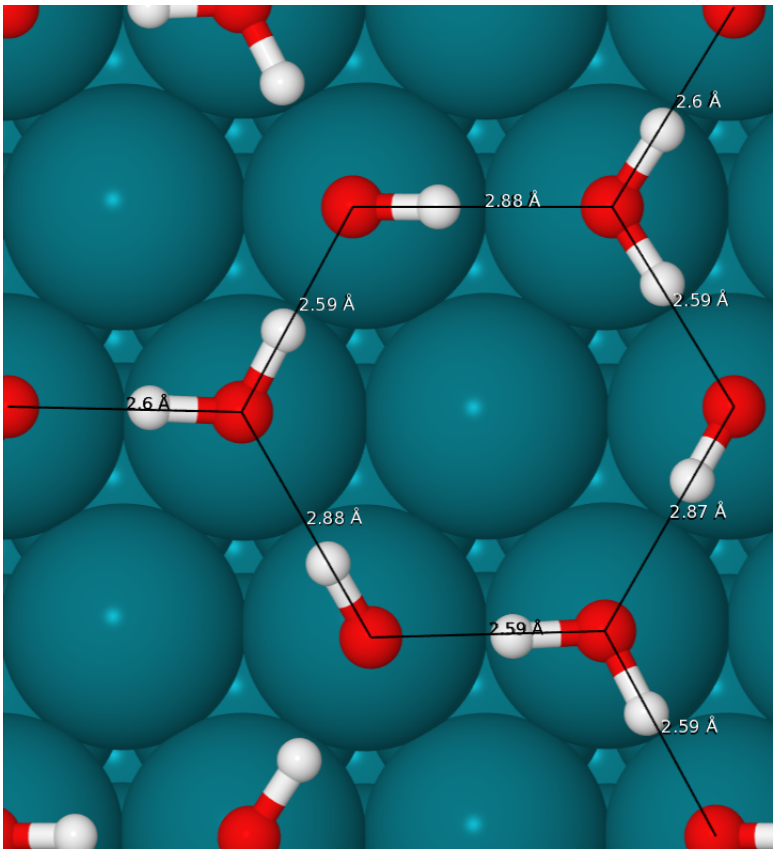

FIGURE 3.21: O-O bond distances for the most stable 1:1 structure

The next overlayer, shown in Figure 3.22 had the hydroxyl molecules in chains of three bonded to other hydroxyl molecules, chains of water molecules have been shown to be preferential on Ru(0001) in pure water systems.[4, 40] This structure is less stable than the previous alternating water and hydroxyl structure, shown in Figure 3.18 and 3.19, as is shown in Table 3.3. The hydroxyl molecules bond closer to the surface again at 2.08Å $\pm$ 0.1Å and the water binds at 2.18Å$\pm$ 0.1Å, these are shown in Figure 3.23, these are very similar to the values found in the alternating structure.

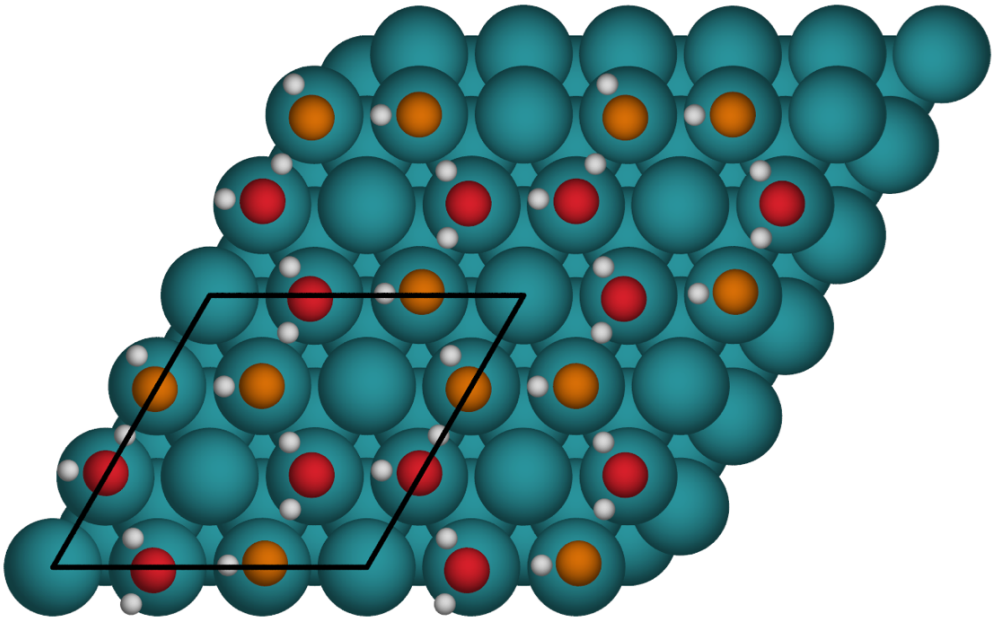

FIGURE 3.22: 1:1 Chain structure with three hydroxyl in a row, water in red and hydroxyl in orange, top view

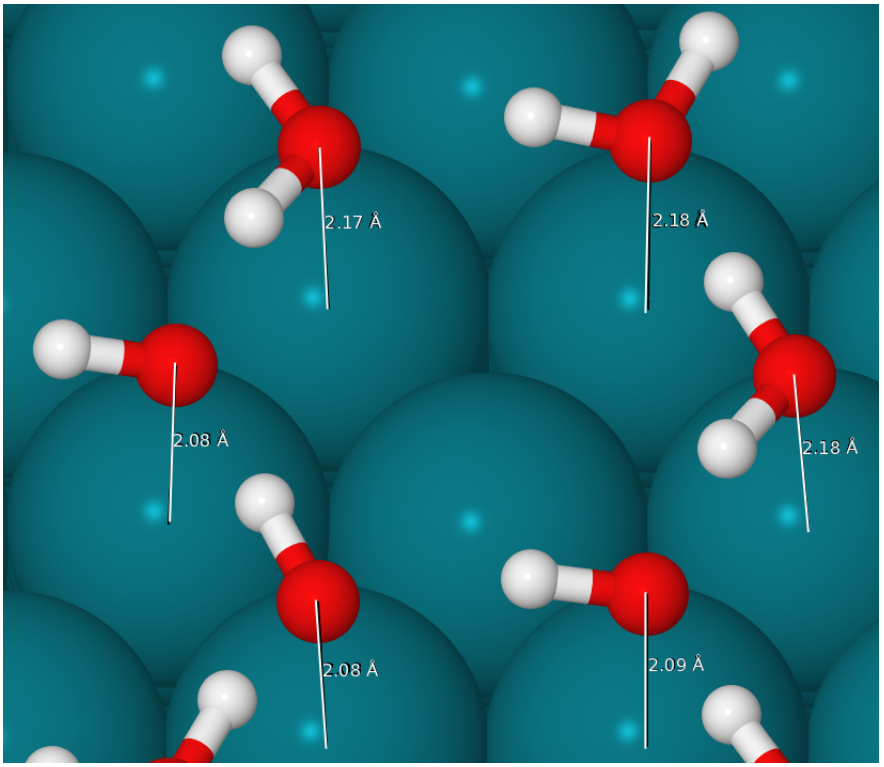

FIGURE 3.23: Height of oxygen in water or hydroxyl molecule above surface atom, in the 1:1 three hydroxyl chain structure

The O-O bond distances, shown in Figure 3.24, are once again closer when the water is the hydrogen donor and the hydroxyl is the acceptor, 2.56Å± 0.6Å

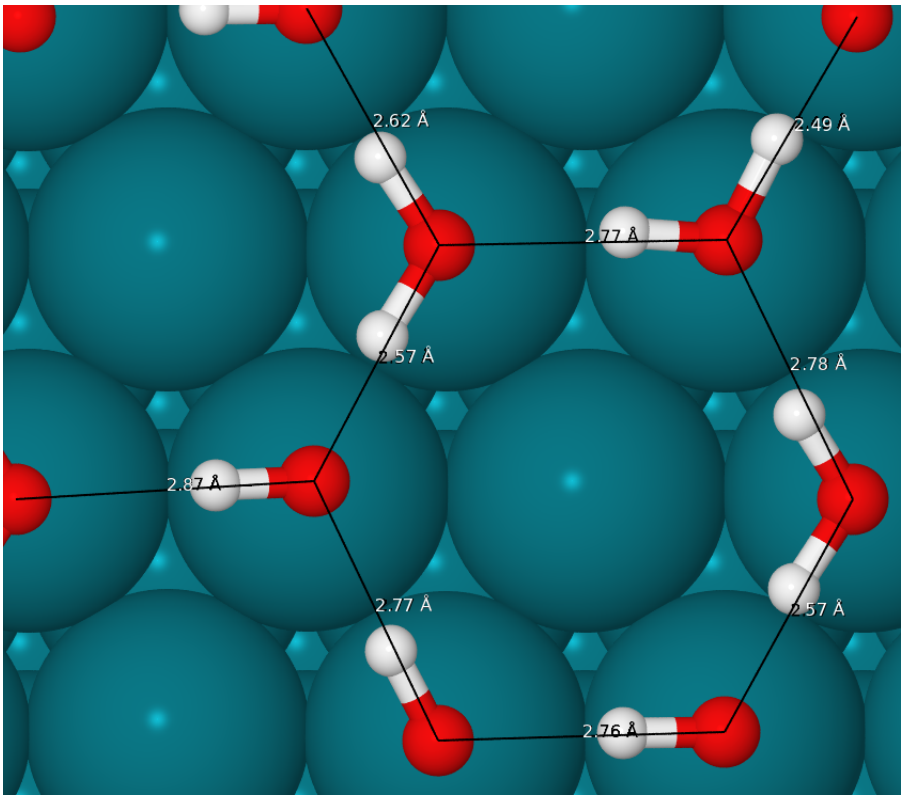

FIGURE 3.24: O-O bond distances, in the 1:1 three hydroxyl chain structure

compared to 2.87Å for donation from OH. The O-O distances when the hydroxyl bonds to another hydroxyl or when water bonds to another water are very similar at 2.77Å$\pm$ 0.1Å.

A larger (6x6) structure has been created, as this will have more possibility for relaxation. It has both alternating water and hydroxyl molecules and chains of bonded hydroxyl molecules present. This structure follows similar binding heights and O-O distances although with slightly more variation in the data collected which is to be expected due to its greater number of inequivalent molecules compared to the smaller (3x3) unit cell size. This structure is 10meV per molecule more stable than the chains structure but 11 meV per molecule less stable than the alternating structure.

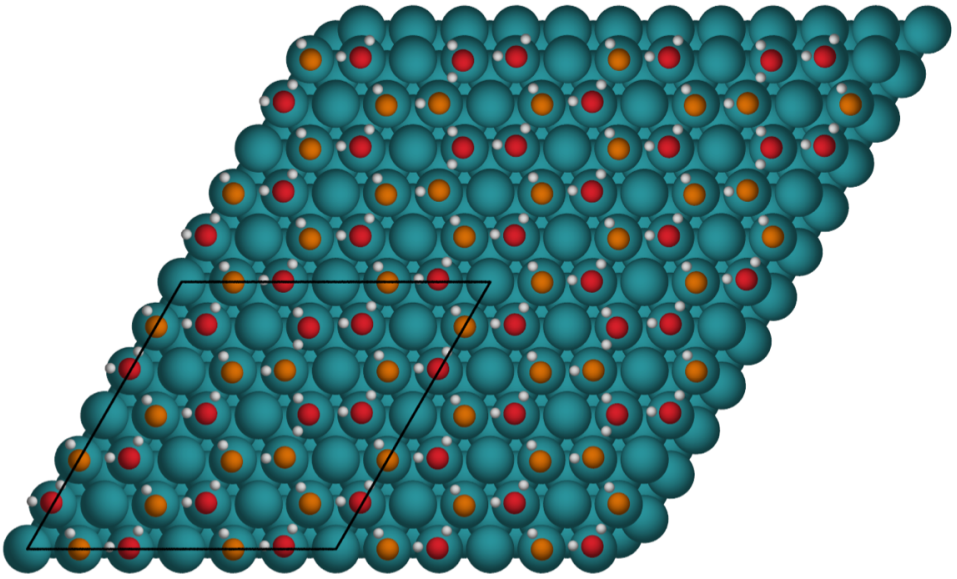

FIGURE 3.25: 1:1 (6x6) structure, has some chains and some alternatingsections, water in red and hydroxyl in orange, top view

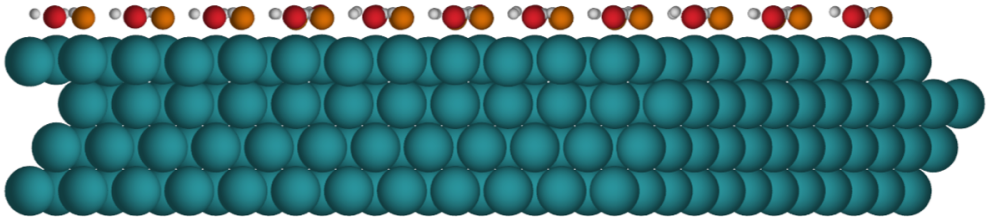

FIGURE 3.26: 1:1 (6x6) structure, has some chains and some alternatingsections, water in red and hydroxyl in orange, side view

3.3.2.2 2:1 H_2O:OH

The $2H_2O$:OH structures need to form Bjerrum defects or have hydrogen pointing to the surface or gas phase. Due to the additional bonds present only the structures containing Bjerrum defects have no hanging hydrogen bonds, unlike with the structures containing no defects.

The height in the most stable $2H_2O$:OH structure, shown in Figure 3.27, for the hydroxyl molecules bound to the surface is higher than the 1:1 H_2O:OH ratio at 2.12Å$\pm$ 0.1Å, compared to 2.09Å in the 1:1 structure. The water molecules also bond further from the surface at 2.22Å$\pm$ 0.6Å for the flat lying water molecules

in this 2:1 structure, rather than 2.16Å in the most stable 1:1 structure. In this structure each of the waters having a dangling bond is a H-bond donator. This may have helped improve the stability of the overlayer as the dangling water molecules are able to bond closer to the surface at 3.11Å± 0.2Å which is much lower than the average for the other structures considered with H-up as will be discussed for other structures.

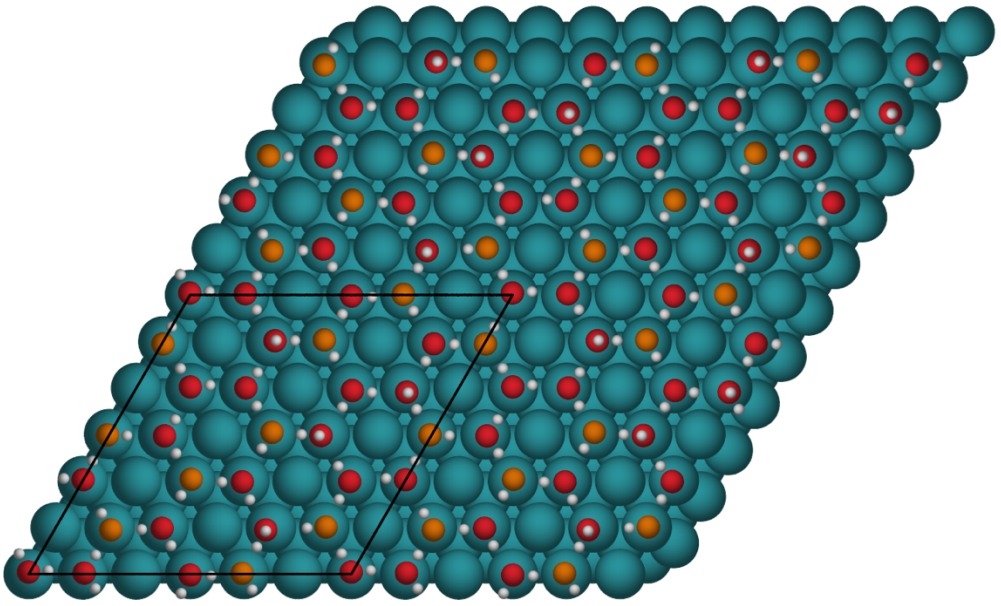

FIGURE 3.27: 2:1 Most stable structure, has four dangling water molecules all of which are donating to a hydroxyl molecule, water molecules shown in red and hydroxyl molecules shown in orange, top view

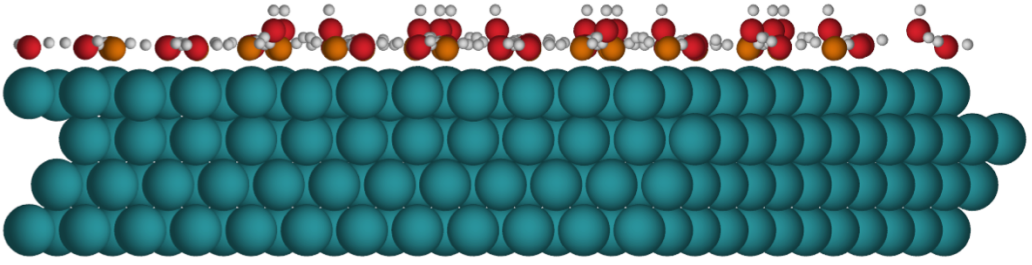

FIGURE 3.28: 2:1 Most stable structure, water molecules shown in red and hydroxyl molecules shown in orange, side view

The O-O distances are not dissimilar with only ± 0.1Å difference between the average distances in the 1:1 structures, i.e. within the variations of the 1:1 structures. When the hydroxyl is donating to the dangling water molecule, the

distance is 3.13Å, 0.24Å greater than any other O-O distance, the hydroxyls ability to donate to the dangling water molecule may have been hindered by the height difference between the two molecules. It is interesting to note that when a hydroxyl is binding to a dangling water it has an angle of 105.30° showing that to donate a stronger bond to the dangling water the angle from the surface has increased by a large amount, shown in Figure 3.29. This angle was calculated by measuring from the centre of the H atom, to the centre of the O atom, to the centre of the Rh atom the O atom was above.

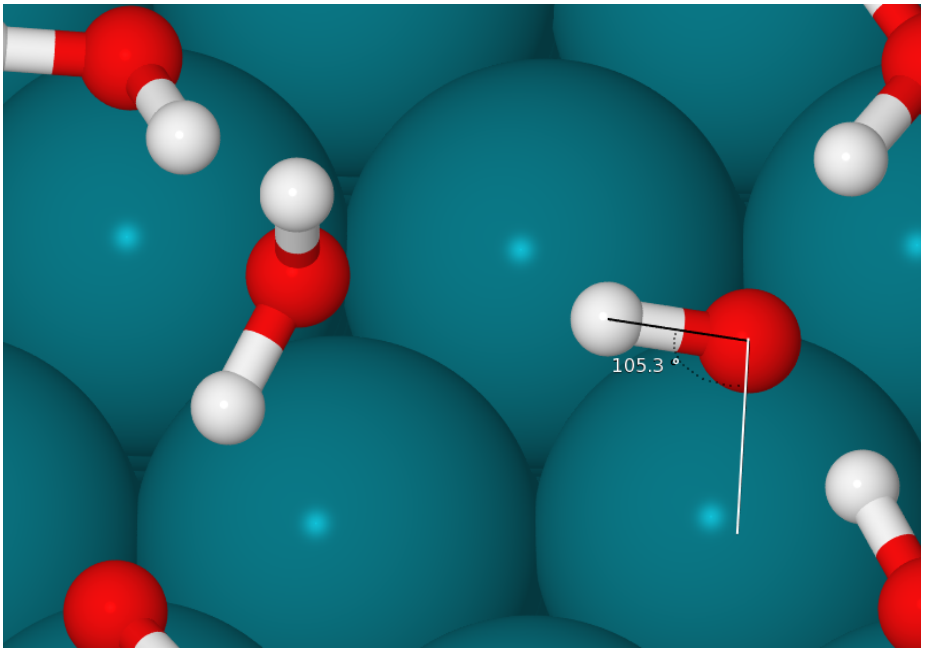

FIGURE 3.29: Angle of hydroxyl in relation to the surface when donating to a dangling water molecule in the most stable structure

For the hydroxyl molecules that are being bound by one dangling water and one flat water the bond angle to the surface is 102.23°±0.52°. For two flat water molecules binding to a hydroxyl molecule this angle is 103.10°±0.10°.

The adsorption energies for all the 2:1 structures run with van der Waals forces are shown in Table 3.4.

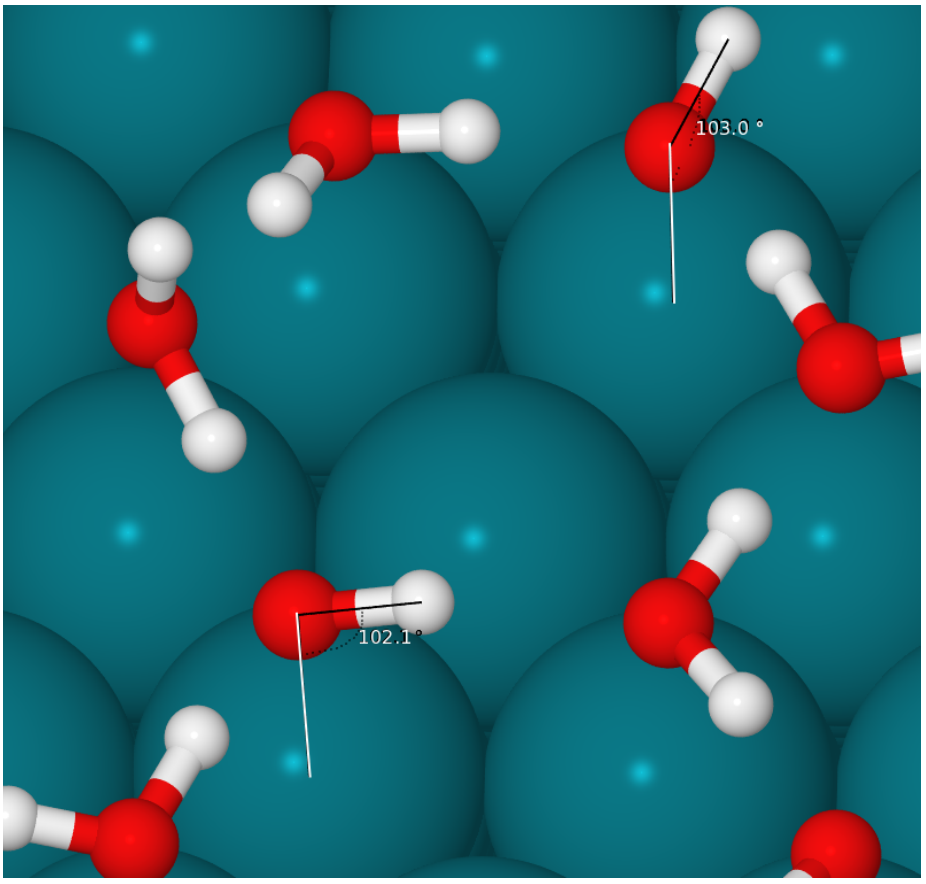

FIGURE 3.30: Angle of hydroxyl in relation to the surface with two flat water molecules donating to it, 103.0° and with one dangling and one flat water molecule donating to it, 102.1°

TABLE 3.4: Calculated adsorption energies of different 2:1 H_2O:OH structures on Rh(111)

Figure	Type	Adsorption Energy (meV)
Figure 3.27	H-up (6x6)	−777
Figure 3.31	H-up (6x6)	−775
Figure 3.34	H-up (3x6)	−774
Figure 3.37	H-up (3x3)	−775
Figure 3.40	H-up (6x6)	−775
Figure 3.42	H-down (6x6)	−754
Figure 3.44	Bjerrum Defect (6x6)	−762

The next most stable structure is one with all of the hydroxyls in the same position as the previous structure, it is shown in Figure 3.31. The section circled in white in the figure shows where the water molecules are arranged differently with different molecules dangling H-up than in the previous structure. The main

difference between the two is that where the previous structure had all of the dangling water molecules binding to a hydroxyl molecule this one has one of the dangling water molecules binding to another dangling water molecule, as shown in the yellow circle.

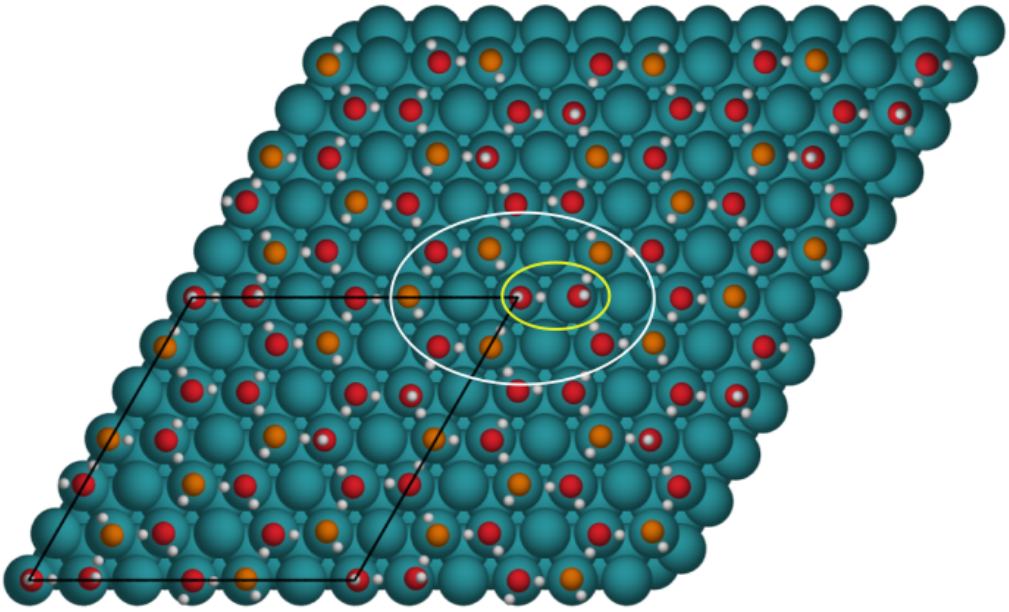

FIGURE 3.31: Yellow circle shows dangling water bonding to another dangling water molcule. White circle shows the section where the water molecules are arranged differently to the previous structure. Water shown in red and hydroxyl shown in orange, top view

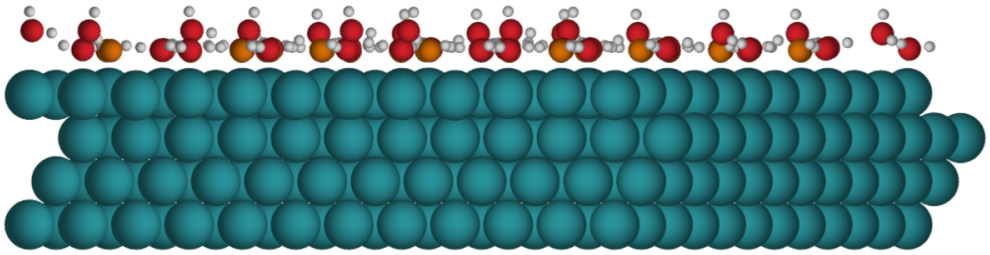

FIGURE 3.32: Water shown in red and hydroxyl shown in orange, side view

The combination of these 2 molecules binding to each other has led to them bonding further away from the surface at 3.23Å and 3.25Å, shown in Figure 3.33. This could be the reason this overlayer has come out 2meV per molecule less stable than the other overlayer structure where the dangling water molecules were

all bound at 3.11Å± 0.2Å which is the case with the other two dangling molecules in this structure.

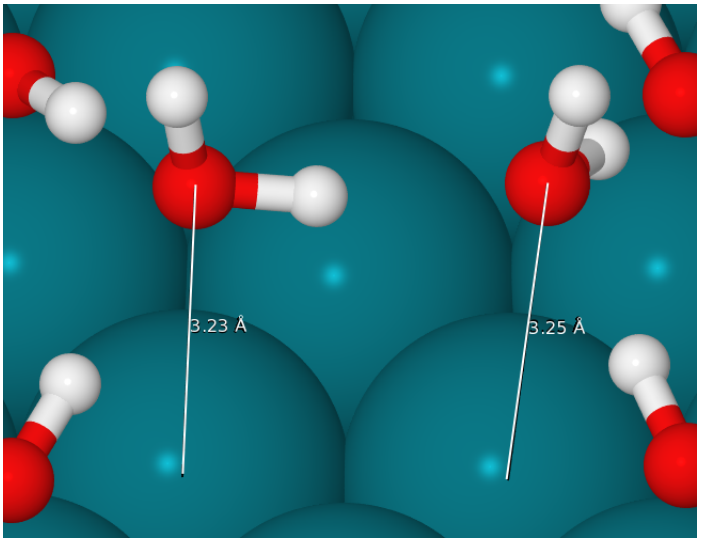

FIGURE 3.33: Heights when one dangling water molecule is donating to another dangling water molecule

There does not seem to be a strong unit cell size preference for the $2H_2O$:OH ratio. This can be seen in Table 3.4, the adsorption energies are very similar -775meV±2meV for the alternating structures in (3 x 3) and (3 x 6) unit cell sizes.

One of the most stable (3x6) unit cell size structures is shown in Figure 3.34, although others were looked at as shown in Figures A.4, A.5 and A.6 in Appendix A. This structure has a dangling water molecule donating to a flat water molecule, shown in the white circle in Figure 3.36, it lies 3.2Å above the surface. Whereas the dangling water donating to a hydroxyl molecule, shown in the yellow circle, is bound closer to the surface at 3.13Å, this trend is found across the 2:1 structures. Also it can be seen that the hydroxyl molecule bonds at a much smaller angle from the surface when donating to a flat water molecule, 101.5°, compared to when it is bonding to a dangling water molecule, 105.4°.

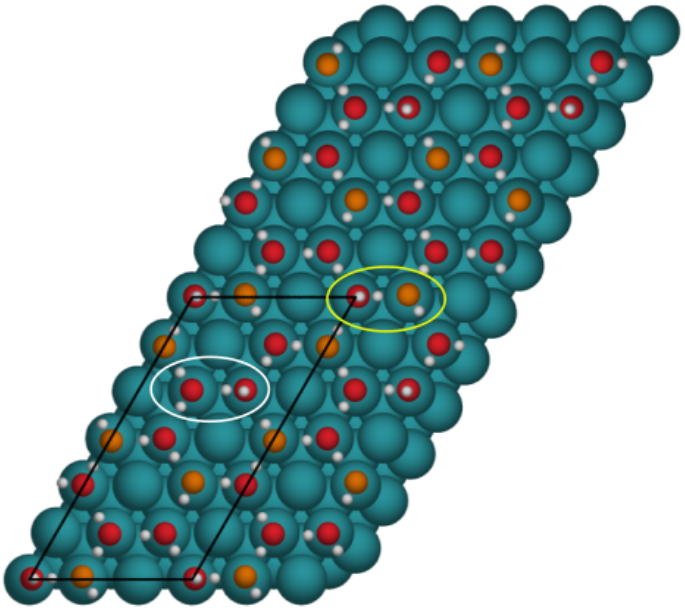

FIGURE 3.34: (3x6) unit cell, white circle shows a dangling water molecule donating to a flat water molecule. Yellow circle shows a dangling water molecule donating to a hydroxyl molecule, with water molecules shown in red and hydroxyls are orange, top view

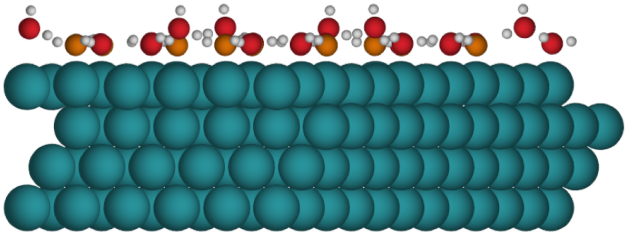

FIGURE 3.35: (3x6) unit cell with water molecules shown in red and hydroxyls are orange, side view

A (3x3) unit cell size structure was also tested, it is shown in Figure 3.37, although the smaller unit cell size means there is less room for relaxation this was still quite a stable structure, with an binding energy of -775meV per molecule. In this case the only H-up dangling molecule accepts and donates H-bonds from and to other water molecules.

A structure was also set up with the hydroxyl molecules in a chain, highlighted in the white circle in Figure 3.39, to test whether such a feature is preferred compared to the hydroxyl molecules binding to water molecules, this was again inspired

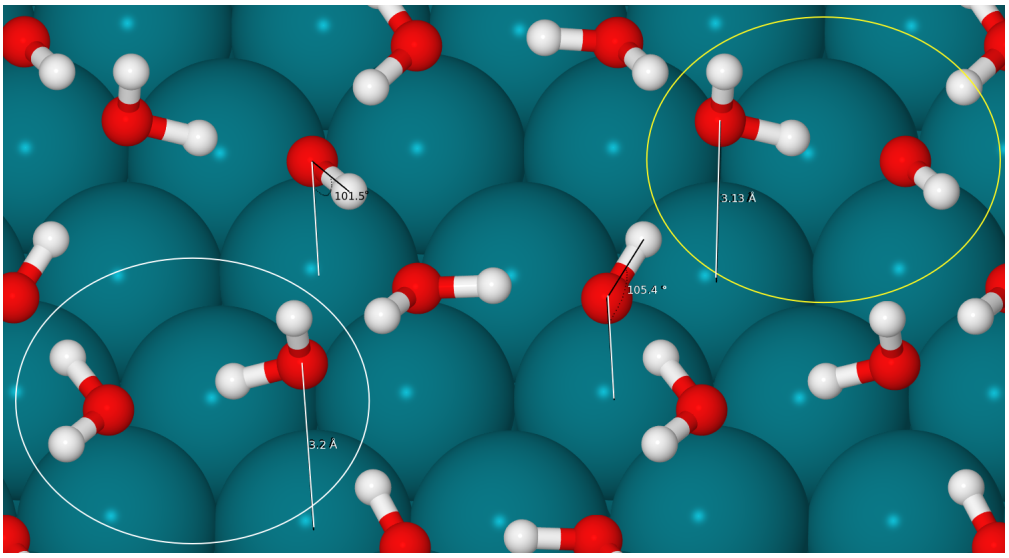

FIGURE 3.36: Angle of hydroxyl in relation to the surface when donating to a dangling, 105.4°, or flat, 101.5°, water molecule. White circle shows a dangling water molecule donating to a flat water molecule. Yellow circle shows a dangling water molecule donating to a hydroxyl molecule.

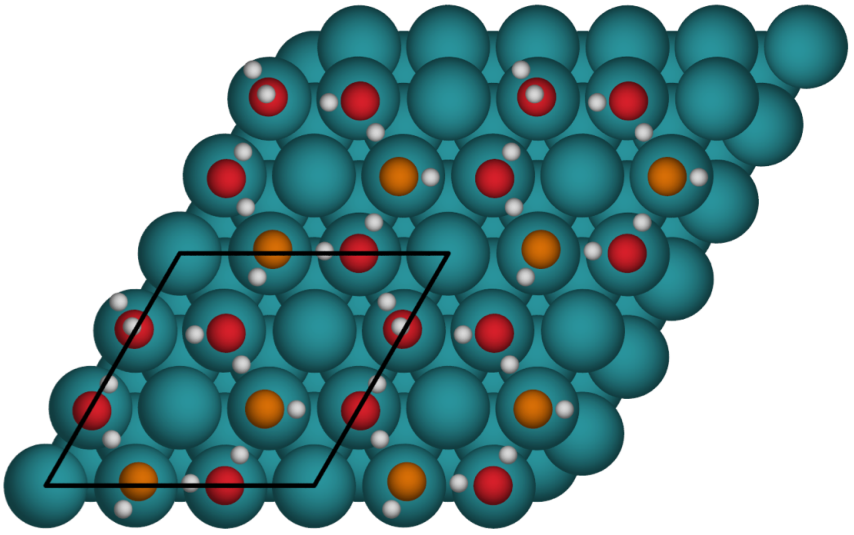

FIGURE 3.37: (3x3) unit cell, one dangling water molecule present, with water molecules shown in red and hydroxyls are orange, top view

by the water chain structure found on Ru(0001).[4] However when this structure was relaxed some water and some hydroxyl molecules have changed identity by transfer of hydrogen atoms from water to hydroxyl, leaving the hydroxyl bound to only water molecules instead of hydroxyls, as can be seen in Figure 3.40. The final structure has no hydroxyl molecules bound to other hydroxyl molecules, i.e.

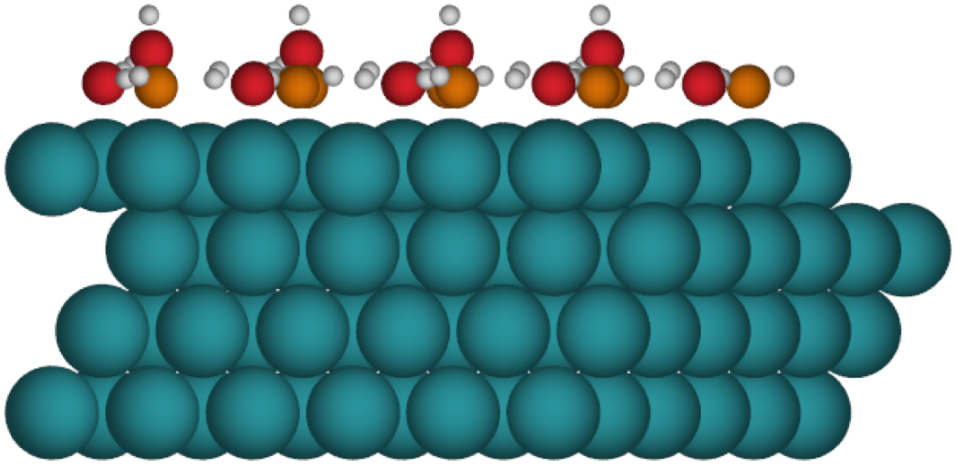

FIGURE 3.38: (3x3) unit cell with water molecules shown in red and hydroxyls are orange, side view

all accept H-bonds from water molecules and donate H-bonds to water molecules. This structure has one H-bond dangling down towards the surface, circled in yellow. This molecule is donating to another dangling up water which has bonded the furthest away from the surface compared to any other water at 3.44Å. Overall this structure still comes out quite stable at -775meV.

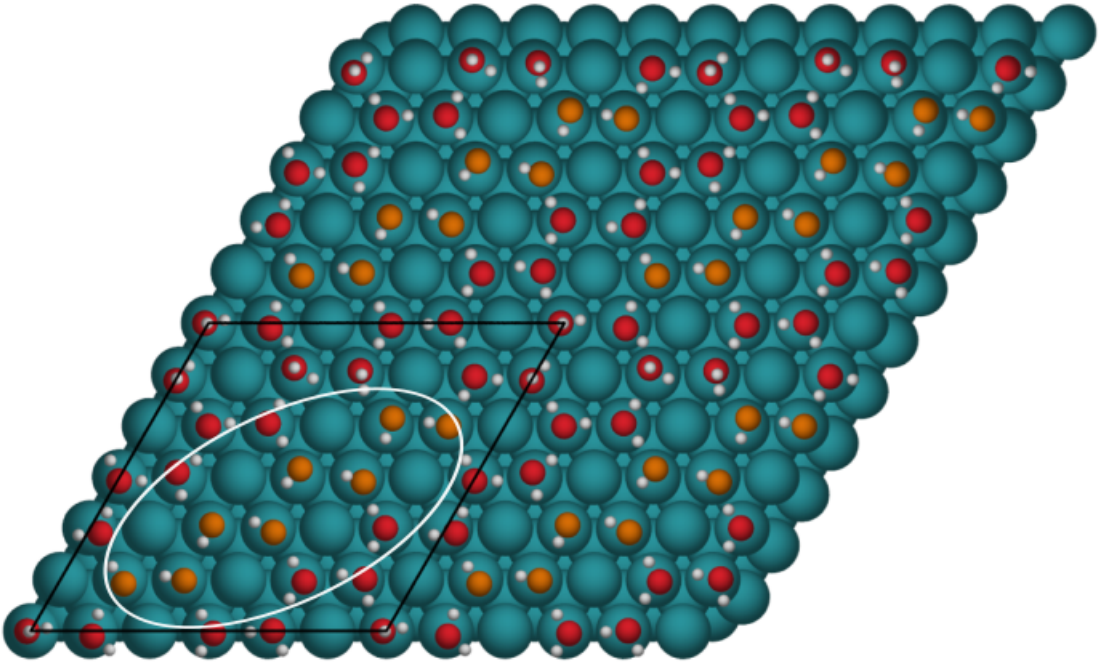

FIGURE 3.39: Original setup for chain structure, with seven hydroxyl molecules donating to other hydroxyl molecules, water shown in red and hydroxyl shown in orange

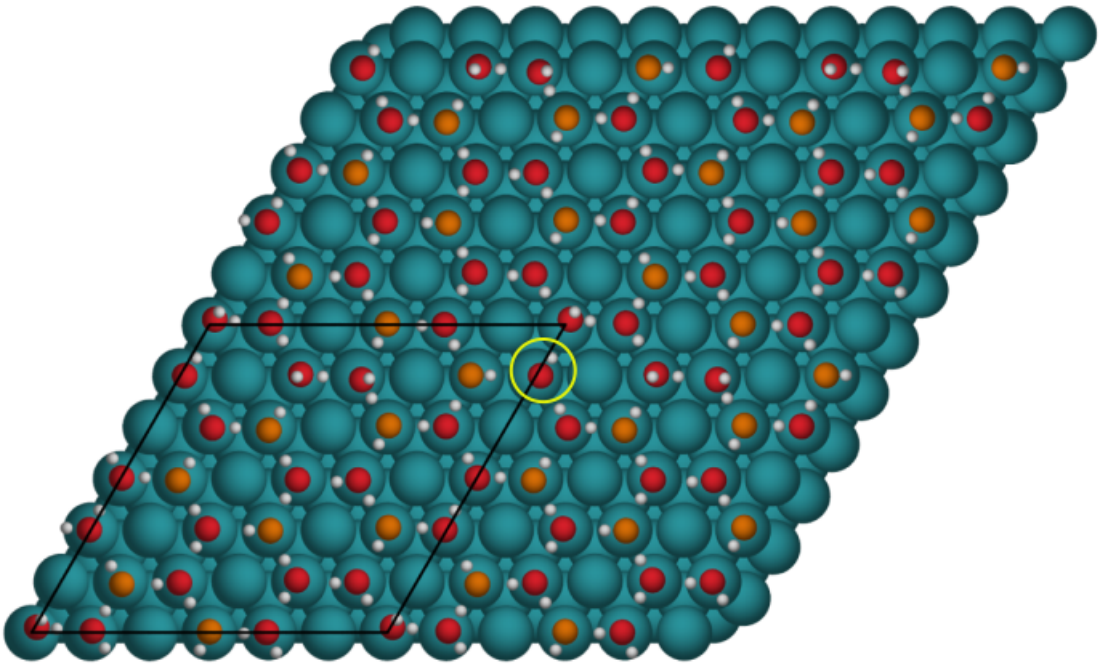

FIGURE 3.40: Final relaxed structure with water shown in red and hydroxyl shown in orange, yellow circle shows the dangling water with hydrogen pointing towards the surface

This structure has the largest O-O distance found in any of the structures examined at 3.29Å, when the hydroxyl tries to bind to the water with the bond dangling down. This hydroxyl is angled much further from the surface than any other hydroxyl molecules in any other alternating structures at 108.7°, shown in Figure 3.41.

One structure was run with all dangling water molecules in the H-down position, shown in Figure 3.42, it is the least stable of all of the 2:1 structures at −754meV, 23meV off the most stable structure shown in Figure 3.27. The dangling water molecules bond closer to the surface than any dangling water molecules in any other 2:1 structures at ∼3.06Å.

Table 3.4 shown gives an indication of how much more stable the alternating

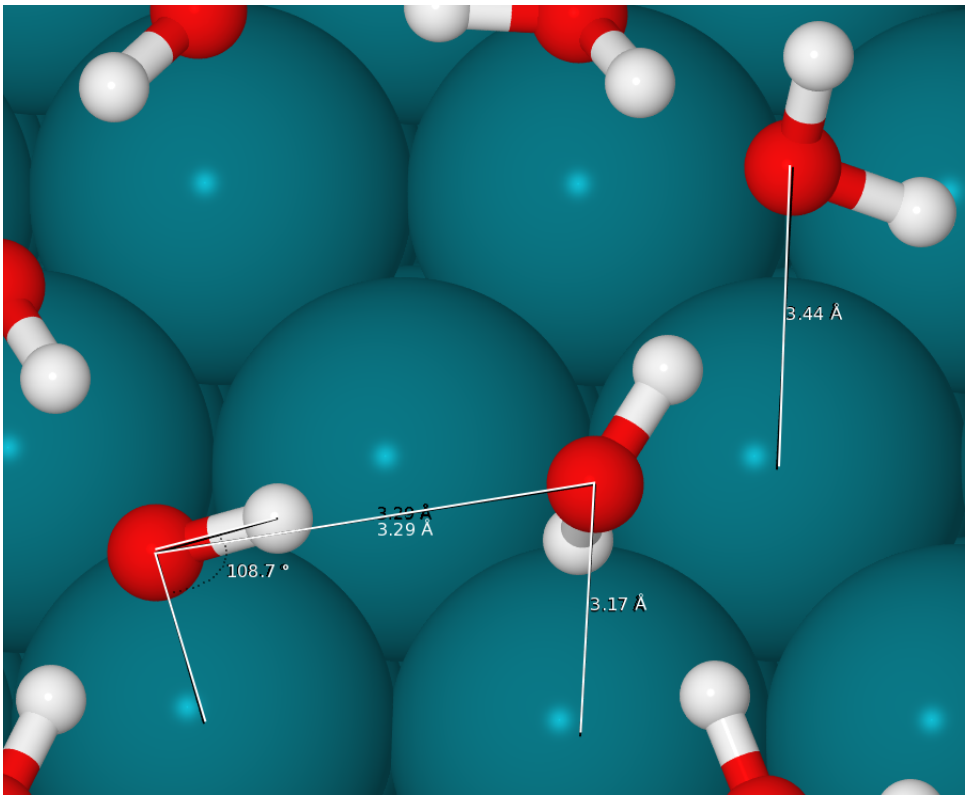

FIGURE 3.41: Heights of H-down dangling water molecule binding to H-up dangling water molecule and angle of hydroxyl molecule to the surface when donating to the H-down dangling water molecule

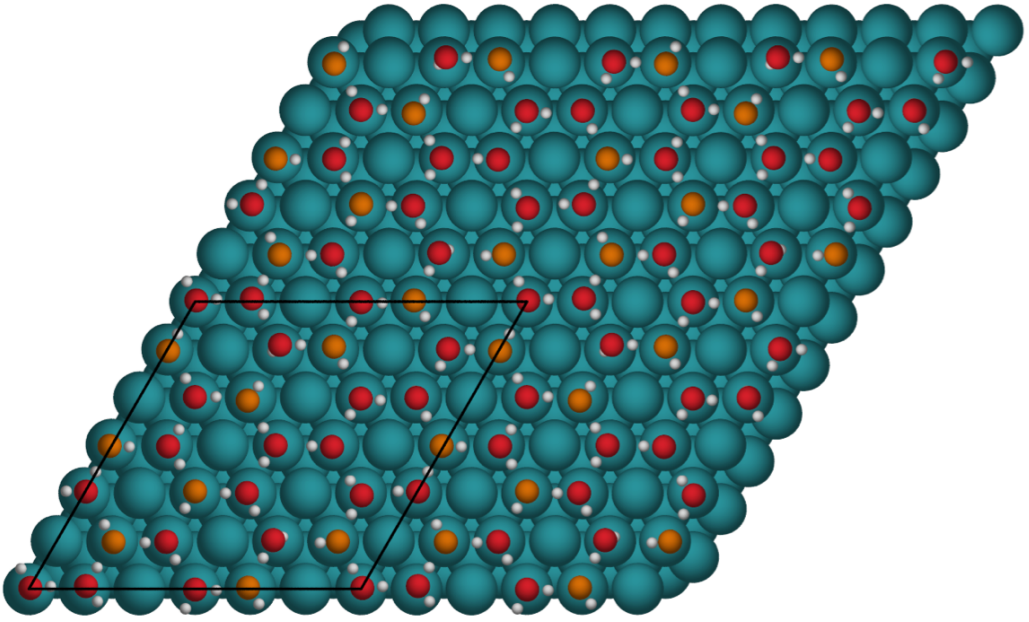

FIGURE 3.42: 2:1 Least stable structure with all dangling water in H-down position, water molecules shown in red and hydroxyl molecules shown in orange, top view

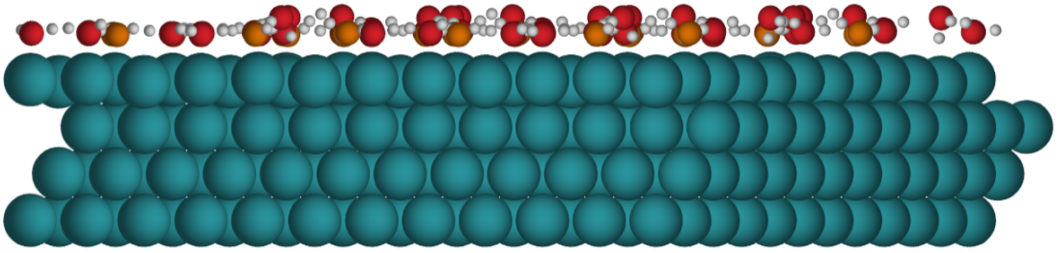

FIGURE 3.43: 2:1 Least stable structure with all dangling water in H-down position, water molecules shown in red and hydroxyl molecules shown in orange, side view

structures are in comparison to a structure with Bjerrum defects. Eighteen overlayers with these defects were tested at the PBE level, as it was initially thought the defects would yield the most stable results as shown on one other surface, Cu(110).[8] The structure shown below in Figure 3.44 was the most stable out of all the overlayer structures with Bjerrum defects at the PBE level, so was the only one to be looked at with van der Waals forces. In this structure every hydroxyl molecule binds further away from the surface than in any other 2:1 or 1:1 structure at 2.18Å ± 0.1Å, as shown in Figure 3.46. In the most stable 2:1 structure the average height for the hydroxyl molecules was 2.12Å ± 0.1Å.

Each of the 8 hydroxyl molecules forming 4 defects has relaxed into a position were the hydrogen's are pointing slightly away from each other rather than straight ahead, this is shown in Figure 3.46. The angles of the hydroxyl molecules relative to the surface show a much greater range, with one even bonding at 110.0°, which is much larger than in any of the defect free alternating structures; the average is ∼102.6° for hydroxyl molecules donating to other flat molecules in 3.27 the average for this structure with Bjerrum defects is 106.6°.

The other defect structures for $2H_2O$:OH shown in Appendix A- all followed similar trends to the one shown above and had poorer binding energies per molecule

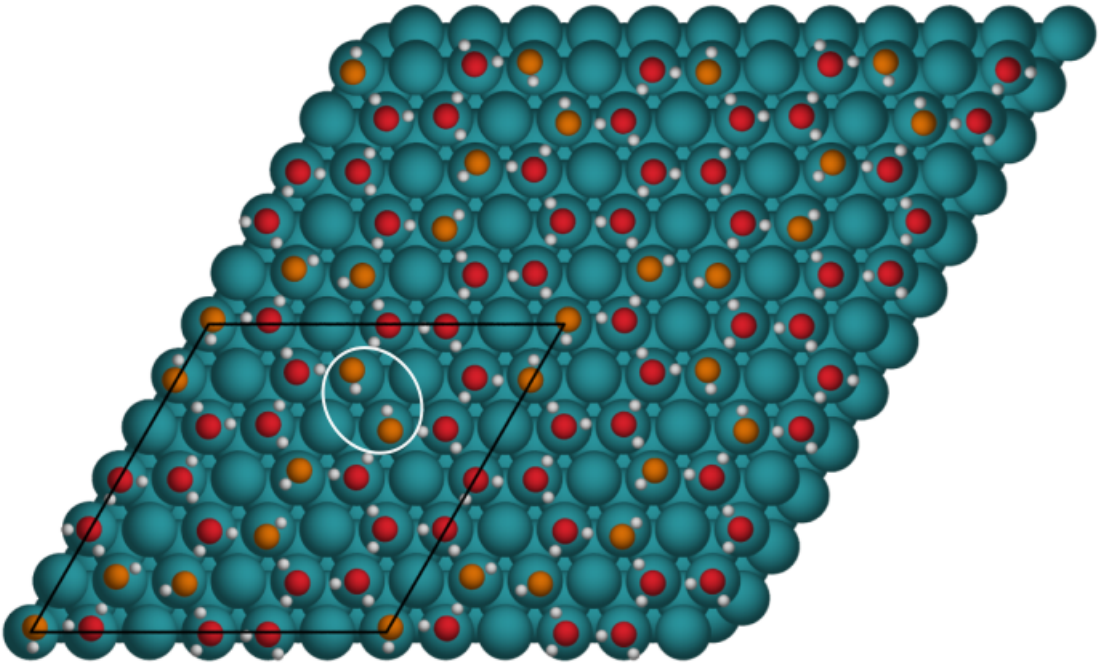

FIGURE 3.44: 2:1 Defect structure, four defects present with white circle showing the defect that is shown in Figure 3.46, water in red and hydroxyl in orange, top view

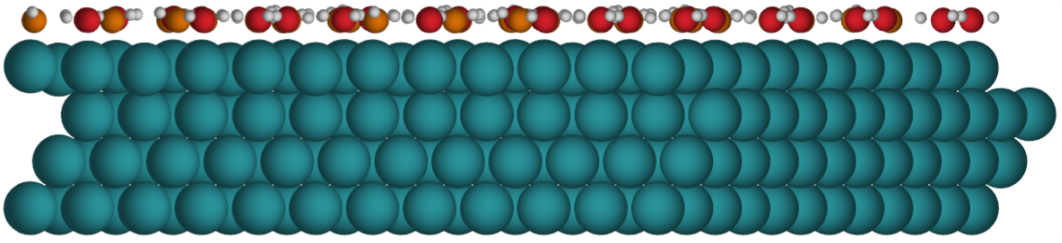

FIGURE 3.45: 2:1 Defect structure, it can be seen that all the water molecules lie flat in this overlayer, water in red and hydroxyl in orange, side view

than the one shown. Interestingly none of the Bjerrum defect structures rearranged to remove the hydroxyl molecules pointing towards each other in the way the chain structure reoriented to remove hydroxyl-hydroxyl bonding.

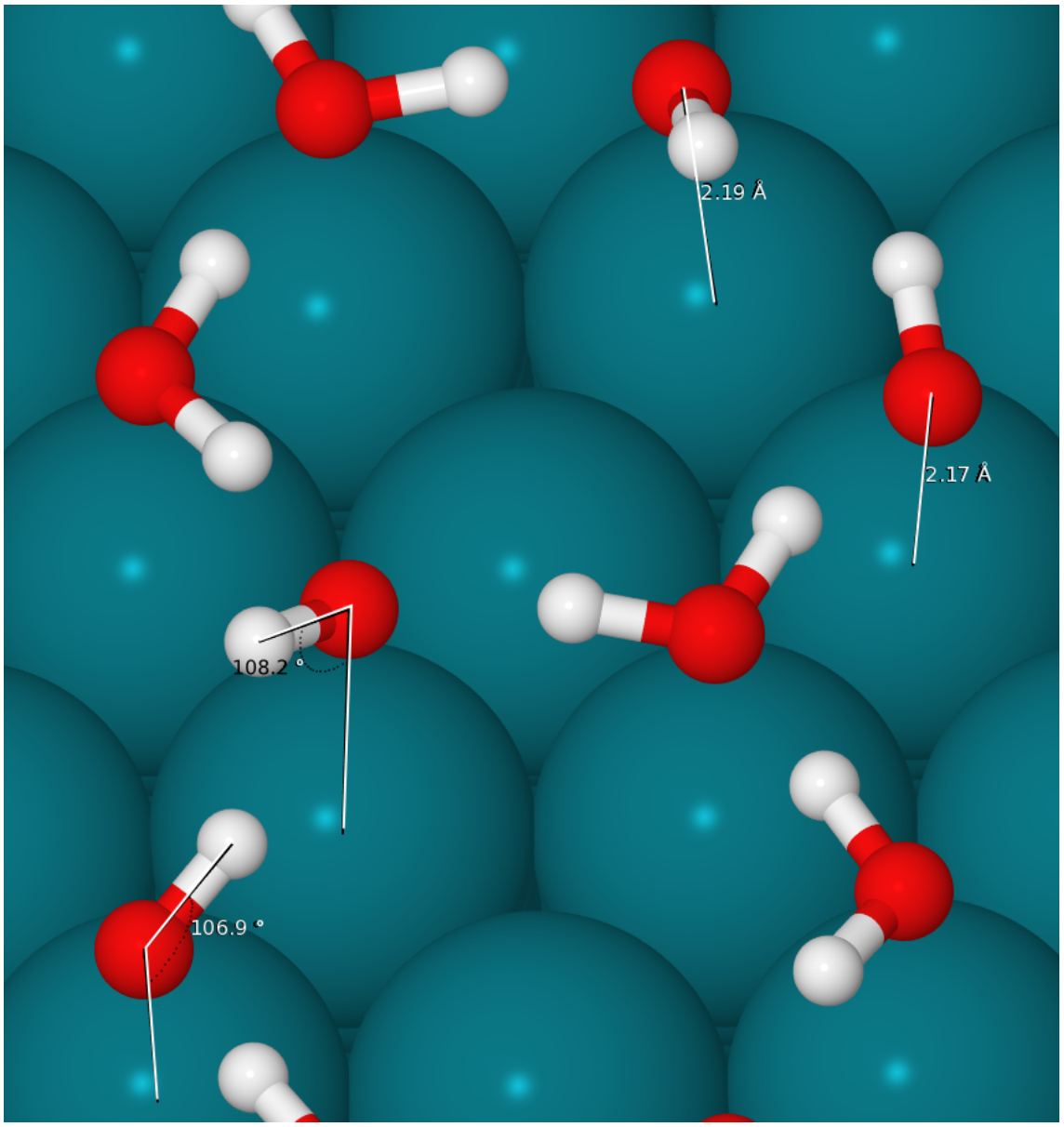

FIGURE 3.46: Heights and angles of hydroxyl molecule in Bjerrum defects

3.3.2.3 3:1 H_2O:OH

The data in Table A.3 shows that as for the $2H_2O$:OH ratio the structures with Bjerrum defects are less stable than structures with dangling H-bonds, at the PBE level. From Table 3.4 it is clear that this is not changed by inclusion of van der Waals so the Bjerrum defect structures have not been repeated with optB86b. All results discussed here are for structures with dangling hydrogens.

The 3:1 overlayer structures have 6 dangling water molecules as opposed to the 4 dangling that were present in the separate 2:1 structures. The hydroxyl molecules bound slightly further away from the surface than the other ratios but there is not quite as large a difference as between the 1:1 and 2:1 overlayers. The most stable 3:1 structure has the hydroxyls bound at 2.14Å ± 0.2Å which is slightly higher than the most stable 2:1 structure that had the hydroxyl molecules bound at 2.12Å ± 0.1Å. Interestingly the most stable 3:1 overlayer structure has one water molecule dangling with the hydrogen pointing down. This molecule is donating to a flat water molecule, as shown in the white circle in Figure 3.47, and is bound at 3.11Å which is closer than most of the other dangling waters in this overlayer which are bound at ∼3.14Å, as it can be seen in Figure 3.49.

The hydroxyl bound to this dangling molecule shows the same trend as in the 2:1 structures with the hydrogen pointing much higher up and less close to parallel to the surface, with an angle of 109.6° to the surface, this is a much larger angle than any of the other hydroxyls in the 3:1 strucutres, this is also shown in Figure 3.49. From Figure 3.47 it can also be seen that all of the dangling water

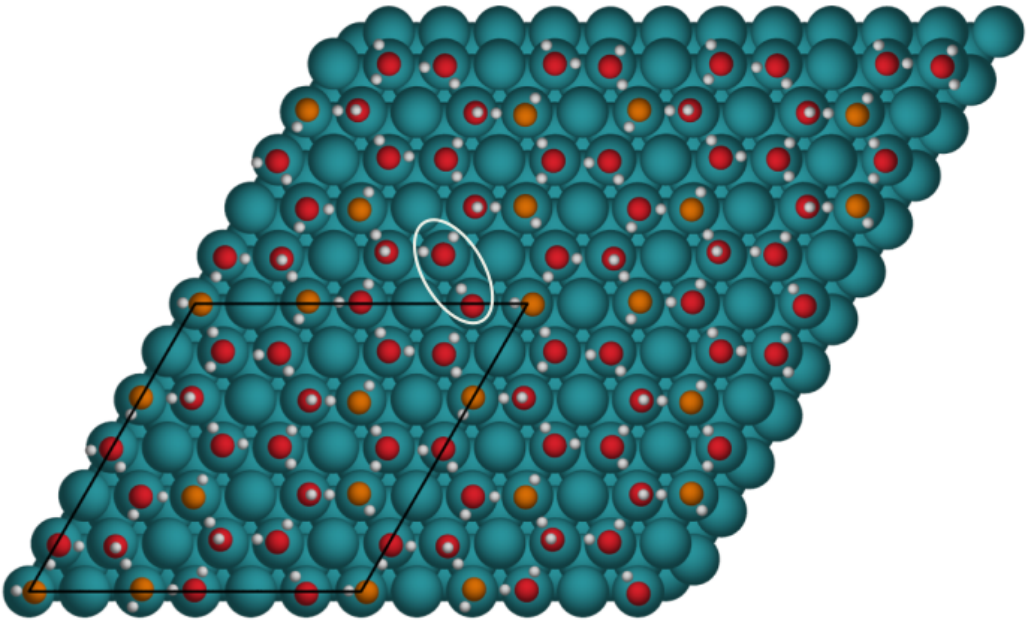

FIGURE 3.47: Most stable 3:1 structure, white circle shows H-down dangling water molecule donating to a flat water, water in red and hydroxyl in orange, top view

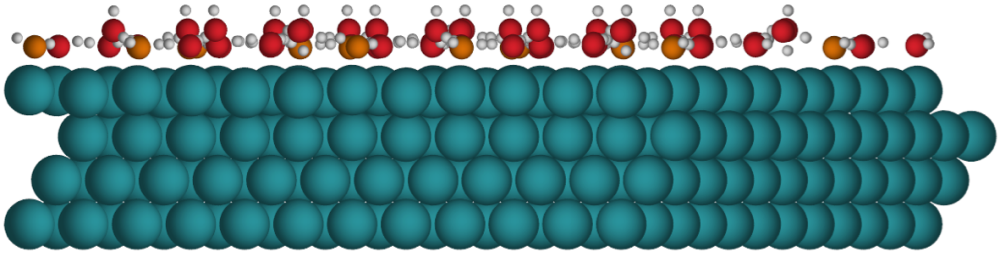

FIGURE 3.48: Most stable 3:1 structure, water in red and hydroxyl in orange, side view

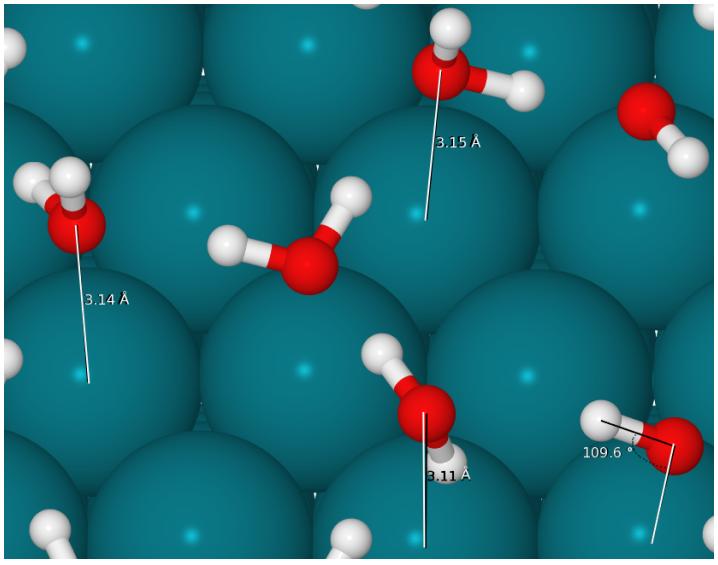

FIGURE 3.49: Heights of three of the dangling water molecules and angle of hydroxyl molecule bonding to the dangling down water molecule

molecules with hydrogen pointing up are donating to a hydroxyl molecule, this may be why this structure is so stable within the 3:1 structures, as this seems to be a preferred arrangement from previously looked at structures, for instance the most stable 2:1 structure followed this trend, shown in Figure 3.27.

TABLE 3.5: Calculated adsorption energies of different 3:1 H_2O:OH structures on Rh(111)

Figure	Type	Adsorption Energy (meV)
Figure 3.47	Five H-up with one H-down (6x6)	−766
Figure 3.50	H-up (6x6)	−765
Figure 3.53	Four H-up with two H-down (6x6)	−761
Figure 3.56	H-up (3x6)	−761
Figure 3.58	H-up (3x6)	−758

The adsorption energies for the most stable 3:1 structures are shown in Table 3.5. As can be seen the next most stable 3:1 structure has a binding energy that is only 1meV per molecule less stable than the most stable structure, it is shown in in Figure 3.50. It also has every dangling water molecule donating to a hydroxyl group. As can be seen in Figure 3.52, every dangling water molecule is bound to the surface at either 3.11Å or 3.12Å. Each of the hydroxyl molecules are donating to a flat lying water molecule and due to this all the bond angles to the surface are quite similar ∼101.8°.

The structure shown in Figure 3.53 initially had all of the dangling water molecules bound H-down and four out of six of these rotated to relax into a structure with the H-bond dangling upwards. The two water molecules dangling H-down are shown in the white circles donating to other flat lying water molecules, they are both bound slightly closer to the surface at 3.07Å and 3.1Å than the other

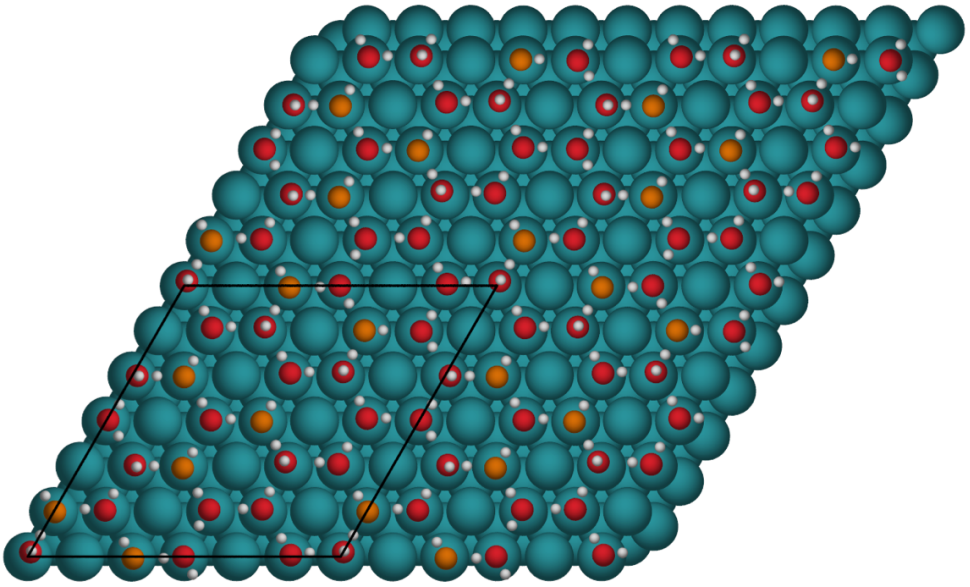

FIGURE 3.50: 3:1 structure with every dangling water molecule donating to a hydroxyl molecule, water are shown in red and hydroxyl in orange, top view

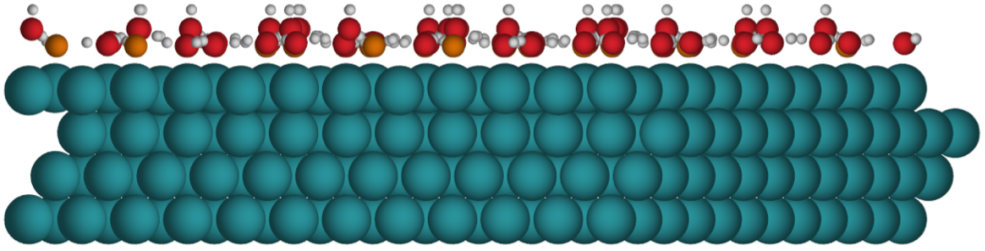

FIGURE 3.51: 3:1 structure, water in red and hydroxyl in orange, side view

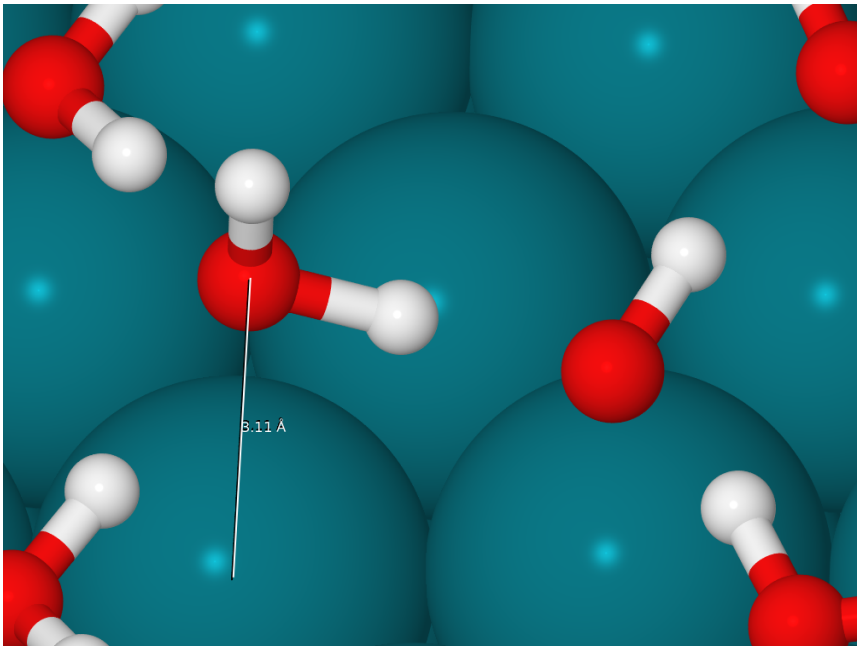

FIGURE 3.52: Every dangling water is donating to a hydroxyl as shown

dangling water molecules, as shown in Figure 3.55. The final relaxed structure is 5meV less stable than the most stable structure.

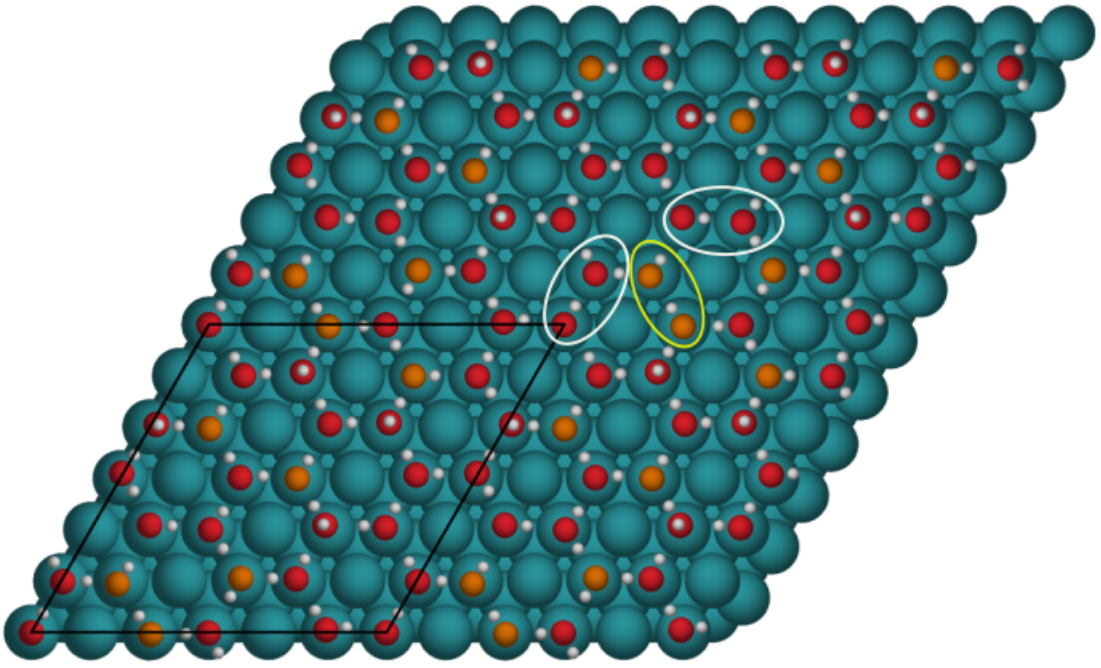

FIGURE 3.53: 3:1 structure two H-down waters shown in white circles and two hydroxyl molecule chain shown in the yellow circle, water in red and hydroxyl in orange, top view

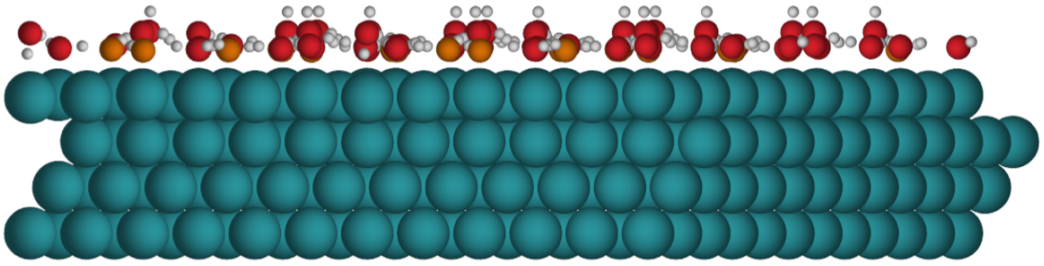

FIGURE 3.54: 3:1 structure started with H-down, water in red and hydroxyl in orange, side view

In the relaxed structure one of the hydroxyl molecules donates to another hydroxyl molecule as can be seen in the yellow circle. The other hydroxyl molecule donates to one of the dangling down water molecules. This has caused it to have a much greater angle to the surface than the hydroxyl donating to it, as can be seen in Figure 3.55. When this structure began relaxing none of the hydroxyl molecules were in a chain this is something that has occurred during optimisation,

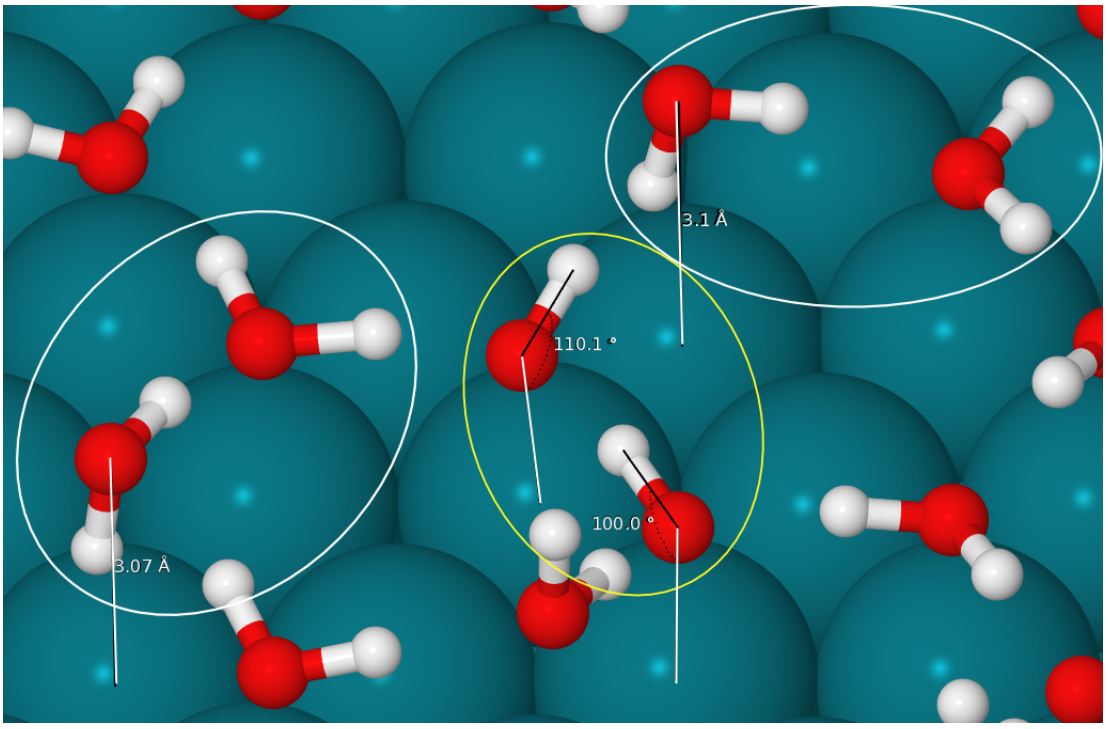

FIGURE 3.55: The two dangling down water molecules and the two hydroxyl chain

possibly due to all the reordering from the water molecules moving from H-down to H-up. It may also be what has made the overlayer less stable rather than the remaining dangling water molecules that are pointing down. Although due to the reorientation it is clear that the H-down configuration is definitely not preferred for all dangling molecules.

Two (3x6) unit cells were also considered with van der Waals interactions as they were quicker to run. The first has one hydroxyl bonding to a dangling water molecule, as can be seen in the white circle in Figure 3.56, which could be the reason it is less stable than the other structures. The O-O distance when the hydroxyl is donating to the buckled water molecule is larger, at 3.05Å, than when hydroxyl is donating to the flat lying waters, 2.87Å, probably due to the height difference between the hydroxyl and dangling water molecule.

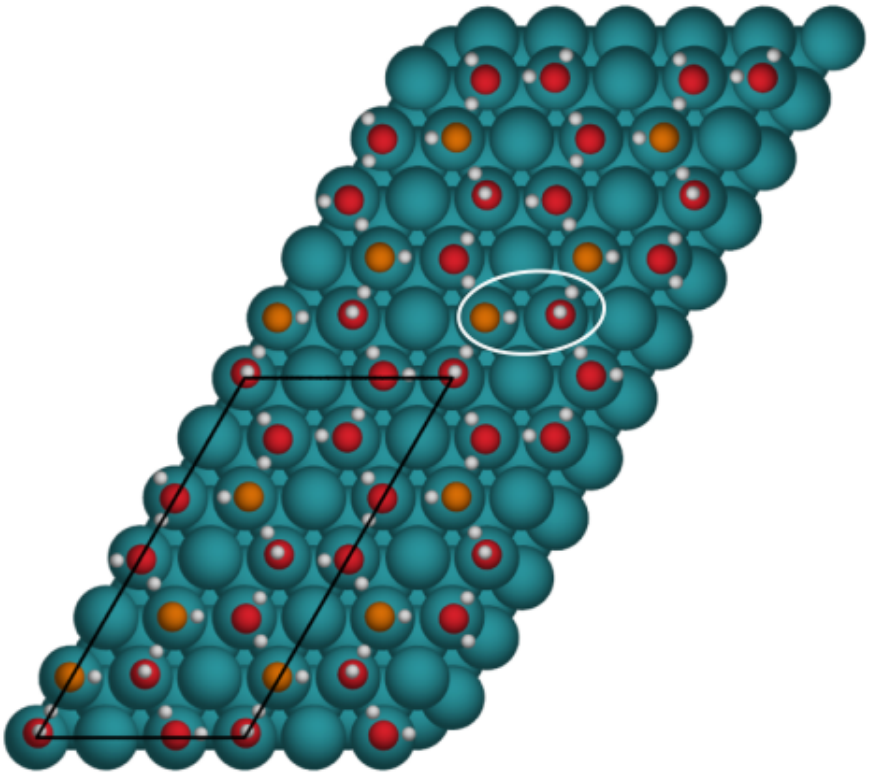

FIGURE 3.56: 3x6 with white circle showing OH donating to dangling water molecule, the other two hydroxyl molecules donate to flat lying waters, water shown in red and hydroxyl shown in orange, top view

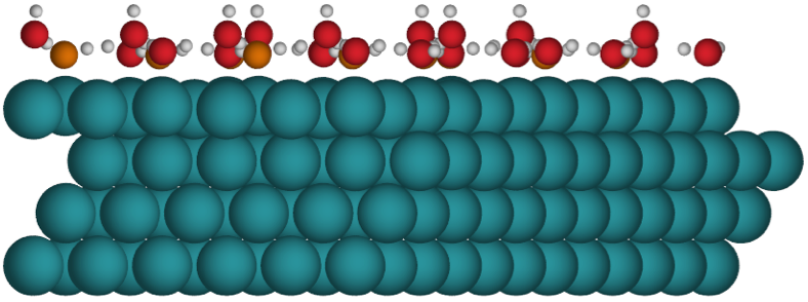

FIGURE 3.57: 3x6, water shown in red and hydroxyl shown in orange, side view

The other (3x6) structure has a dangling hydroxyl molecule; this structure has come out 8meV less stable than the most stable structure in the 3:1 overlayers. This structure is shown in Figure 3.58, with the dangling hydroxyl highlighted by the yellow circle, the remaining two dangling water molecules are bound to the other two hydroxyl molecules that are not pointing away from the surface.

Although the dangling hydroxyl is bound significantly further away than any

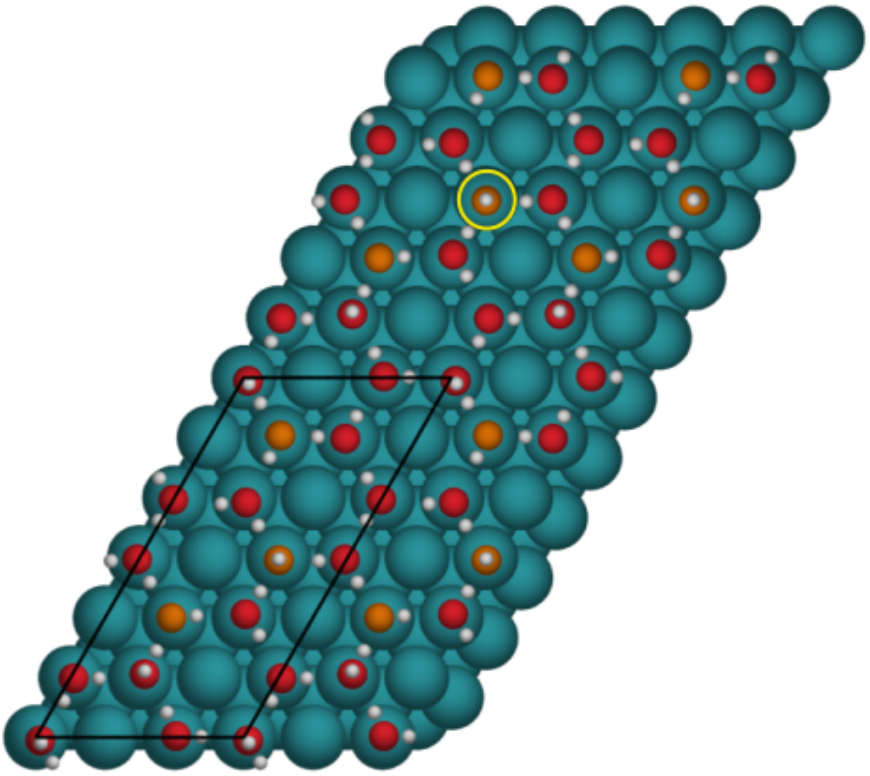

FIGURE 3.58: Only structure ran with van der Waals with dangling OH highlighted by the yellow circle, water shown in red and hydroxyl shown in orange, top view

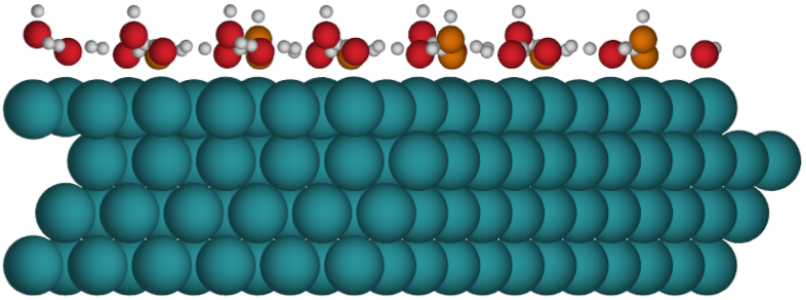

FIGURE 3.59: The only structure completed with van der Waals with dangling OH, water shown in red and hydroxyl shown in orange, side view

other hydroxyl at 2.93Å, the other hydroxyls are bound at 2.13Å and 2.14Å in this overlayer, it is still bound much closer than the dangling water molecules, which bind at 3.12Å and 3.14Å, as shown in Figure 3.60.

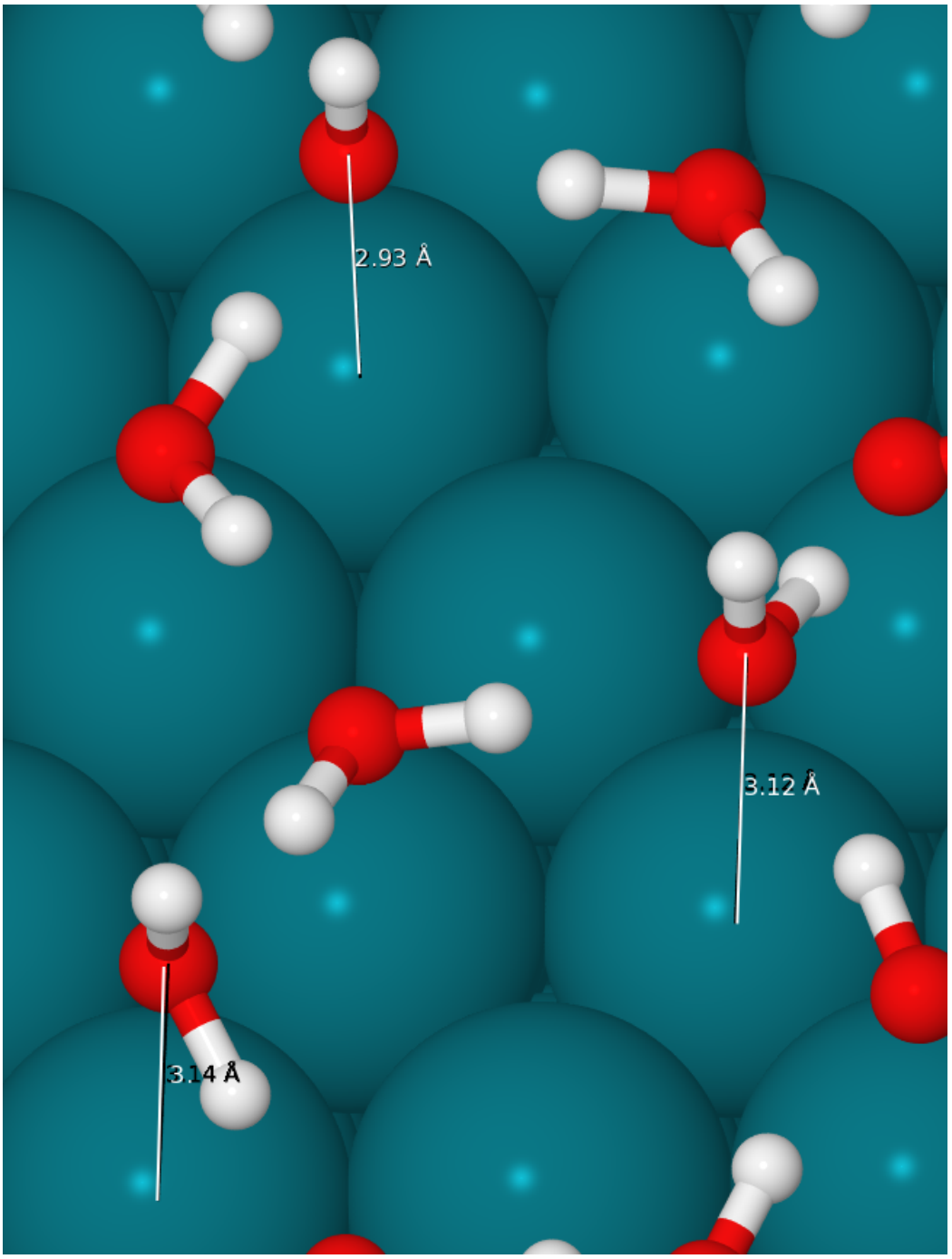

FIGURE 3.60: Heights of the dangling hydroxyl, 2.93Å and the dangling waters, 3.12Å and 3.14Å, are shown

3.3.2.4 5:1 H_2O:OH

A 5:1 structure was created, resembling the set up for the ice-like bilayer as can be seen in Figure 3.61, however 4 of the dangling H-up molecules have been replaced with hydroxyl molecules. This overlayer structure with the larger quantity of water molecules sees itself binding on average further away from the surface. This balance between the hydrogen bonding network and the bonding to the surface is clearly not preferred as this is the least stable ratio that has been tried. It also is the only network with no dangling water molecules binding to hydroxyl molecules and no flat lying water bound to another flat lying water.

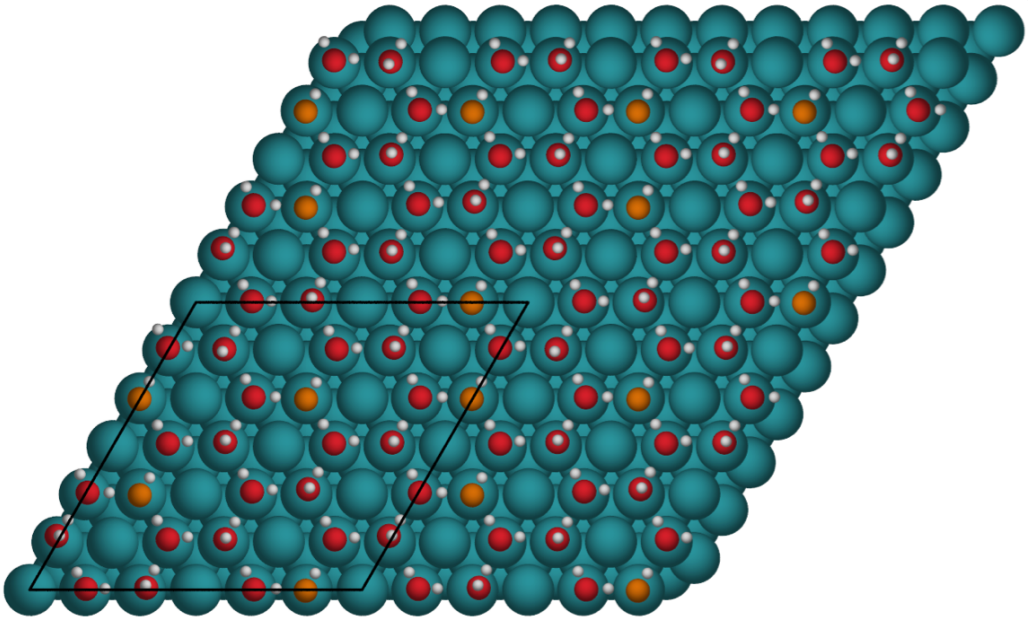

FIGURE 3.61: 5:1 structure resembling the ice-like bilayer with four hydroxyl molecules, water shown in red and hydroxyl shown in orange, top view

The main reason for running the 5:1 structures was to try and understand at what ratio of H_2O:OH the overlayers would prefer the dangling water molecules to be H-down. As this is preferred for the pure water overlayers as will be discussed in 3.3.3. An overlayer was created with the same structure shown in Figure 3.61

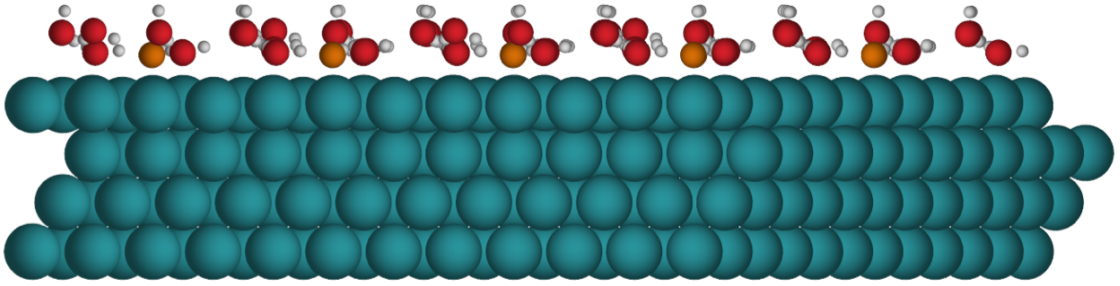

FIGURE 3.62: 5:1 structure resembling the ice-like bilayer with four hydroxyl molecules, water shown in red and hydroxyl shown in orange, side view

except with the dangling water molecules pointing H-down instead of H-up, as shown in Figure 3.63. As can be seen in Table 3.6 this structure has come out the most stable of all the 5:1 structures by 7meV per molecule compared to the H-up variation.

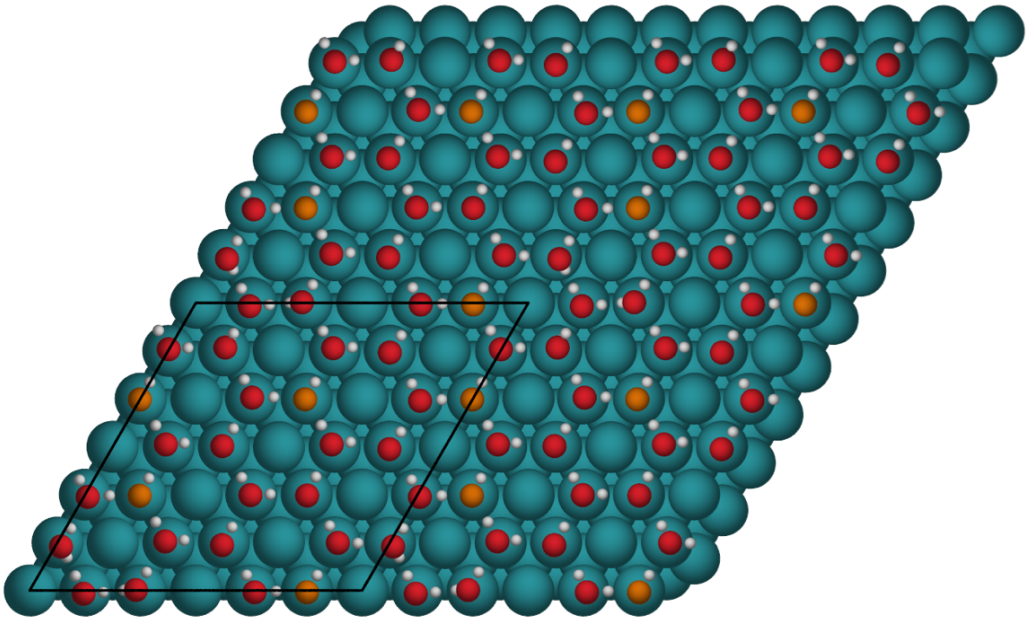

FIGURE 3.63: 5:1 structure resembling the ice-like bilayer with dangling water molecules in H-down position, with water shown in red and hydroxyl shown in orange, top view

This structure includes one flat water that is 4.4Å away from the surface, this is 2.13Å higher than the average flat lying water molecule that is bonded at 2.27Å. Figure 3.65 shows this water molecules highlighted in the yellow circle, the other 2 flat lyting water molecules are bonded and 2.25Å and 2.29Å as shown. As

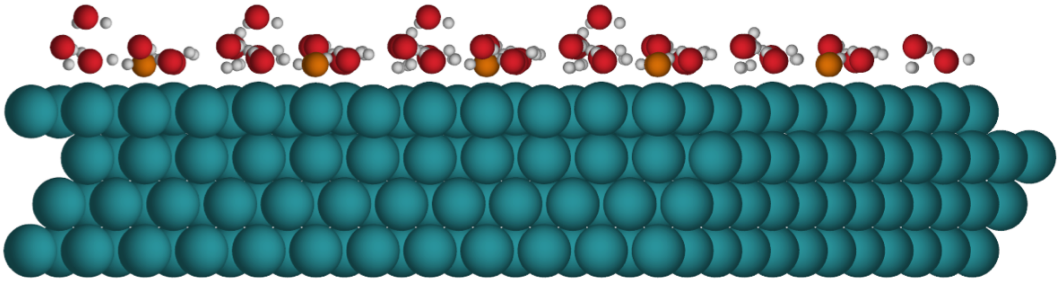

FIGURE 3.64: 5:1 structure resembling the ice-like bilayer with dangling water molecules in H-down position, with water shown in red and hydroxyl shown in orange, side view

TABLE 3.6: Calculated adsorption energies of different 5:1 H_2O:OH structures on Rh(111)

Figure	Type	Adsorption Energy (meV)
Figure 3.61	H-up (6x6)	−745
Figure 3.63	H-down (6x6)	−752
Figure 3.66	Bjerrum defect, H-up (6x6)	−741

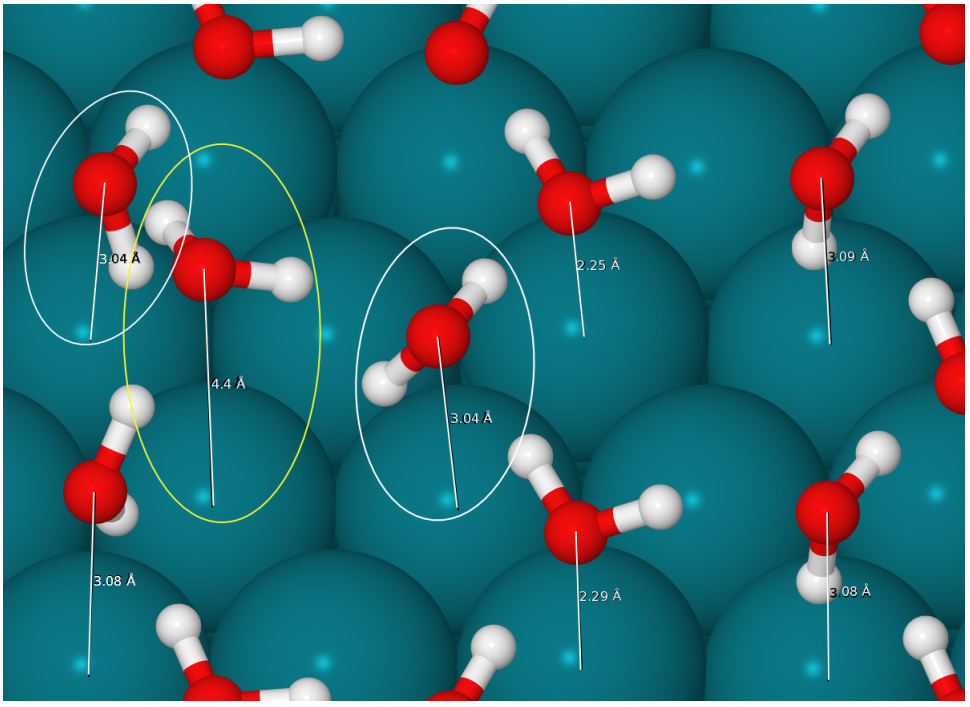

FIGURE 3.65: Yellow circle shows the water that is bonded 4.4Å from the surface, white cirles show the two dangling water molecules that are closer to the surface due to this height difference. Heights of other flat water and dangling waters are shown at the heights more in keeping with the trend across this structure.

can also be seen by the dangling water molecuels highted in the white circles this height difference has caused these molecules to bond closer to the surface at 3.04Å

compared to the average of 3.09Å of all other dangling water molecules. Being closer to the surface has also caused these to rotate slightly away from the surface so they are not as straight on as the other dangling water molecules.

A Bjerrum defect in the 5:1 ratio, Figure 3.66, has the hydroxyl molecules all bonding at about the same distance away from the surface as for the defect structures at 2:1 ratio. This overlayer structure came out 4meV per molecule less stable than Figure 3.61, as shown in Table 3.6, so it seems the Bjerrum defects are once again not more stable.

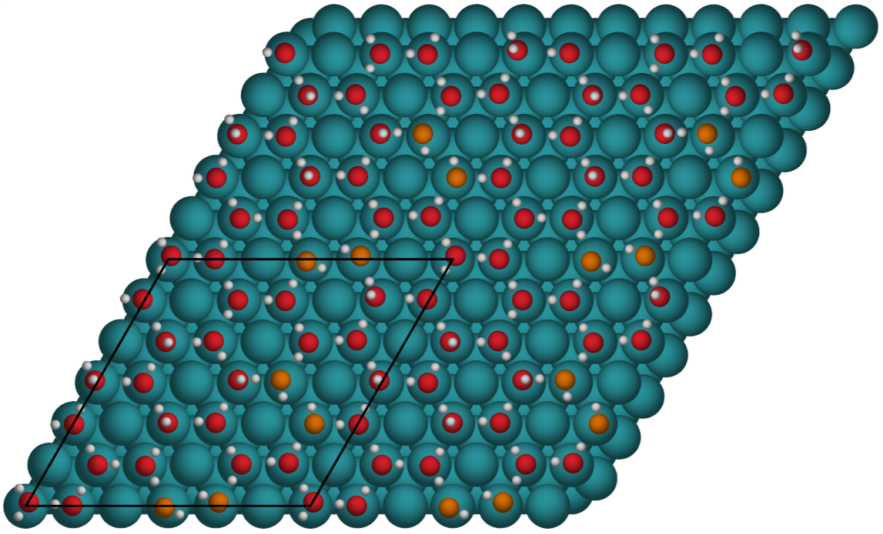

FIGURE 3.66: 5:1 Bjerrum defect structure, with water shown in red and hydroxyl shown in orange, top view

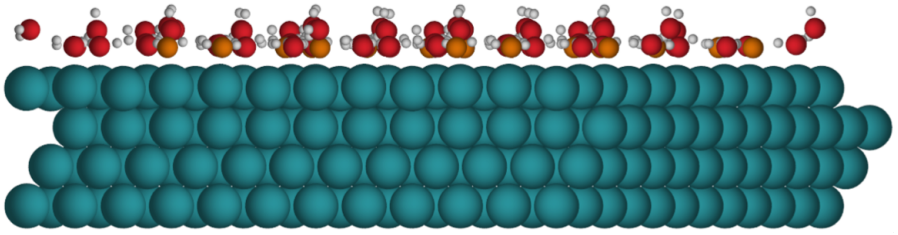

FIGURE 3.67: 5:1 Bjerrum defect structure, with water shown in red and hydroxyl shown in orange, side view

3.3.3 Pure Water Overlayers

Due to the oxygen precoverage of the surface used in these experiments it is unlikely that pure water overlayers would be found on the surface. Also at low coverage dissociation to form two OH's has been found to be favoured making the pure water overlayers even less likely. Howevere six pure water overlayers were still calculated for comparison and to determine whether a bilayer would form on Rh(111). To calculate the adsorption energies for the pure overlayers either equation 3.3 or 3.4 were used.

The adsorption energies for the pure water overlayers can be seen in Table 3.7. The most stable pure water structure is shown in Figure 3.68, it has been created in a different unit cell size to get continuous chains of dangling H-down water molecules and chains of flat water lying molecules. The height of every flat water molecule is at 2.32Å and the height of every buckled water is 3.23Å. These are very similar heights to the chains structure created in the (3 x 3) unit cell shown in Figure 3.70, it has three H-down dangling water molecules donating in a chain, shown by the white circle, and three flat water molecules donating in a chain, shown by the yellow circle. These had a height of ∼2.33Å for the flat water molecules and ∼3.18Å for the buckled H-down molecules. However the second chain structure showed more variation in these heights.

These chains do not carry on indefinitely they are continuous chains of three, with each of the dangling hydrogens pointing towards the surface. In the mixed

TABLE 3.7: Calculated adsorption energies of different pure H_2O structures on Rh(111)

Figure	Type	Adsorption Energy (meV)
Figure 3.68	H-down $(2\sqrt{3} \times \sqrt{3})$R30°	−795
Figure 3.70	H-down (3x3)	−769
Figure 3.72	H-down (3x3)	−756
Figure 3.75	H up and down (3x3)	−735
Figure 3.80	H-up (3x3)	−715
Figure 3.78	H-down (3x3)	−707
Figure 3.82	H-down (3x3)	−675

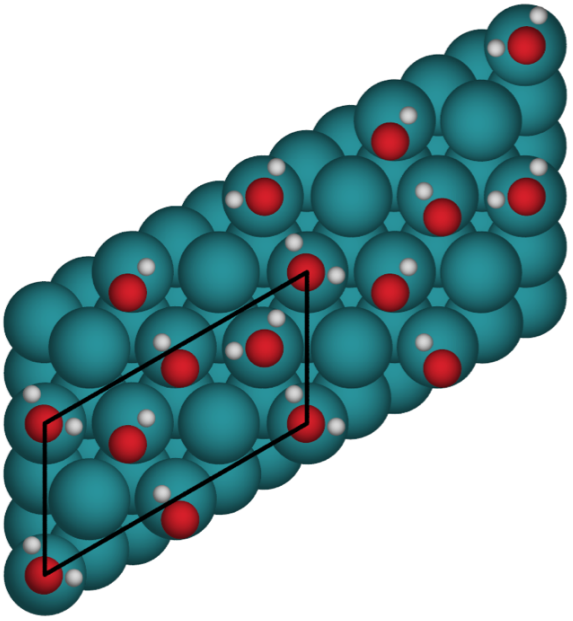

FIGURE 3.68: Pure water chains of flat lying water molecules and chains of buckled water molecules, top view

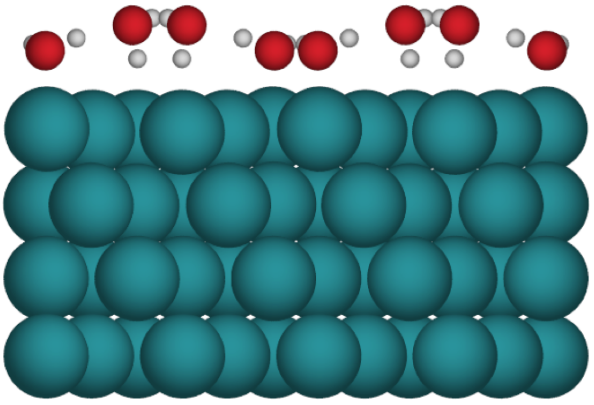

FIGURE 3.69: Pure water chainsof flat lying water molecules and chains of buckled water molecules, side view

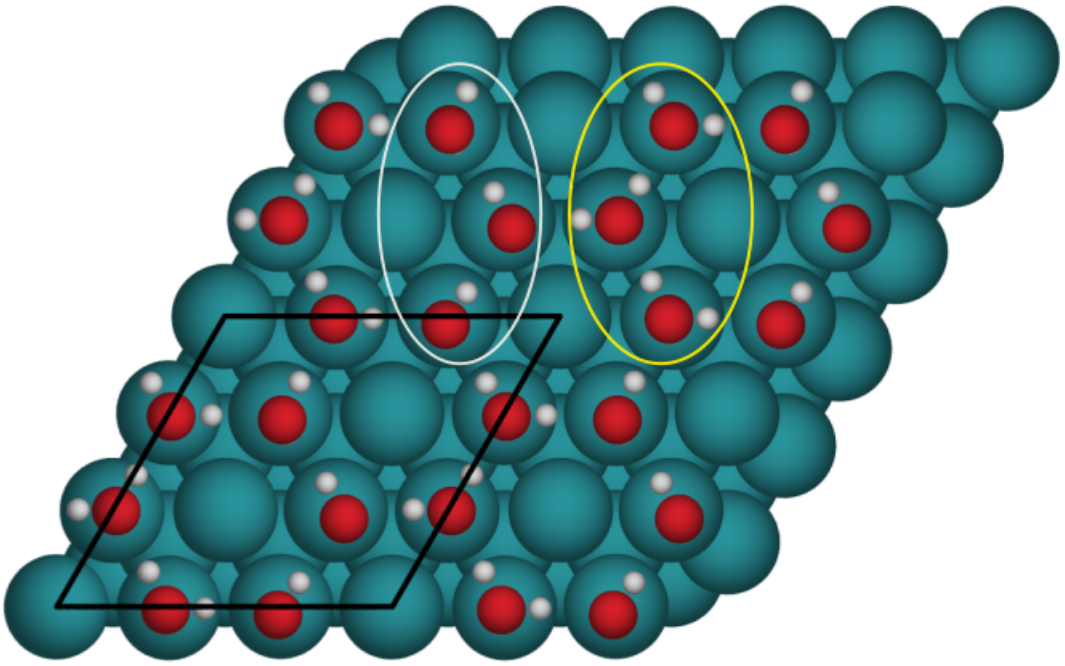

FIGURE 3.70: Pure water chains, 3 flat followed by 3 dangling down water molecules, top view

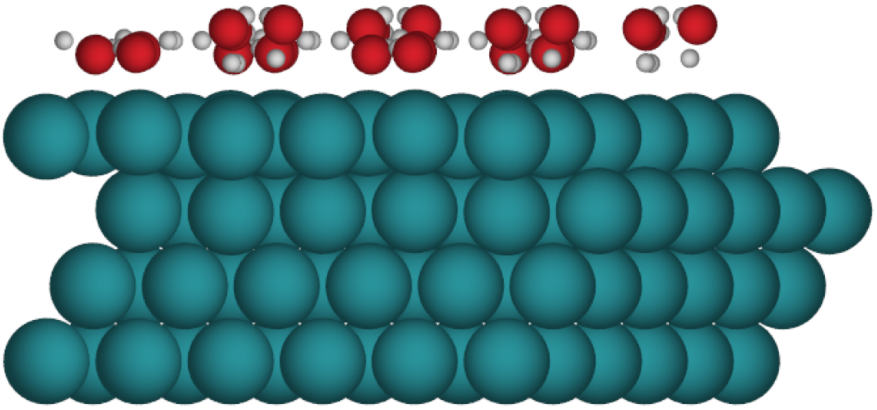

FIGURE 3.71: Pure water chains, 3 flat followed by 3 dangling down water molecules, side view

H_2O/OH structures the 5:1 ratio found that the H-down configuration became more stable, as expected this is also the case with the pure water structures.

The next most stable structure after the chains structure has alternating dangling water molecules and flat lying molecules with the dangling hydrogens pointing towards the surface again it can be seen in Figure 3.72 and 3.73.

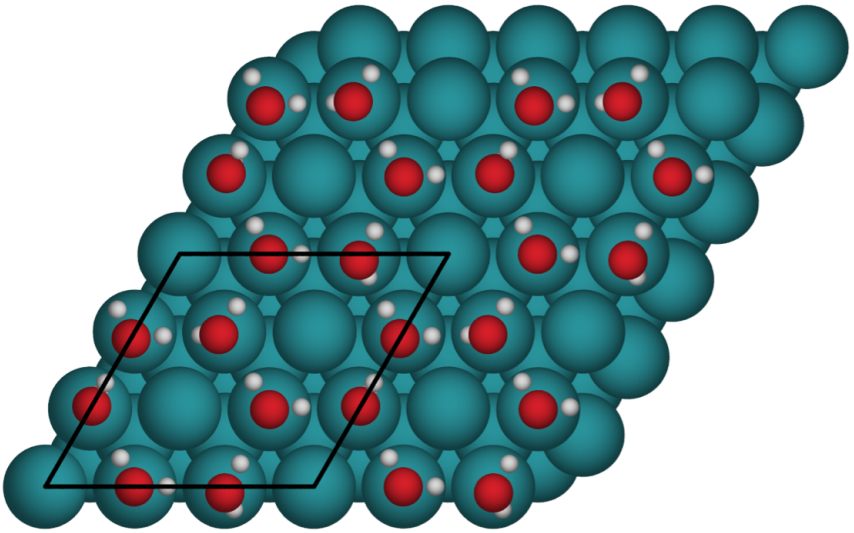

FIGURE 3.72: Pure water H-down dangling water molecules alternating with flat water top view

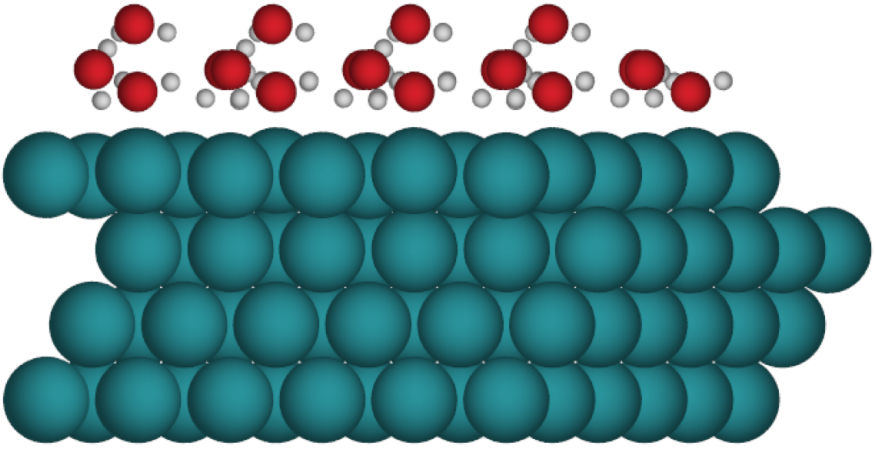

FIGURE 3.73: Pure water H-down dangling water molecules alternating with flat water side view

This calculation was set up with the molecules arranged similarly to an ice-like bilayer, however one of the flat lying water molecules was positioned to be bonding significantly further from the surface than any of the other water molecules. This calculation was performed to see if one of the molecules being further from the surface reduced the strain of the hexagonal network in such a small (3x3) unit cell and allowed for a more stable structure. After optimisation it ended up bonding 2.08Å higher than any of the other flat water molecules in the structure, as shown in Figure 3.74.

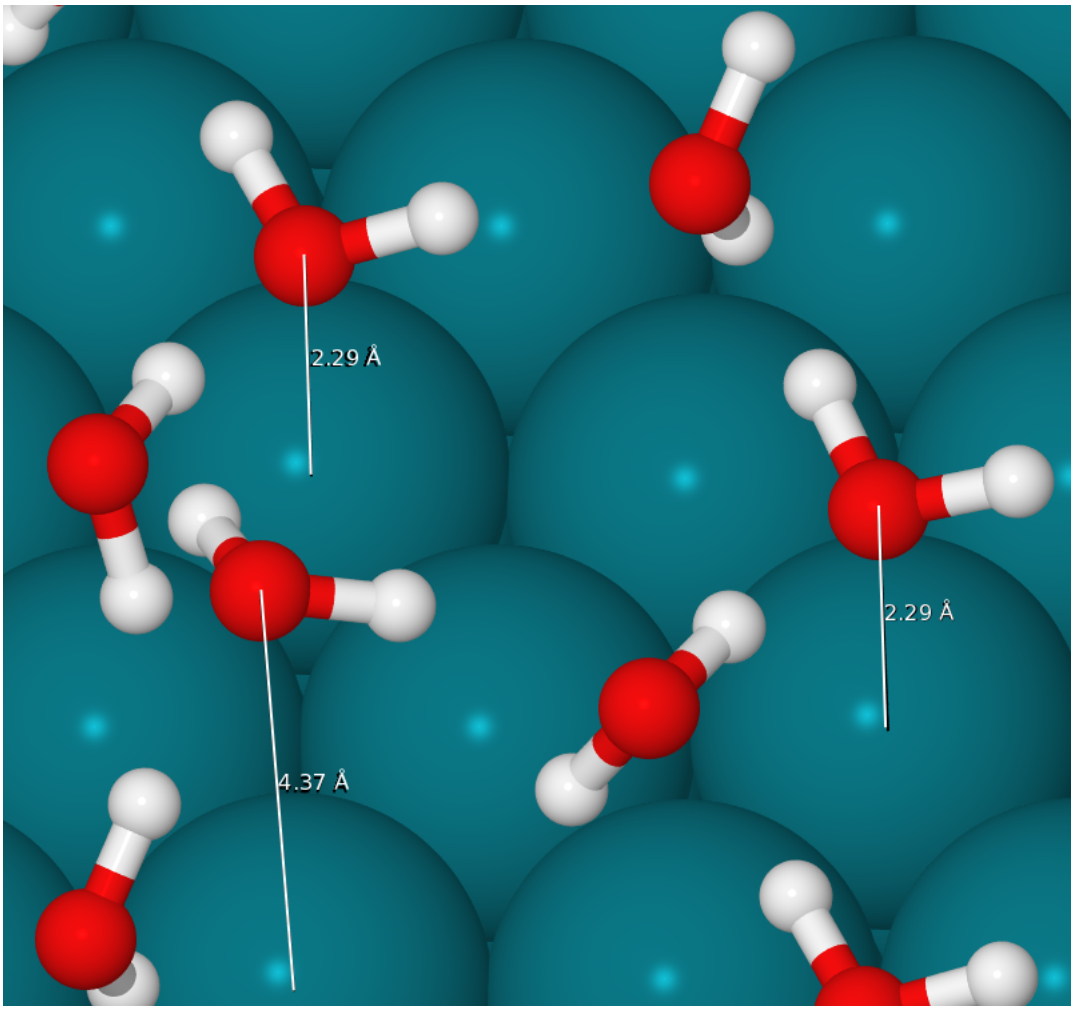

FIGURE 3.74: Height of water that is furthest away from the surface, 4.37Å, in comparison to the other two flat water molecules, 2.29Å.

Two overlayers were calculated with the classic ice-like bilayer structure, alternating dangling molecules with flat lying molecules close to the surface, one with the dangling hydrogen atoms in a H-up orientation and the other in a H-down orientation. The structure with the dangling hydrogens pointing up, relaxed to have one of the dangling hydrogens pointing down in a chain with a dangling water donating to it, as can be seen circled in Figure 3.75. Although this structure does contain a chain of two dangling water molecules the fact that only one is pointing down appears to make this structure less stable than the short chains structure, shown in Figure 3.70.

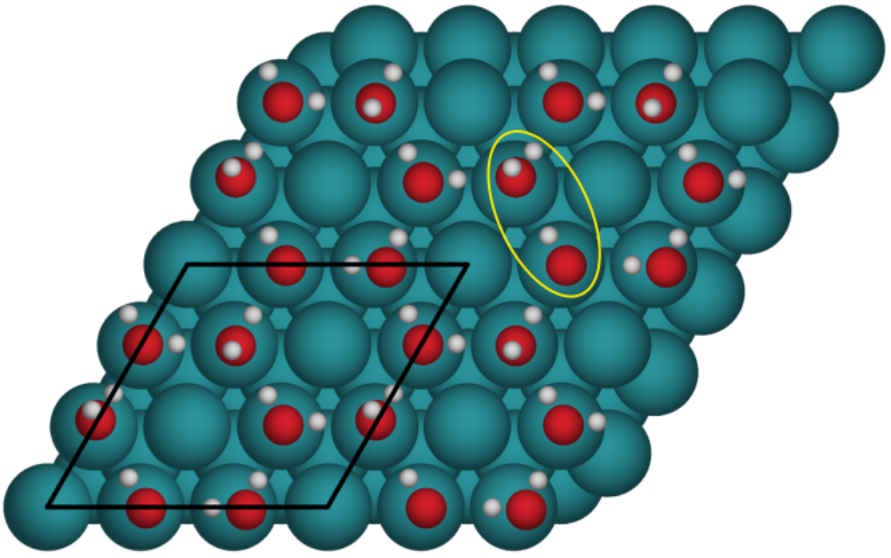

FIGURE 3.75: One H-down and two H-up dangling water molecules, chain dangling water is circled top view

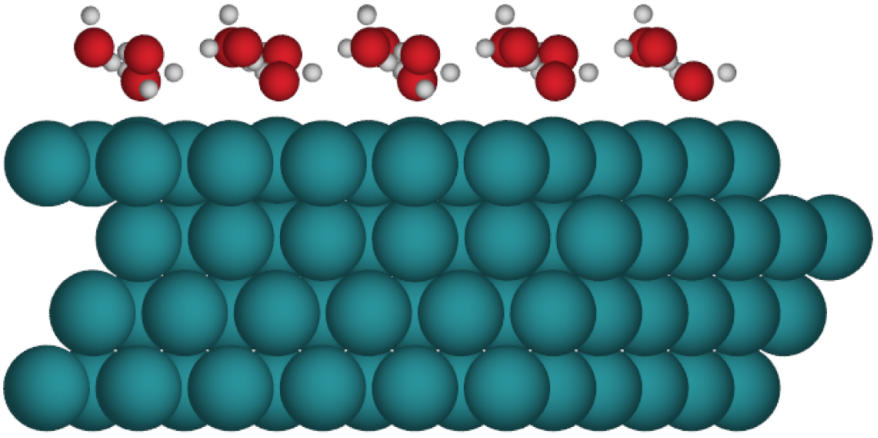

FIGURE 3.76: One H-down and two H-up dangling water molecules side view

As was seen in the previous structure 3.72 one of the flat water molecules is again bonding further from the surface, at 3.41Å, after the reordering of the molecules, compared to the other two flat water molecules that are bonding at 2.29Å and 2.31Å, shown in Figure 3.77. This may be what has caused this structure to be more stable than the H-down structure shown in Figure 3.78.

The other classic ice-like bilayer structure studied with H-down, shown in Figure 3.78 is 28meVper molecule less stable than the H-up structure; this is

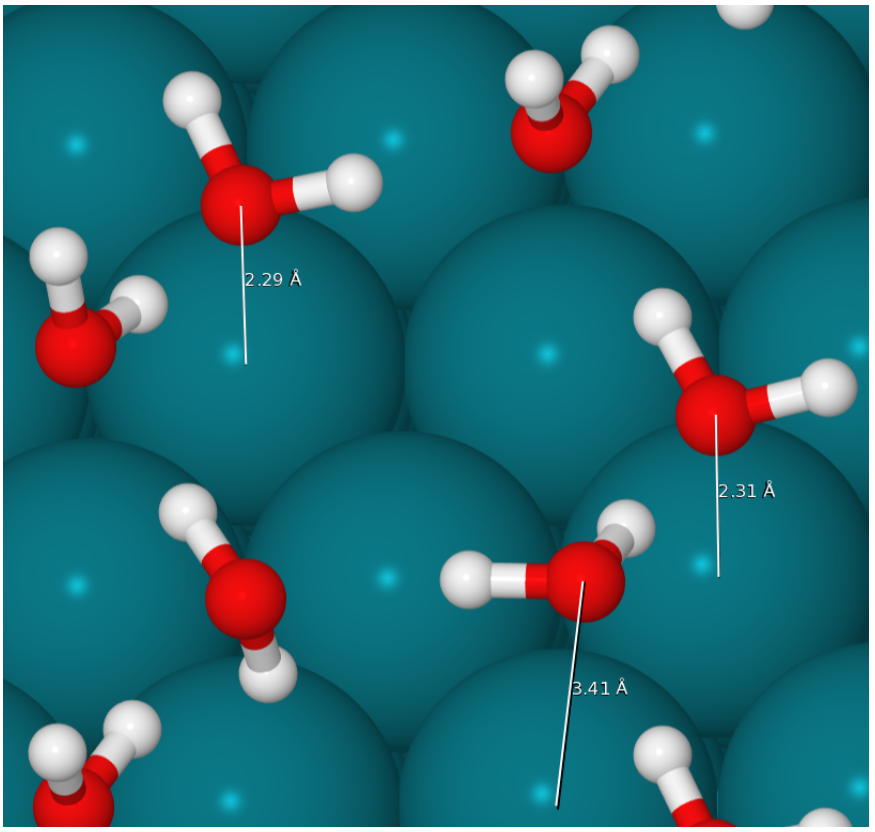

FIGURE 3.77: Height of water that is furthest away from the surface, 3.41Å, in comparison to the other two flat water molecules, 2.29Å and 2.31Å.

possibly due to the lack of chains of dangling water molecules present or that there are no water molecules further from the surface as seen in Figure 3.72. The optimised positions are close to the initial ones, i.e. it has remained a strictly alternating bilayer.

A final two structures were constructed with the dangling water molecules in exactly the same position as each other however on one those molecules were dangling H-up and on the other those molecules were dangling H-down and the both relaxed keeping these positions. Interestingly the structure with the H-up dangling water molecules, shown in Figure 3.80, came out much more stable than the structure with the H-down dangling water molecules by 40meV, shown in Figure 3.82, this structure mimics the proton order shown in the structure shown

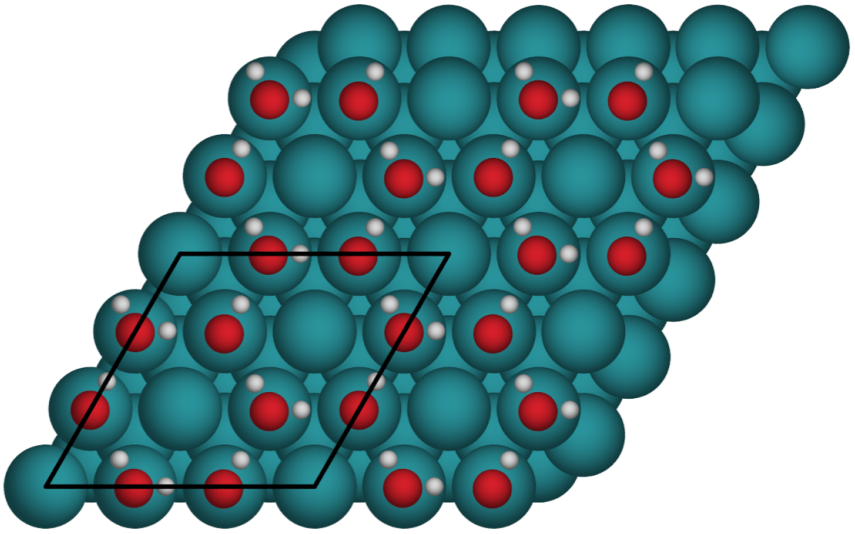

FIGURE 3.78: H-down ice-like bilayer, proton ordered, top view

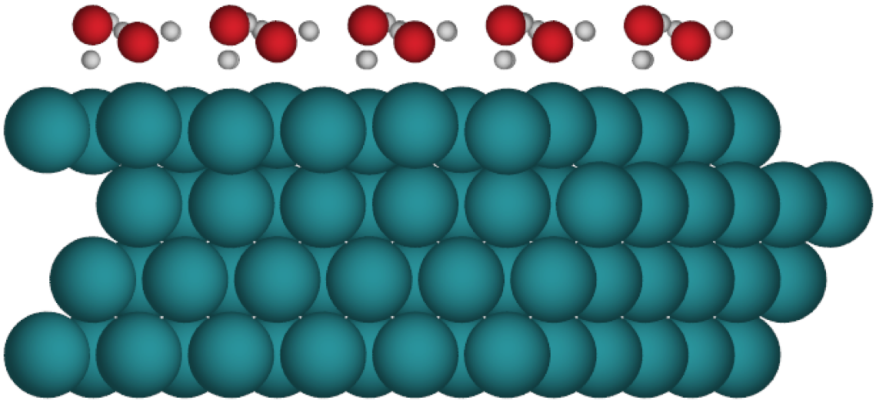

FIGURE 3.79: H-down ice-like bilayer side view

in Figure 3.78.

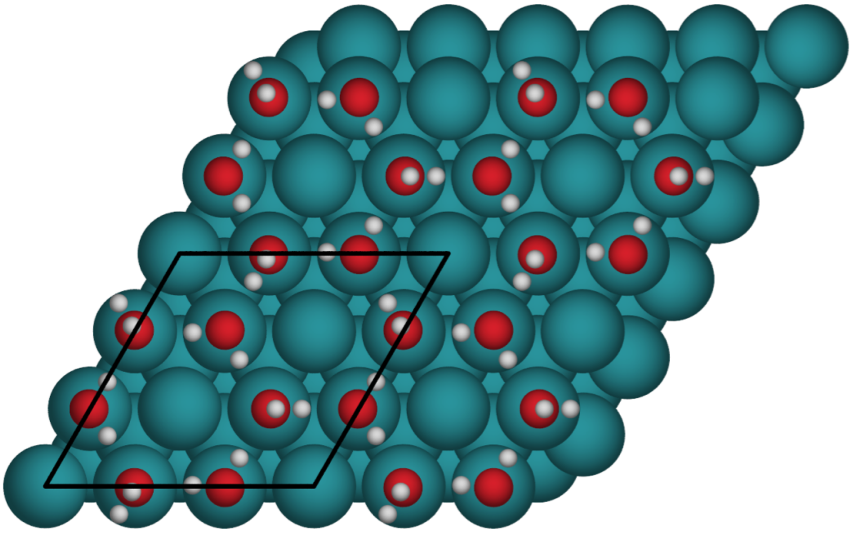

FIGURE 3.80: Structure with dangling water molecules pointing up, top view

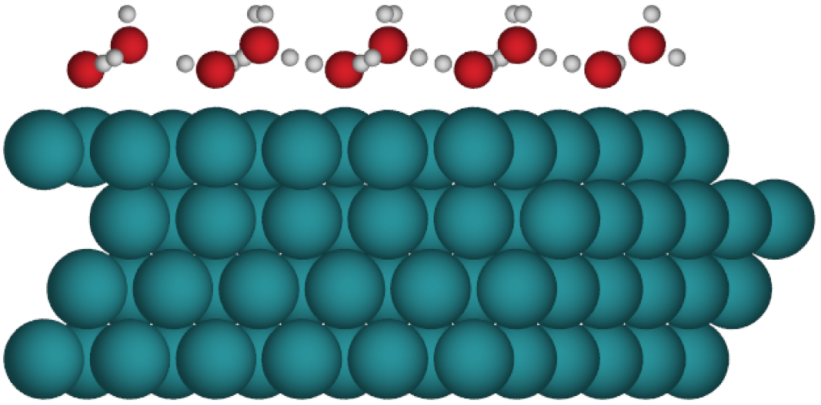

FIGURE 3.81: Structure with dangling water molecules pointing up, side view

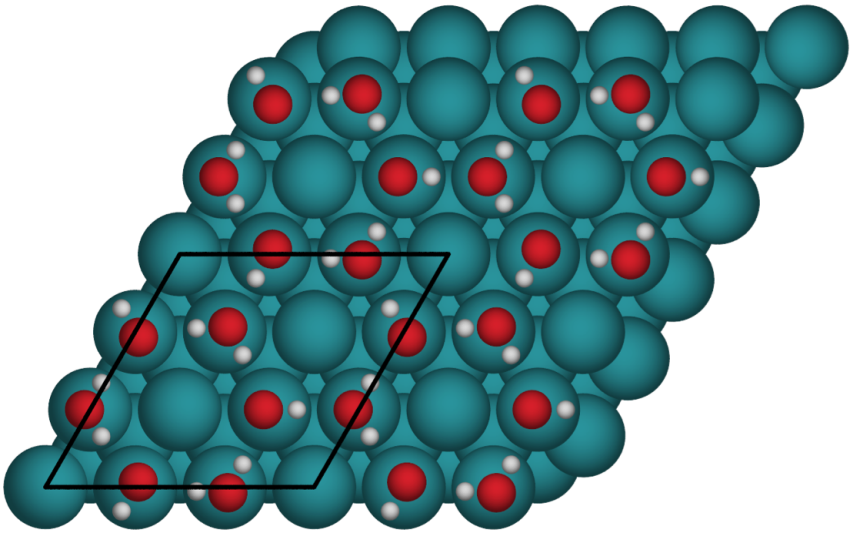

FIGURE 3.82: Structure with dangling water molecules pointing down, top view

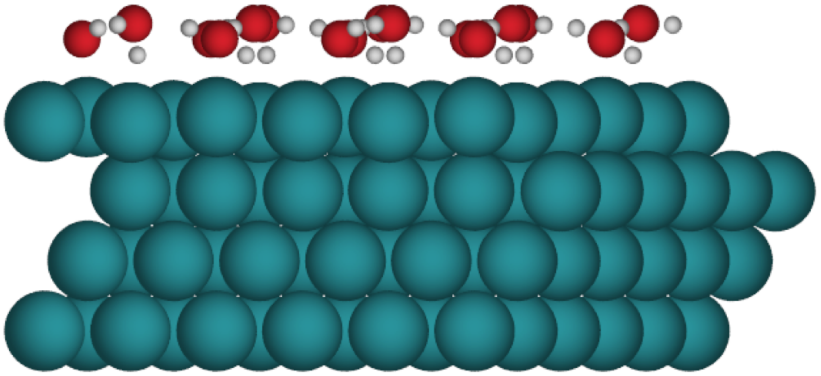

FIGURE 3.83: Structure with dangling water molecules pointing down, side view

3.3.4 Convex hull calculations

For each of the ratios the most stable structures energy has been found, this is then used to compare if it is more stable than combinations of the other ratios. If the energy of the single phase structure is lower, it will likely form, whereas if the energy of multiple competing compositions is lower then it is likely that the surface will segregate into patches of these competing phases. For instance, in Table 3.8, the adsorption energy for the 1:1 ratio alone, shown by the red dot in Figure 3.84, is more stable than any combination of 2:1, 3:1 and pure water (in the form of the most stable lines structure Figure 3.68) structures combined with free oxygen.

TABLE 3.8: Convex hull results for 1:1 ratio

1:1 ratio with 36 H's and 24 O's		Adsorption Energy (eV)
1:1		-956.606
2:1 + free O	9/10 in 2:1 + 1/10 of O/Rh	-954.866
3:1 + free O	6/7 in 3:1 + 1/7 of O/Rh	-953.840
lines + free O	3/4 in lines + O	-951.496

For the 2:1 ratio, shown in Table 3.9, the full 2:1 structure comes out the most stable once again rather than any combination to make up the correct number of H's and O's. The red dot in Figure 3.85 shows the most stable.

TABLE 3.9: Convex hull results for 2:1 ratio

2:1 ratio with 40 H's and 24 O's		Adsorption Energy (eV)
2:1		-970.886
1:1 + lines	2/3 of 1:1 + 1/3 of lines	-970.548
1:1 + 3:1	1/3 of 1:1 + 2/3 of 3:1	-970.668
3:1 + free O	20/21 of 3:1 + 1/21 of O	-969.746
lines + free O	5/6 of lines +1/6 of O	-967.142

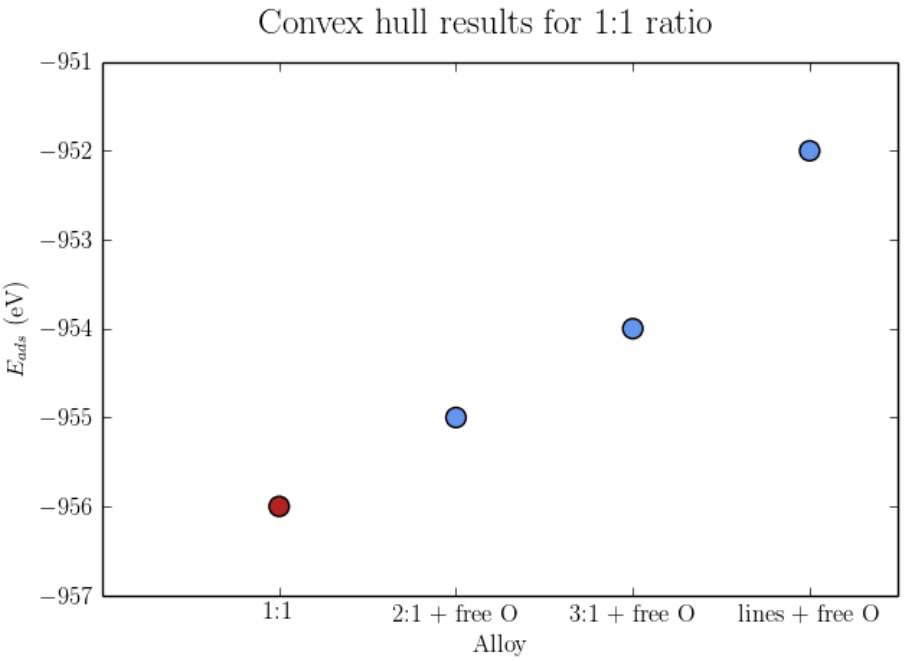

FIGURE 3.84: Convex hull results for 1:1 ratio

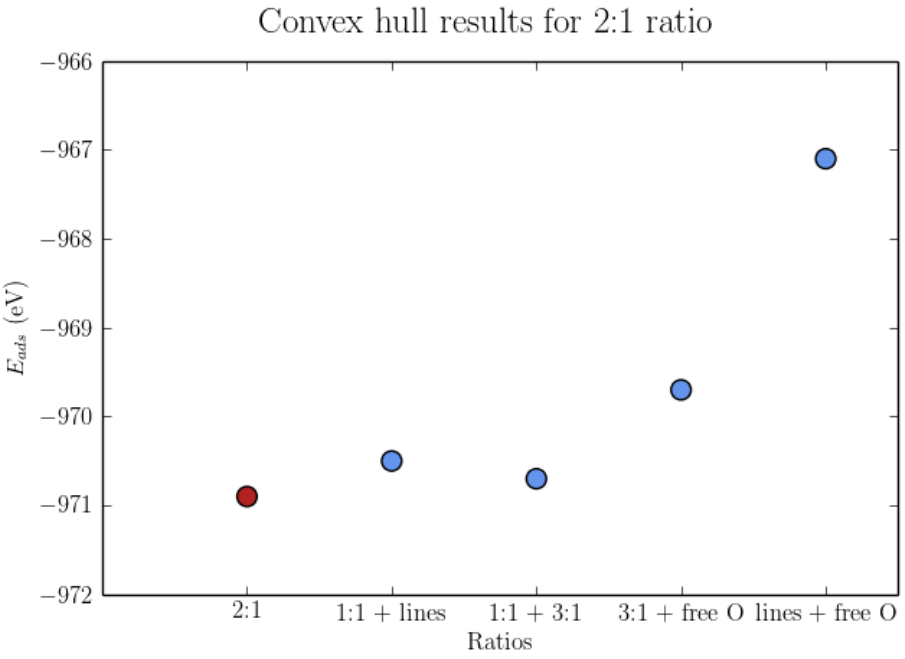

FIGURE 3.85: Convex hull results for 2:1 ratio

Table 3.10 shows that the 2:1 ratio combined with the lines structure is more stable than the 3:1 structure alone, this result shows that the 3:1 structures are unlikely to form, although the energy difference is only 70meV. The grey dot in Figure 3.86 shows the single pahse structure everything is being compared to,

while the red dot shows the most stable adsorption energy.

TABLE 3.10: Convex hull results for 3:1 ratio

3:1 ratio with 42 H's and 24 O's		Adsorption Energy (eV)
3:1		-977.699
1:1 + lines	1/2 of 1:1 + 1/2 of lines	-977.520
2:1 + lines	3/4 of 2:1 + 1/4 of lines	-977.773
lines + free O	7/8 of lines +1/8 of O	-974.964

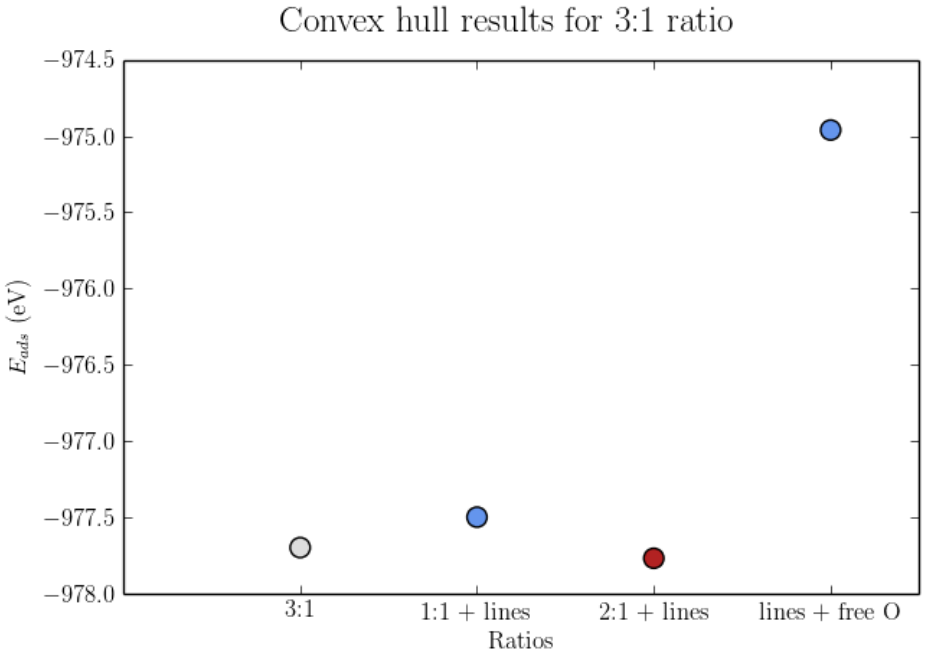

FIGURE 3.86: Convex hull results for 3:1 ratio

3.4 Summary

The aim of this work was to determine the composition and probable structures of mixed H_2O:OH overlayers on the Rh(111) surface. An initial objective was to test the suggestion that, as found on the Cu(110) surface, the structures are stabliised by Bjerrum defects where dangling OH bonds point towards each other on the surface rather than participating in a hydrogen bonding network or pointing towards or away from the surface.[8] The initial set of calculations performed with the PBE functional showed clearly that on the Rh(111) surface Bjerrum defects do not produce the most stable structures and instead the bonding within the overlayer obeys the ice rules.

Although the adsorption energies were calculated with the same method and DFT functional(the second set of calculations was repeated with van der Waals corrected DFT, specifically the optB86b functional), different H_2O:OH ratios are composed of different numbers of H and O atoms, therefore the energies are not directly comparable across different compositions. To account for this, we have to compare the energy of each composition with the energies obtained for combinations of the competing compositions that would yield the same numbers of each atom type. For instance, the most stable 1:1 structure has an adsorption energy of -956 meV (per adsorbed molecule) and is composed of 36 H atoms and 24 O atoms. This composition can also be achieved with part (9/10) of the surface covered by a 2:1 structure (having 40 H's and 24 O's) and the remainder (1/10) with only adsorbed O on the surface. We therefore compare the energy of the 1:1 ratio with 0.9 $E_{2:1}$ + 0.1 E_O, where E_O is the energy of a surface covered with O

atoms only. If the energy of the single phase structure is lower, it will likely form, whereas if the energy of multiple competing compositions is lower then it is likely that the surface will segregate into patches of these competing phases. The set of the lowest energy combinations found for all possible compositions is said to form the "convex hull".

The convex hull calculations show that both the 1:1 and 2:1 ratios are stable in comparison to competing phases. However the 3:1 structures are found to be less stable relative to a combination of 3/4 of the 2:1 ratio with 1/4 of the structure for a pure water overlayer, indicating that 3:1 should be ruled out as a likely composition ratio.

Chapter 4

Surface Alloys with Sn

4.1 Introduction

4.1.1 Surface alloys

Surface structure and composition are known to impact properties of metals and alloys. Heterogeneous catalysts are one of the main areas of study for alloy surfaces.[76, 77] Platinum or palladium catalysts are used in industry on a regular basis, they can be less selective or have a shorter lifetime than a bimetallic catalyst.[78–80] A second metal type can be introduced that changes the electronic structure of the surfaces and results in a surface with different characteristics, including increased selectivity and resistance to poisoning.[81, 82] It is known that adsorption can modify the structure of surfaces and this can result in substitution of atoms in the outer most layer creating surface alloys.[83]

Sn surface alloy phases are common and include the formation of a $(\sqrt{3} \times \sqrt{3})$R30° phase by substitution of 1/3 surface atoms on an fcc(111) surface, it is this surface alloy type that is studied here.[84, 85] Atoms displaced from the surface terraces migrate to steps. Many studies have been done to confirm that this substitution only occurs in the top layer.[84–87] Strain due to differences in size between the Sn and M atoms can result in surface rumpling within the alloy overlayer.[87]

This chapter looks at different Sn surface alloys including AgSn, PdSn, PtSn and RhSn. These structures were studied as experimental and theory agree for PtSn and PdSn structures but not for other metals such as Cu. The AgSn alloy surface studied here has not been seen experimentally and is modelled here to study the trends seen for these alloy surfaces. The purpose of this chapter is to assess the adsorption site preference of a single water and determine if it is intact or dissociated.

4.1.2 Adsorption on surface alloys

Hydrogen adsorption has been studied before on three out of four of the surface alloys looked at here, as these type of bimetallic catalysts are often used in reactions such as hydrogenation.[78, 88, 89] A study of PtSn found hydrogen moving away from the Sn in the surface on most occasions except for when the hydrogen is present on top on the Sn atom. Also other studies have found a decreased binding energy for hydrogen when Sn is present and in the presence of Sn, hydrogen

has been known to have increased barriers to diffusion along the surfaces of the alloys.[88, 89]

The bimetallic alloys have also be seen to preferentially increase the oxidation of CO, this is important for fuel cells as it removes CO that would otherwise block reactions.[90] For PtSn CO is found to bind preferentially to the Pt atoms while the hydroxyl that the CO reacts with binds preferentially to the Sn atoms in the surface.[91]

Understanding the wetting behaviour of metal surfaces is important for many reasons as it can influence various molecular properties. For PtSn a H-down bilayer forms, this is preferred on this surface due to the rumpling causing the H-down positions to not be bonded too closely to the surface.[3] The water bonds flat on the Sn atoms and H-down on the Pt in this bilayer.

4.1.3 Adsorption of water molecules on non-alloy surfaces

Adsorption of water on the Pt(111) surface has been extensively studied.[2] Thermodynamically, partial dissociation appears to be favoured,[27] but with careful preparation, surfaces composed of intact molecules can be obtained.[2] The water overlayers form in structures with large $(\sqrt{39}\times\sqrt{39})$ or $(\sqrt{37}\times\sqrt{37})$ supercells dependent on coverage. The atomistic details of these structures have still to be fully established. On Pd(111), experiment shows roughly commensurate $(\sqrt{3}\times\sqrt{3})$R30° clusters form at low coverage, but on completing the monolayer, much larger approximately (7×7) supercells form. He atom scattering, LEED measurements and

DFT calculations indicate that as many water molecules as possible try to bond lying flat on the surface atop the Pd atoms. This can occur at low coverage, but at high coverage a complete network requires some H-down or H-up bonding, and the large-supercells are likely forming as domain boundaries of H-down molecules (within which a certain degree of randomness can be accommodated) between patches of flat-lying molecules.

4.2 Method

4.2.1 Calculation Details

The DFT calculations were once again carried out using Vienna *ab-initio* Simulation Package (VASP), discussed in chapter 2. The Perdew-Burke-Ernzerhof (PBE) exchange correlation functional with the projector augmented wave (PAW) method was used with the optB86b van der Waals functional.[52] A Monkhorst-Pack grid of 5 x 5 x 1 was used for the k-point sampling of the Brillouin zone in the $(2\sqrt{3} \times 2\sqrt{3})$R30° {111} unit cell with a cut off energy set at 400 eV. The ratio of M to Sn was 2:1 in the surface layer, with M representing either Ag, Pd, Pt or Rh, the other 4 layers representing the bulk were pure M, with the bottom 2 layers constrained. Each unit cell has a 13Å vacuum to reduce any interaction due to the periodicity of the cell.

4.2.2 Adsorption Energies

The adsorption energies were calculated using the equation shown in 4.1.

$$E_{\text{ads}} = E(Total) - E(clean) - E(water) \tag{4.1}$$

Where E(Total) is the total energy of the relaxed bulk with alloy surface with H_2O present or dissociated into hydroxyl and hydrogen. E(clean) is the total energy of the bulk with alloy surface, with nothing present on the surface. E(water) is the energy of one H_2O molecule in the gas-phase.

4.3 Results

Each of the surface alloys were analysed with no adsorbate to check how flat the surfaces were. Then for each of the alloys a water was bound either on the Sn or on M, with M being either Ag, Pd, Pt or Rh. Each surface was also studied with a dissociated H_2O molecule present and the hydroxyl and hydrogen binding at different points on the surface. The starting structures for the dissociated H_2O molecule included both the hydroxyl and hydrogen present on separate Sn atoms, or both present on separate M atoms. The hydroxyl binding on top of Sn with hydrogen binding on top of a M atom and vice versa were also examined. This was to try and understand the preferred binding sites as well as studying the effect the molecules have on the surface and how much they distort it from the clean surface.

4.3.1 Clean alloy surfaces

Within the top layer as shown in Figure 4.1 the distance between two Ag atoms in the top layer is 2.89Å and there is only a small increase to 2.9Å between a Sn and Ag atom in the top layer. For the AgSn clean alloy surface the average Ag-Ag atom distance between the bottom 4 layers was 2.9Å, this is shown marked on the bottom layer in Figure 4.3. This increased for the top alloy layer the Ag-Ag distance between the 1st and 2nd layer atoms being 2.95Å and the Sn-Ag distance being 3.11Å.

For the PdSn surface alloy the distance between Pd atoms in the top layer is 2.75Å and this is the same for the difference between Pd and Sn atoms, as shown in Figure 4.2. It can be seen in Figure 4.4 that PdSn is the most flat alloy surface of those looked at, this can be confirmed by looking at the atom distances between the layers, for instance the lower 4 layers have an average Pd-Pd distance of 2.79Å between each layer. The top layer is however pulled slightly away from the bulk and the distance becomes 2.81Å between a Pd in the 1st layer and a Pd in the 2nd layer. There is a small increase in distance between a Sn in the 1st layer and a Pd in the 2nd layer at 2.82Å, however this is the smallest difference of any of the surface alloys looked at. Table 4.1 shows this is the least rumpled surface.

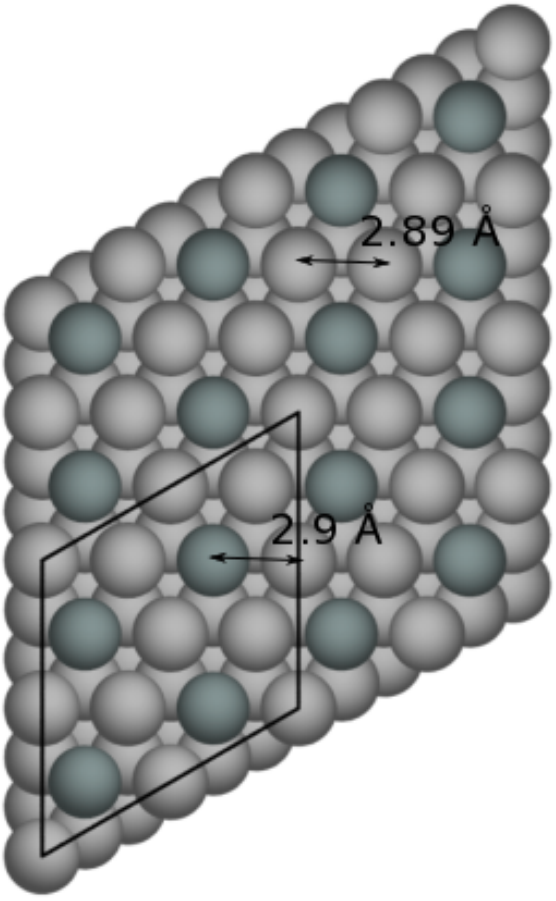

FIGURE 4.1: AgSn alloy top view

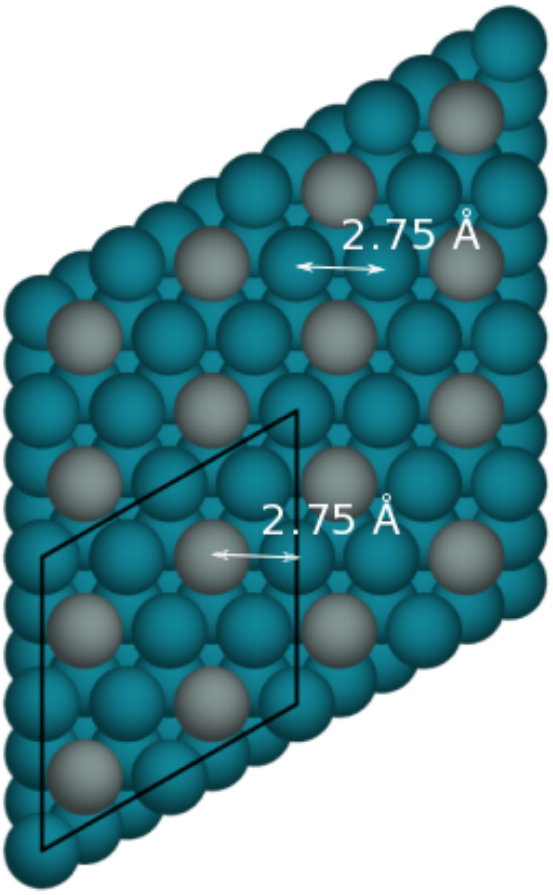

FIGURE 4.2: PdSn alloy top view

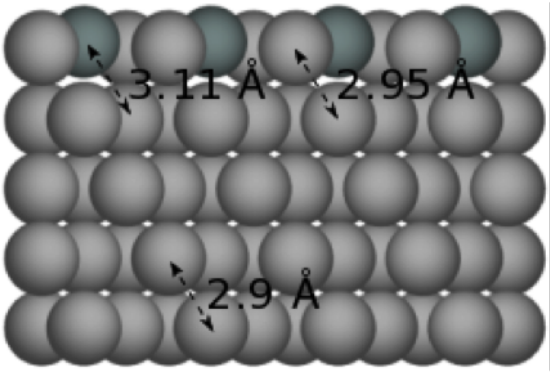

FIGURE 4.3: AgSn alloy side view

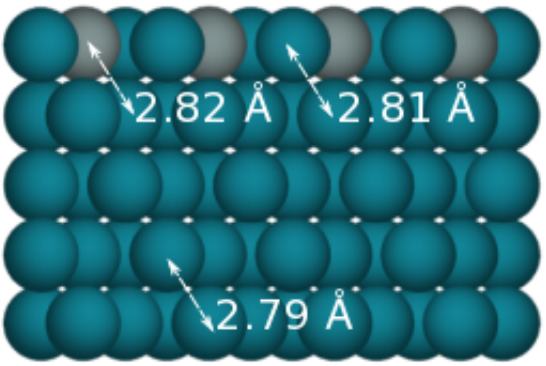

FIGURE 4.4: PdSn alloy side view

The RhSn alloy surface is the most rumpled of all the clean surfaces looked at here, shown in Figure 4.7. The Rh-Rh atom distance in the bottom 4 layers is 2.69Å and as was also seen in platinum, Figure 4.6 & 4.8, this is reduced slightly to a distance of 2.68Å between a Rh atom in the 1st and an atom in the 2nd layer. The Sn-Rh distance reduces slightly between the 1st and 2nd layers is 3.03Å. For RhSn the largest difference in atom distance is shown in the top layer, shown in Figure 4.5, the distance between two Rh atoms is 2.69Å whereas the difference between a Rh and Sn atom is 2.73Å, these are also the smallest distances between atoms within a layer shown in these alloys because Rh has the smallest lattice constant. As can be seen in Table 4.1 only the Rh-Rh distance gets smaller between the 1st and 2nd layer, in every other case this distance increases. The rhodium surface is the most rumpled, at 0.44Å, as shown by the distances in Table 4.2, however the experimental value for the rumpling is 0.29Å so theory is clearly not able to get the correct rumpling values.

The PtSn alloy surface has been looked at previously,[78, 83] and can be seen in Figure 4.8. The Pt-Pt atom distances for the bottom 4 layers is 2.82Å. Interestingly the distance between the Pt- Pt atoms in the 1st and 2nd layer is

slightly smaller at 2.81Å, this is not the case for the Sn-Pt distance which is 3.02Å. Within the top layer the distance between two Pt atoms is 2.77Å this is slightly smaller than between a Sn and Pt atom at 2.79Å as shown in Figure 4.6. The surface rumpling for PtSn in these calculations comes out at 0.26Å while the experimental value is 0.225Å.

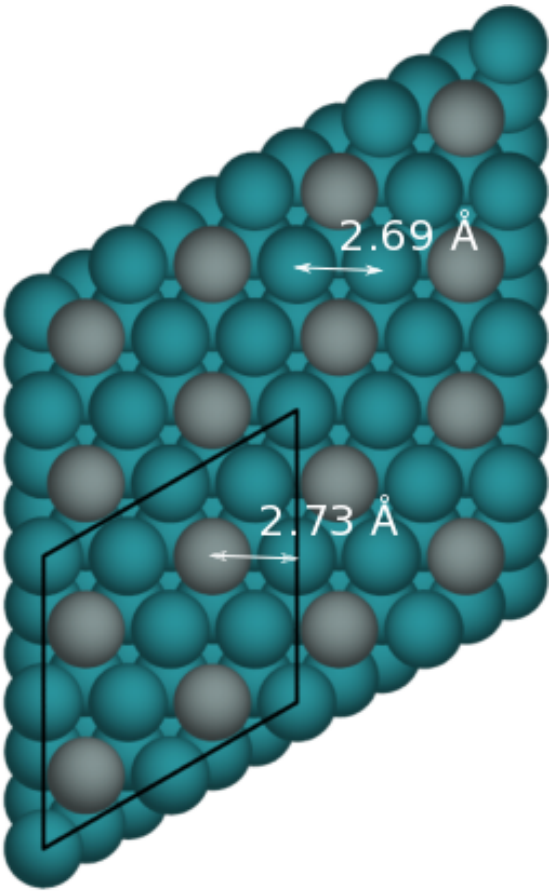

FIGURE 4.5: RhSn alloy top view

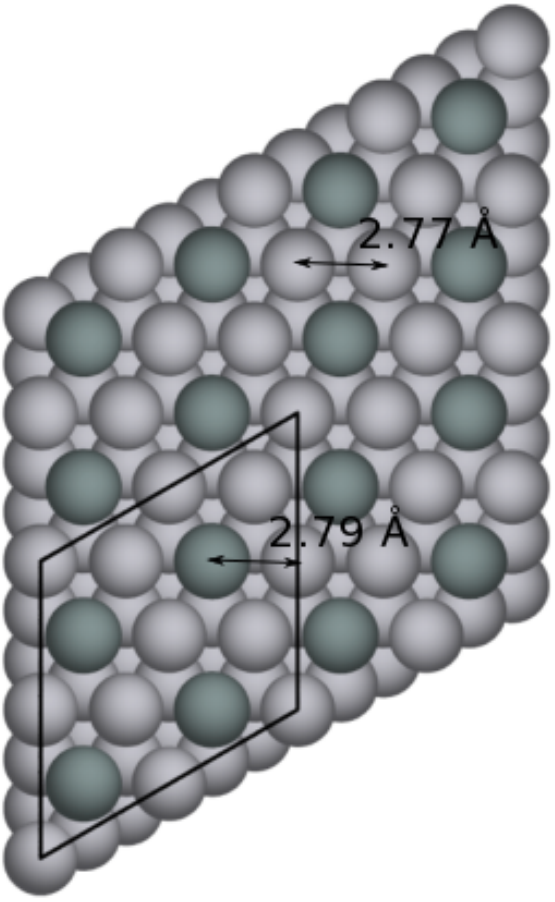

FIGURE 4.6: PtSn alloy top view

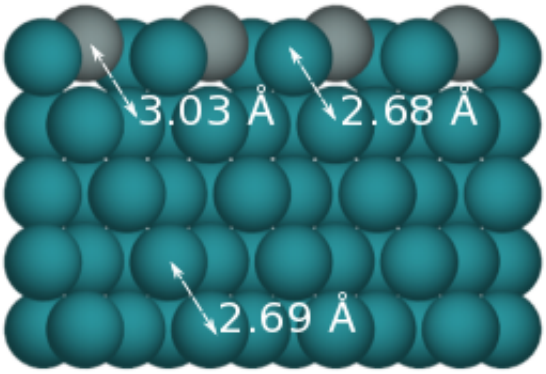

FIGURE 4.7: RhSn alloy side view

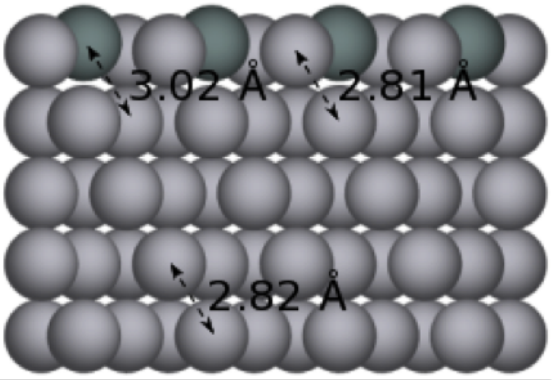

FIGURE 4.8: PtSn alloy side view

TABLE 4.1: Distances between atoms in the surface alloys

Atom type	Distance between 1st-1st layer atoms (Å)	Distance between 1st-2nd layer atoms (Å)	Diffence between 1st-1st & 1st-2nd atom distances(Å)
Ag-Ag	2.89	2.95	0.06
Ag-Sn	2.90	3.11	0.21
Pd-Pd	2.75	2.81	0.06
Pd-Sn	2.75	2.82	0.07
Rh-Rh	2.69	2.68	−0.01
Rh-Sn	2.73	3.03	0.30
Pt-Pt	2.77	2.81	0.04
Pt-Sn	2.79	3.02	0.23

TABLE 4.2: Surface rumpling (Å) for each of the different surface alloys

Surface alloy type	Surface Rumpling (Å)
AgSn	0.21
PdSn	0.02
RhSn	0.44
PtSn	0.26

4.3.2 Intact water bound to the alloy surfaces

Each of the surfaces had one intact water molecule per $(2\sqrt{3} \times 2\sqrt{3})$R30° unit cell bound either on the Sn atom or on the M atom that makes up the alloy surface. Table 4.3 shows the adsorption energies for the water molecule bound to the two locations on AgSn surface. Also the height at which the water molecule is adsorbed to the surface is shown, as expected O-adsorption site distance is shorter in the more stable structure. The water was started in the same starting position on each surface and rotates from this position in only two of the structures shown. If there was more time these calculations would have been run with more than one starting orientation.

TABLE 4.3: Calculated adsorption energies and binding height of water binding to the AgSn surface

Adsorption site	E_{ads} (eV)	O-adsorption site distance (Å)
Sn	−0.239	2.87
Ag	−0.245	2.76

As can be seen from the energies the water binds more strongly to the Ag than the Sn. When looking at the adsorption positions on the surface it can also be seen that although the water molecule binds with the O atom directly atop the Ag atom, shown in Figure 4.10, it is displaced when bound to the Sn atom, shown in Figure 4.9. Also it can be noted that the atoms the water molecules are bound to are pulled slightly away from the bulk in both cases, this atom is the only one shifted from the clean surface position looked at above. Although when the Sn atom has the water bound to it it is pulled a further 0.6Å from the rest of

the bulk, as shown in Figure 4.11, compared with when the water binds to the Ag atom which is only pulled a further 0.2Å away, as shown in Figure 4.12.

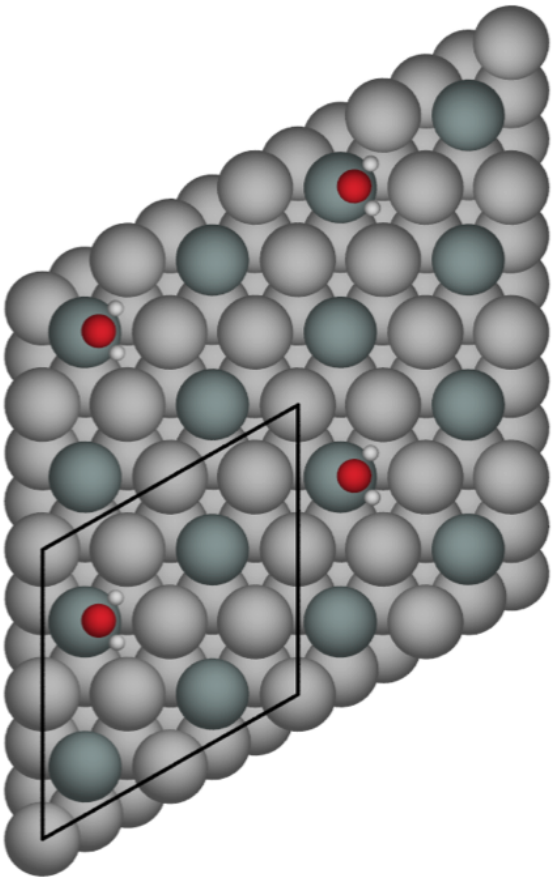

FIGURE 4.9: $E_{ads} = -0.239$ (eV), AgSn alloy with water bound to Sn atom top view

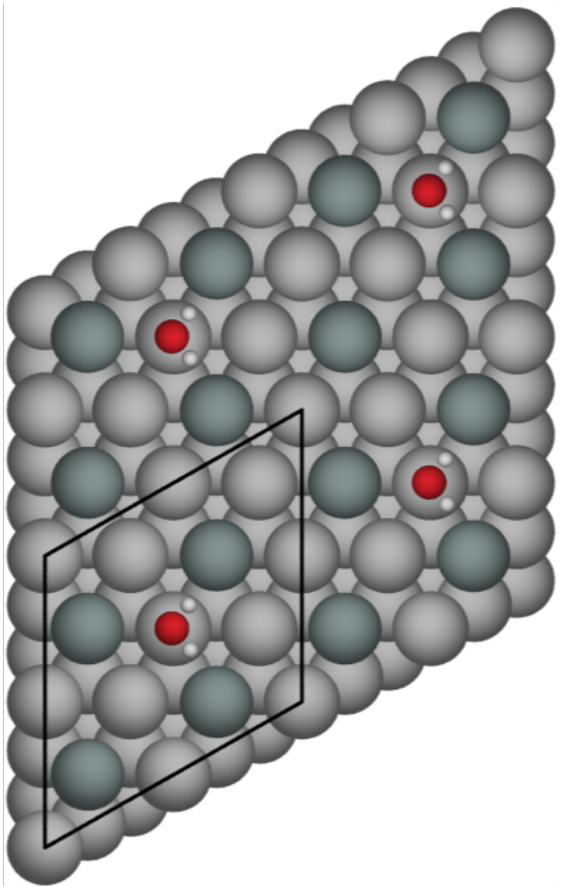

FIGURE 4.10: $E_{ads} = -0.245$ (eV), AgSn alloy with water bound to Ag atom top view

Table 4.4 shows the adsorption energies for the water molecules binding in different places to the PdSn surface.

TABLE 4.4: Calculated adsorption energies and binding height of water binding to the PdSn surface

Adsorption site	E_{ads} (eV)	O-adsorption site distance (Å)
Sn	−0.258	2.75
Pd	−0.264	2.61

As can be seen from the energies the water binds more strongly to the Pd than the Sn. Once again it can be seen that the water is bound in a much more

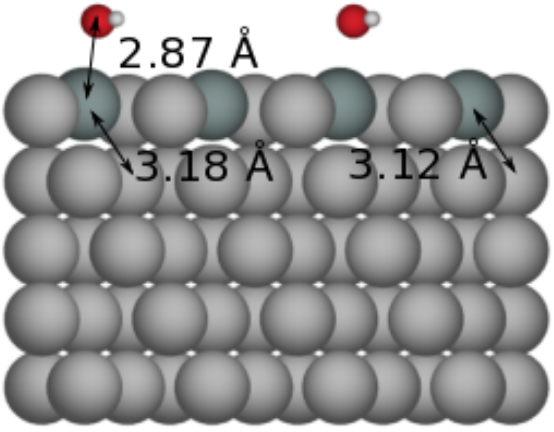

FIGURE 4.11: $E_{ads} = -0.239$(eV), AgSn alloy with water bound to Sn atom side view

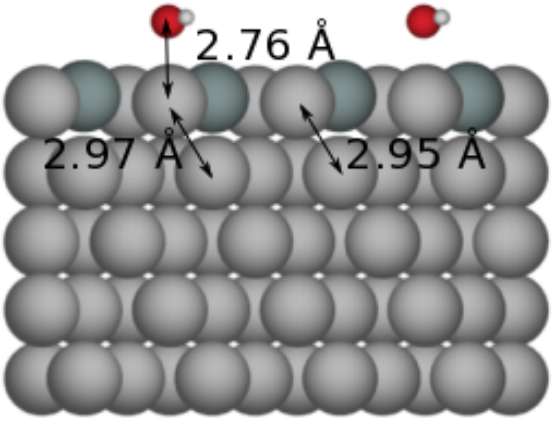

FIGURE 4.12: $E_{ads} = -0.245$(eV), AgSn alloy with water bound to Ag atom side view

displaced position when bound to the Sn atom, shown in Figure 4.13. Figure 4.14 shows the more expected atop position on the Pd atom. Once again the atom the water molecules are bound to are pulled slightly away from the bulk in both cases and once again this is the only atom shifted from the clean surface positions.

For the RhSn alloy surface the adsorption energies and adsorption heights of the water are shown in Table 4.5.

TABLE 4.5: Calculated adsorption energies and binding height of water binding to the RhSn surface

Adsorption site	E_{ads} (eV)	O-adsorption site distance (Å)
Sn	−0.341	2.64
Rh	−0.212	2.76

With the RhSn alloy the water bonds stronger and closer to the Sn atom, shown in Figure 4.17, although again it is in the more shifted atop position. The water bound to the rhodium atom has moved to have the hydrogens pointing away from one of the Sn atoms, shown in Figure 4.18 this Sn atom is bound closer to the 2nd layer than the other Sn atoms at 2.96Å and the Sn furthest away from

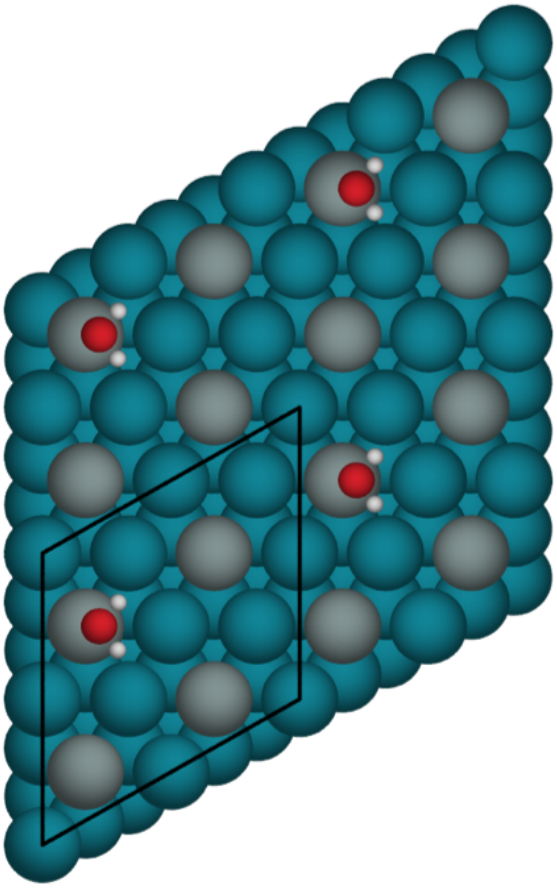

FIGURE 4.13: $E_{ads} = -0.258$ (eV), PdSn alloy with water bound to Sn atom top view

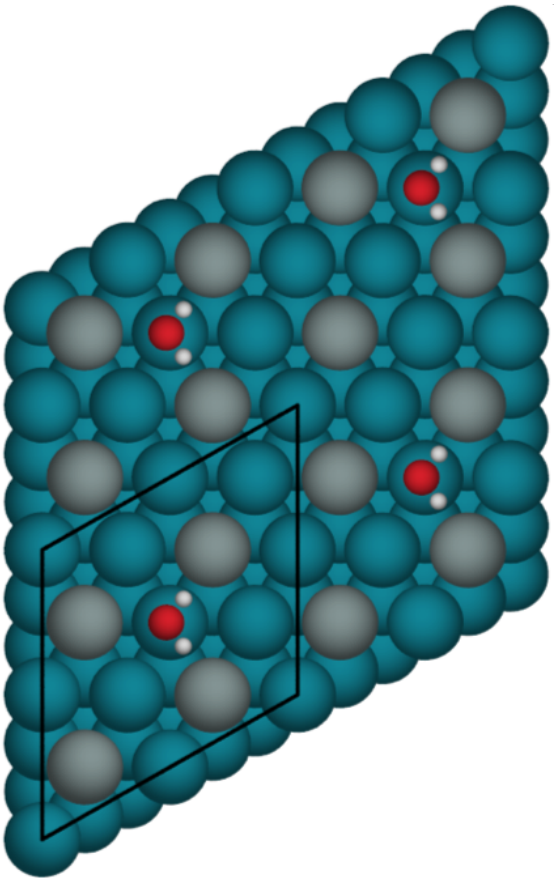

FIGURE 4.14: $E_{ads} = -0.264$ (eV), PdSn alloy with water bound to Pd atom top view

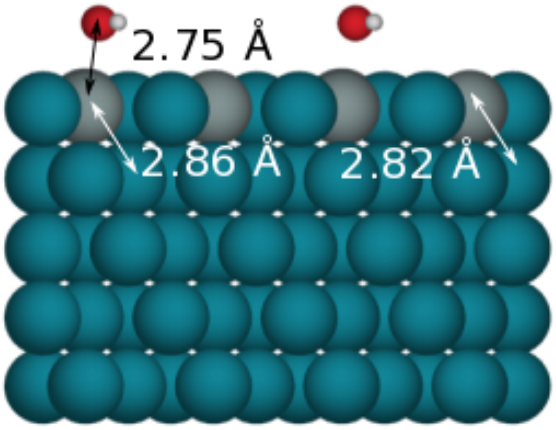

FIGURE 4.15: $E_{ads} = -0.258$ (eV), PdSn alloy with water bound to Sn atom side view

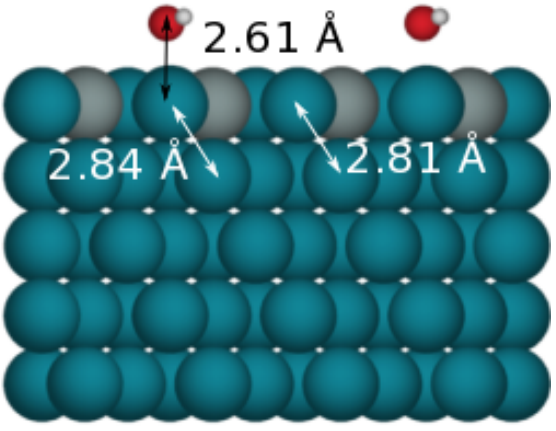

FIGURE 4.16: $E_{ads} = -0.264$ (eV), PdSn alloy with water bound to Pd atom side view

the water is the highest at 3.05Å, this is quite a range compared to the 3.03Å Sn-Rh distance that was shown between the 1st and 2nd layer for the clean surface. These changes were not witnessed in either the AgSn or PdSn surfaces alloys.

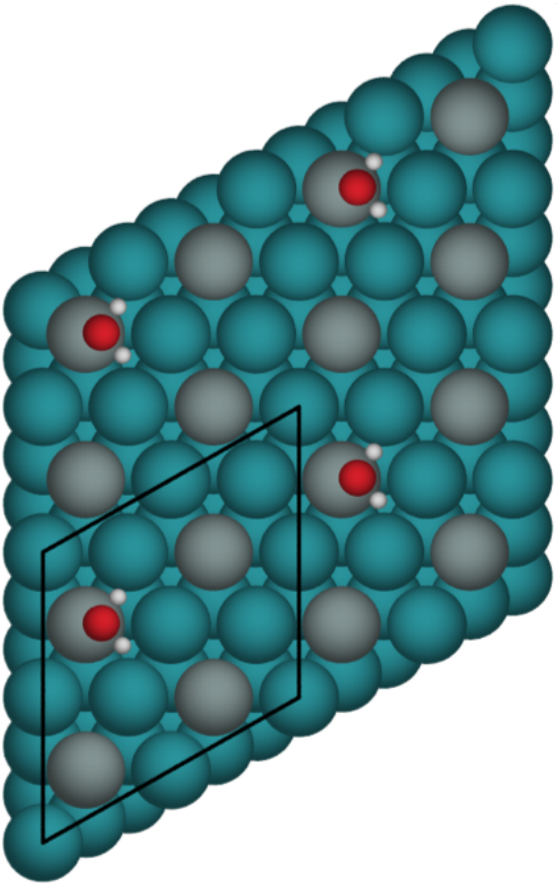

FIGURE 4.17: $E_{ads} = -0.341$(eV), RhSn alloy with water bound to Sn atom top view

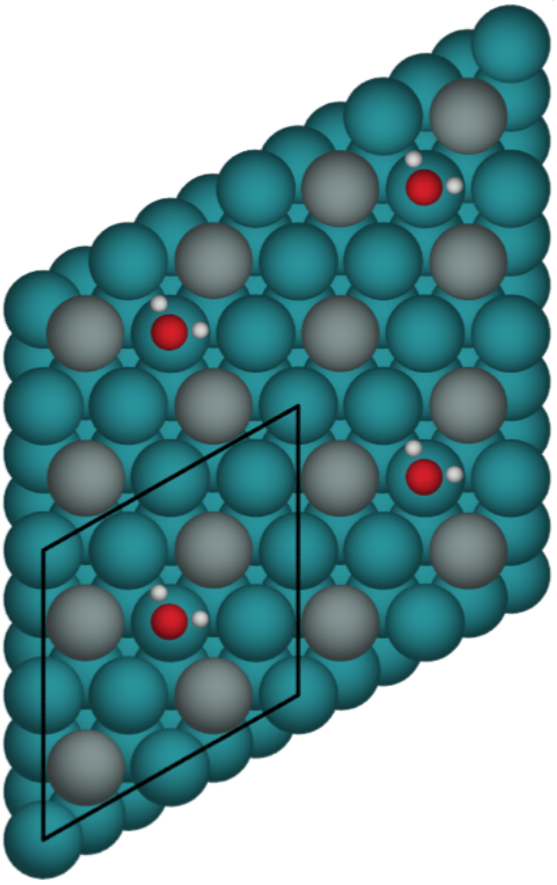

FIGURE 4.18: $E_{ads} = -0.212$(eV), RhSn alloy with water bound to Rh atom top view

The PtSn surface alloy has been previously looked at in other papers and has been studied again here for comparison. The Table 4.6 shows the binding energies and the height water has adsorbed in this study.

TABLE 4.6: Calculated adsorption energies and binding height of water binding to the PtSn surface

Adsorption site	E_{ads} (eV)	O-adsorption site distance (Å)
Sn	−0.437	2.53
Pt	−0.204	3.28

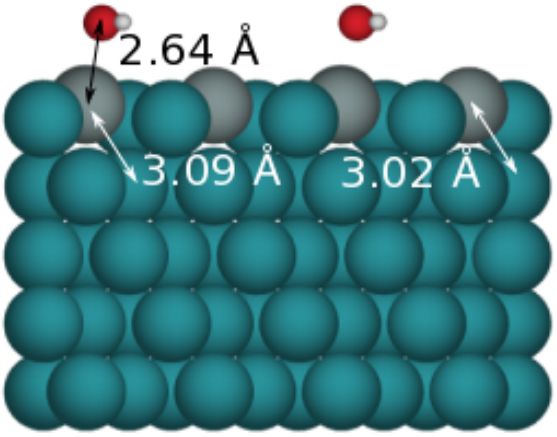

FIGURE 4.19: $E_{ads} = -0.341$(eV), RhSn alloy with water bound to Sn atom side view

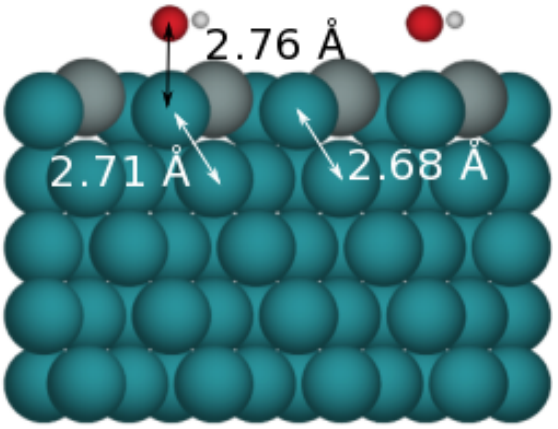

FIGURE 4.20: $E_{ads} = -0.212$(eV), RhSn alloy with water bound to Rh atom side view

This structure once again has the water binding closer to the surface and in a more stable position on the tin atom, which is shown in Figure 4.21. The structure with the water binding to the platinum is not as stable, the water is further from the surface and is tilted with its hydrogens pointed towards the surface as can be seen in Figure 4.24. This is the only surface calculation that was performed with the water further from the surface, which may be the cause of the tilting towards the surface, as when the structure started with the intact water above the Pt atom, at the height of the water molecules on other surfaces it rearranged to be above the Sn atom. This is also the only calculation that the M atom in the 1st layer is bound closer to the 2nd layer when the water is binding to it.

Table 4.7 shows the adsorption energies and the O-adsorption site distance for all alloys considered. It can be seen that for silver and palladium the water binds stronger to the M type than to the tin, this is also shown in Figure 4.25. These structures were less rumpled, with Pd showing a very flat surface and Ag showing one slightly more flat than the Rh and Pt. For both rhodium and platinum the

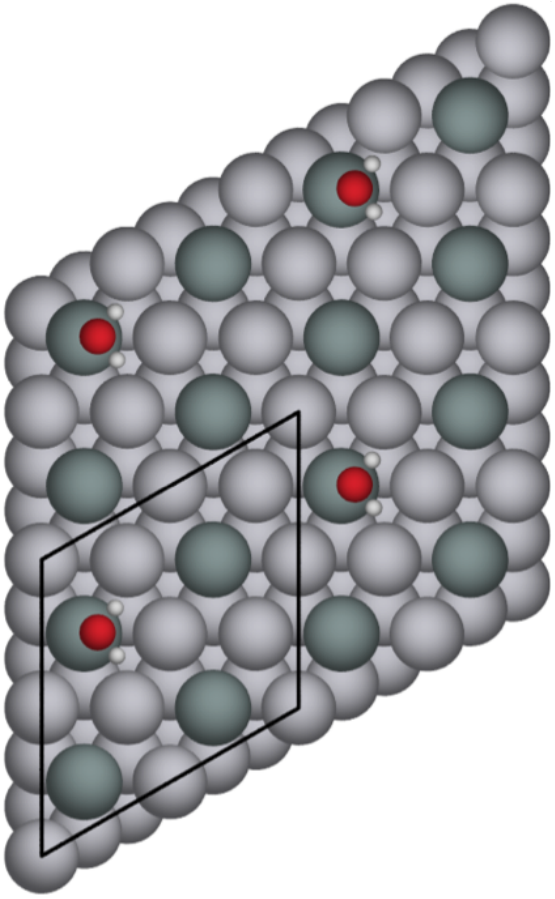

FIGURE 4.21: $E_{\text{ads}} = -0.437$ (eV), PtSn alloy with water bound to Sn atom top view

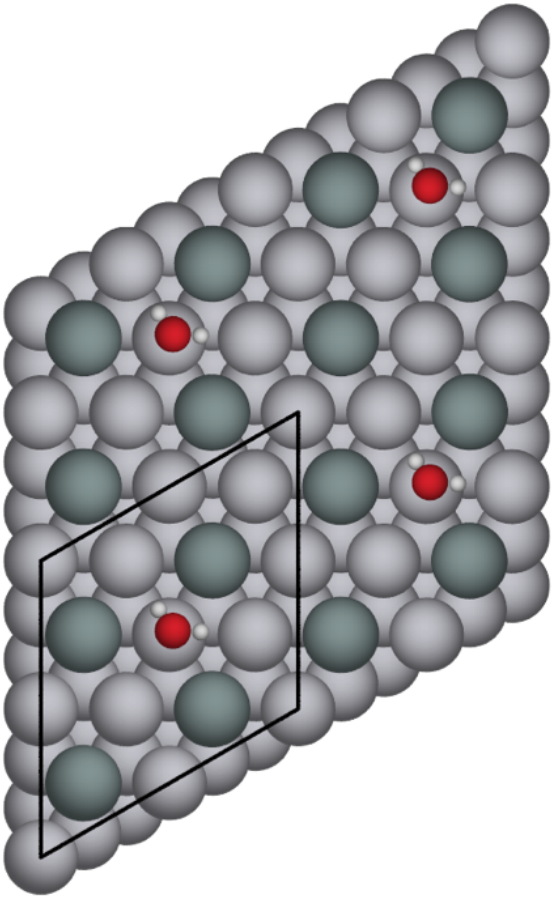

FIGURE 4.22: $E_{\text{ads}} = -0.204$(eV), PtSn alloy with water bound to Pt atom top view

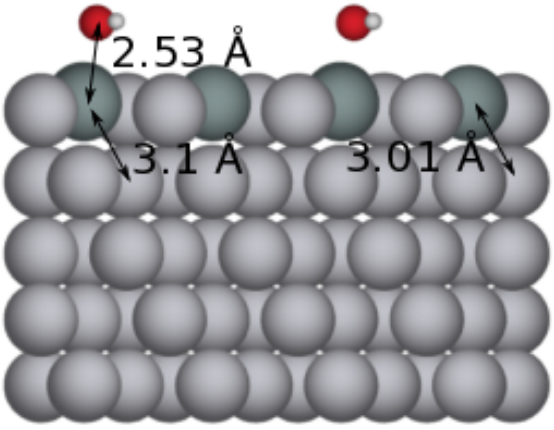

FIGURE 4.23: $E_{\text{ads}} = -0.437$ (eV), PtSn alloy with water bound to Sn atom side view

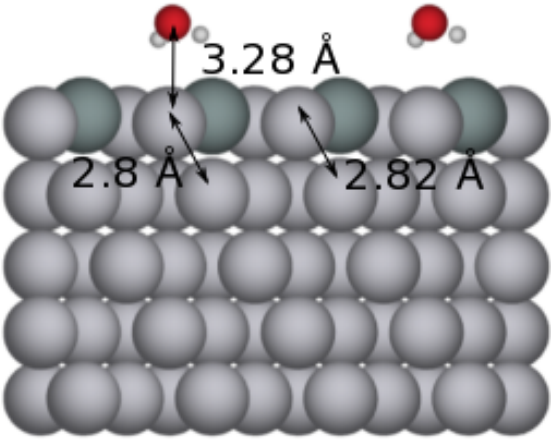

FIGURE 4.24: $E_{\text{ads}} = -0.204$(eV), PtSn alloy with water bound to Pt atom side view

water preferred to bind to the tin, these two surfaces also show the most surface rumpling. Every alloy type has the oxygen in water bonding closer to the surface atom it is bound to in the most stable structure, as can be expected.

TABLE 4.7: Calculated adsorption energies and binding height of water binding all alloy surfaces

Alloy type	Adsorption site	E_{ads} (eV)	O-adsorption site distance (Å)
AgSn	Sn	−0.239	2.87
AgSn	Ag	−0.245	2.76
PdSn	Sn	−0.258	2.75
PdSn	Pd	−0.264	2.61
RhSn	Sn	−0.341	2.64
RhSn	Rh	−0.212	2.76
PtSn	Sn	−0.437	2.53
PtSn	Pt	−0.204	3.28

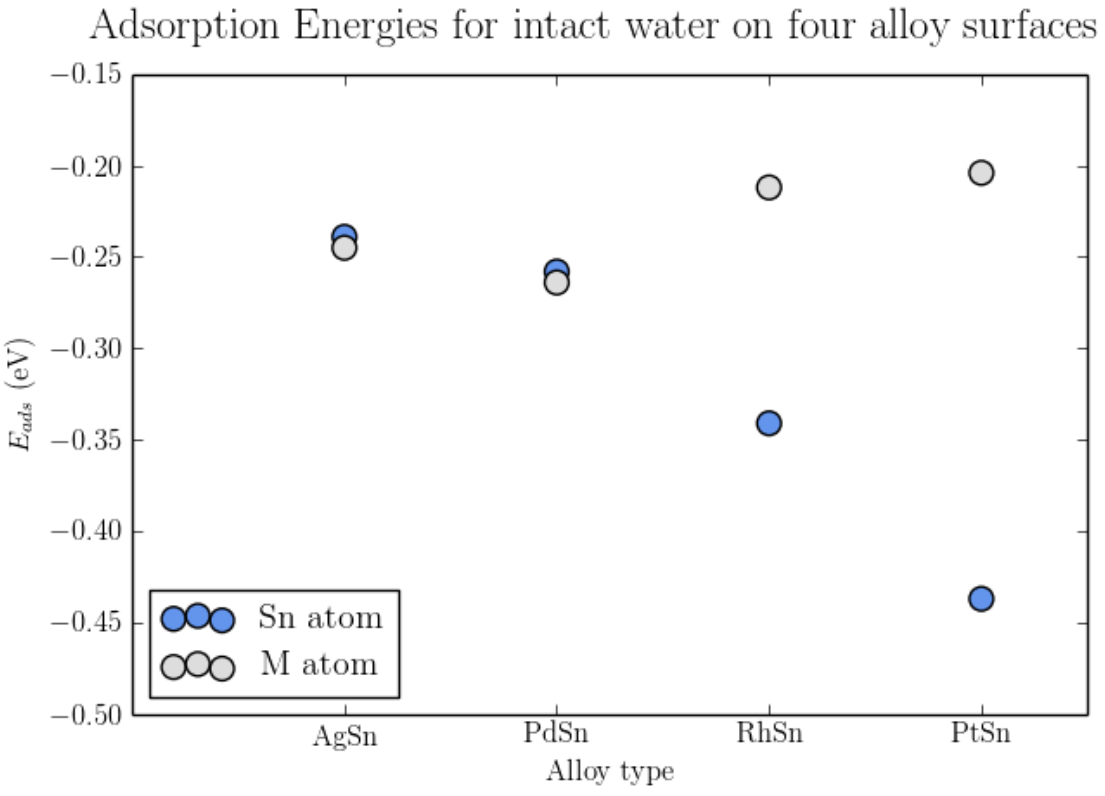

FIGURE 4.25: Adsorption energies for intact H_2O on either the bulk M atom or a Sn atom on four alloy surfaces.

4.3.3 Dissociated water bound to the alloy surfaces

Dissociated water has also been studied on these surfaces, these were looked at with hydroxyl and hydrogen binding to different atoms on the surface alloy. Four different variations were used as starting points these included hydroxyl and hydrogen both bonded to different Sn atoms. Hydroxyl and hydrogen both bonded to different M atoms on the surface. Hydroxyl bonded to Sn with hydrogen bonded to M and vice versa. These radicals did not always keep those positions on optimisation as will be discussed for each surface alloy.

The adsorption energies and O-adsorption site distances of the dissociated water structures for the AgSn alloy surface are shown in Table 4.8. The adsorption energies were calculated as for an intact water molecule so they could be directly comparable to the above calculations.

TABLE 4.8: Calculated adsorption energies and binding height of hydroxyl and hydrogen binding to the AgSn surface

Start position	End position	E_{ads} (eV)	O-adsorption site distance (Å)
OH on Sn H on Sn	OH on Sn H on Sn	0.794	2.03 1.76
OH on Ag H on Ag	OH on Sn H in hollow	0.863	2.03 1.92
OH on Sn H on Ag	OH on Sn H in hollow	0.850	2.03 1.90
OH on M H on Ag	OH on Sn H in hollow	0.863	2.03 1.92

As can be seen none of these structures are stable relative to the gas phase. It can also be noted that in every situation the hydroxyl has moved onto the Sn atom. Three out of four structures have had the hydrogen relax into the shifted hollow position with it furthest away from the Sn atom, even one of the structures

that initially had the hydrogen on top of the tin atom. However it can be seen from the adsorption energies that when the hydrogen in bound on top of the Sn atom, as shown in Figure 4.26, it is preferred compared to being in the shifted hollow site, shown in Figure 4.27.

In each situation the hydroxyl molecule binds closer to the surface, with an O-adsorption site distance of 2.03Å, compared to the most stable intact water structure that is 2.76Å. Also in each structure the atom the hydroxyl or hydrogen are bonded above has been pulled away from the bulk. The hydroxyl molecule pulls the Sn atom ∼0.5Å higher than the other tin atoms in each model. The hydrogen bound in the atop position shown in Figure 4.26 pulls the Sn 0.36Å above the other tin atoms. The three structures that have the hydrogen in the shifted hollow position do not show a rise in any of the metal atoms surrounding the hollow position.

As the positions are very similar for all three of the structures that had the hydrogen bound in the shifted hollow position only one has been shown here. The 0.863eV energies were due to the hydrogen occupying a *fcc* hollow site compared to the 0.850eV which was due to the hydrogen occupying a *hcp* hollow site.

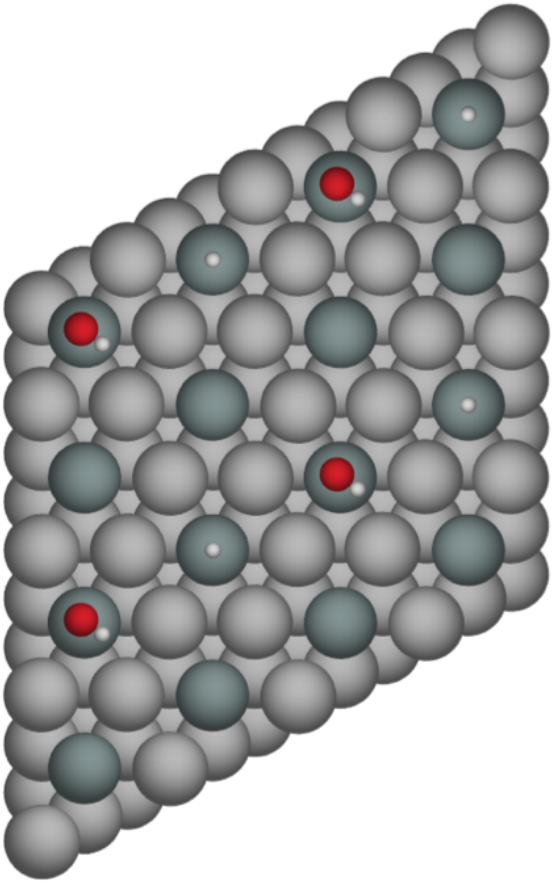

FIGURE 4.26: $E_{\text{ads}} = 0.794$(eV), AgSn alloy with OH & H on Sn top view

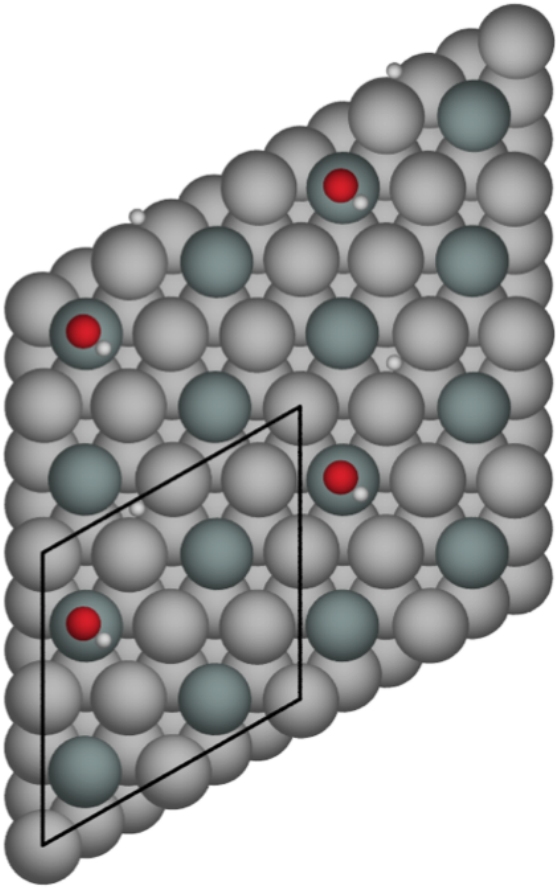

FIGURE 4.27: $E_{\text{ads}} = 0.863$ (eV), AgSn alloy with OH on Sn & H in a fcc shifted hollow position, started with OH & H on Ag, top view

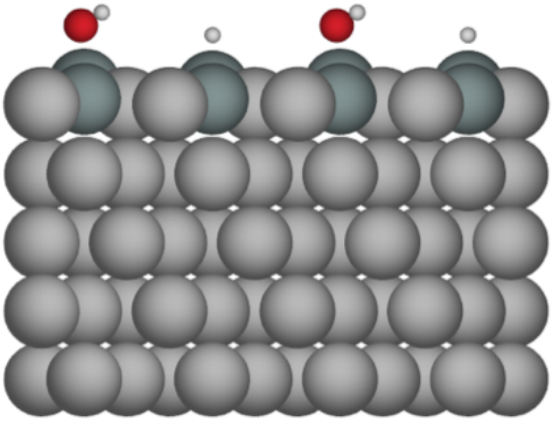

FIGURE 4.28: $E_{\text{ads}} = 0.794$ (eV), AgSn alloy with OH & H on Sn side view

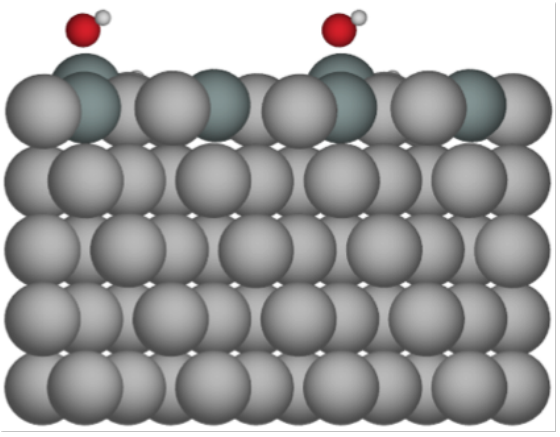

FIGURE 4.29: $E_{\text{ads}} = 0.863$ (eV), AgSn alloy with OH on Sn & H in a fcc shifted hollow position, started with OH & H on Ag, side view

The adsorption energies and O-adsorption site distances of the dissociated water structures for the PdSn alloy surface are shown in Table 4.9.

TABLE 4.9: Calculated adsorption energies and binding height of hydroxyl and hydrogen binding to the PdSn surface

Start position	End position	E_{ads} (eV)	O-adsorption site distance (Å)
OH on Sn H on Sn	OH on Sn H on Sn	1.564	2.04 1.78
OH on Pd H on Pd	OH in bridge H on Pd	0.944	2.22 1.58
OH on Sn H on Pd	OH on Sn H on Pd	0.692	2.03 1.57
OH on Pd H on Sn	OH on Pd H on Sn	1.954	2.04 1.77
OH on Pd H in hollow	OH on Pd H in bridge	0.604	2.03 1.76

Once again none of these structures are stable. As can be seen from Table 4.9 the hydroxyl and hydrogen molecules each have remained bonded to the same metal type they began on. This however is not the full story as can be seen in Figure 4.31 which has had the hydroxyl that was in the atop position on a palladium move into the bridge position between two of palladium atoms. Also again the atom the hydroxyl or hydrogen are bonded to is pulled away from the bulk, it is only when the hydroxyl is in the bridge position that this is not seen. The most stable has OH on Sn and H between two Pd atoms in the bridge position. As shown in the silver structures the hydroxyl molecules bind closer to the surface, at ∼2.04Å compared to the most stable water which was bonded at 2.61Å.

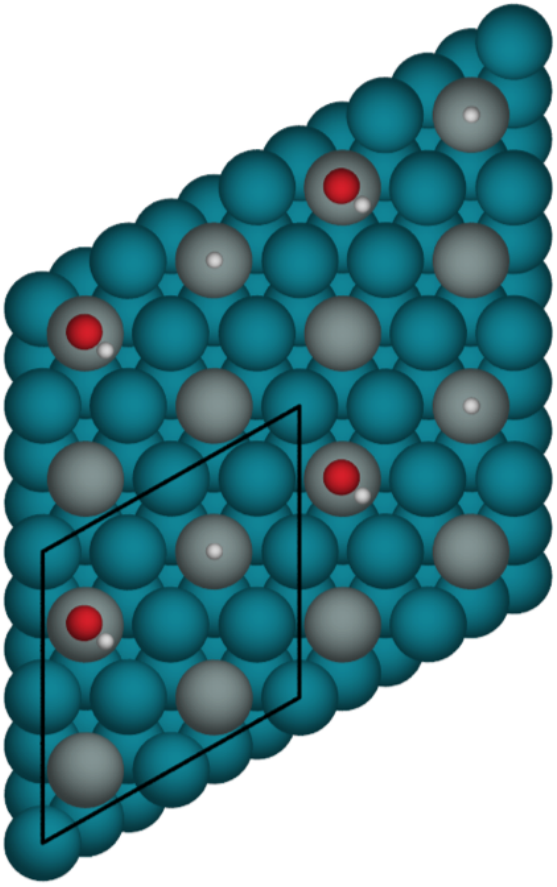

FIGURE 4.30: $E_{\text{ads}} = 1.564$ (eV), PdSn alloy with OH & H on Sn, started with OH & H on Sn, top view

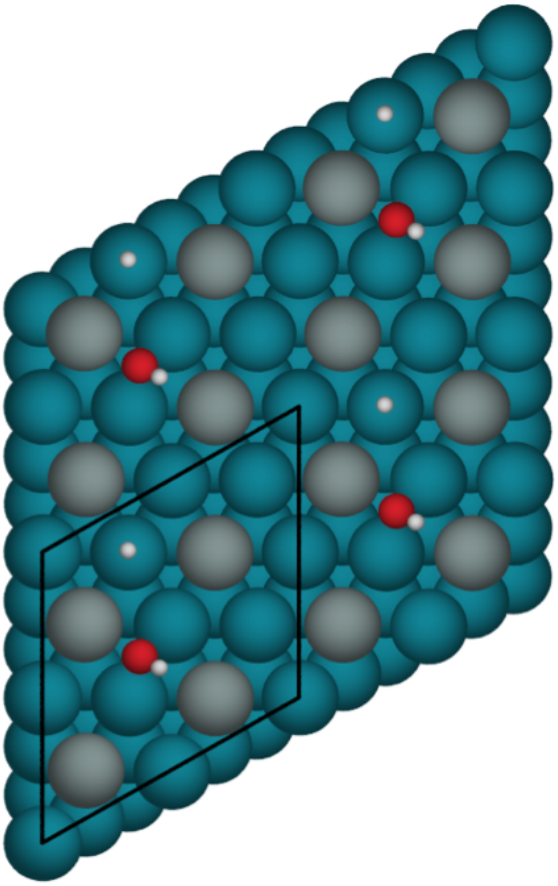

FIGURE 4.31: $E_{\text{ads}} = 0.944$ (eV), PdSn alloy with OH in bridge position on Pd & H on Pd, started with OH & H on Pd, top view

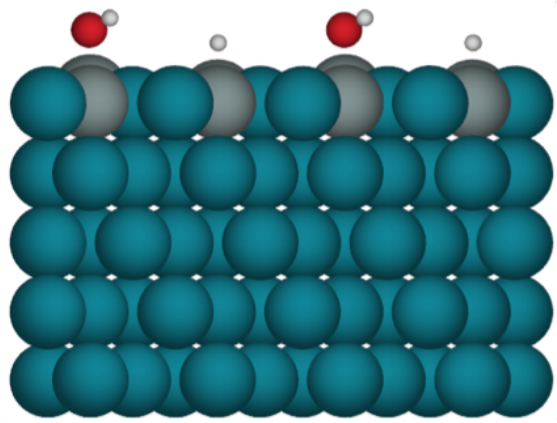

FIGURE 4.32: $E_{\text{ads}} = 1.564$ (eV), PdSn alloy with OH & H on Sn, started with OH & H on Sn, side view

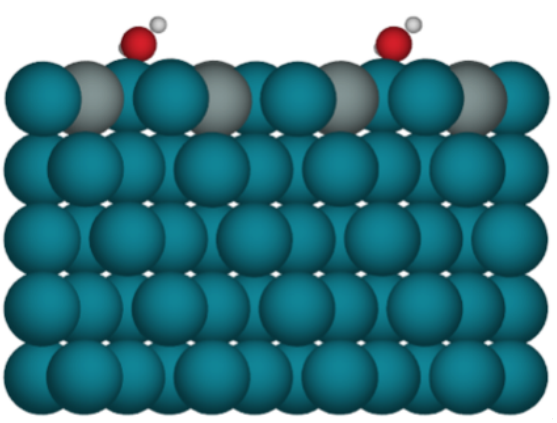

FIGURE 4.33: $E_{\text{ads}} = 0.944$ (eV), PdSn alloy with OH in bridge position between Pd & H on Pd, started with OH & H on Pd, side view

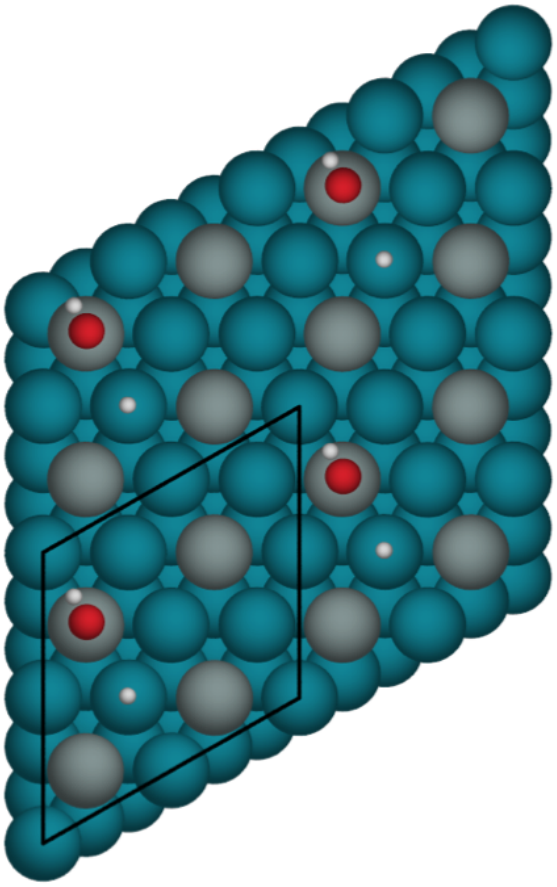

FIGURE 4.34: $E_{\text{ads}} = 0.692$ (eV), PdSn alloy with OH on Sn & H on Pd, started with OH on Sn & H on Pd, top view

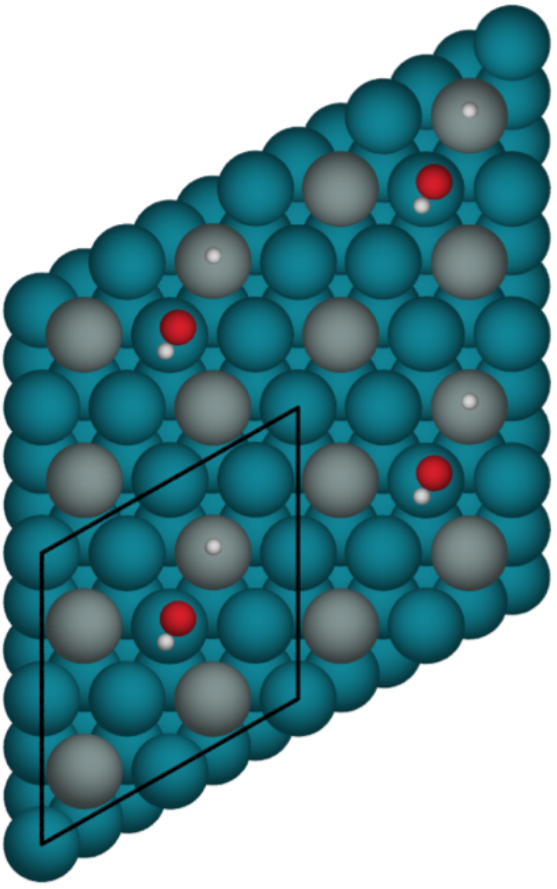

FIGURE 4.35: $E_{\text{ads}} = 1.954$ (eV), PdSn alloy with OH on Pd & H on Sn, started with OH on Pd & H on Sn, top view

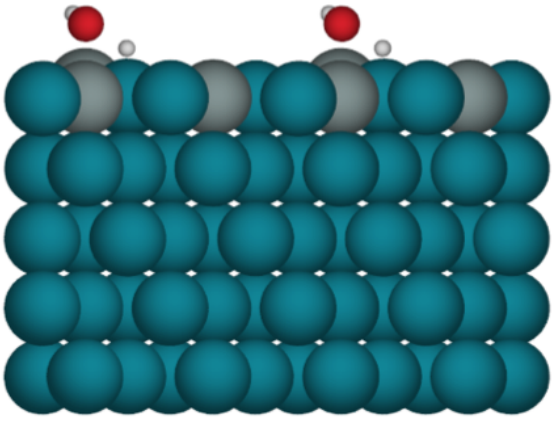

FIGURE 4.36: $E_{\text{ads}} = 0.692$ (eV), PdSn alloy with OH on Sn & H on Pd, started with OH on Sn & H on Pd, side view

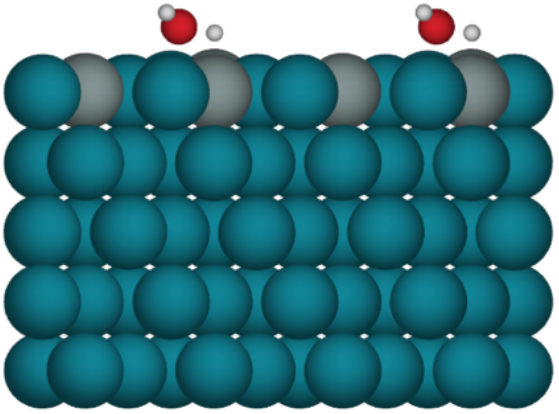

FIGURE 4.37: $E_{\text{ads}} = 1.954$ (eV), PdSn alloy with OH on Pd & H on Sn, started with OH on Pd & H on Sn, side view

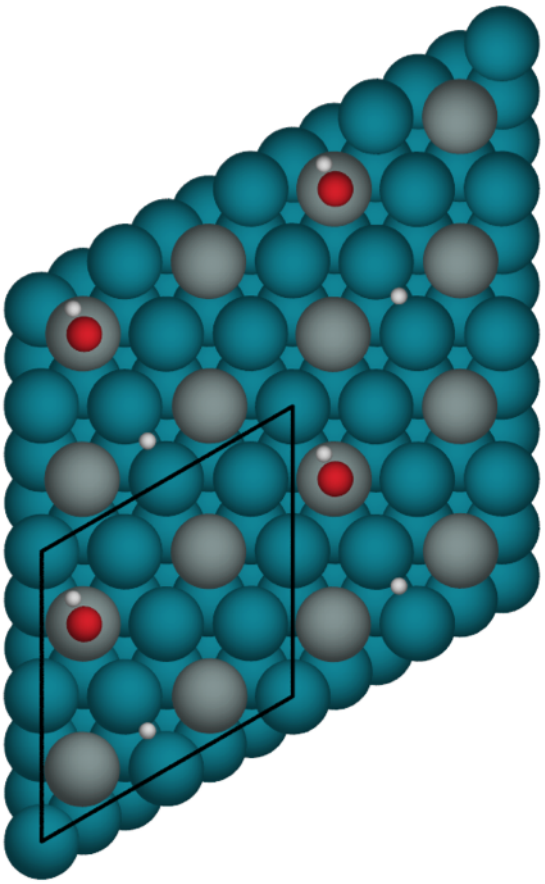

FIGURE 4.38: $E_{\text{ads}} = 0.603$ (eV), PdSn alloy with OH on Sn & H in bridge position between two Pd atoms, started with OH on Sn & H in hollow, top view

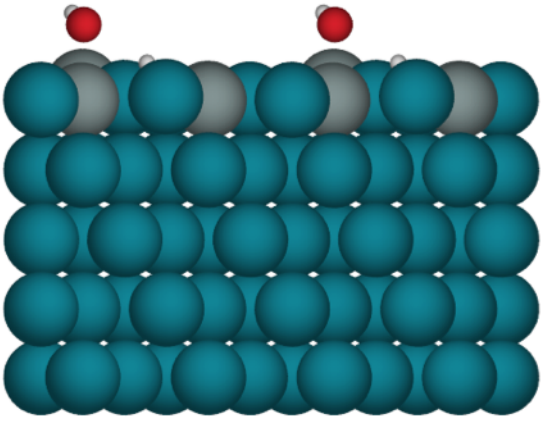

FIGURE 4.39: $E_{\text{ads}} = 0.603$ (eV), PdSn alloy with OH on Sn & H in bridge position between two Pd atoms, started with OH on Sn & H in hollow, side view

The adsorption energies and O-adsorption site distances of the dissociated water structures for the RhSn alloy surface are shown in Table 4.10.

TABLE 4.10: Calculated adsorption energies and binding height of hydroxyl and hydrogen binding to the RhSn surface

Start position	End position	E_{ads} (eV)	O-adsorption site distance (Å)
OH on Sn H on Sn	OH on Sn H on Sn	1.055	2.02 1.76
OH on Rh H on Rh	OH in bridge H on Rh	0.276	2.20 1.59
OH on Sn H on Rh	OH on Sn H on Rh	0.100	2.02 1.59
OH on Rh H on Sn	OH on Rh H on Sn	1.290	2.06 1.75

None of these structures come out stable again, as can be seen from Table 4.10. The most stable structure, Figure 4.44 has the hydroxyl binding to the Sn atom and the H binding to a Rh atom, as the intact water was more stable on the Sn atom this is expected. Figure 4.41 has had the hydroxyl move into the bridge position between one of the rhodium atoms and one of the tin atoms. Once again the atom the hydroxyl or hydrogen are bonded to is pulled away from the bulk including the atoms bonded to the bridge positioned hydroxyl. The most stable has OH on Sn and H on the bulk metal, in this case Rh. This was the most rumpled surface out of all the clean alloy structures studied and with the dissociated water bound to it this becomes even more apparent.

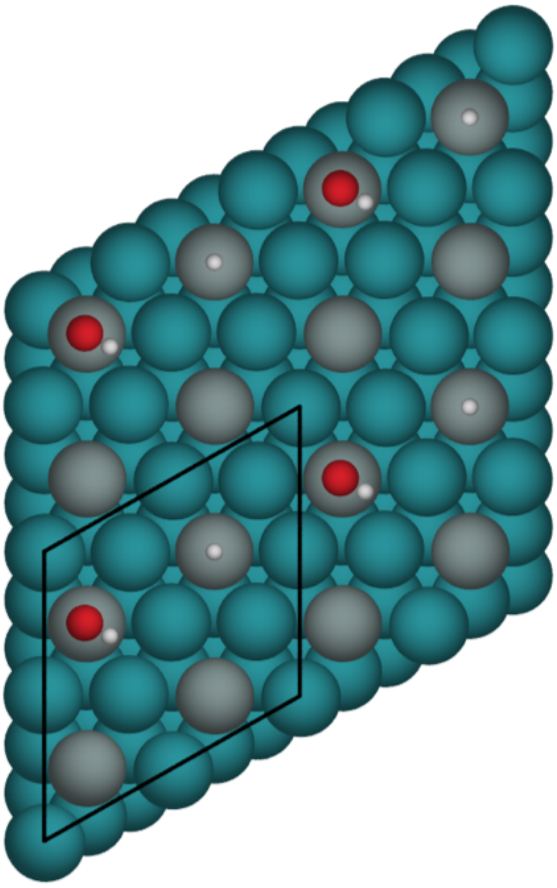

FIGURE 4.40: $E_{\text{ads}} = 1.055$ (eV), RhSn alloy with OH & H on Sn, started with OH & H on Sn, top view

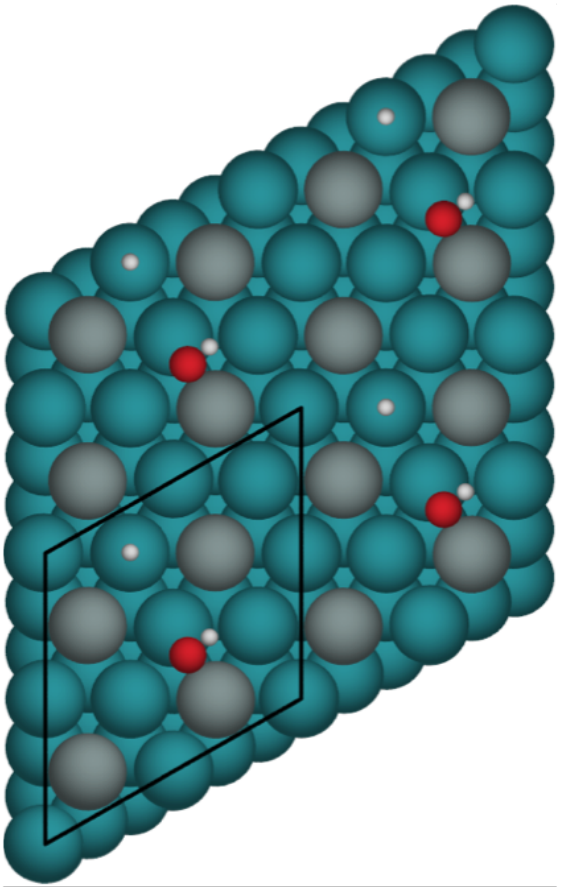

FIGURE 4.41: $E_{\text{ads}} = 0.276$ (eV), RhSn alloy with OH in bridge position on M & H on M, started with OH & H on M, top view

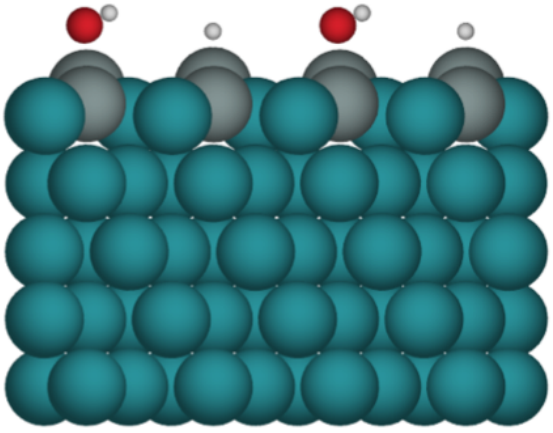

FIGURE 4.42: $E_{\text{ads}} = 1.055$ (eV), RhSn alloy with OH & H on Sn, started with OH & H on Sn, side view

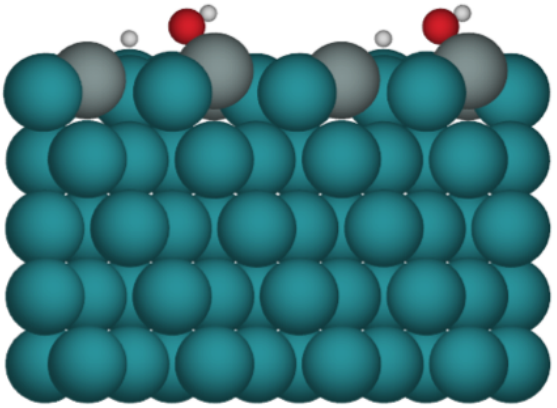

FIGURE 4.43: $E_{\text{ads}} = 0.276$ (eV), RhSn alloy with OH in bridge position between Rh and Sn & H on Rh, started with OH & H on Rh, side view

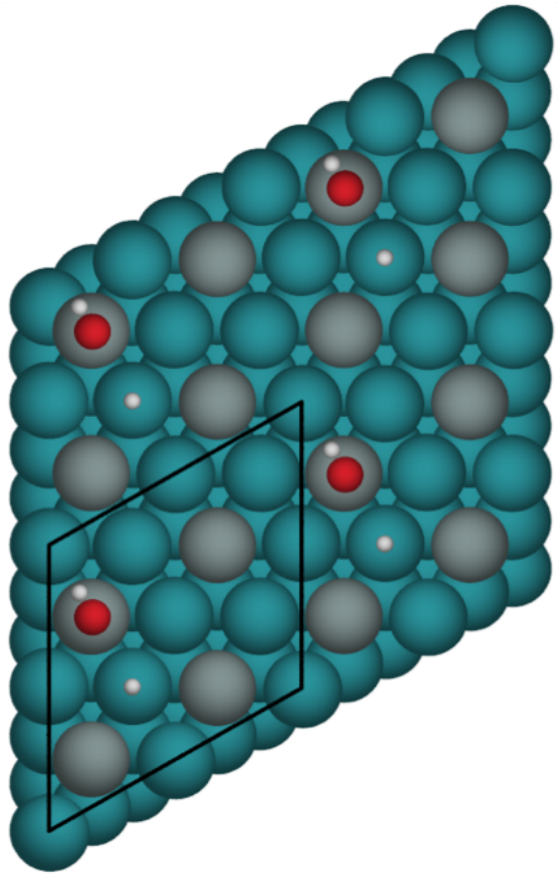

FIGURE 4.44: E_{ads} = 0.100 (eV), RhSn alloy with OH on Sn & H on Rh, started with OH on Sn & H on Rh, top view

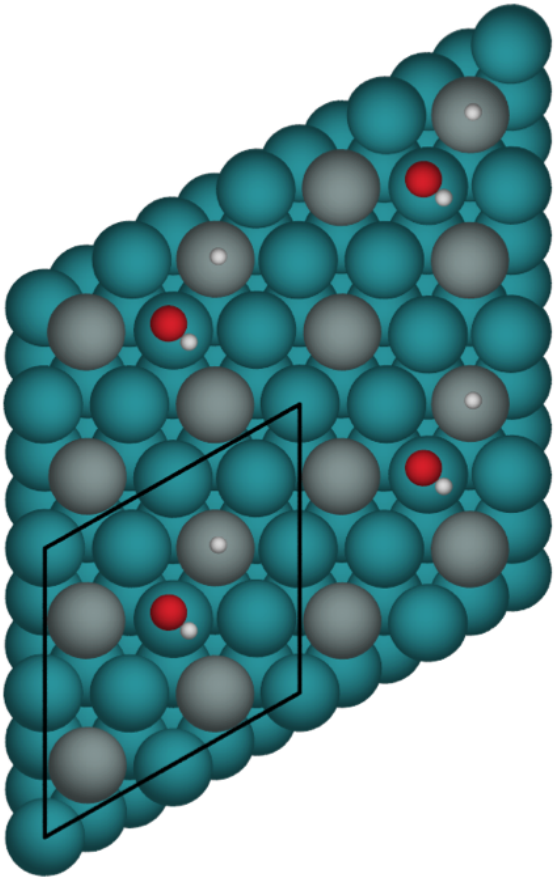

FIGURE 4.45: E_{ads} = 1.290 (eV), RhSn alloy with OH on Rh & H on Sn, started with OH on Rh & H on Sn, top view

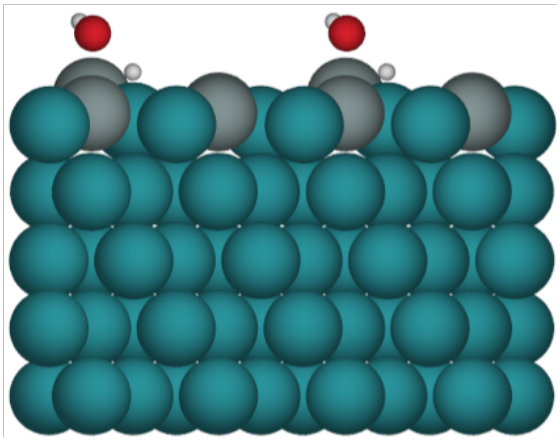

FIGURE 4.46: E_{ads} = 0.100 (eV), RhSn alloy with OH on Sn & H on Rh, started with OH on Sn & H on Rh, side view

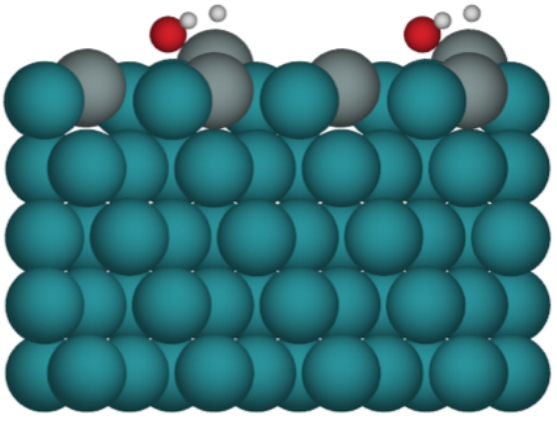

FIGURE 4.47: E_{ads} = 1.290 (eV), RhSn alloy with OH on Rh & H on Sn, started with OH on Rh & H on Sn, side view

The adsorption energies and O-adsorption site distances of the dissociated water structures for the PtSn alloy surface are shown in Table 4.11.

TABLE 4.11: Calculated adsorption energies and binding height of hydroxyl and hydrogen binding to the PtSn surface

Start position	End position	E_{ads} (eV)	O-adsorption site distance (Å)
OH on Sn H on Sn	OH on Sn H on Sn	0.860	2.01 1.75
OH on Pt H on Pt	OH on Sn H on Pt	−0.195	2.01 1.58
OH on Sn H on Pt	OH on Sn H on Pt	−0.220	2.01 1.57
OH on Pt H on Sn	OH on Pt H on Sn	1.325	2.04 1.74
OH on Pt H in hollow	OH on Pt H in bridge	0.225	2.01 1.79

As can be seen in Table 4.11 two of the structures have come out stable, this is the only alloy that any of the dissociated water structures have come out stable relative to the gas phase. Both of these structures have hydroxyl on the Sn atom and the H on a Pt atom as shown in Figures 4.49 & 4.52. It can be seen in Figure 4.53 that having hydroxyl on the Pt atom is the least stable set up, with Figure 4.49 having rearranged to have the hydroxyl on the Sn atom. The height of the hydroxyl above the Sn atom was smaller ar 2.01Å compared to when the hydroxyl was present over the Pt atom and it was bound at 2.04Å. One structure was run with the hydrogen in the hollow site, this structure relaxed to have the hydrogen bound in the bridge position between two platinum atoms and was not stable in comparison to the gas phase, shown in Figure 4.56.

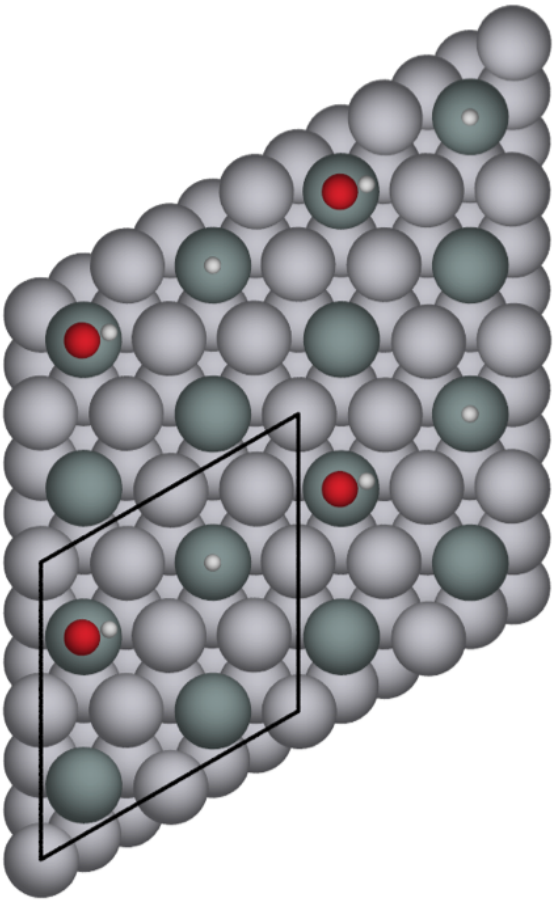

FIGURE 4.48: $E_{\text{ads}} = 0.860$ (eV), PtSn alloy with OH & H on Sn, started with OH & H on Sn, top view

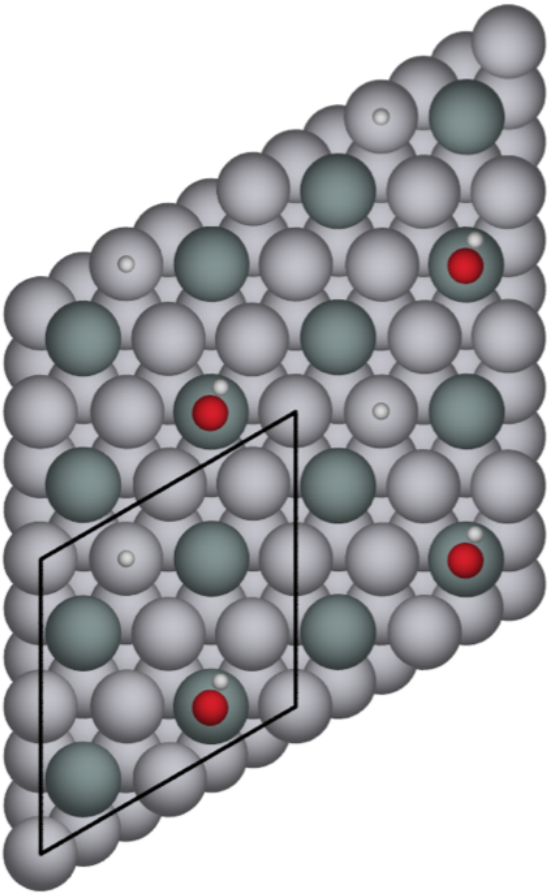

FIGURE 4.49: $E_{\text{ads}} = -0.195$(eV), PtSn alloy with OH on Sn & H on Pt, started with OH & H on Pt, top view

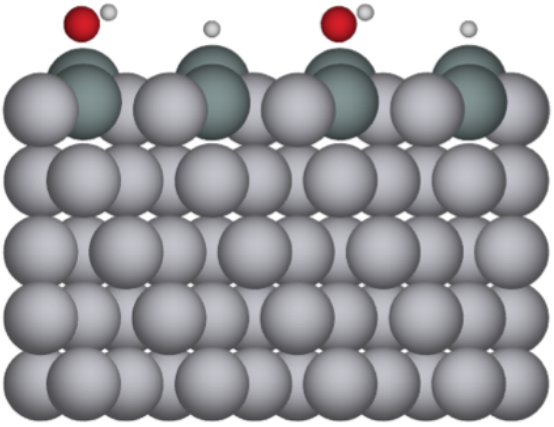

FIGURE 4.50: $E_{\text{ads}} = 0.860$ (eV), PtSn alloy with OH & H on Sn, started with OH & H on Sn, side view

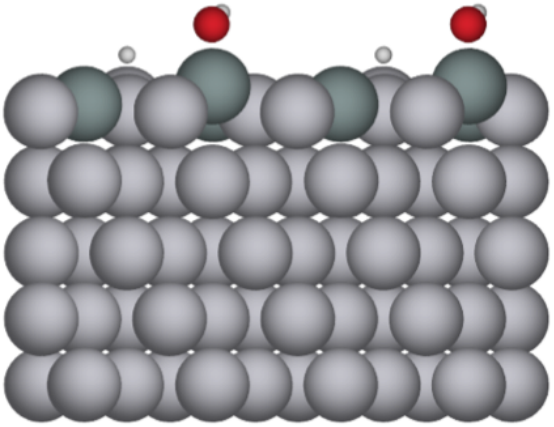

FIGURE 4.51: $E_{\text{ads}} = -0.195$ (eV), PtSn alloy with OH on Sn & H on Pt, started with OH & H on Pt, side view

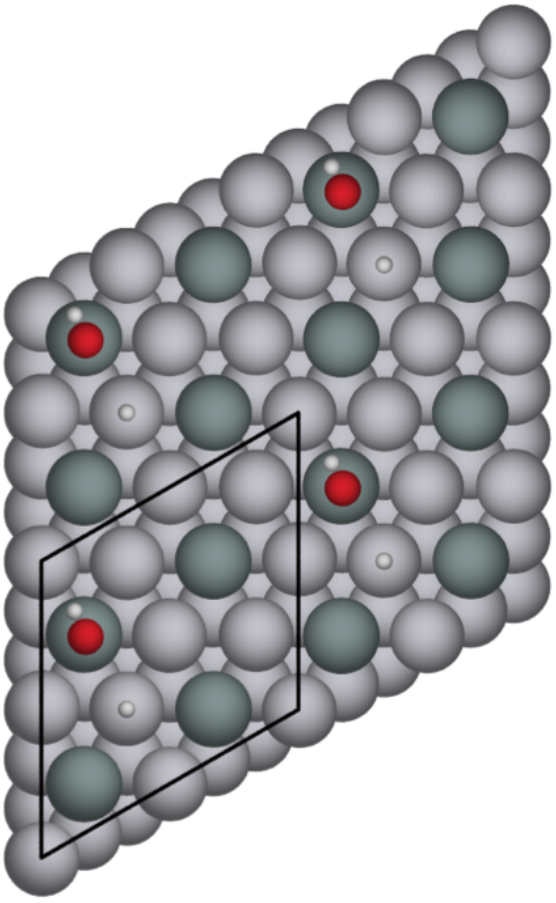

FIGURE 4.52: $E_{\text{ads}} = -0.220$ (eV), PtSn alloy with OH on Sn & H on Pt, started with OH on Sn & H on Pt, top view

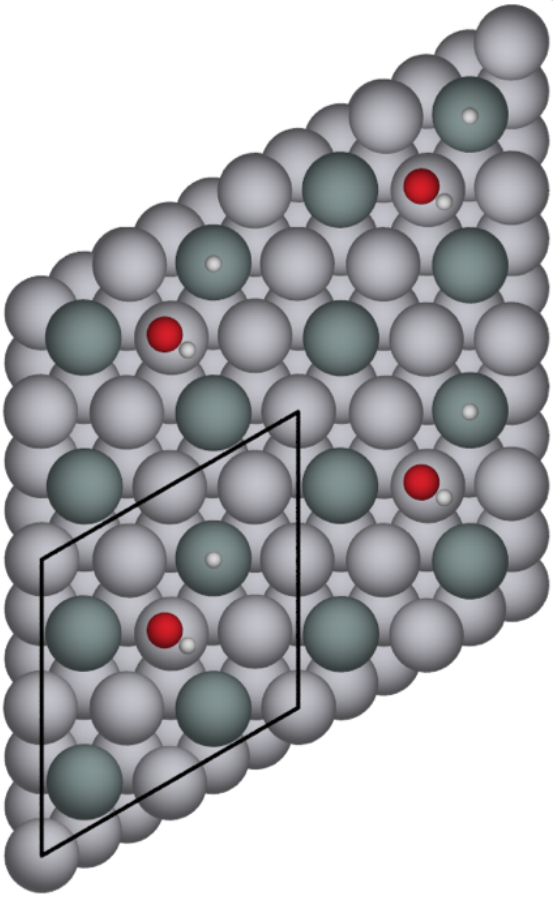

FIGURE 4.53: $E_{\text{ads}} = 1.325$ (eV), PtSn alloy with OH on M & H on Sn, started with OH on Pt & H on Sn, top view

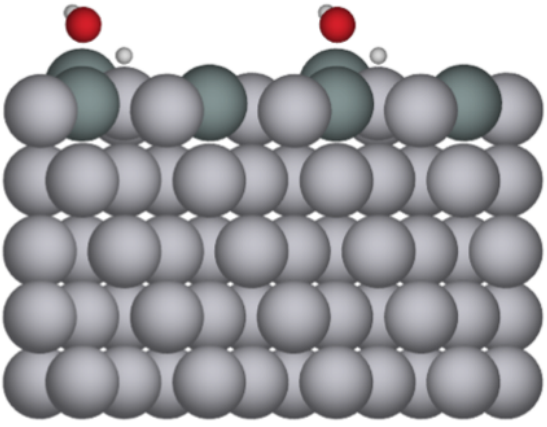

FIGURE 4.54: $E_{\text{ads}} = -0.220$(eV), PtSn alloy with OH on Sn & H on Pt, started with OH on Sn & H on Pt, side view

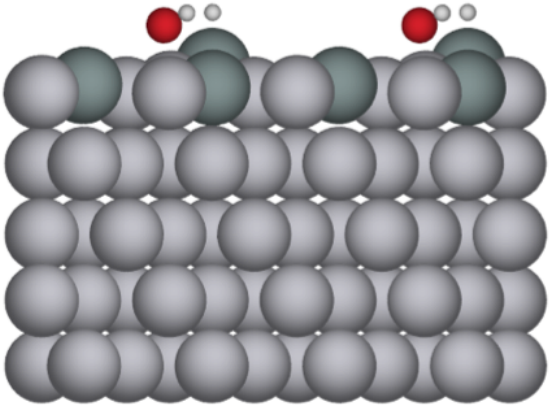

FIGURE 4.55: $E_{\text{ads}} = 1.325$ (eV), PtSn alloy with OH on M & H on Sn, started with OH on Pt & H on Sn, side view

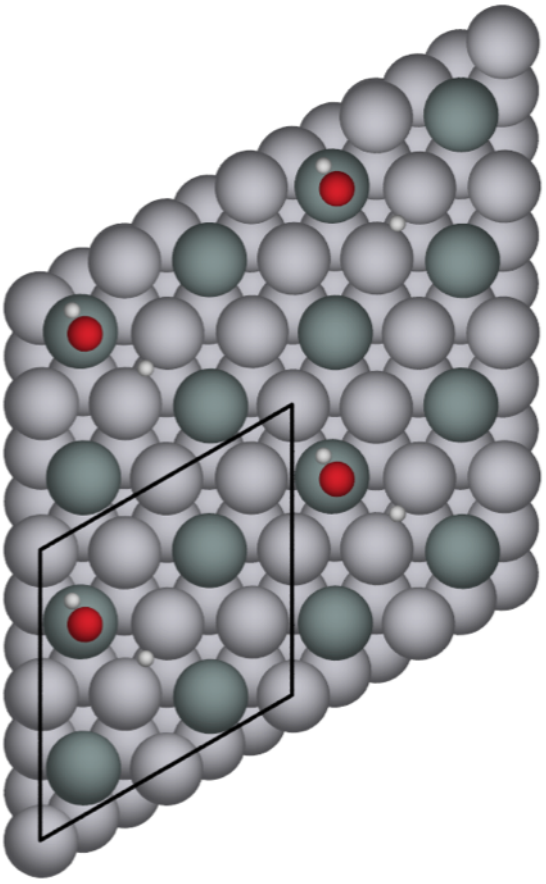

FIGURE 4.56: $E_{\text{ads}} = 0.225$ (eV), PtSn alloy with OH on Sn & H in bridge position between two Pt atoms, started with OH on Sn & H in hollow, top view

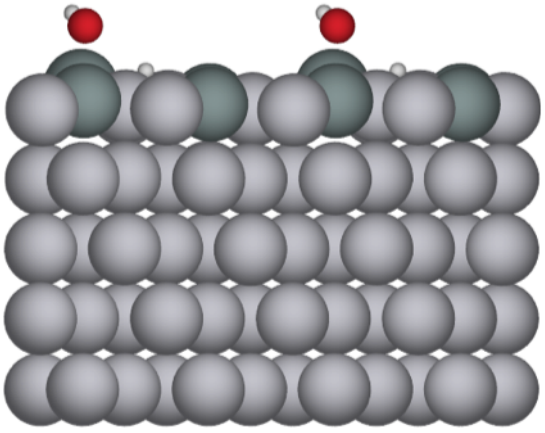

FIGURE 4.57: $E_{\text{ads}} = 0.225$ (eV), PtSn alloy with OH on Sn & H in bridge position between two Pt atoms, started with OH on Sn & H in hollow, side view

4.4 Conclusion

The surface rumpling varied across the different surface alloys with PdSn being the flattest surface and RhSn being the most rumpled surface.

From the models studied here the preferred adsorption site for intact water on different M alloys can be determined, as shown in Figure 4.58. For both rhodium and platinum it is clear that there is a very strong preference for the water to bind intact to a Sn atom present in the surface alloy. Silver and palladium show a much smaller adsorption energy difference and it was found in each that adsorption onto the bulk metal atom type in the surface alloy is marginally preferred. The adsorption energies for the most stable dissociated water structures have been shown with lines to show the general trends.

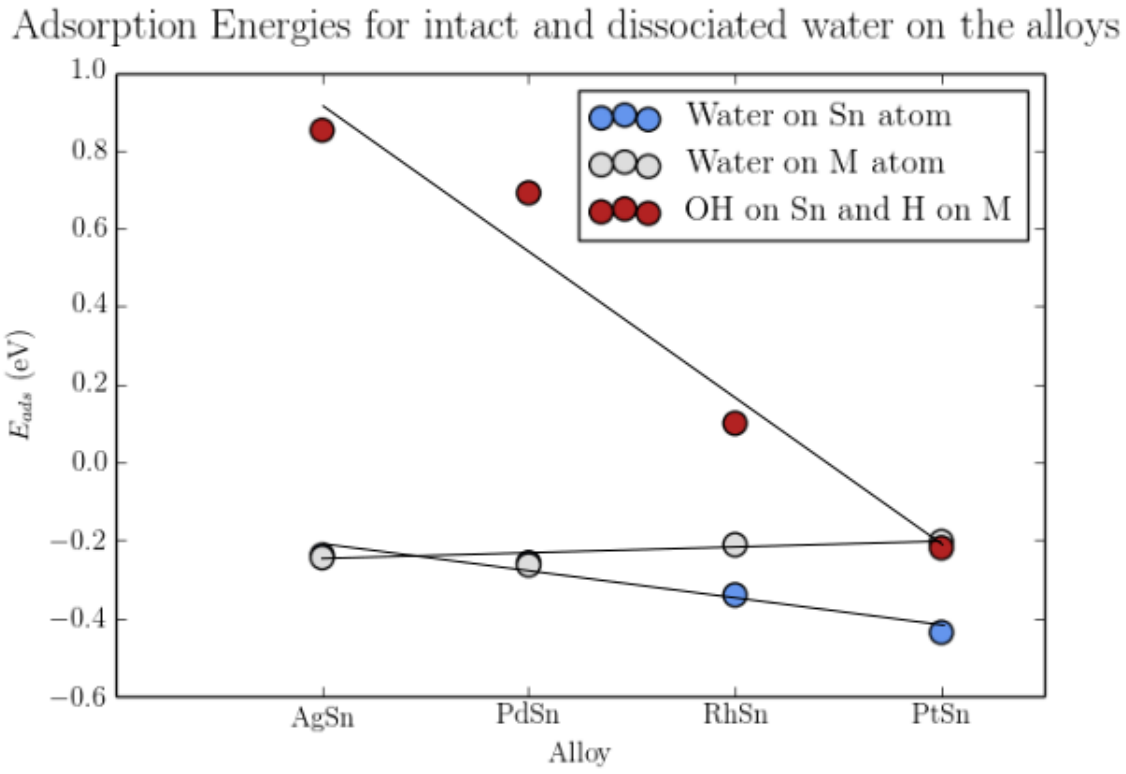

FIGURE 4.58: Adsorption energies for intact and dissociated H_2O on four alloy surfaces.

For the dissociated water it was found that only the PtSn alloy surface formed a stable dissociated structure relative to the gas phase, this had the hydroxyl bonded to a Sn atom and hydrogen bonded atop a Pt atom. Hydrogen binding on top of a Sn atom or hydroxyl bonding to a Pt atom led to unstable dissociation structures. Although rhodium had no stable dissociated structures it followed the same pattern as the platinum structure. In all cases adsorption of intact water was favoured.

The AgSn alloy also had no stable structures and the hydroxyl binds to the Sn atom in every structure no matter where it began in the relaxation. It was also the only surface alloy to have hydrogen move into a shifted hollow position furthest from the Sn atom, although this was less stable than when the hydrogen bonded to the atop position on the Sn atom.

The PdSn had no stable dissociated structures and preferred the hydrogen bonding to the palladium atom. The two most stable structures for this alloy had the hydroxyl bound either in the atop position on Sn or in the bridge position between two palladium atoms. The structures that had hydrogen bonded to the Sn atoms were the least stable with the hydroxyl bound to the Sn atom slightly more stable out of the two structures.

4.4.1 Future work

The electronic structure for the Sn-surface alloys could have been studied with more time; specifically the d-band center theory could have been used.[92] The

main idea of this theory is that the adsorption energy of an adsorbate on a metal surface is dependent on the electronic structure. The bonding orbital of the adsorbate hybridizes with the metal d-band forming bonding and anti-bonding states. The filling of the anti-bonding states of the metals depends on the surface density of states, i.e. the local electronic structure at the surface.[93] The adsorbate bonds more weakly to the surface with an increased filling of the anti-bonding states. The higher the d-band center is the higher the energy (relative to the Fermi level), this corresponds to a decrease in the filling of the anti-bonding state, resulting in stronger binding between the metal and the adsorbate. This model was created for hydrogen on metal surfaces, however it is also reasonable for oxygen or an oxygen containing species also.[94]

Pt binds oxygen very strongly; therefore the d-band center is too high. When Pt is alloyed with other non-precious metals, i.e. Ni, it lowers the d-band center and therefore the binding of the oxygen. Different alloys therefore show a means of tweaking the electronic structure. Looking at the electronic structures for each of the alloys studied here may have led to a better understanding of why certain surface alloys had the molecules and atoms bind in specific positions.

Chapter 5

CO + O catalysis on Cu(110)

5.1 Introduction

This chapter studies carbon monoxide oxidation on a Cu(110) surface, first the adsorption sites were studied and then the actual oxidation. Reactions pathways were being studied to try and understand what was being seen in the experimental calculations. Carbon monoxide reacting with oxygen that is part of the oxide surface was going to be compared to carbon monoxide reacting with an oxygen that was present on and separate to the oxide surface. However the latter calculation had some problems and it never converged.

Heterogeneous catalysis of CO oxidation has been studied using many noble metal catalysts and metal oxides previously, however these can be expensive so other metals are being considered including Cu.[95] In heterogeneous catalysis reactions proceed via many steps, each can influence the rate at which the reaction

proceeds by. The most common reaction mechanism in heterogeneous reactions is the Langmuir-Hinshelwood (L-H) mechanism which has both reactants adsorbed on the surface, these proceed to migrate to each other and collide causing a reaction leading to a product which then desorbs from the surface.

5.1.1 Oxygen adsorption on Cu(110)

Catalysts made out of copper are used in many industrial processes such as fuel cell electrodes or treatment of waste water. Exposure to oxygen at different pressures and temperatures will vary whether surface oxidation occurs or if the oxygen is just chemisorbed onto the surface.[96] Oxidation of the Cu surface is believed to play an important role in catalytic reactions.[9] Oxidation of Cu(110) can result in a p (4×1) added row (AR) structure at 1/4ML coverage or p (2×1) added row (AR) reconstructed surface, which corresponds to half a monolayer coverage of oxygen in the long-bridge sites, or a c (6×2) phase with 2/3 ML coverage, all shown in Figure 5.1.[97–99] The added row structure results in a decrease in the reactivity of the oxygen atoms.[100] At low pressure and low coverage oxygen will bind preferentially to the shifted hollow site on the non-reconstructed surface, shown in Figure 5.2.[9]

5.1.2 Carbon monoxide on Cu(110)

Carbon monoxide interacting with metal surfaces has been studied extensively with previous studies finding carbon monoxide adsorbs at the atop site on most

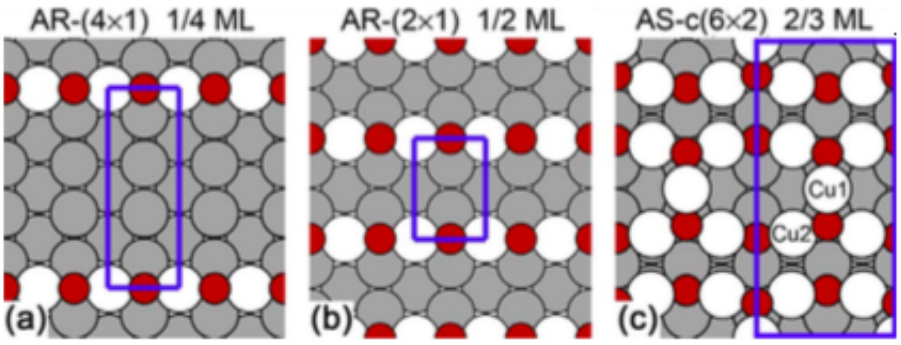

FIGURE 5.1: Top views of the favourable oxygen adsorption structures on Cu 110. Shown are (a) the 1/4 ML oxygen coverage added row (4×1) structure characterized by Cu-O chains in the 100 direction, (b) the added row (2×1) structure with 1/2 ML coverage with a closer spacing of the Cu-O chains, and (c) the *c* (6×2) structure with 2/3 ML oxygen. Large white and gray circles represent top and second layer Cu atoms, respectively. Small dark red circles represent O atoms. The rectangles indicate the surface unit cells used in the calculations. In the *c* (6×2) structure, the non-equivalent Cu atom sites Cu1 and Cu2 are indicated. Reproduced from [9].

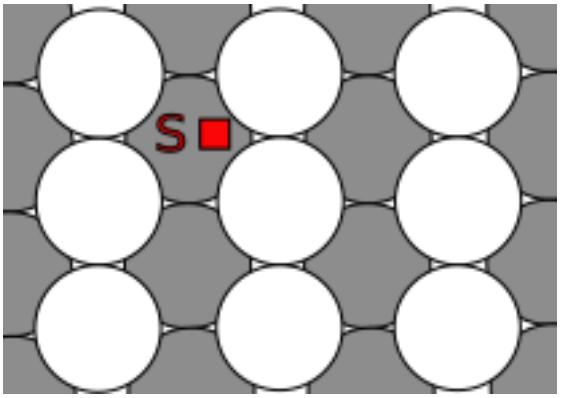

FIGURE 5.2: Non-reconstructed Cu(110) surface with the shifted hollow site highlighted by the red square. Top layer Cu atoms are coloured white and second layer Cu atoms are coloured grey. Adapted from [9].

Cu surfaces, including Cu(110).[101] It was also found at coverages up to 0.5ML that the CO molecule is in the upright position.[102, 103] When the monolayer coverage of CO is increased tilting of the CO molecule from the upright position may occur, shown in Figure 5.3.[10] Another study has shown carbon monoxide to bond to the Cu(110) surface preferentially in the short bridge position, with an adsorption energy of -1.13eV. The atop position was nearly as stable at -1.09eV and then the longbridge site quite a bit less stable at -0.66eV, this is a similar trend to some of the data found in this chapter.[104]

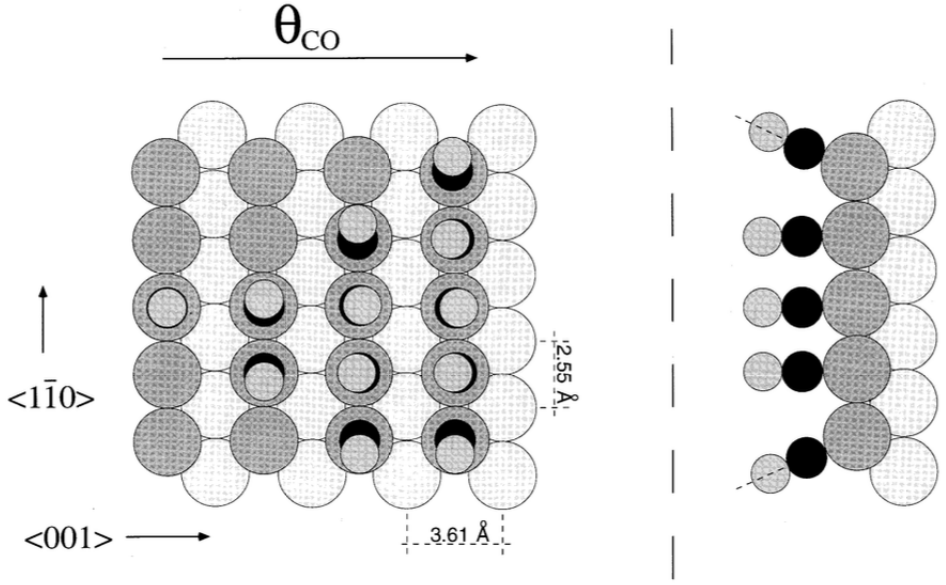

FIGURE 5.3: Linear chain model for the adsorption of CO on Cu 110 , schematically shown for increasing coverage moving from left to right. Reproduced from [10].

5.1.3 CO oxidation on Cu(110)

When one CO binds onto the Cu(110) reconstructed oxide surface it binds to the Cu atom in the Cu-O- chains in either the tilted or straight up orientation.[105] The oxidation of CO to CO_2 on oxygen covered Cu(110) occurs between two adsorbed species, as shown in Equation 5.1.[11, 106] Oxygen atoms on unreconstructed Cu(110) surface are 25 times more likely to react compared to the oxygens in the reconstructed surface.[107]

$$CO_{(ad)} + O_{(ad)} \rightarrow CO_{2(g)} \tag{5.1}$$

5.1.4 Slab geometries

This chapter will show many figures of the surface to make it clear what the colour of the atoms refers to shown in Figure 5.4. This shows the overall view of the bulk oxide surface without the presence of any oxygen, this is to make it clear what each of the colours show. Each colour is still a copper atom, with the darkened atoms being the bulk of the system and the lighter atoms being the top atoms. The intermediate coloured show the first full row of atoms. The normal Cu(110), non reconstructed surfaces have the same colouring just without the top lighter atoms.

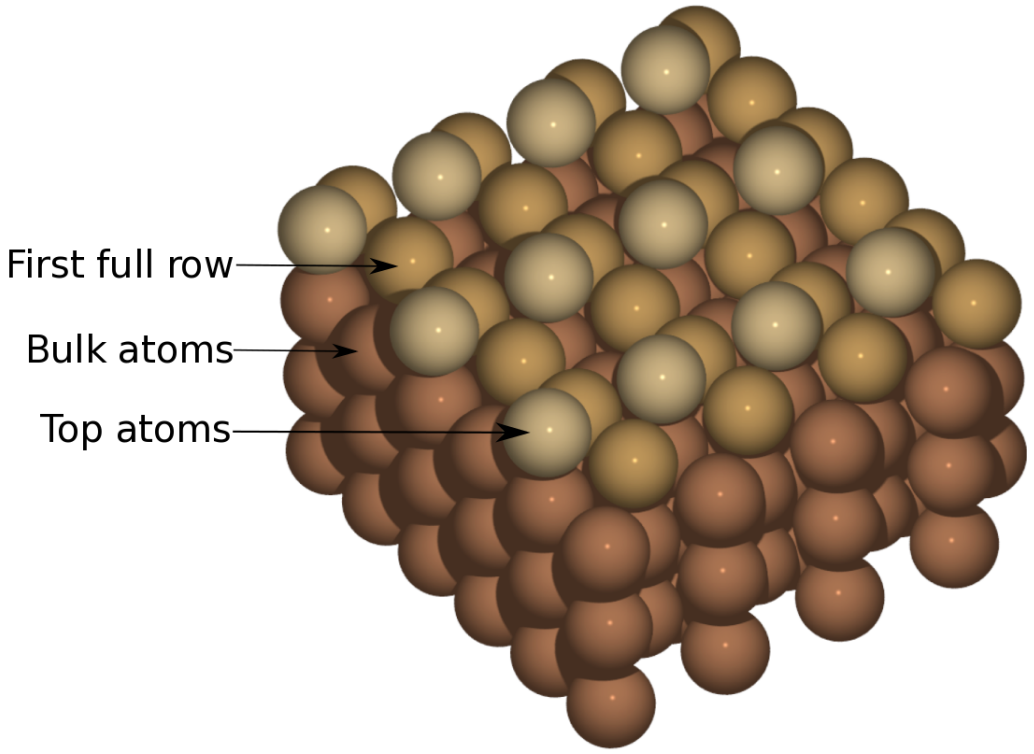

FIGURE 5.4: Cu reconstructed added row surface without oxygen present showing what the colours refer to which layer

Most of the figures will show a top view and side view so the unit cell size can be shown in the top view figures. For the reconstructed oxide surface these will

look as follows in Figures 5.5 and 5.6 the colours are the same as in the previous Figure 5.4.

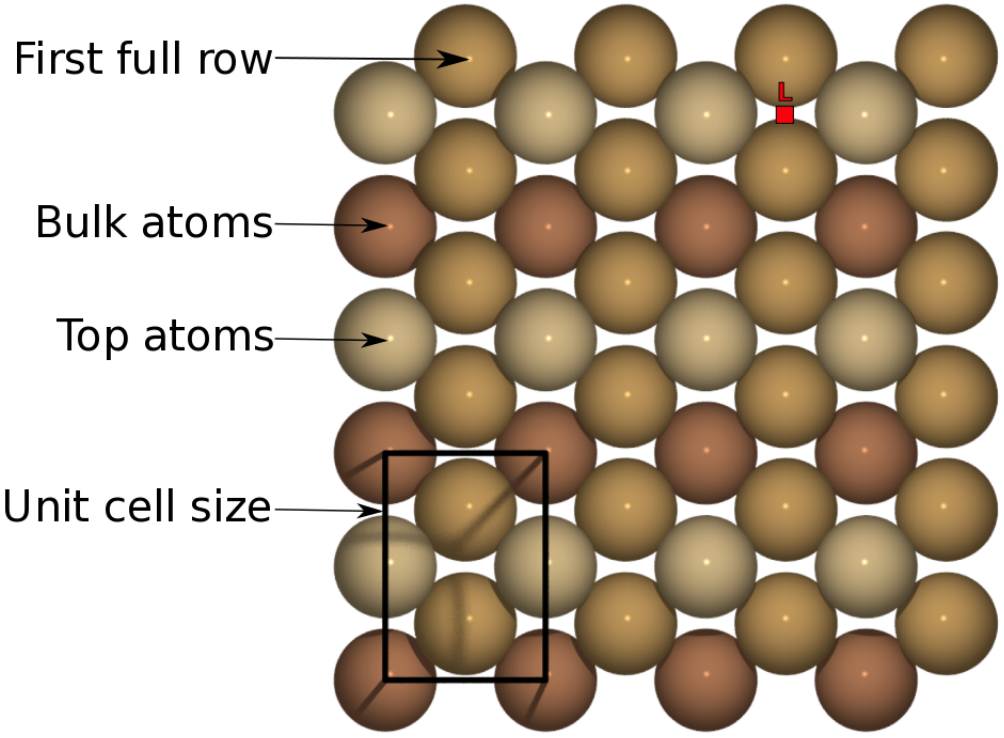

FIGURE 5.5: Cu(110) added row oxide surface without oxygen present showing which colours refer to which layer. Also shown by red squares L shows the longbridge position that oxygen takes in this added row reconstruction.

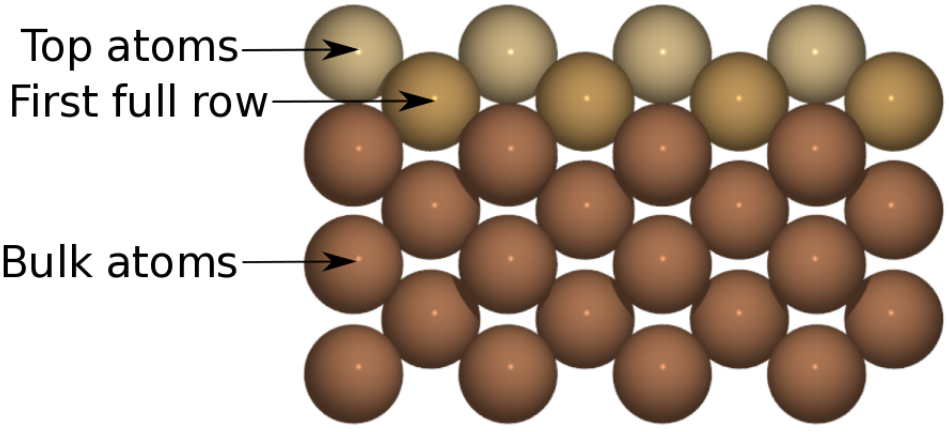

FIGURE 5.6: Cu surface without oxygen present showing which the colours refer to which layer

Figure 5.7 shows the unreconstructed Cu(110) surface from above with the possible adsorption sites present. The side view has also been shown in Figure 5.8. Cu(110) is important to study with its stepped surface and many possible adsorption sites.

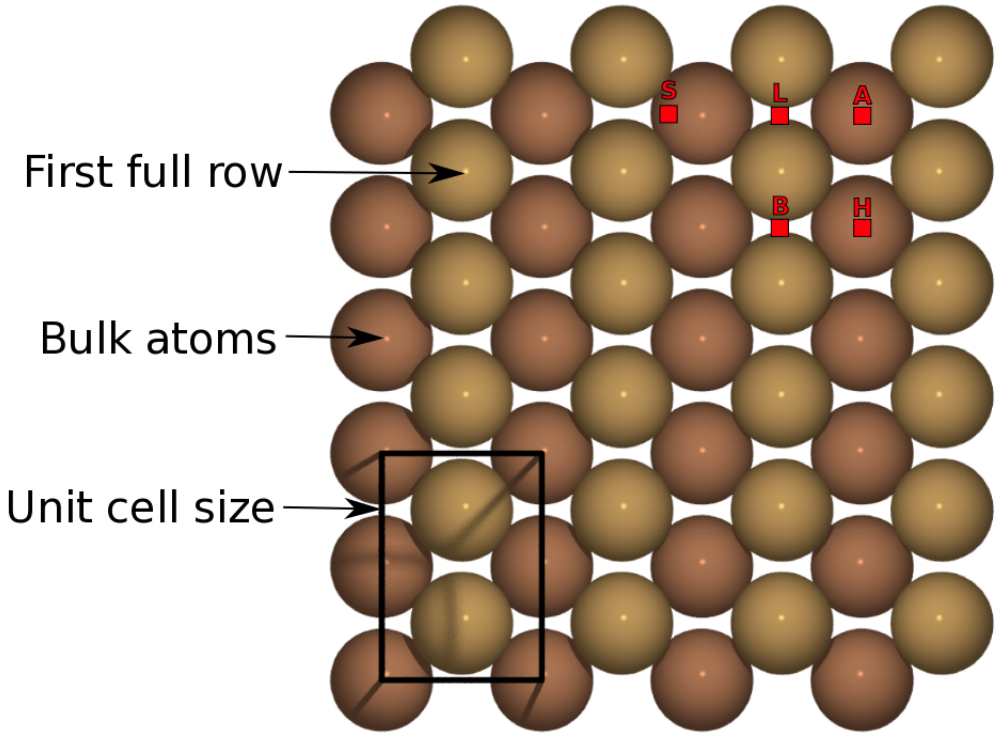

FIGURE 5.7: Cu(110) surface without oxygen present showing which colours refer to which layer. Also shown by red squares A shows atop site, B shows bridge site, H shows hollow site, L shows the longbridge position and S shows the shifted hollow position.

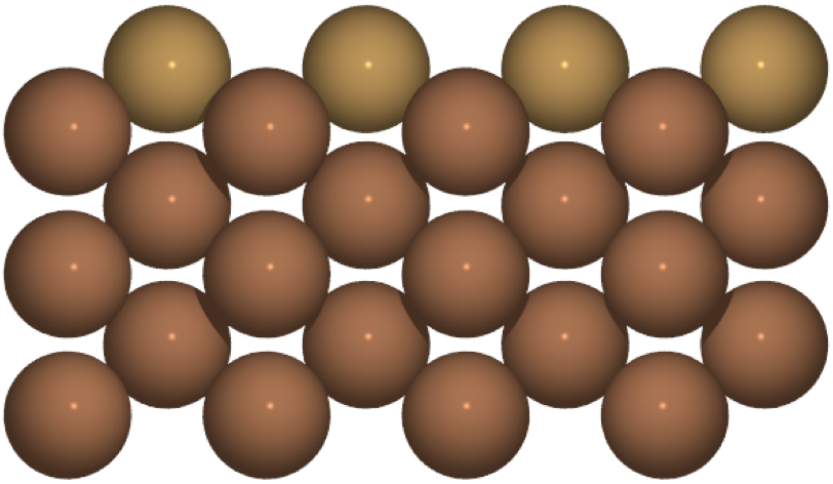

FIGURE 5.8: Cu(110) surface just no longer has the top atoms, side view.

5.2 Method

5.2.1 Calculation Details

The DFT calculations were once again carried out using Vienna *ab-initio* Simulation Package (VASP) with electron-ion core interactions described using the Projecter Augmented Wave (PAW) method with a plane wave basis-set, discussed in chapter 2. A Gamma centered grid of 5 x 5 x 1 was used for the k-point sampling of the Brillouin zone in the (4 x 3) unit cell, which was 10.6Å x 10.92Å and a 16 x 11 x 1 k- point grid was used for the (2 x 1) unit cell size, 4.46Å x 5.15Å. These had a cut off energy of 400 eV. This simulation was performed using a 7-layer Cu(110) slab. The bottom 3 layers of the metal in each system are constrained with only the top 4 allowed to relax. Each unit cell has a 13Å vacuum gap to reduce any interaction due to the periodicity of the cell. The structures were relaxed so that all the ionic forces were < 0.01 eV Å^{-1}. The O_2 molecule been given an electron spin = 1 as the triplet state of oxygen is energetically more favourable.

5.2.2 Adsorption Energies

The adsorption energies were calculated using the equation shown in 5.2.

$$E_{\text{ads}} = \frac{1}{n}\left(E(Total) - E(Cu) - n(oxygen) \times \frac{1}{2}E(O_2)\right) \tag{5.2}$$

Where E(Total) is the total energy of the relaxed Cu(110) surface with oxygen present, E(Cu) is the total energy of the clean Cu(110) surface, n(oxygen) is the number of oxygen atoms present in the overlayer and E(O_2) is the total energy of an oxygen molecule in the gas-phase, this is divided by 2 to get the energy for a single oxygen atom. This was calculated with spin polarised corrections. Where n is the total number molecules adsorbed on the surface.

There is a constant shift between calculated and experimental findings estimated at -1.36eV per O_2 molecule with GGA.[108] This is due to adding electrons to the oxygen p orbital in O_2 to form O^2- when the surface oxide is made. As this would change every adsorption energy equally it has not been taken into account.

5.3 Results

5.3.1 Oxygen adsorption on Cu(110) in a (2x1) unit cell

Calculations were performed to identify the preferred position of oxygen on a Cu(110) surface. It can be seen from Table 5.1 that oxygen was bound more strongly in the shifted hollow position. The calculations that started out in the atop, bridge and hollow position relaxed into the shifted hollow position, shown in Figure 5.9.

TABLE 5.1: Calculated adsorption energies of different adsorption positions of oxygen on Cu(110)

Position	Adsorption Energy (eV)
Longbridge	−2.186
Shifted hollow	−2.333

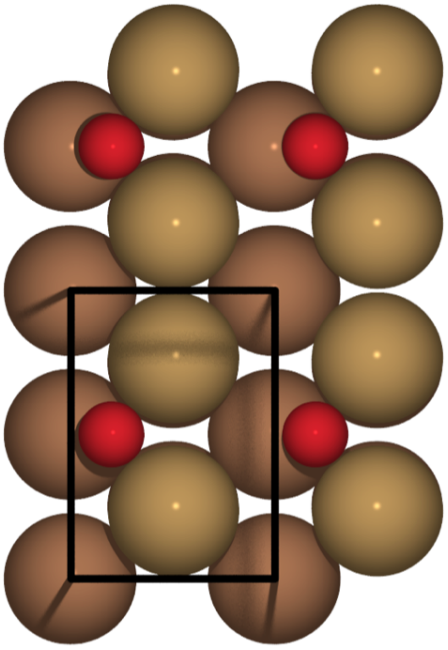

FIGURE 5.9: Oxygen in shifted hollow on Cu(110) top view

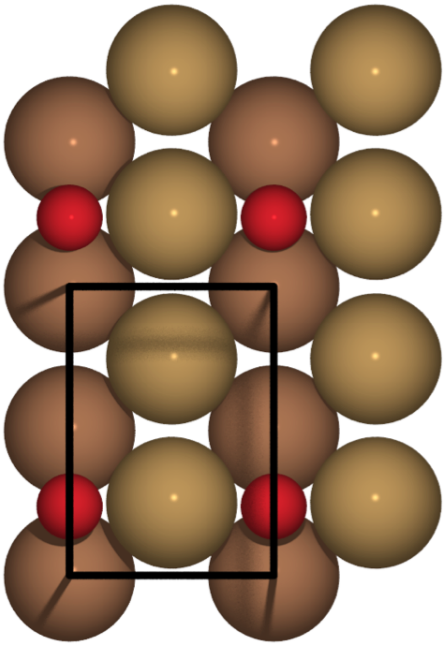

FIGURE 5.10: Oxygen in longbridge on Cu(110) top view

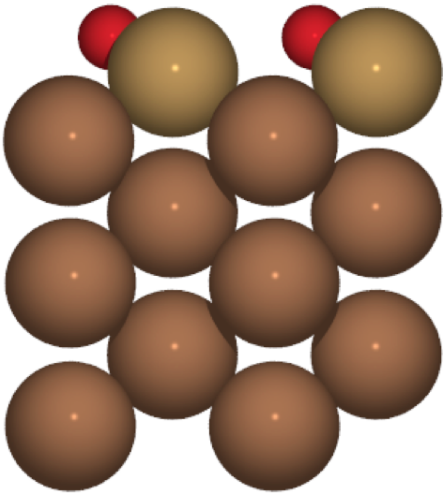

FIGURE 5.11: Oxygen in shifted hollow on Cu(110) side view

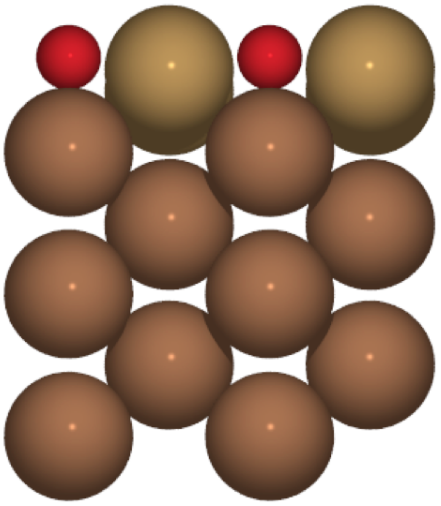

FIGURE 5.12: Oxygen in longbridge on Cu(110) side view

The longbridge calculation relaxed to have the Cu atoms in the row with the oxygen atoms pulled slightly out from the bulk, as can be seen slightly in Figure 5.12, while the other Cu atoms in the first full row remained in the expected position.

5.3.2 CO adsorption on Cu(110) in a (2x1) unit cell

Calculations were performed to identify the preferred position of carbon monoxides on a Cu(110) surface. As can be seen from Table 5.2 it was bound more strongly in the bridge position, as is shown in Figure 5.13. The structure that began relaxation with CO in the hollow site had the CO molecule relax into the bridge position also. There is not too much difference between the adsorption energies and the results found here agree with some previous studies for one single CO molecule.[104] The atop geometry is almost as tightly bound as the bridge and is shown in Figure 5.15. While the longbridge calculation has the CO molecule pulled away from the

surface, which probably explains the weaker adsorption energy, as can be seen in Figure 5.18.

TABLE 5.2: Calculated adsorption energies of different adsorption positions of carbon monoxide on Cu(110)

Position	Adsorption Energy (eV)
Bridge	−0.977
Atop	−0.972
Longbridge	−0.645

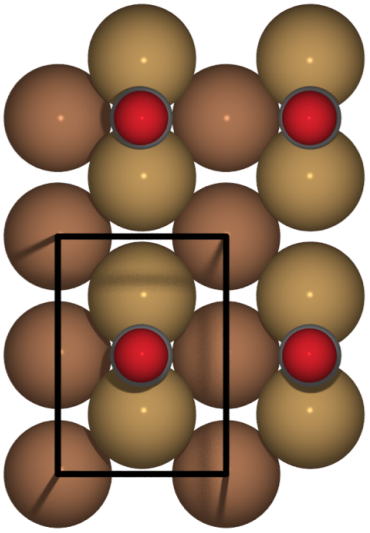

FIGURE 5.13: Carbon monoxide in the bridge position on Cu(110) top view

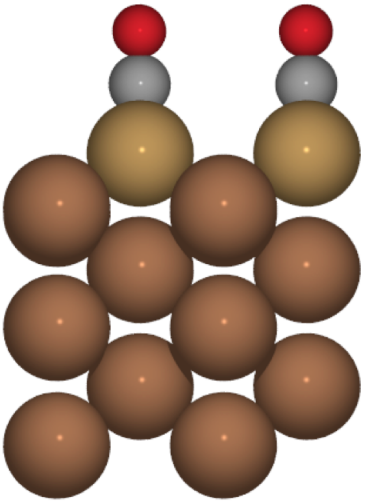

FIGURE 5.14: Carbon monoxide in the bridge position on Cu(110) side view

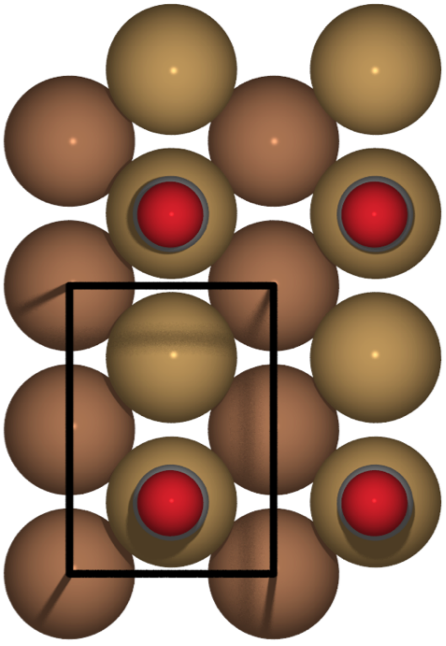

FIGURE 5.15: Carbon monoxide in the atop position on Cu(110) top view

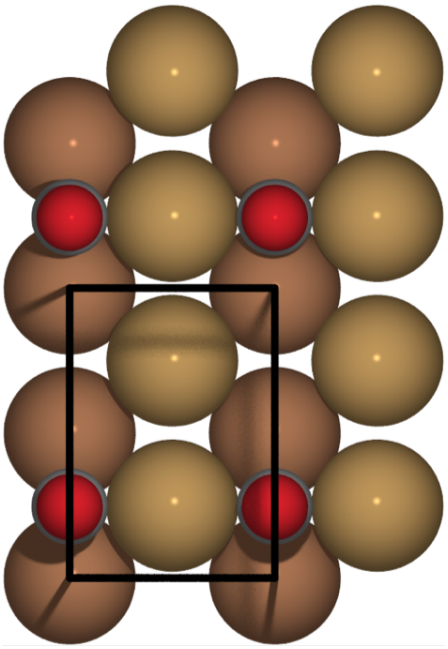

FIGURE 5.16: Carbon monoxide in the long-bridge position on Cu(110) top view

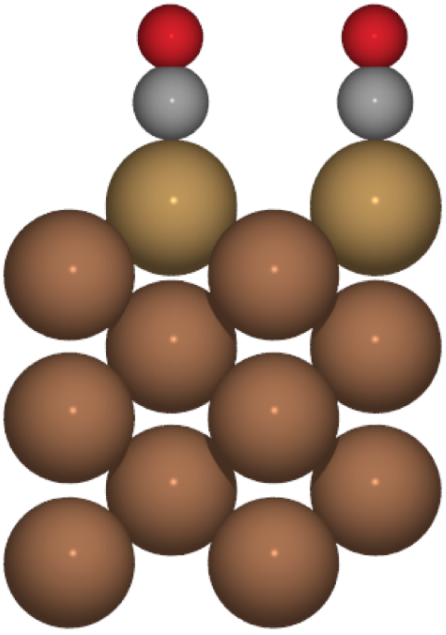

FIGURE 5.17: Carbon monoxide in the atop position on Cu(110) side view

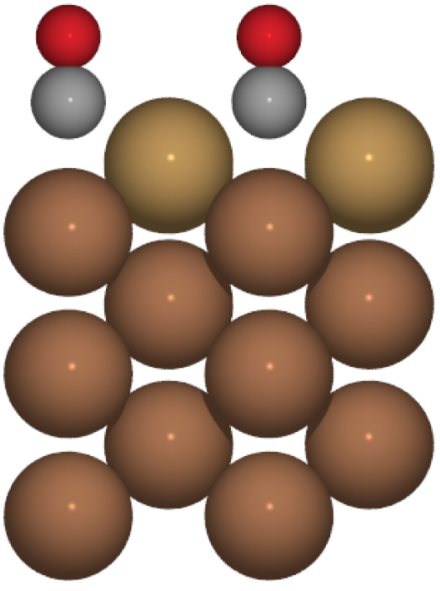

FIGURE 5.18: Carbon monoxide in the long-bridge position on Cu(110) side view

5.3.3 Oxygen adsorbed in a reconstructed added row (2x1) & (4x3) unit cell size

A small (2x1) reconstructed overlayer was looked at first to relax the surface into the preferred structure quickly before creating the larger (4x3) unit cell. The adsorption energy per oxygen molecule can be seen in Table 5.3.

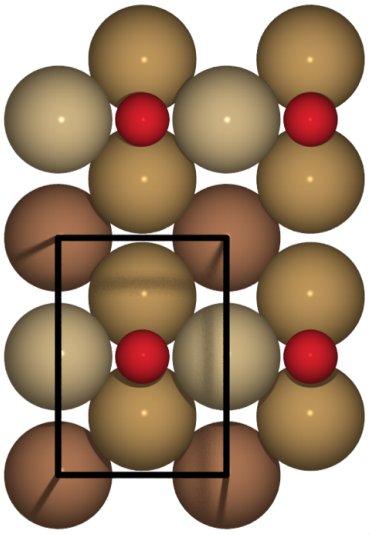

FIGURE 5.19: Oxygen in longbridge on reconstructed added row Cu(110) (2x1) top view

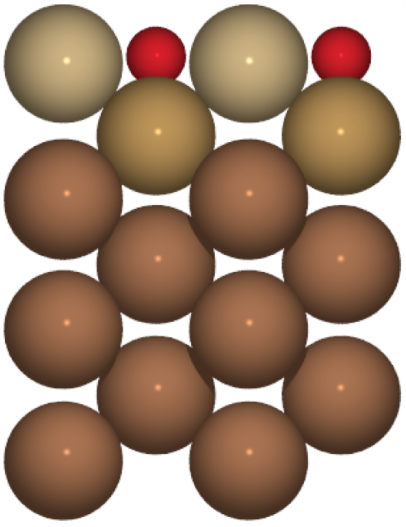

FIGURE 5.20: Oxygen in longbridge on reconstructed added row Cu(110) (2x1) side view

TABLE 5.3: Calculated adsorption energies of different adsorption positions of oxygen on Cu(110)

Unit cell size	Number oxygen present	Adsorption Energy (eV)
(2x1)	1 oxygen in longbridge	−2.289
(4x3)	6 oxygen in longbridge	−2.290
(4x3)	5 oxygen in longbridge	−2.253

A larger (4x3) unit cell size was then looked at as this is the size we would be looking at the reactions in, as can be seen in Table 5.3. Figure 5.21 shows the six oxygens adsorbed in each of the longbridge sites in a reconstructed added row structure in a (4x3) unit cell.

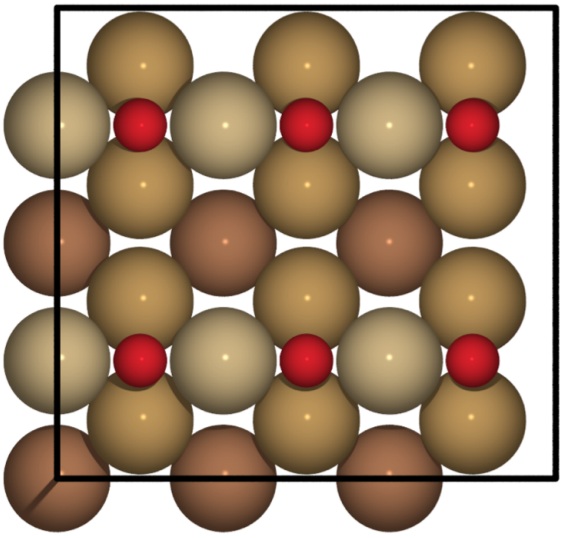

FIGURE 5.21: 6 oxygens in longbridge site on Cu(110) (4x3) unit cell size top view

When one of these oxygens is removed the remaining oxygens are bound less strongly to the surface as can be seen from the energies in Table 5.3. The surface with five oxygens present in the (4x3) unit cell size is shown in Figure 5.23, it can be seen that the copper atoms in the position adjacent to the gap caused by the removal of one oxygen have moved slightly in toward the gap.

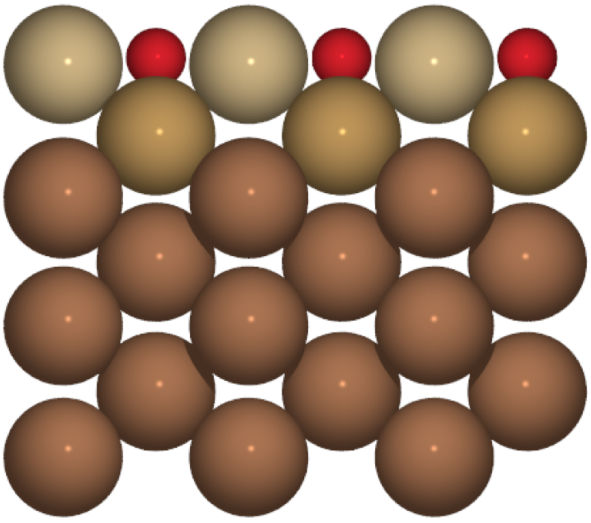

FIGURE 5.22: 6 oxygens in longbridge site on Cu(110) (4x3) unit cell size side view

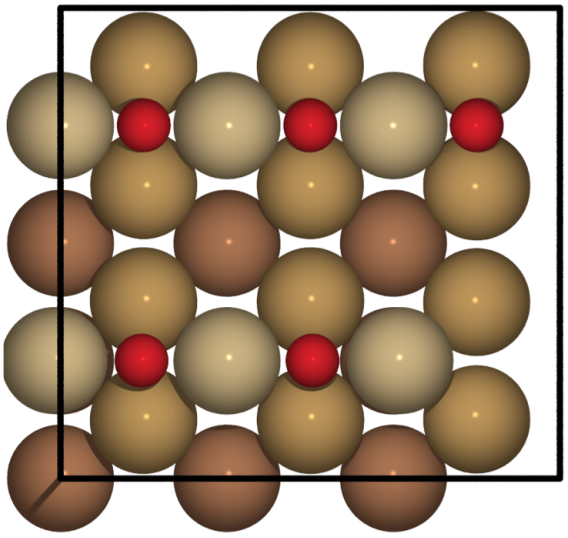

FIGURE 5.23: 5 oxygens in longbridge site on Cu(110) (4x3) unit cell size top view

5.3.4 Carbon monoxide bonding to pre-oxidised surface

Some calculations have been performed to try and look at carbon monoxide and oxygen bonding to form carbon dioxide. This has first been looked at with carbon monoxide bonding to the oxide surface shown in Figure 5.21. The carbon monoxide was initially positioned above the surface as a gas phase molecule, to look at where on the surface it would bond. The calculation relaxed to have the carbon monoxide bonding to the surface in the atop site position- as shown in Figure 5.25 it is

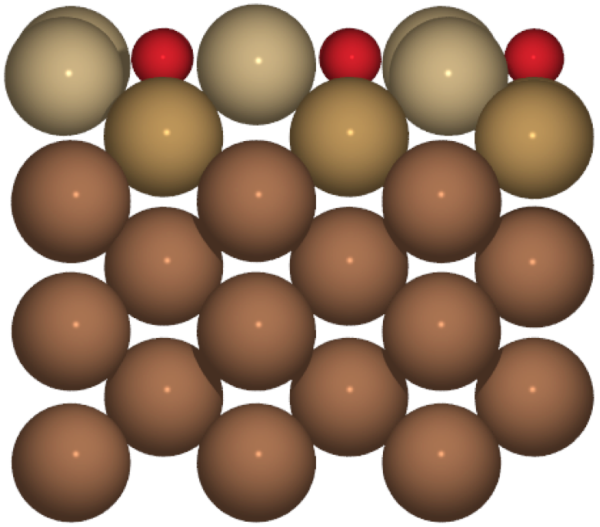

FIGURE 5.24: 5 oxygens in longbridge site on Cu(110) (4x3) unit cell size side view

slightly tilted. Another calculation was performed with the carbon monoxide in the straight up atop position- it can be seen in Figure 5.26. It was found to remain in this position with the same adsorption energy, of −0.467eV. These differences are probably more to do with the minimisation pathway followed in each structure as opposed to the CO molecule always being tilted if it bonds to the surface from the gas phase. It has simply found a low energy configuration and stayed there.

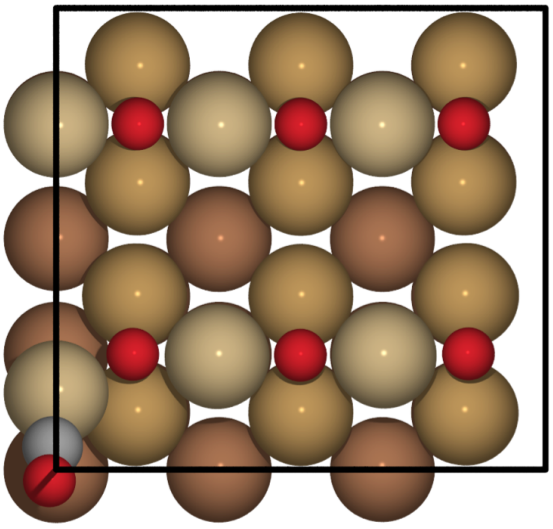

FIGURE 5.25: One carbon monoxide molecule adsorbed from the gas phase onto the oxide top view

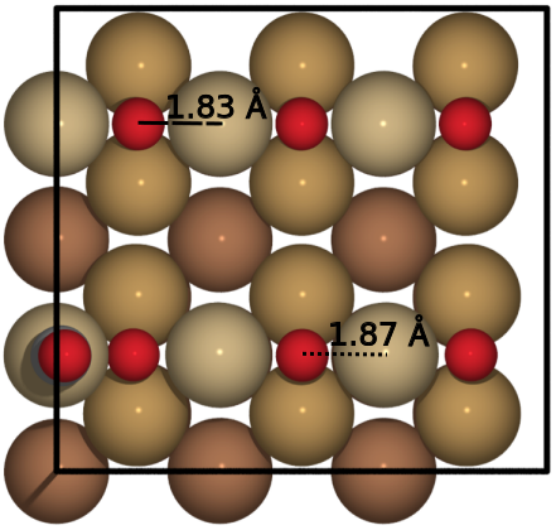

FIGURE 5.26: One carbon monoxide on the oxide in the atop position top view

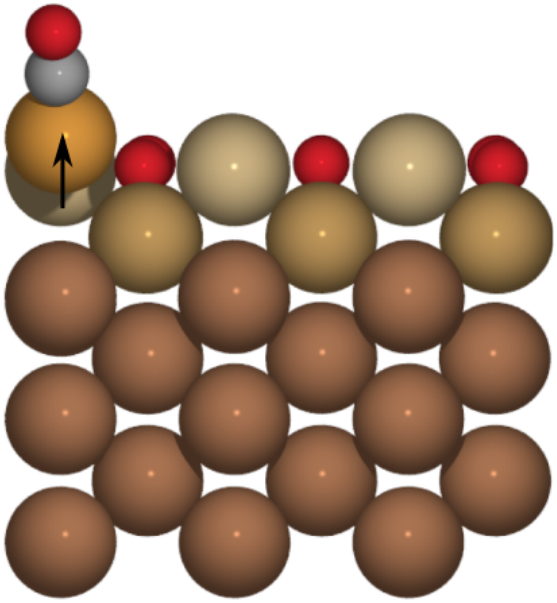

FIGURE 5.27: One carbon monoxide molecule adsorbed from the gas phase onto the oxide side view

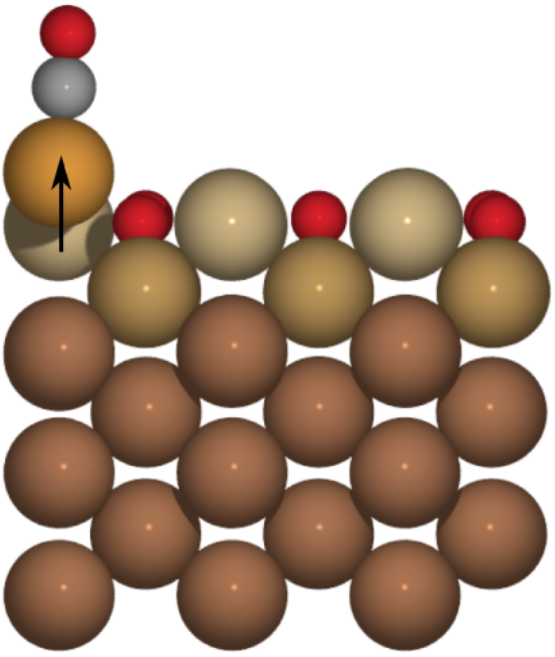

FIGURE 5.28: One carbon monoxide on the oxide in the atop position side view

Both structures show little difference in bonding within the overlayer, the carbon monoxide bonds 1.8Å± 0.1Å above the copper atom, which is pulled approximately 1Å away from its usual position, as shown with the arrows in the figures. The bond distance between the oxygens and copper atoms in the rows is smaller in the row that does not have the carbon monoxide bound to one of the copper atoms at 1.83Å as shown by the dashed line in Figure 5.26, than in the other row. This has them all bonding at 1.87Å, shown by the dotted line in Figure 5.26, except for the oxygens bonding to the copper atom that have been pulled away from the surface which have a slightly larger distance of ∼2Å.

A structure was relaxed with CO_2 above the oxide structure with one oxygen removed as shown in Figure 5.29. This calculation was performed to look at CO and O reacting to result in CO_2 so nudged elastic band calculations could be

performed, however these did not converge. As can be seen in Figure 5.30 the structure has had the two copper atoms on either side of the vacant oxygen site moved towards each other and the bulk slightly. This is very different from the copper atoms pulled away from the surface when the CO is bound atop one of them, as seen in figures 5.25 and 5.26.

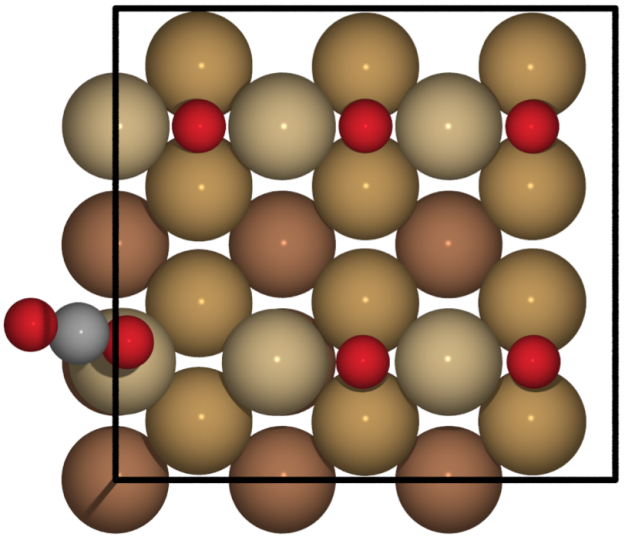

FIGURE 5.29: CO_2 above 5 oxygens in longbridge site on Cu(110) (4x3) unit cell size top view

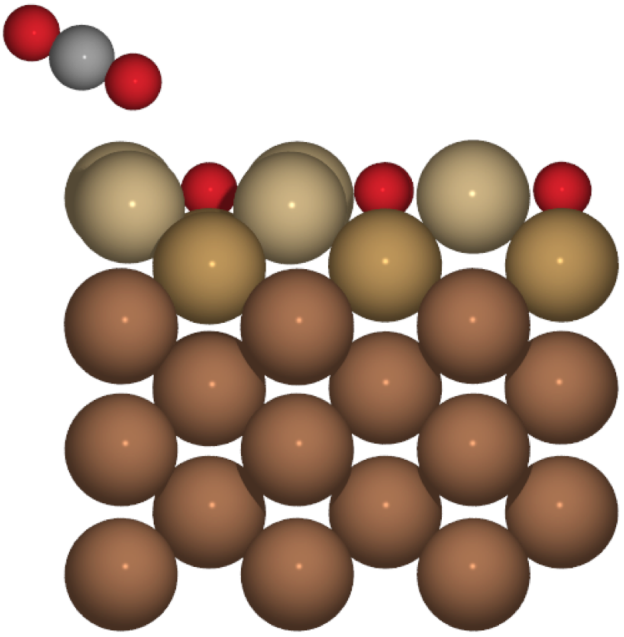

FIGURE 5.30: CO_2 above 5 oxygens in longbridge site on Cu(110) (4x3) unit cell size side view

The total energies of carbon monoxide on the oxide surface and CO_2 desorbed off the Cu(110) added row oxide surface are shown in Table 5.4. Looking at the total energies CO_2 desorbed from the surface is shown to be preferential so the barrier for CO_2 desorption must be large for it to not happen.

TABLE 5.4: Total energies of carbon monoxide on oxide surface and CO_2 desorbed off Cu(110)

Structure	Total Energy (eV)
CO on oxide surface	−326.147
CO_2 desorbed	−326.624

The adsorption energies per CO molecule for different numbers of carbon monoxide adsorbed onto the oxide surface are shown in Table 5.5. As it can be seen the more carbon monoxide molecules present the less strongly bound to the surface they are.

TABLE 5.5: Calculated adsorption energies of different adsorption positions of carbon monoxide on Cu(110)

Number carbon monoxide present	Adsorption Energy (eV)
1CO on oxide surface	−0.467
5CO on oxide surface	−0.395
6CO on oxide surface	−0.384

An oxide surface was calculated with 6CO present as can be seen in Figure 5.31 this caused quite a shift with none of the CO in an upright position and some of the top layer copper atoms shifted so they are no longer between the oxygen atoms. As can be seen in Figure 5.33 every copper atom that a CO is adsorbed onto has been pulled away from the bulk as was seen when one CO was adsorbed in the atop position.

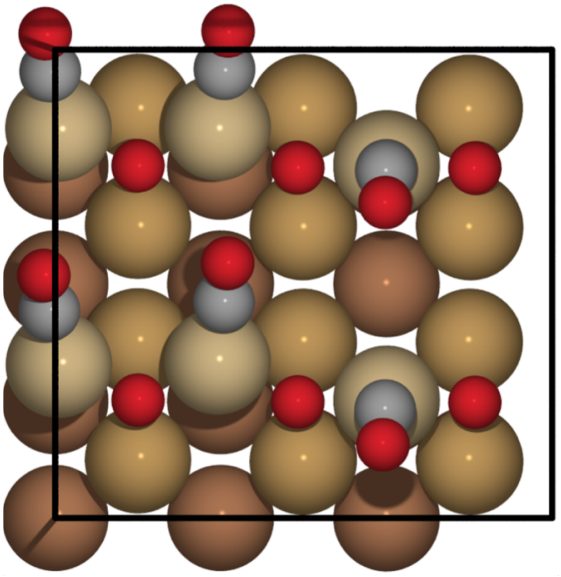

FIGURE 5.31: Six carbon monoxide molecule adsorbed onto the oxide top view

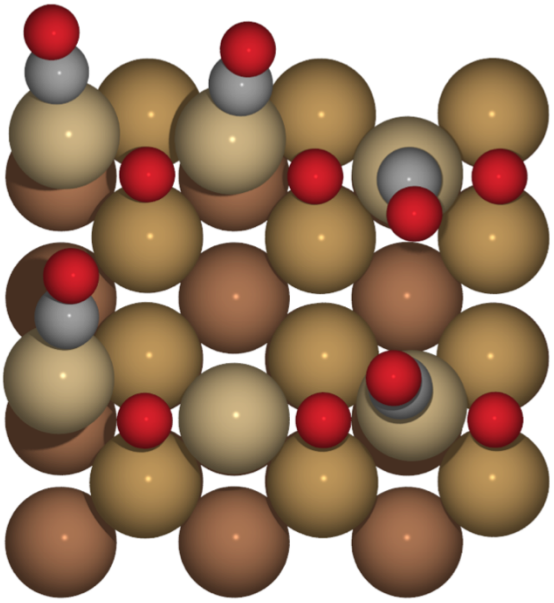

FIGURE 5.32: Five carbon monoxide on the oxide in the atop position top view

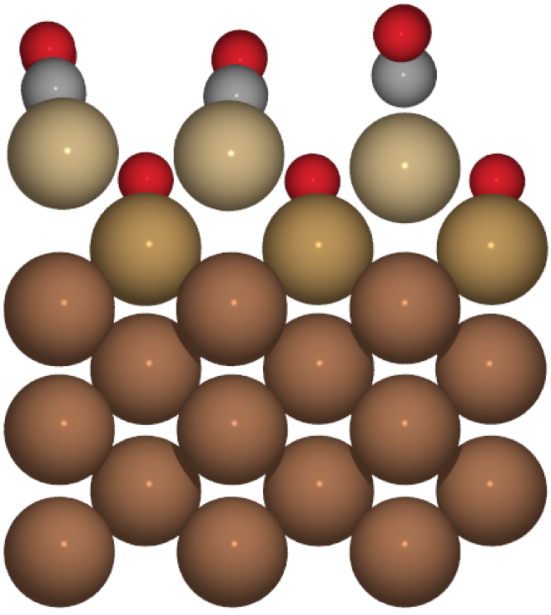

FIGURE 5.33: Six carbon monoxide molecule adsorbed onto the oxide side view

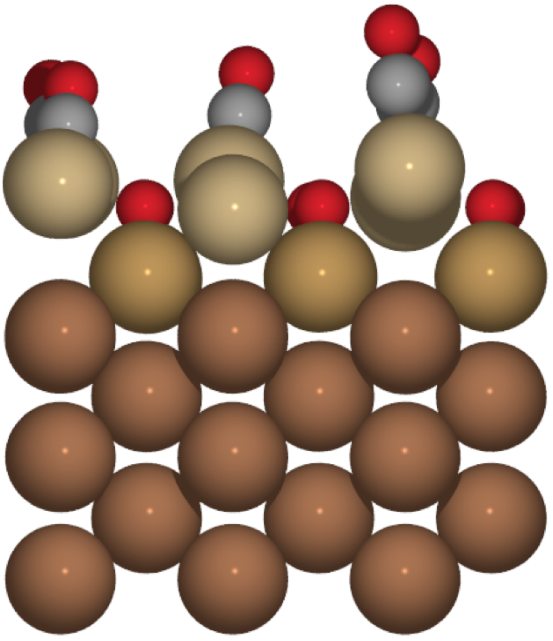

FIGURE 5.34: Five carbon monoxide on the oxide in the atop position side view

Another oxide surface with 5 carbon monoxide molecules present was looked at to study the energy needed to remove one CO molecule from the surface. As can be seen in Figure 5.32 the molecules are once again very unorganised as seen in Figure 5.31. Figure 5.34 shows that only the copper atom in the top layer that has no carbon monoxide adsorbed on top is close to the bulk as seen in the clean oxide surface.

5.4 Conclusion

This study found that on the non-reconstructed (2x1) Cu(110) surface the shifted hollow site was the preferred position for O to bind. It binds less strongly than in the added row reconstruction that has oxygen in the longbridge position, -1.653eV compared to -2.289eV.

Carbon monoxide was found to bind preferentially in the bridge site on the non-reconstructed surface, however there was only a very small difference between that and the atop site of -0.005eV. When carbon monoxide was in the gas phase above the added row oxide surface it moved to the surface and bound in the atop position. The Cu atom the carbon monoxide molecule binds to on the oxide surface is always pulled away from the surface.

As expected oxygen will not readily be removed from the oxide surface to form CO_2, even with increasing quantities of carbon monoxide. This is interesting as the total energies show a preference for CO_2 desorption compared to CO being bound to the oxide surface, as shown in Table 5.4, therefore the barrier to this

desorption must be large. The more carbon monoxide molecules bonded to the Cu(110) added row oxide structure the less strongly bound to the surface they are, as shown in Table 5.5.

It can also be observed that CO molecules are less strongly bound on the oxide than the clean surfaces. On the clean surface one CO molecule adsorbs strongest in the bridge position at -0.977eV. For the oxide surface one CO molecule adsorbs in the atop position at -0.467eV showing it is bound much weaker to the oxide.

Chapter 6

Concluding remarks

The work presented in this thesis has been studied to try and understand how different adsorbates bond to transition metals. Water has been studied closely here as it is readily available in the atmosphere and is also a by product of some common catalytic processes as both reactants and intermediates.

First the overlayers formed on Rh(111) were studied as the bilayer model has been shown to be an oversimplification. The structure of the water overlayers created on metals are a balance between the optimisation of the water-metal interaction and the water-water hydrogen bonding.[24–26] From experimental work presented for the water overlayers on Rh(111) it was known that the unit cell size was likely (6x6) and the ratio on water to hydroxyl was likely 2:1 or 3:1. A mixed rather than pure water overlayer was expected due to the surface being predosed with oxygen which was therefore likely to cause dissociation of some of the water

molecules. From the structures considered it was possible to confirm that Bjerrum defects were not favoured on Rh(111). For mixed H_2O:OH overlayers it was found that the 2:1 structures with no hydroxyl molecules binding to other hydroxyl molecules were the most stable out of all the structures studied. However it is not possible to confirm a specific structure due to how close the energies lie between the most stable structures. The 1:1 structure with strictly alternating hydroxyl and water molecules was the only other structure that was similar in stability to the 2:1 structures, this however would have had a smaller (3x3) unit cell size.

Although the way the experiment was performed did not yield in pure water overlayers these were examined to understand if the water would bond in a H-down or H-up orientation. For the mixed overlayers the H-up orientation was preferred until the 5:1 ratio of water to hydroxyl, at this point the H-down overlayer was preferred. For the pure water structures the H-down position was preferred for the dangling water molecules, also it can be confirmed that chains or lines of dangling or flat water molecules gives the preferred pure water structures.

Single water molecules on different surface alloys were looked at namely AgSn, PdSn, PtSn and RhSn. The water molecules were studied both intact and dissociated to determine the preferred binding positions and ability to dissociate on the surfaces. These were being studied to see if there was a reasonable pattern across the series for preferred binding positions possibly due to charges on atoms or the surface rumpling.

The surface rumpling varied across the different surface alloys with PdSn being the flattest surface and RhSn being the most rumpled surface. However

there were no clear correlations in whether the water or hydroxyl molecules chose to bind to specific atoms. For all the systems studied intact water was more stable on the surface compared to in the gas phase. AgSn and PdSn both show no preference for adsorption on the Sn or transition metal surface atoms. For RhSn and PtSn the water was bound more strongly to the Sn atom in both cases.

The PtSn surface alloy was the only one that formed a stable dissociated structure compared to gas phase water with the hydroxyl molecule bound to the Sn atom and the hydrogen bonded atop the Pt atom. For every alloy surface the hydroxyl molecule preferred to bind to the Sn atom in the surface and for most the hydrogen was bonded to the transition metal in the surface. The only exception to this was AgSn were the hydrogen preferred to bind atop one of the Sn atoms. Although the charges and various structure characteristics of the surface were studied from the information available a pattern explaining preferred binding positions was not found.

For the CO oxidation on Cu(110) firstly the adsorption sites on the non-reconstructed surface were studied followed by carbon monoxide bonding onto the oxidised surface. This was done to increase our knowledge and get a better understanding of CO oxidation on Cu(110). On the non-reconstructed (2x1) Cu(110) surface the shifted hollow site was the preferred position for O to bind although it was bound less strongly than in the added row reconstruction that has oxygen binding in the longbridge position, forming an oxide structure.

Carbon monoxide was found to bind preferentially in the bridge site on the non-reconstructed surface in this study although the atop site had a very similar

adsorption energy and it is the atop position that has been found to be preferential before.[10] When carbon monoxide bonded to the oxide surface it did so in the atop position on the Cu in the Cu-O chains. This Cu atom was pulled away from the rest of the surface.

The more carbon monoxide molecules bonded to the Cu(110) added row oxide structure the less strongly bound to the surface they are. The total energies shown in Table 5.4 show a preference for CO_2 desorbed above the surface with oxygen having been removed compared to CO being bound to the full oxide surface, therefore the barrier to this desorption must be large. CO molecules are also shown to bond more strongly to the clean surface than the oxide surface.

In summary this work has endeavoured to increase the understanding of some small molecules bonding to surfaces. To achieve a fuller understanding the combination of experimental and theory work is required as alone there are still many questions to be answered.

Furthermore, the range of systems investigated here emphasise important aspects of similar systems that attention should be paid to in future computational work. These include, trying to gain a better understanding of alloy structures, including bulk alloys, as aposed to just the surface alloys shown here, and also nano alloy particles. The reactions of carbon monoxide with hydrogen could also be studied to understand the energetics to make methanol and water which would link well with the work studied in this thesis.

Appendix A

PBE data for Rh(111)

The data obtained with the Perdew-Burke-Ernzerhof exchange correlation functional is presented in this appendix. These calculations were done as a starting point to work out which overlayer structures were preferred. From this knowledge the structures that were to be calculated with the van der Waals functional were decided and it is those that are discussed in the main rhodium Chapter 3.

A.1 1:1 H_2O:OH

A table showing the adsorption energies of the 1:1 H_2O:OH structures is shown below in Table A.1. Both of these strucutres were then also looked at with van der Waals forces and are discussed in the main rhodium Chapter 3.

TABLE A.1: Calculated adsorption energies of PBE 1:1 H_2O:OH structures on Rh(111)

Figure	Type	PBE E_{ads} (meV)	Run with VdW
Figure A.1	(3x3) Alternating	-567	Yes
Figure A.2	(3x3) 3 OH Chains	-547	Yes

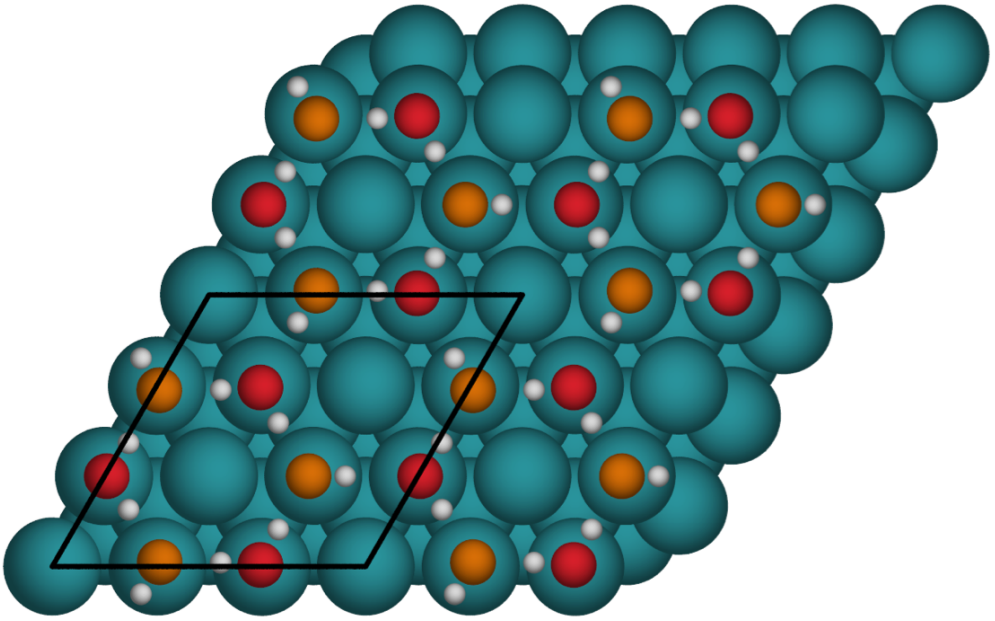

FIGURE A.1: 1:1 Alternating water(red) and hydroxyl(orange) overlayer top view. Calculated with van der Waals and shown in Figure 3.18.

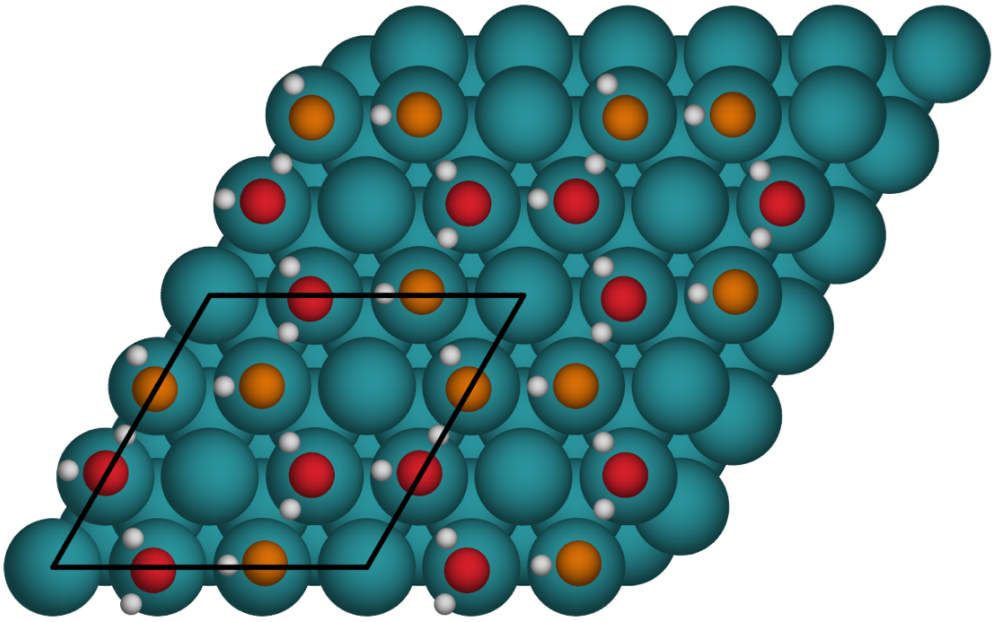

FIGURE A.2: 1:1 Chains water(red) and hydroxyl(orange) overlayer top view. Calculated with van der Waals and shown in Figure 3.22.

A.2 2:1 H_2O:OH

A table showing the adsorption energies of the 2:1 H_2O:OH structures is shown below in Table A.2. From these calculations it was clear that the Bjerrum defects were less stable than the structures with the hydroxyl molecules not donating to other hydroxyl molecules. This led to only one of the Bjerrum defect overlayers being looked at with van der Waals and more structures being made with the hydroxyl molecules separate from each other.

TABLE A.2: Calculated adsorption energies of different 2:1 H_2O:OH structures on Rh(111)

Figure	Type	PBE E_{ads} (meV)	Run with VdW
Figure A.3	(3x3) Bjerrum defects	-559	No
Figure A.4	(3x6) Bjerrum defects	-557	No
Figure A.5	(3x6) Bjerrum defects	-557	No
Figure A.6	(3x6) Bjerrum defects	-554	No
Figure A.7	(6x6) Bjerrum defects	-560	No
Figure A.8	(6x6) Bjerrum defects	-562	No
Figure A.9	(6x6) Bjerrum defects	-559	No
Figure A.10	(6x6) Bjerrum defects	-559	No
Figure A.11	(6x6) Bjerrum defects	-561	No
Figure A.12	(6x6) Bjerrum defects	-558	No
Figure A.13	(6x6) Bjerrum defects	-561	No
Figure A.14	(6x6) Bjerrum defects	-560	No
Figure A.15	(6x6) Bjerrum defects	-560	No
Figure A.16	(6x6) Bjerrum defects	-559	No
Figure A.17	(6x6) Bjerrum defects	-553	No
Figure A.18	(6x6) Bjerrum defects	-561	No
Figure A.19	(6x6) Bjerrum defects	-563	Yes
Figure A.20	(6x6) Bjerrum defects	-555	No
Figure A.21	(6x6) Chains of 2 hydroxyls	-560	No
Figure A.22	(6x6) Alternating	-592	Yes
Figure A.23	(6x6) Alternating	-593	Yes

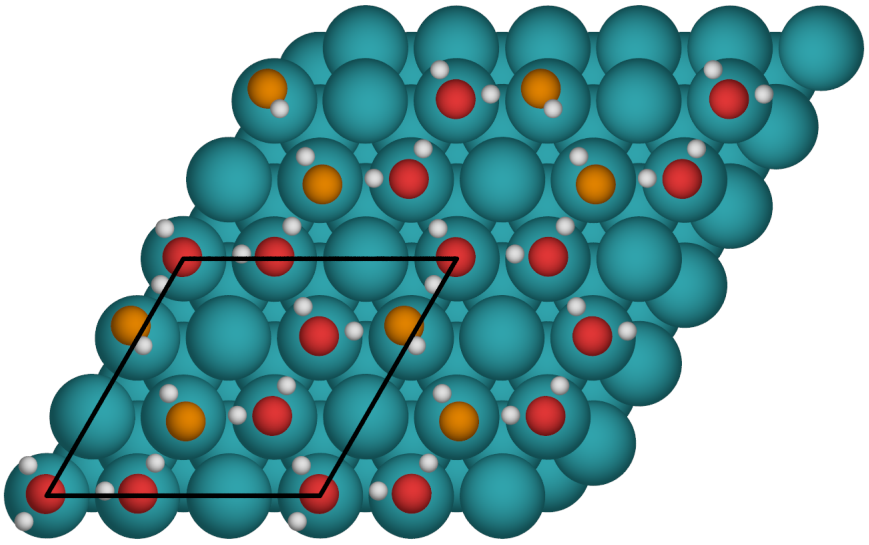

FIGURE A.3: 2:1 (3x3) Bjerrum defect, water(red) and hydroxyl(orange) overlayer top view

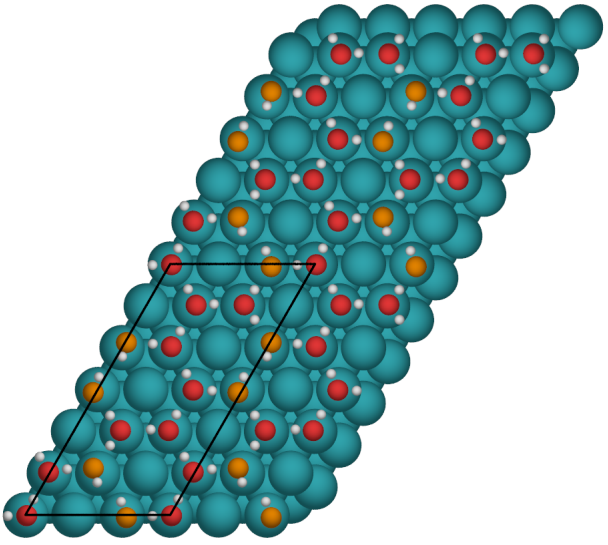

FIGURE A.4: 2:1 (3x6) Bjerrum defect, water(red) and hydroxyl(orange) overlayer top view

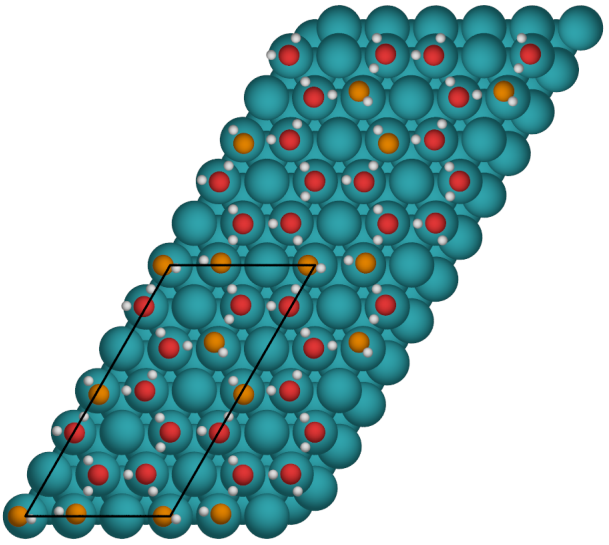

FIGURE A.5: 2:1 (3x6) Bjerrum defect, water(red) and hydroxyl(orange) overlayer top view

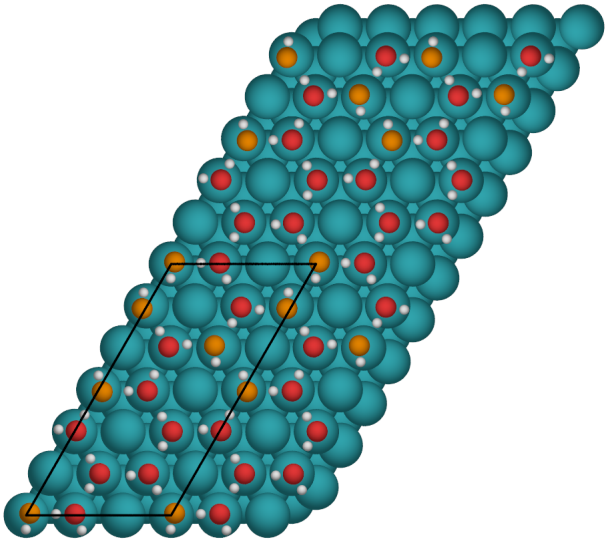

FIGURE A.6: 2:1 (3x6) Bjerrum defect, water(red) and hydroxyl(orange) overlayer top view

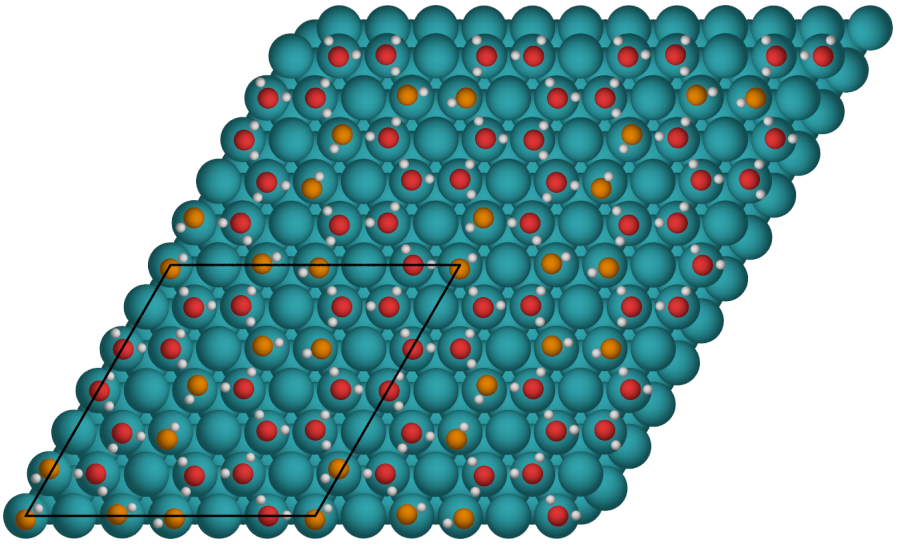

FIGURE A.7: 2:1 (6x6) Bjerrum defect, water(red) and hydroxyl(orange) overlayer top view

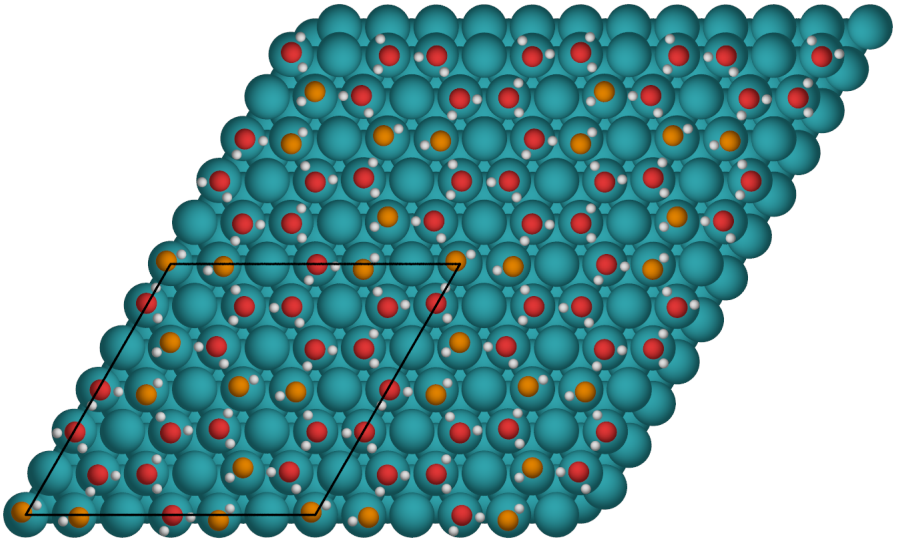

FIGURE A.8: 2:1 (6x6) Bjerrum defect, water(red) and hydroxyl(orange) overlayer top view

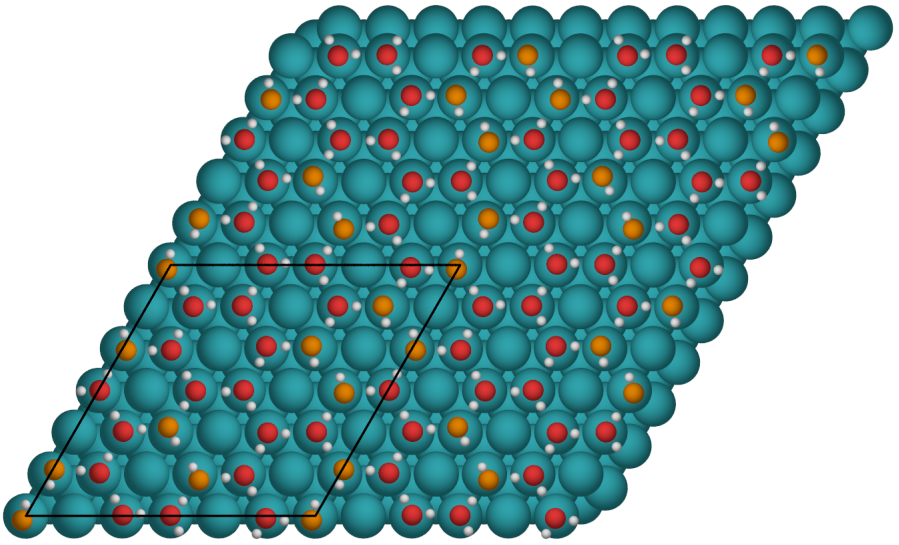

FIGURE A.9: 2:1 (6x6) Bjerrum defect, water(red) and hydroxyl(orange) overlayer top view

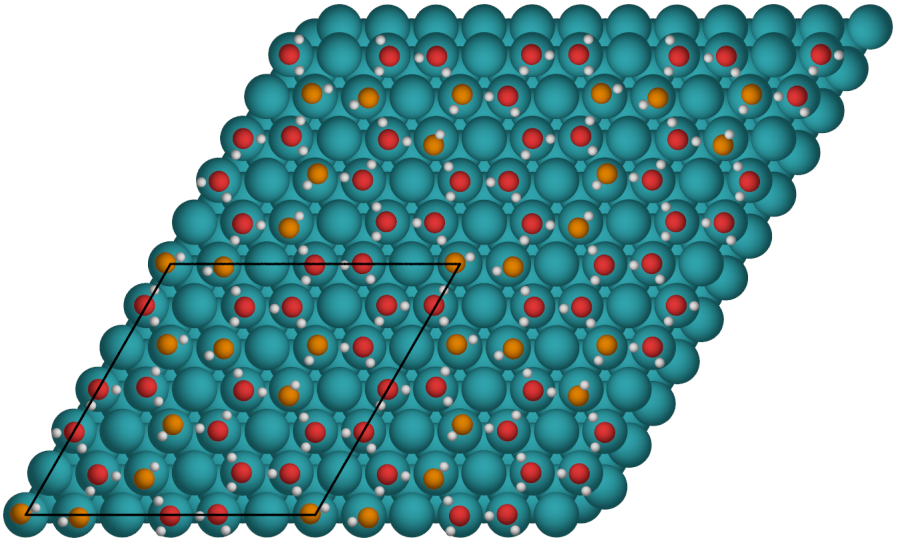

FIGURE A.10: 2:1 (6x6) Bjerrum defect, water(red) and hydroxyl(orange) overlayer top view

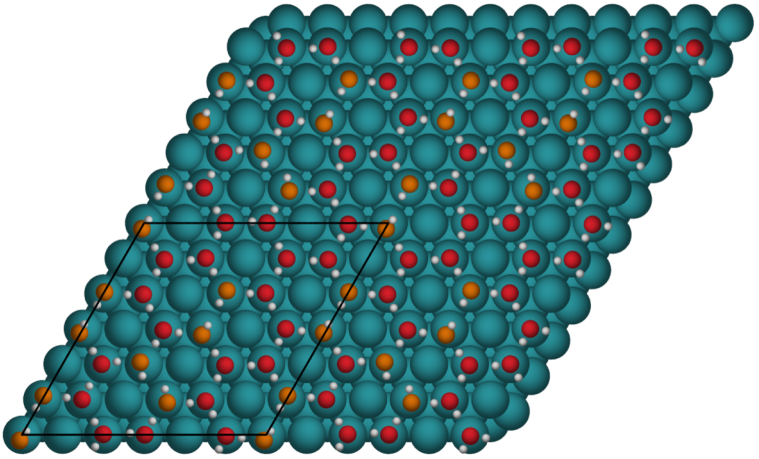

FIGURE A.11: 2:1 (6x6) Bjerrum defect, water(red) and hydroxyl(orange) overlayer top view

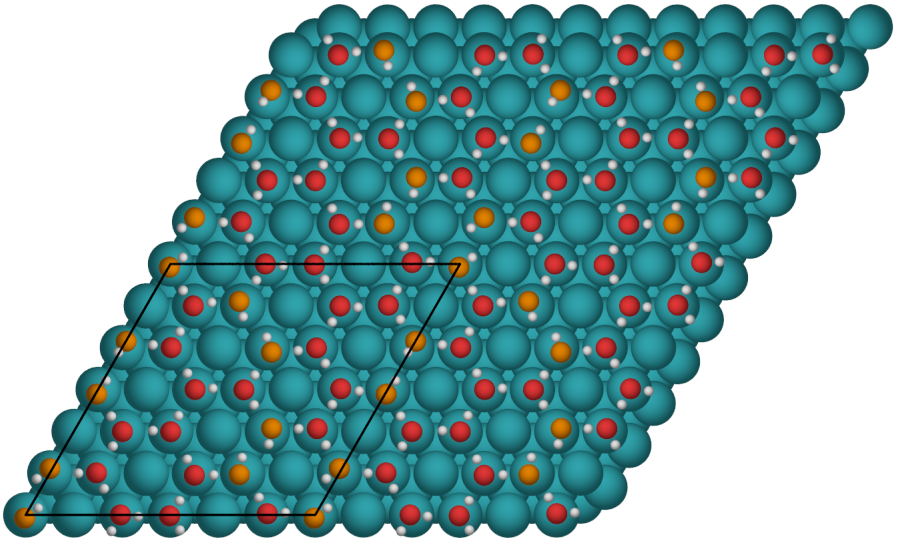

FIGURE A.12: 2:1 (6x6) Bjerrum defect, water(red) and hydroxyl(orange) overlayer top view

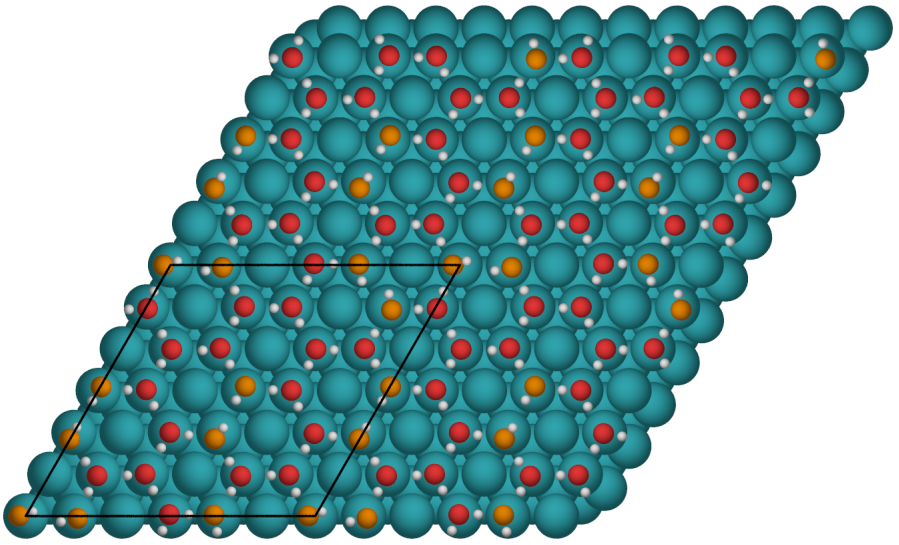

FIGURE A.13: 2:1 (6x6) Bjerrum defect, water(red) and hydroxyl(orange) overlayer top view

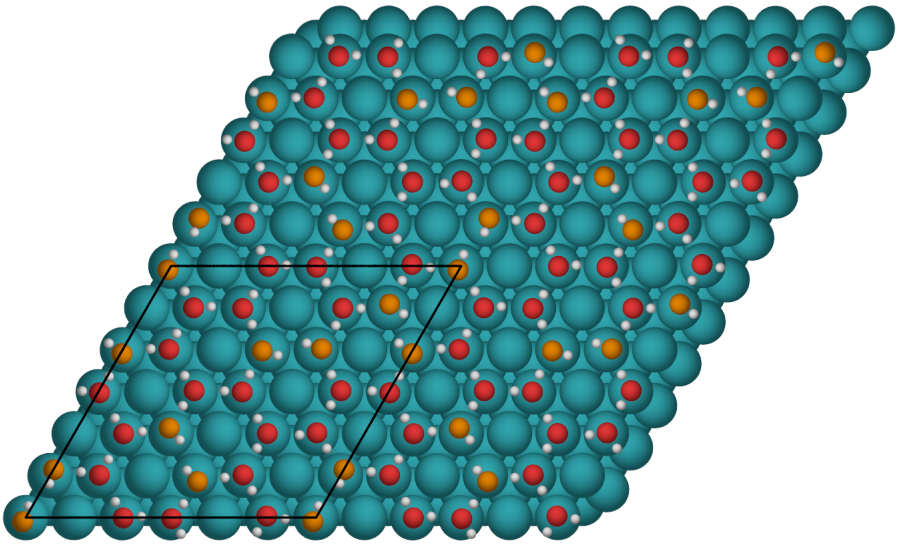

FIGURE A.14: 2:1 (6x6) Bjerrum defect, water(red) and hydroxyl(orange) overlayer top view

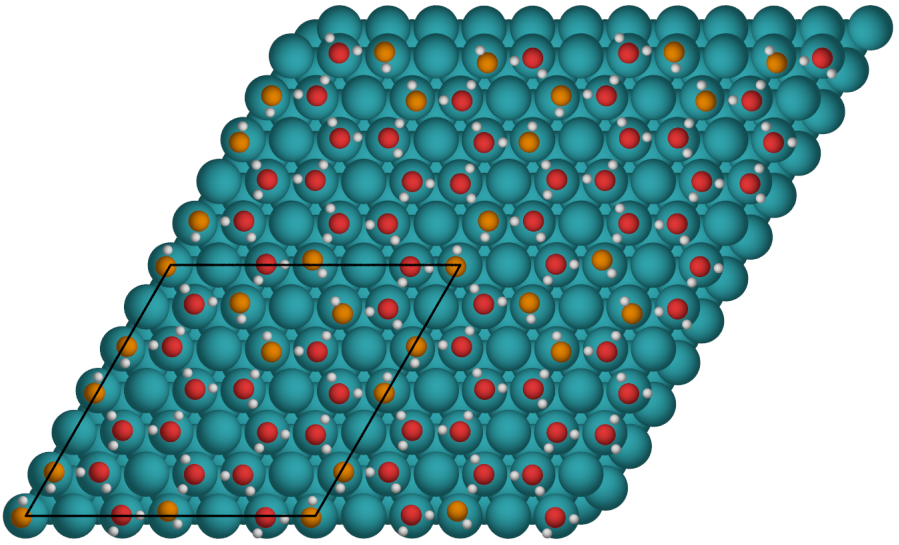

FIGURE A.15: 2:1 (6x6) Bjerrum defect, water(red) and hydroxyl(orange) overlayer top view

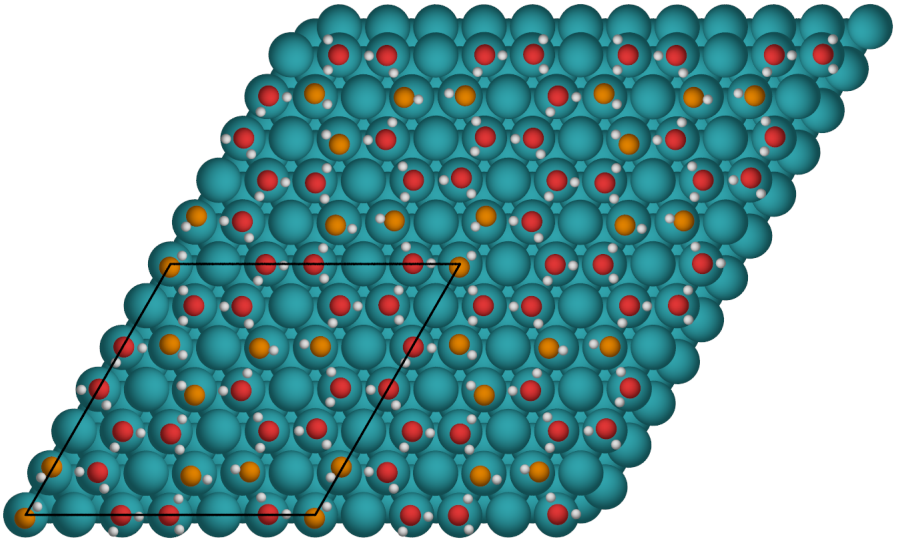

FIGURE A.16: 2:1 (6x6) Bjerrum defect, water(red) and hydroxyl(orange) overlayer top view

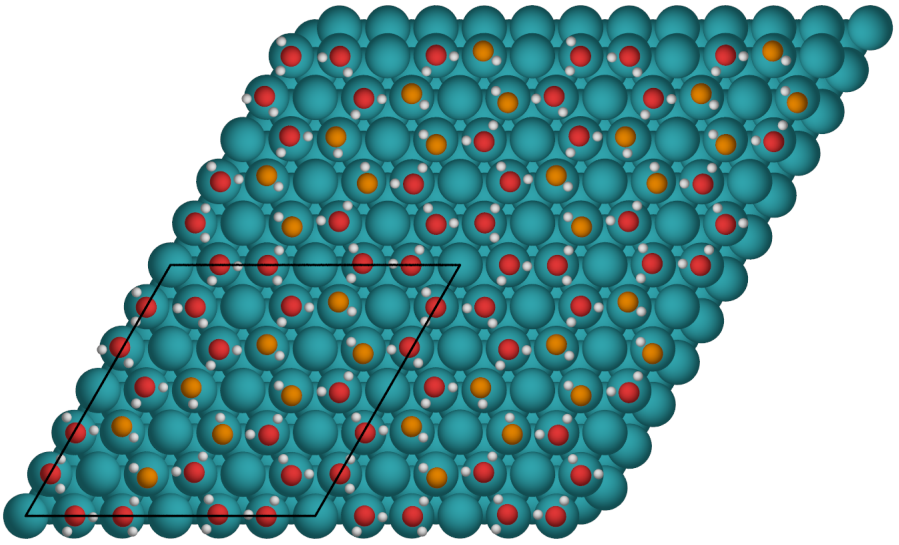

FIGURE A.17: 2:1 (6x6) Bjerrum defect, water(red) and hydroxyl(orange) overlayer top view

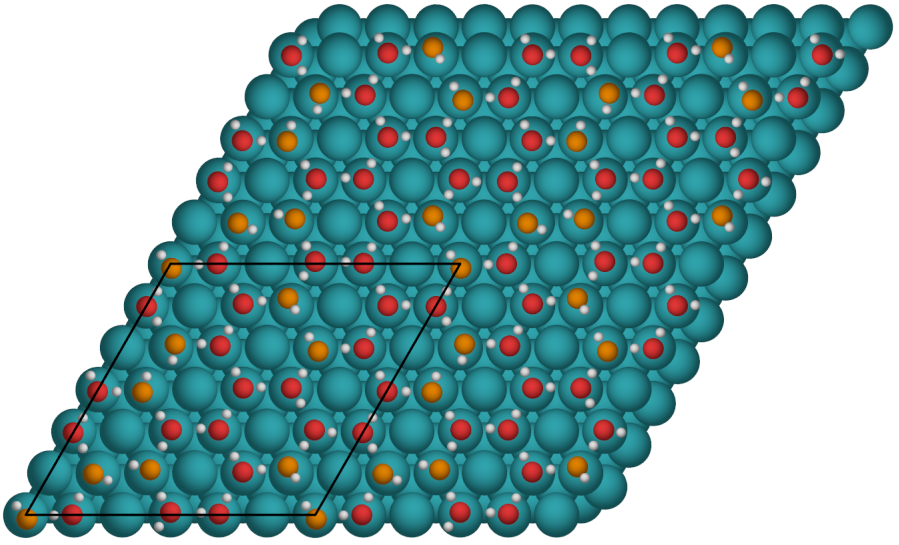

FIGURE A.18: 2:1 (6x6) Bjerrum defect, water(red) and hydroxyl(orange) overlayer top view

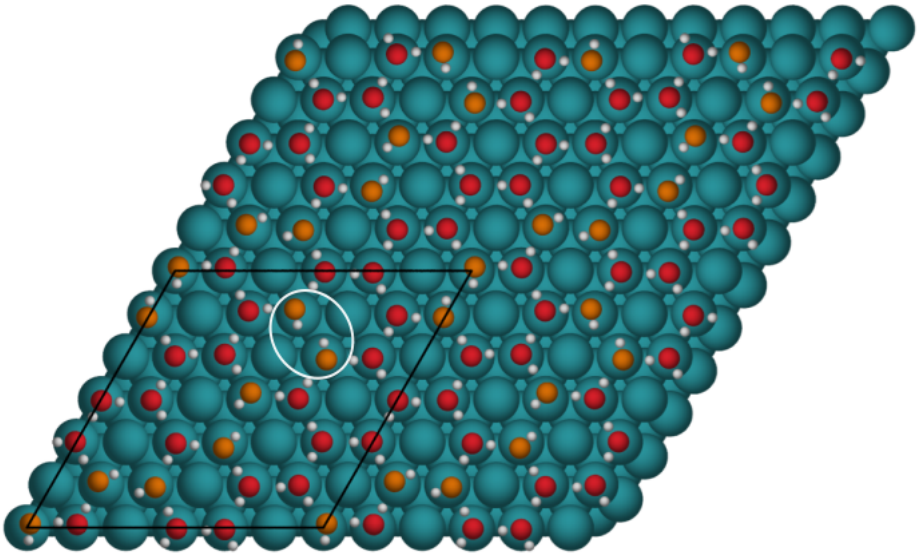

FIGURE A.19: 2:1 (6x6) Bjerrum defect, water(red) and hydroxyl(orange) overlayer top view. This is also shown in Figure 3.44, it is the structure with best binding energy.

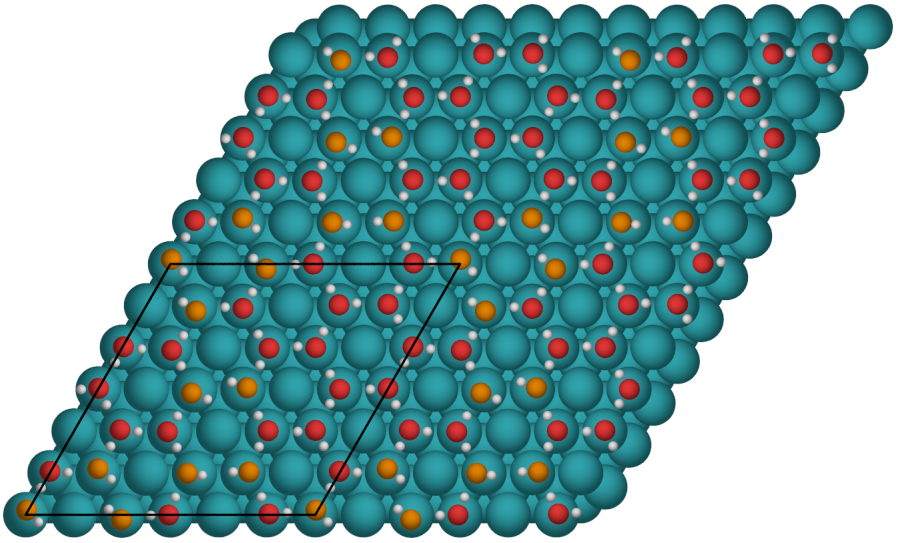

FIGURE A.20: 2:1 (6x6) Bjerrum defect, water(red) and hydroxyl(orange) overlayer top view

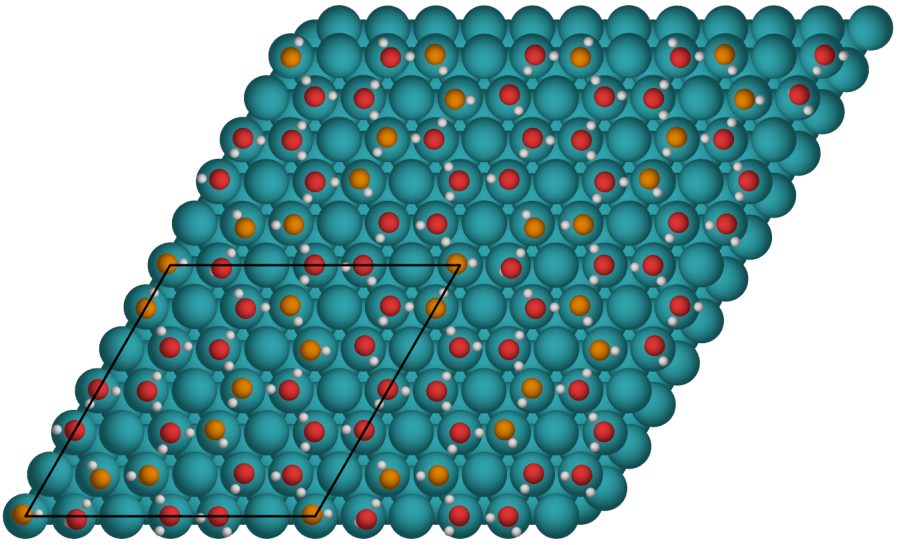

FIGURE A.21: 2:1 (6x6) Two molecule hydroxyl chains, water(red) and hydroxyl(orange) overlayer top view

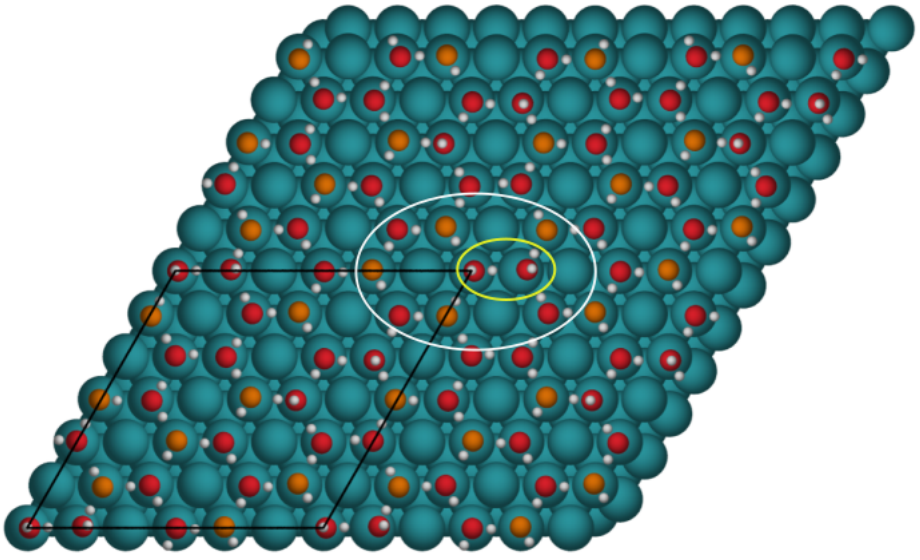

FIGURE A.22: 2:1 (6x6) Alternating, water(red) and hydroxyl(orange) overlayer top view. Calculated with van der Waals and shown in Figure 3.31.

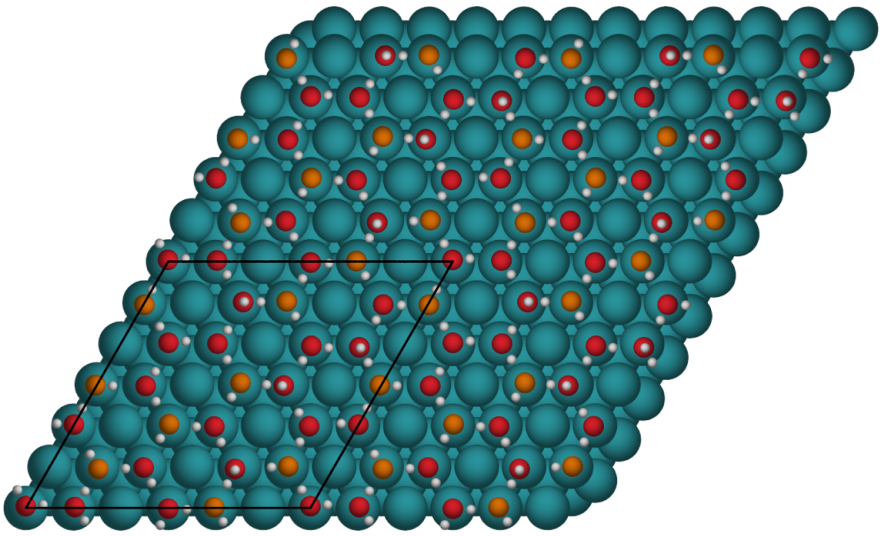

FIGURE A.23: 2:1 (6x6) Alternating, water(red) and hydroxyl(orange) overlayer top view. Calculated with van der Waals and shown in Figure 3.27.

A.3 3:1 H_2O:OH

A table showing the adsorption energies of the 3:1 H_2O:OH structures is shown below in Table A.3. From the structures run here it was clear that the 2:1 overlayers were on the whole preferred, this led to only a handful of these structures being looked at with van der Waals forces for completeness. Some of the calculations were started with hydroxyl molecules pointing straight up, the overlayers that kept that position were never the most stable structures. The lowest energy structure was not fully converged when the van der Waals calculations were started hence it not being run with those.

TABLE A.3: Calculated adsorption energies of different 3:1 H_2O:OH structures on Rh(111)

Figure	Type	PBE E_{ads} (meV)	Run with VdW
Figure A.24	(3x6)	-567	Yes
Figure A.25	(3x6)	-570	Yes
Figure A.26	(6x6)	-581	Yes
Figure A.27	(6x6)	-581	No
Figure A.28	(6x6)	-580	No
Figure A.29	(6x6)	-559	No
Figure A.30	(6x6)	-578	No
Figure A.31	(6x6)	-572	No
Figure A.32	(6x6)	-582	No
Figure A.33	(6x6)	-573	No
Figure A.34	(6x6)	-581	No
Figure A.36	(6x6)	-576	Yes
Figure A.35	(6x6)	-581	Yes
Figure A.37	(6x6)	-575	No
Figure A.38	(6x6) Bjerrum defects	-554	No
Figure A.39	(6x6) Bjerrum defects	-552	No

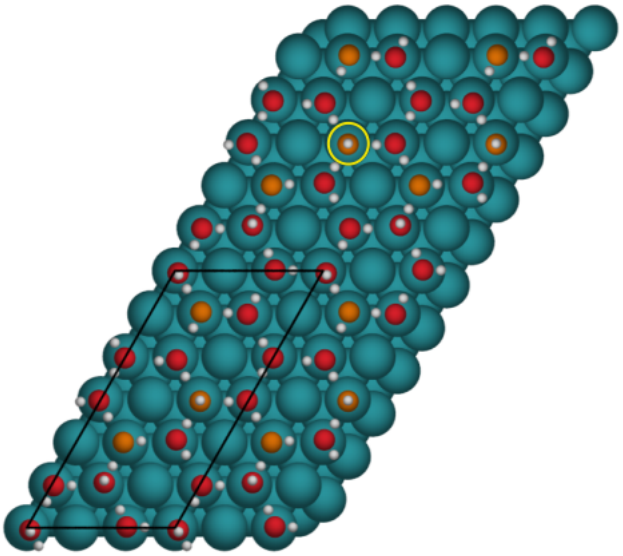

FIGURE A.24: 3:1 (3x6) Alternating, with OH pointing up, water(red) and hydroxyl(orange) overlayer top view. Calculated with van der Waals and shown in Figure 3.58.

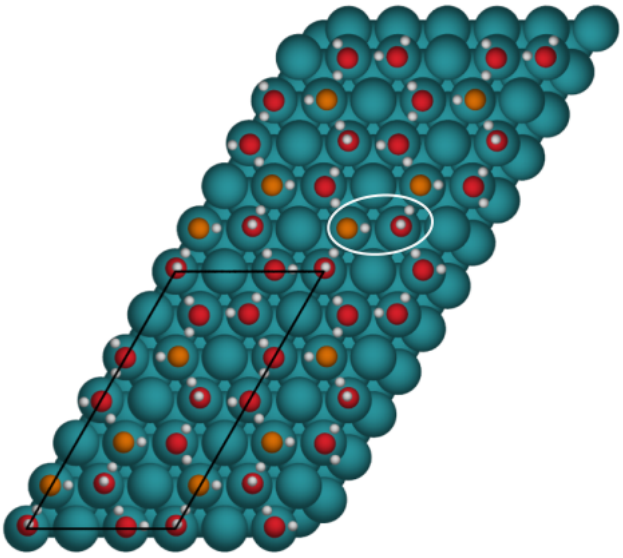

FIGURE A.25: 3:1 (3x6) Alternating, water(red) and hydroxyl(orange) overlayer top view. Calculated with van der Waals and shown in Figure 3.56.

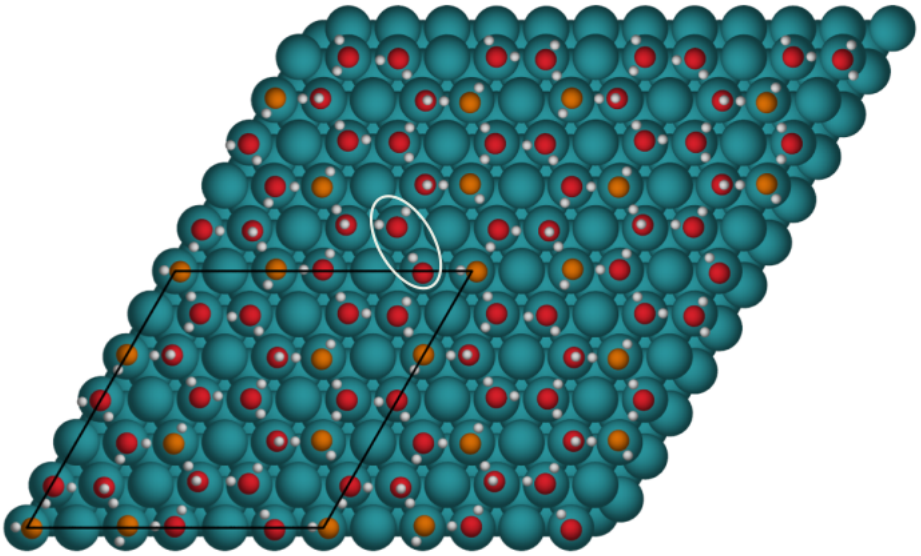

FIGURE A.26: 3:1 (6x6) Alternating, water(red) and hydroxyl(orange) overlayer top view. Calculated with van der Waals and shown in Figure 3.47.

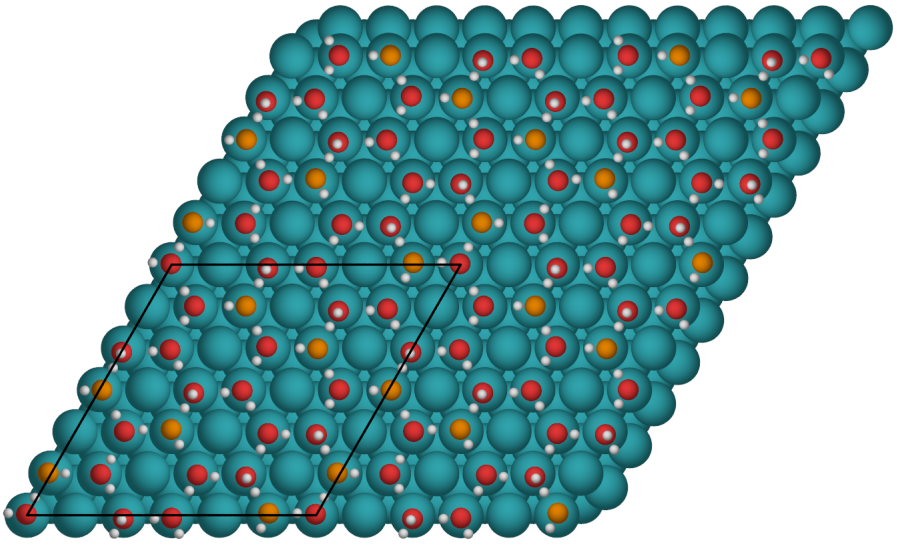

FIGURE A.27: 3:1 (6x6) Alternating, water(red) and hydroxyl(orange) overlayer top view

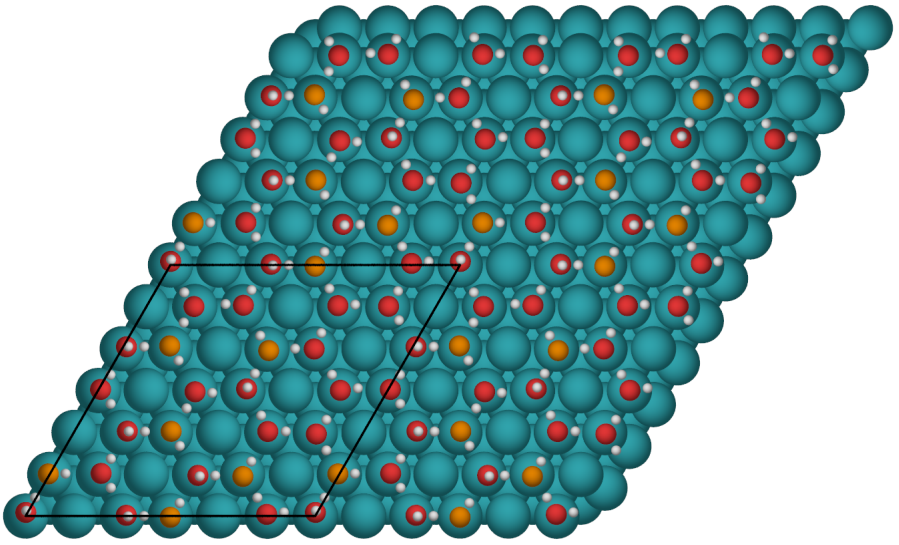

FIGURE A.28: 3:1 (6x6) Alternating, water(red) and hydroxyl(orange) overlayer top view

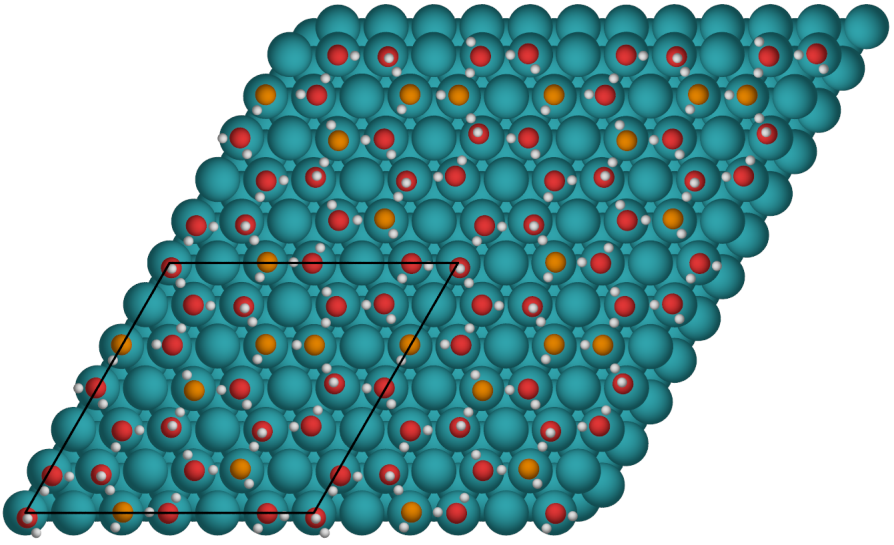

FIGURE A.29: 3:1 (6x6) Has two hydroxyl molecules which has given it an unfavourbale binding energy, water(red) and hydroxyl(orange) overlayer top view

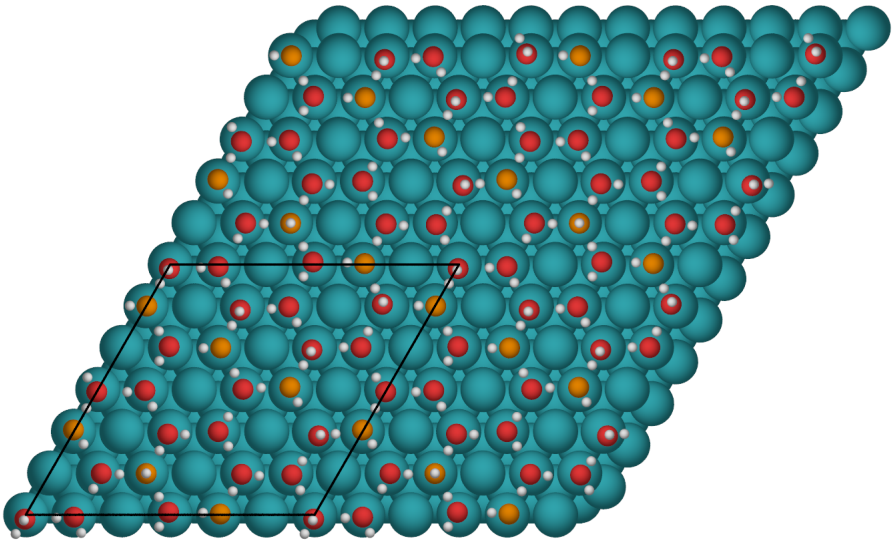

FIGURE A.30: 3:1 (6x6) Alternating, with one OH dangling, water(red) and hydroxyl(orange) overlayer top view

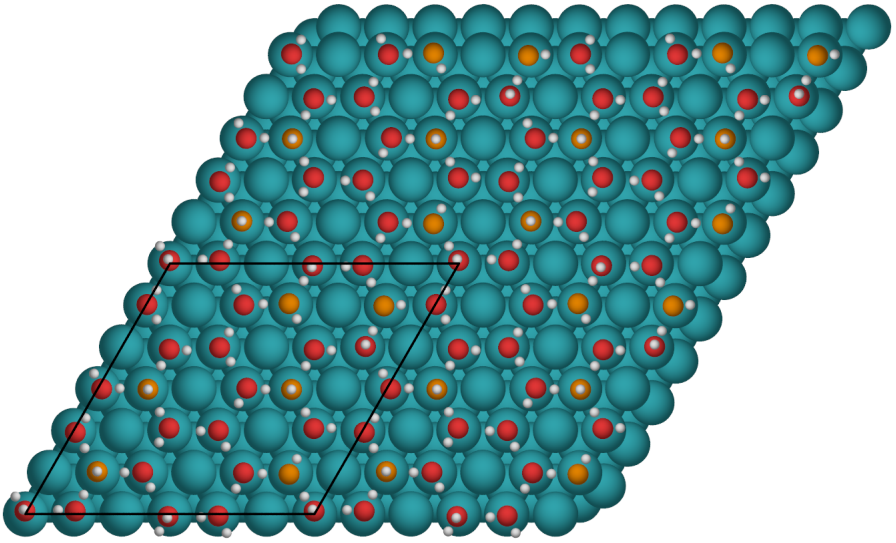

FIGURE A.31: 3:1 (6x6) Alternating, with 3 OH pointing up, water(red) and hydroxyl(orange) overlayer top view

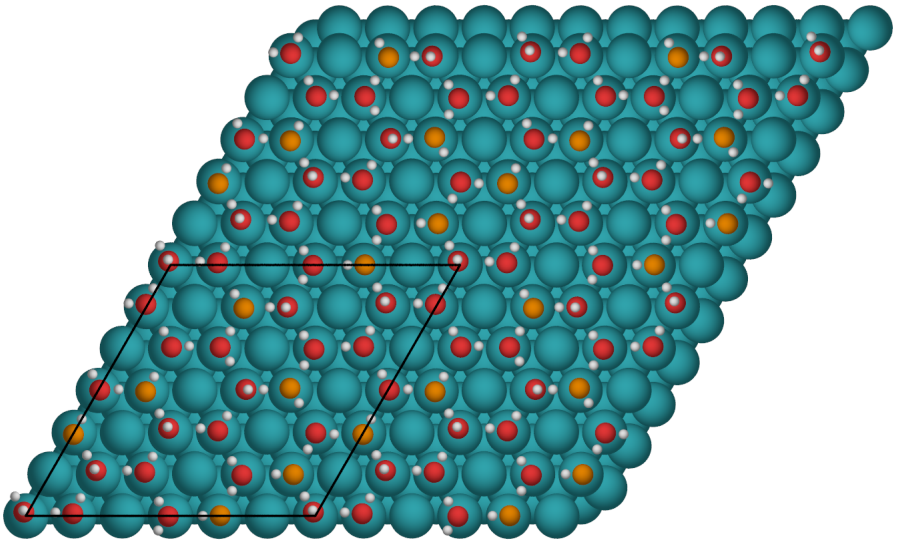

FIGURE A.32: 3:1 (6x6) Alternating, water(red) and hydroxyl(orange) overlayer top view. This is the lowest energy at PBE level

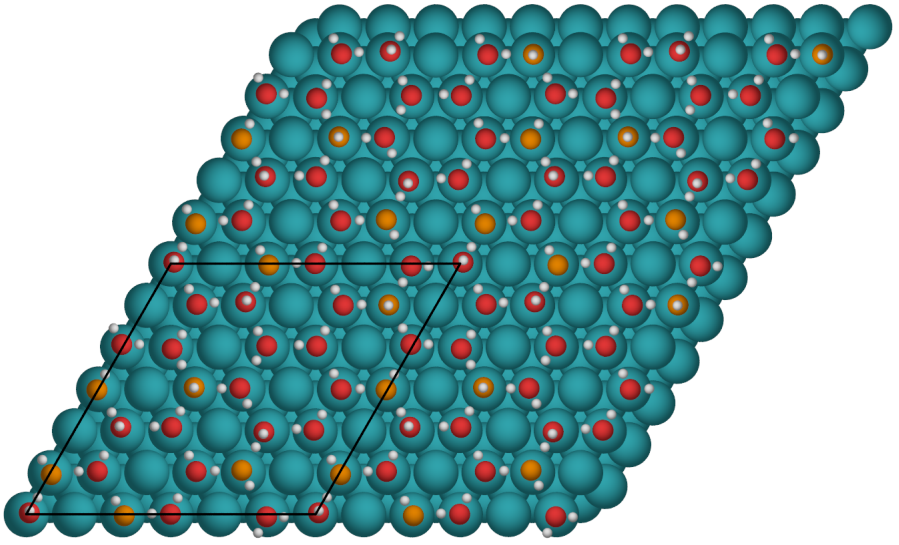

FIGURE A.33: 3:1 (6x6) Alternating, with 2 OH pointing up, water(red) and hydroxyl(orange) overlayer top view

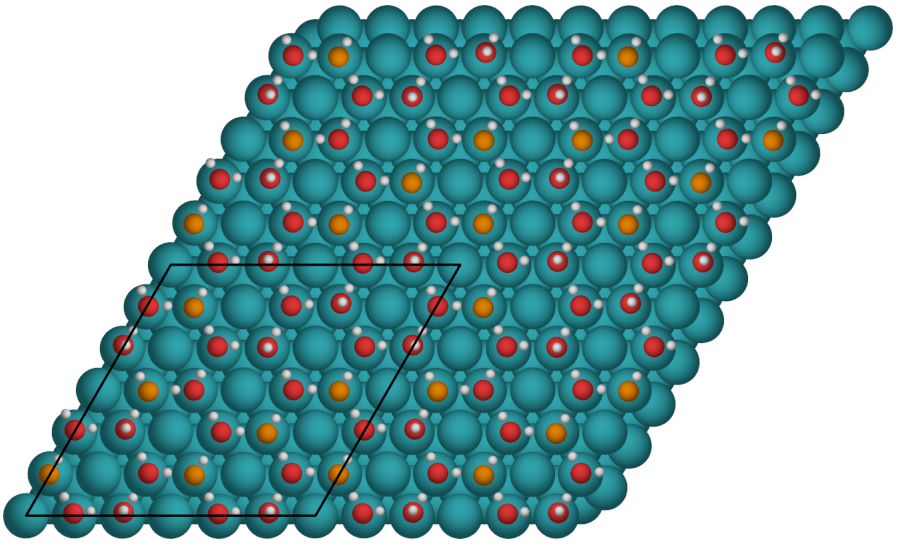

FIGURE A.34: 3:1 (6x6) Alternating, water(red) and hydroxyl(orange) overlayer top view

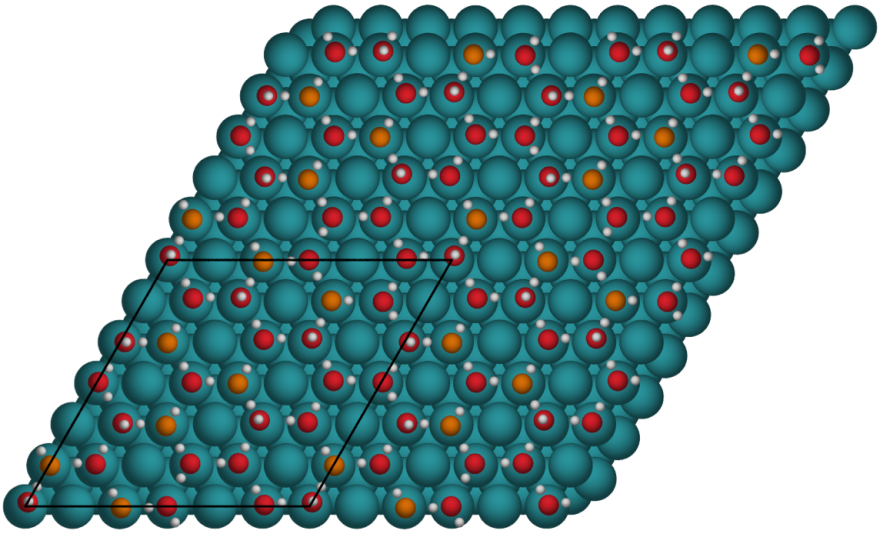

FIGURE A.35: 3:1 (6x6) Alternating, water(red) and hydroxyl(orange) overlayer top view. Calculated with van der Waals and shown in Figure 3.50.

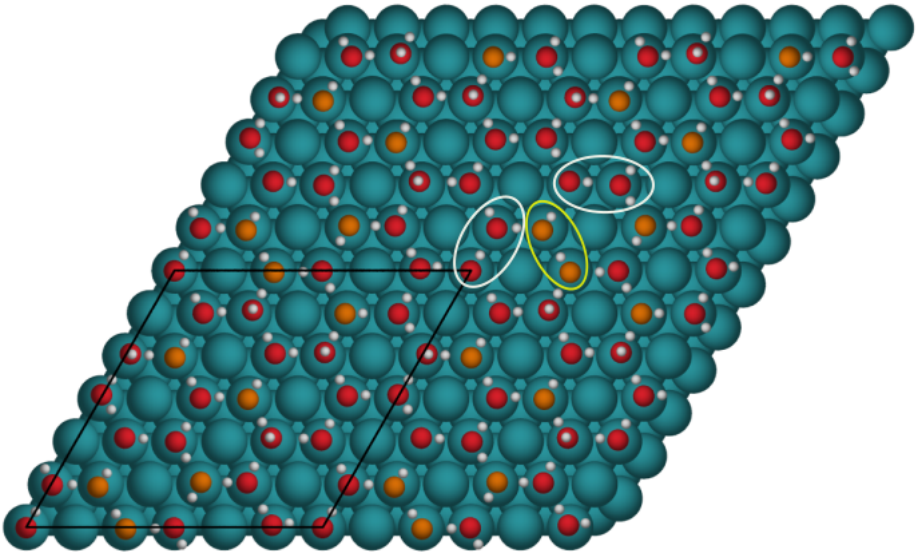

FIGURE A.36: 3:1 (6x6) Alternating, water(red) and hydroxyl(orange) overlayer top view. Calculated with van der Waals and shown in Figure 3.53.

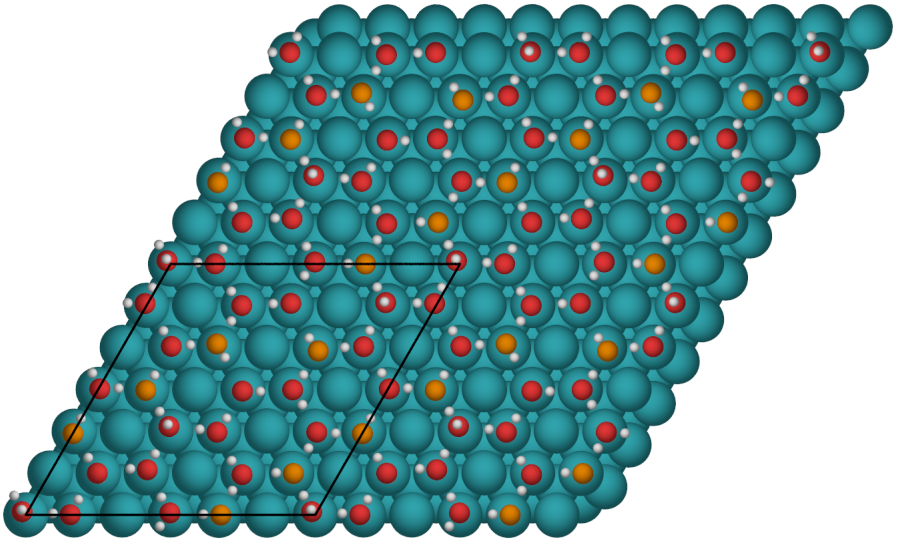

FIGURE A.37: 3:1 (6x6) Alternating, water(red) and hydroxyl(orange) overlayer top view

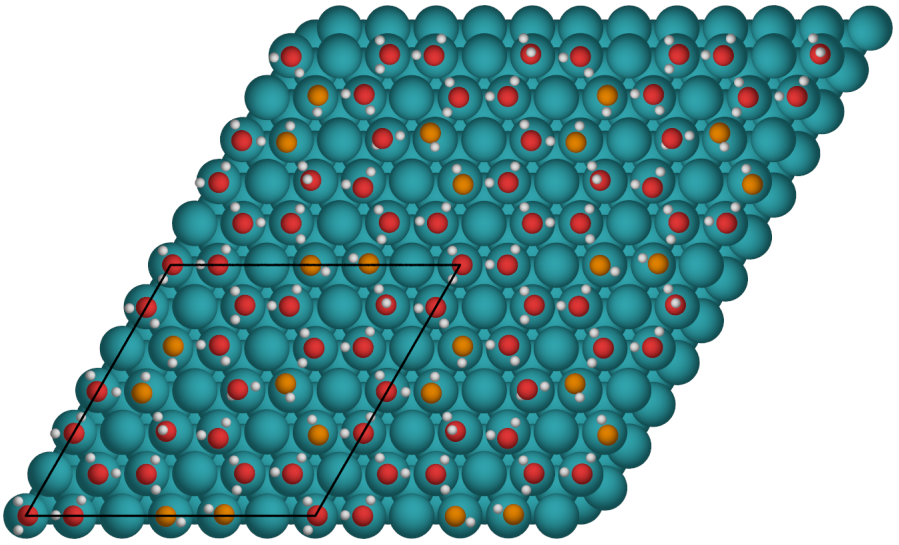

FIGURE A.38: 3:1 (6x6) Bjerrum defects with one water dangling down, started with all 4 dangling down, water(red) and hydroxyl(orange) overlayer top view

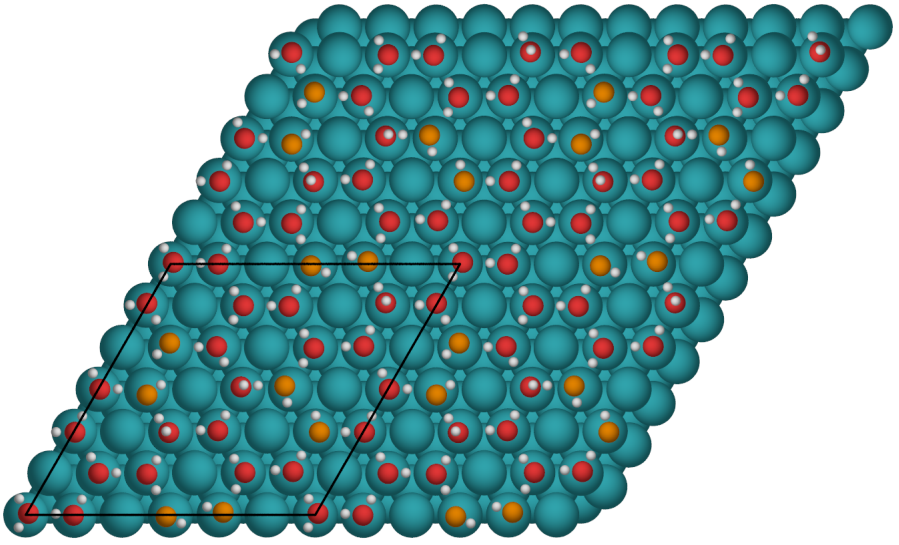

FIGURE A.39: 3:1 (6x6) Bjerrum defects with water dangling up, water(red) and hydroxyl(orange) overlayer top view

A.4 5:1 H_2O:OH

A table showing the adsorption energies of the 5:1 H_2O:OH structures is shown below in Table A.4. These calculations were done to show the trend continued of decreasing stability with increasing water fraction, also to look at which ratio of hydroxyl to water the dangling water molecules preferred to point down as is seen in the pure water structures.

TABLE A.4: Calculated adsorption energies of different 5:1 H_2O:OH structures on Rh(111)

Figure	Type	PBE E_{ads} (meV)	Run with VdW
Figure A.40	H-up	-567	Yes
Figure A.41	H-up Bjerrum defects	-556	Yes

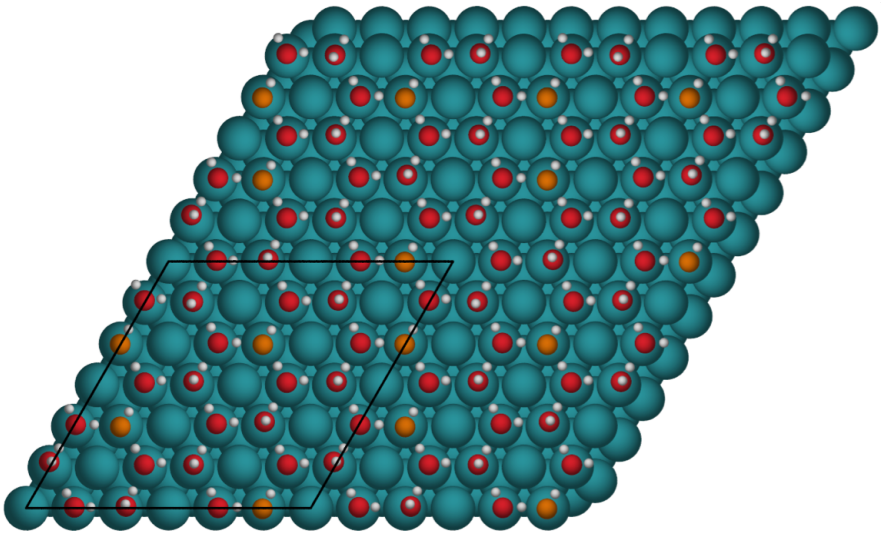

FIGURE A.40: 5:1 (6x6) Alternating, water(red) and hydroxyl(orange) overlayer top view. Calculated with van der Waals and shown in Figure 3.61.

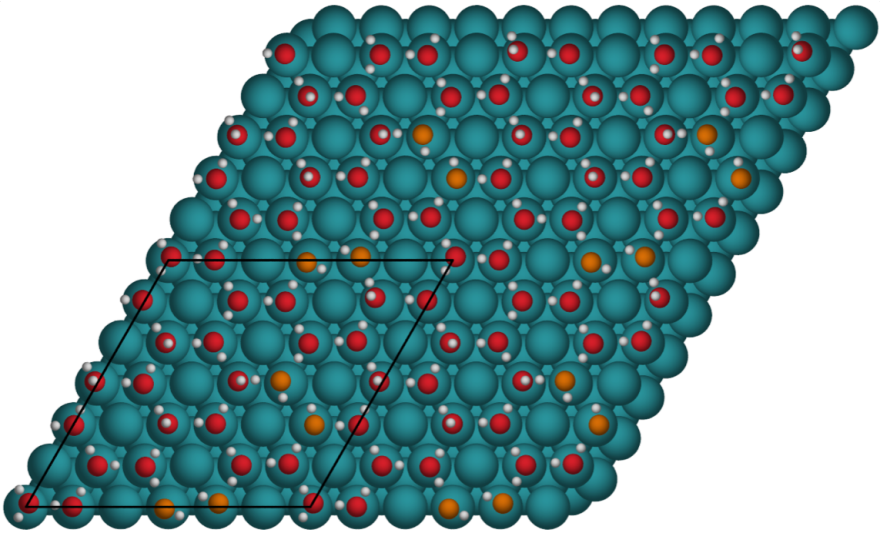

FIGURE A.41: 5:1 (6x6) Bjerrum defects, water(red) and hydroxyl(orange) overlayer top view. Calculated with van der Waals and shown in Figure 3.66.

Bibliography

[1] D. L. Doering and T. E. Madey. The adsorption of water on clean and oxygen-dosed Ru(011). *Surface Science*, 123:305–337, December 1982. doi: 10.1016/0039-6028(82)90331-4.

[2] A. Hodgson and S. Haq. Water adsorption and the wetting of metal surfaces. *Surface Science Reports*, 64(9):381–451, 2009.

[3] F. McBride, G. R. Darling, K. Pussi, and A. Hodgson. Tailoring the structure of water at a metal surface: A structural analysis of the water bilayer formed on an alloy template. *Physical Review Letters*, 106(22):226101, 2011.

[4] M. Gallagher, A. Omer, G. R. Darling, and A. Hodgson. Order and disorder in the wetting layer on Ru (0001). *Faraday Discussions*, 141:231–249, 2009.

[5] S. Nie, P. J. Feibelman, N. C. Bartelt, and K. Thürmer. Pentagons and heptagons in the first water layer on Pt (111). *Physical Review Letters*, 105 (2):026102, 2010.

[6] R. M. Martin. *Electronic structure: basic theory and practical methods*. Cambridge, 2004.

[7] W. Lew, M. C. Crowe, C. T. Campbell, J. Carrasco, and A. Michaelides. The energy of hydroxyl coadsorbed with water on Pt (111). *The Journal of Physical Chemistry C*, 115(46):23008–23012, 2011.

[8] M. Forster, R. Raval, A. Hodgson, J. Carrasco, and A. Michaelides. c (2× 2) water-hydroxyl layer on Cu (110): A wetting layer stabilized by bjerrum defects. *Physical Review Letters*, 106(4):046103, 2011.

[9] X. Duan, O. Warschkow, A. Soon, B. Delley, and C. Stampfl. Density functional study of oxygen on Cu(100) and Cu(110) surfaces. *Phys. Rev. B*, 81:075430, Feb 2010. doi: 10.1103/PhysRevB.81.075430. URL http://link.aps.org/doi/10.1103/PhysRevB.81.075430.

[10] J. Ahner, D. Mocuta, R. D. Ramsier, and J. T. Yates Jr. Adsorbate-adsorbate repulsions: The coverage dependence of the adsorption structure of CO on Cu(110) as studied by electron-stimulated desorption ion angular distribution. *The Journal of Chemical Physics*, 105(15):6553–6559, 1996. doi: 10.1063/1.472464. URL http://dx.doi.org/10.1063/1.472464.

[11] W. W. Crew and R. J. Madix. Monitoring surface reactions with scanning tunneling microscopy: CO oxidation on p(2 × 1)-O pre-covered Cu(110) at 400 K. *Surface Science*, 319:L34–L40, November 1994. doi: 10.1016/0039-6028(94)90587-8.

[12] M. M. V. M. Souza, N. F. P. Ribeiro, and M. Schmal. Influence of the support in selective CO oxidation on Pt catalysts for fuel cell applications. *International Journal of Hydrogen Energy*, 32(3):425 – 429,

2007. ISSN 0360-3199. doi: http://dx.doi.org/10.1016/j.ijhydene.2006.10.057. URL http://www.sciencedirect.com/science/article/pii/S0360319906005349. Fuel Cells.

[13] E. McCarthy, J. Zahradnik, G.C. Kuczynski, and J.J. Carberry. Some unique aspects of CO oxidation on supported Pt. *Journal of Catalysis*, 39(1):29 – 35, 1975. ISSN 0021-9517. doi: http://dx.doi.org/10.1016/0021-9517(75)90278-X. URL http://www.sciencedirect.com/science/article/pii/002195177590278X.

[14] W. Taifan, J. F. Boily, and J. Baltrusaitis. Surface chemistry of carbon dioxide revisited. *Surface Science Reports*, 71(4):595 – 671, 2016. ISSN 0167-5729. doi: http://dx.doi.org/10.1016/j.surfrep.2016.09.001. URL http://www.sciencedirect.com/science/article/pii/S016757291630022X.

[15] H. J. Freund and M. W. Roberts. Surface chemistry of carbon dioxide. *Surface Science Reports*, 25(8):225 – 273, 1996. ISSN 0167-5729. doi: http://dx.doi.org/10.1016/S0167-5729(96)00007-6. URL http://www.sciencedirect.com/science/article/pii/S0167572996000076.

[16] M. Gattrell, N. Gupta, and A. Co. A review of the aqueous electrochemical reduction of CO_2 to hydrocarbons at copper. *Journal of Electroanalytical Chemistry*, 594(1):1 – 19, 2006. ISSN 1572-6657. doi: http://dx.doi.org/10.1016/j.jelechem.2006.05.013. URL http://www.sciencedirect.com/science/article/pii/S0022072806002853.

[17] W. Kuch, M. Schulze, W. Schnurnberger, and K. Bohwin. Kinetics of H_2O adsorption on clean and potassium precovered Ni(111) surfaces. 97(3):356–359, 1993. ISSN 0005-9021. doi: 10.1002/bbpc.19930970318. URL http://dx.doi.org/10.1002/bbpc.19930970318.

[18] J. K. Gregory, D. C. Clary., K. Liu, M. G. Brown, and R. J. Saykally. The water dipole moment in water clusters. *Science*, 275(5301):814–817, 1997. ISSN 0036-8075. doi: 10.1126/science.275.5301.814. URL http://science.sciencemag.org/content/275/5301/814.

[19] P. A. Thiel and T. E. Madey. The interaction of water with solid surfaces: Fundamental aspects. *Surface Science Reports*, 7(68):211 – 385, 1987. ISSN 0167-5729. doi: http://dx.doi.org/10.1016/0167-5729(87)90001-X. URL http://www.sciencedirect.com/science/article/pii/016757298790001X.

[20] D. Pan, L-M. Liu, G. A. Tribello, B. Slater, A. Michaelides, and E. Wang. Surface energy and surface proton order of ice I*h*. *Phys. Rev. Lett.*, 101:155703, Oct 2008. doi: 10.1103/PhysRevLett.101.155703. URL http://link.aps.org/doi/10.1103/PhysRevLett.101.155703.

[21] J. Carrasco, B. Santra, J. Klimeš, and A. Michaelides. To wet or not to wet? dispersion forces tip the balance for water ice on metals. *Physical Review Letters*, 106(2):026101, 2011.

[22] A. Beniya, Y. Sakaguchi, T. Narushima, K. Mukai, Y. Yamashita, S. Yoshimoto, and J. Yoshinobu. The growth process of first water layer and crystalline ice on the Rh (111) surface. *The Journal of Chemical Physics*, 130: 034706, 2009.

[23] J. Carrasco, A. Hodgson, and A. Michaelides. A molecular perspective of water at metal interfaces. *Nature Materials*, 11(8):667–674, 2012.

[24] F. McBride, A. Omer, C.M. Clay, L. Cummings, G. R. Darling, and A. Hodgson. Strain relief and disorder in commensurate water layers formed on Pd (111). *Journal of Physics: Condensed Matter*, 24(12):124102, 2012.

[25] O. Bjorneholm, M. H. Hansen, A. Hodgson, L. Liu, D. T. Limmer, A. Michaelides, P. Pedevilla, J. Rossmeisl, H. Shen, G. Tocci, E. Tyrode, M. Walz, J. Werner, and H. Bluhm. Water at interfaces. *Chemical Reviews*, 116(13):7698–7726, 2016. doi: 10.1021/acs.chemrev.6b00045. URL http://dx.doi.org/10.1021/acs.chemrev.6b00045. PMID: 27232062.

[26] T. Schiros, K. J. Andersson, L. G. M. Pettersson, A. Nilsson, and H. Ogasawara. Chemical bonding of water to metal surfaces studied with core-level spectroscopies. *Journal of Electron Spectroscopy and Related Phenomena*, 177(2-3):85–98, 2010. ISSN 0368-2048. doi: 10.1016/j.elspec.2009.09.009.

[27] P. J. Feibelman. A wetting layer breaks the ice rules. *Chemical Physics Letters*, 410(1):120–124, 2005.

[28] J. Li, S. Zhu, H. Li, E. E. Oguzie, Y. Li, and F. Wang. Bonding nature of monomeric H2O on Pd: Orbital cooperation and competition. *The Journal*

of Physical Chemistry C, 113(5):1931–1938, 2009. doi: 10.1021/jp809595y. URL http://dx.doi.org/10.1021/jp809595y.

[29] A. Michaelides and K. Morgenstern. Ice nanoclusters at hydrophobic metal surfaces. *Nat Mater*, 6(8):597–601, 08 2007. URL http://dx.doi.org/10.1038/nmat1940.

[30] C. Clay, S. Haq, and A. Hodgson. Hydrogen bonding in mixed OH+ H_2O overlayers on Pt (111). *Physical Review Letters*, 92(4):046102, 2004.

[31] A. Michaelides. Density functional theory simulations of water–metal interfaces: waltzing waters, a novel 2D ice phase, and more. *Applied Physics A*, 85(4):415–425, 2006.

[32] P. J. Feibelman. The first wetting layer on a solid. *Physics Today*, 63(2):34, 2010. doi: 10.1063/1.3326987.

[33] M. Sacchi and S. J. Jenkins. Co-adsorption of water and glycine on cu110. *Phys. Chem. Chem. Phys.*, 16:6101–6107, 2014. doi: 10.1039/C3CP55094J. URL http://dx.doi.org/10.1039/C3CP55094J.

[34] T. Schiros, S. Haq, H. Ogasawara, O. Takahashi, H. Öström, K. Andersson, L. G. M. Pettersson, A. Hodgson, and A. Nilsson. Structure of water adsorbed on the open Cu (110) surface: H-up, H-down, or both? *Chemical Physics Letters*, 429(4):415–419, 2006.

[35] G. Jones and S. J. Jenkins. Water and ammonia on Cu110: comparative structure and bonding. *Phys. Chem. Chem. Phys.*, 15:4785–4798, 2013. doi: 10.1039/C3CP42658K. URL http://dx.doi.org/10.1039/C3CP42658K.

[36] H. Ogasawara, B. Brena, D. Nordlund, M. Nyberg, A. Pelmenschikov, L. G. M. Pettersson, and A. Nilsson. Structure and bonding of water on Pt (111). *Physical Review Letters*, 89(27):276102, 2002.

[37] J. Cerda, A. Michaelides, M. L. Bocquet, P. J. Feibelman, T. Mitsui, M. Rose, E. Fomin, and M. Salmeron. Novel water overlayer growth on Pd (111) characterized with scanning tunneling microscopy and density functional theory. *Physical Review Letters*, 93(11):116101, 2004.

[38] M. Tatarkhanov, D. F. Ogletree, F. Rose, T. Mitsui, E. Fomin, S. Maier, M. Rose, J. I. Cerdá, and M. Salmeron. Metal-and hydrogen-bonding competition during water adsorption on Pd (111) and Ru (0001). *Journal of the American Chemical Society*, 131(51):18425–18434, 2009.

[39] S. Maier and M. Salmeron. How does water wet a surface? *Accounts of Chemical Research*, 48(10):2783–2790, 2015. doi: 10.1021/acs.accounts.5b00214. URL http://dx.doi.org/10.1021/acs.accounts.5b00214. PMID: 26418288.

[40] A. Michaelides, A. Alavi, and D. A. King. Different surface chemistries of water on Ru (0001): From monomer adsorption to partially dissociated bilayers. *Journal of the American Chemical Society*, 125(9):2746–2755, 2003.

[41] K. Thurmer and N. C. Bartelt. Growth of multilayer ice films and the formation of cubic ice imaged with STM. 77(19):195425, May 2008. doi: 10.1103/PhysRevB.77.195425.

[42] G. A. Kimmel, N. G. Petrik, Z. Dohnalek, and B. D. Kay. Crystalline ice growth on Pt(111) and Pd(111): Nonwetting growth on a hydrophobic water monolayer. *The Journal of Chemical Physics*, 126(11):114702, 2007. doi: 10.1063/1.2672869. URL http://aip.scitation.org/doi/abs/10.1063/1.2672869.

[43] K. Burke and L. O. Wagner. DFT in a nutshell. *International Journal of Quantum Chemistry*, 113(2):96–101, 2013.

[44] C. A. Ullrich. *Time-dependent density-functional theory: concepts and applications*. Oxford University Press, 2011.

[45] A. Hinchliffe. *Molecular Modelling for Beginners*. Wiley. com, 2005.

[46] W. Kohn. Nobel lecture: Electronic structure of matter, wave functions and density functionals. *Rev. Mod. Phys.*, 71:1253–1266, Oct 1999. doi: 10.1103/RevModPhys.71.1253. URL http://link.aps.org/doi/10.1103/RevModPhys.71.1253.

[47] P. Hohenberg and W. Kohn. Inhomogeneous electron gas. *Phys. Rev.*, 136: B864–B871, Nov 1964. doi: 10.1103/PhysRev.136.B864. URL http://link.aps.org/doi/10.1103/PhysRev.136.B864.

[48] E. Teller. On the stability of molecules in the Thomas-Fermi theory. *Rev. Mod. Phys.*, 34:627–631, Oct 1962. doi: 10.1103/RevModPhys.34.627. URL http://link.aps.org/doi/10.1103/RevModPhys.34.627.

[49] W. Kohn and L. J. Sham. Self-consistent equations including exchange and correlation effects. *Phys. Rev.*, 140:A1133–A1138, Nov 1965. doi: 10.1103/

PhysRev.140.A1133. URL http://link.aps.org/doi/10.1103/PhysRev.140.A1133.

[50] J. Hafner. Materials simulation using VASP a quantum perspective to materials science. *Computer Physics Communications*, 177:6 – 13, 2007. ISSN 0010-4655. doi: http://dx.doi.org/10.1016/j.cpc.2007.02.045. URL http://www.sciencedirect.com/science/article/pii/S001046550700080X.

[51] J. Klimes, D. R. Bowler, and A. Michaelides. Chemical accuracy for the van der Waals density functional. *Journal of Physics: Condensed Matter*, 22(2):022201, 2010. URL http://stacks.iop.org/0953-8984/22/i=2/a=022201.

[52] J. Klimes, D. R. Bowler, and A. Michaelides. Van der Waals density functionals applied to solids. *Phys. Rev. B*, 83:195131, May 2011. doi: 10.1103/PhysRevB.83.195131. URL http://link.aps.org/doi/10.1103/PhysRevB.83.195131.

[53] J. P. Perdew, J. A. Chevary, S. H. Vosko, J. A. Koblar, M.R. Pederson, D. J. Singh, and C. Fiolhais. Atoms, molecules, solids, and surfaces: Applications of the generalized gradient approximation for exchange and correlation. *Phys. Rev. B*, 46:6671–6687, Sep 1992. doi: 10.1103/PhysRevB.46.6671. URL http://link.aps.org/doi/10.1103/PhysRevB.46.6671.

[54] J. P. Perdew, K. Burke, and M. Ernzerhof. Generalized gradient approximation made simple. *Phys. Rev. Lett.*, 77:3865–3868, Oct 1996. doi:

10.1103/PhysRevLett.77.3865. URL http://link.aps.org/doi/10.1103/PhysRevLett.77.3865.

[55] J. Carrasco, W. Liu, A. Michaelides, and A. Tkatchenko. Insight into the description of van der Waals forces for benzene adsorption on transition metal (111) surfaces. *The Journal of Chemical Physics*, 140(8):084704, 2014. doi: http://dx.doi.org/10.1063/1.4866175. URL http://scitation.aip.org/content/aip/journal/jcp/140/8/10.1063/1.4866175.

[56] M. Dion, H. Rydberg, E. Schröder, D. C. Langreth, and B. I. Lundqvist. Van der Waals density functional for general geometries. *Phys. Rev. Lett.*, 92:246401, Jun 2004. doi: 10.1103/PhysRevLett.92.246401. URL http://link.aps.org/doi/10.1103/PhysRevLett.92.246401.

[57] G. Román-Pérez and J. Soler. Efficient implementation of a van der waals density functional: Application to double-wall carbon nanotubes. *Phys. Rev. Lett.*, 103:096102, 2009. doi: 10.1103/PhysRevLett.103.096102. URL https://link.aps.org/doi/10.1103/PhysRevLett.103.096102.

[58] F. Hanke, M. S. Dyer, J. Bjork, and M. Persson. Structure and stability of weakly chemisorbed ethene adsorbed on low-index cu surfaces: performance of density functionals with van der waals interactions. *Journal of Physics: Condensed Matter*, 24(42):424217, 2012. URL http://stacks.iop.org/0953-8984/24/i=42/a=424217.

[59] J. Hafner. Ab-initio simulations of materials using VASP: Density-functional theory and beyond. *Journal of Computational Chemistry*, 29(13):2044–2078,

2008. ISSN 1096-987X. doi: 10.1002/jcc.21057. URL http://dx.doi.org/10.1002/jcc.21057.

[60] H. J. Monkhorst and J. D. Pack. Special points for Brillouin-zone integrations. *Phys. Rev. B*, 13:5188–5192, Jun 1976. doi: 10.1103/PhysRevB.13.5188. URL http://link.aps.org/doi/10.1103/PhysRevB.13.5188.

[61] J. S. Lin, A. Qteish, M. C. Payne, and V. Heine. Optimized and transferable nonlocal separable ab initio pseudopotentials. *Physical Review B*, 47(8):4174, 1993.

[62] P. E. Blöchl. Projector augmented-wave method. *Phys. Rev. B*, 50:17953–17979, Dec 1994. doi: 10.1103/PhysRevB.50.17953. URL http://link.aps.org/doi/10.1103/PhysRevB.50.17953.

[63] C. J. Cramer and D. G. Truhlar. Density functional theory for transition metals and transition metal chemistry. *Phys. Chem. Chem. Phys.*, 11:10757–10816, 2009. doi: 10.1039/B907148B. URL http://dx.doi.org/10.1039/B907148B.

[64] G. S. Karlberg. Adsorption trends for water, hydroxyl, oxygen, and hydrogen on transition-metal and platinum-skin surfaces. *Phys. Rev. B*, 74:153414, Oct 2006. doi: 10.1103/PhysRevB.74.153414. URL http://link.aps.org/doi/10.1103/PhysRevB.74.153414.

[65] A. Michaelides and P. Hu. Catalytic water formation on platinum: A first-principles study. *Journal of the American Chemical Society*, 123(18):4235–4242, 2001. doi: 10.1021/ja003576x. URL http://dx.doi.org/10.1021/ja003576x. PMID: 11457189.

[66] P. J. Feibelman. Partial dissociation of water on Ru (0001). *Science*, 295 (5552):99–102, 2002.

[67] J. Derouin, R. G. Farber, and D. R. Killelea. Combined STM and TPD study of Rh(111) under conditions of high oxygen coverage. *The Journal of Physical Chemistry C*, 119(26):14748–14755, 2015. doi: 10.1021/acs.jpcc.5b00635. URL http://dx.doi.org/10.1021/acs.jpcc.5b00635.

[68] M. Forster, R. Raval, J. Carrasco, A. Michaelides, and A. Hodgson. Water-hydroxyl phases on an open metal surface: breaking the ice rules. *Chem. Sci.*, 3:93–102, 2012. doi: 10.1039/C1SC00355K. URL http://dx.doi.org/10.1039/C1SC00355K.

[69] T. Schiros, L. A. Naeslund, K. Andersson, J. Gyllenpalm, G. S. Karlberg, M. Odelius, H. Ogasawara, L. G. M. Pettersson, and A. Nilsson. Structure and bonding of the water-hydroxyl mixed phase on Pt(111). *The Journal of Physical Chemistry C*, 111(41):15003–15012, 2007. doi: 10.1021/jp073405f. URL http://dx.doi.org/10.1021/jp073405f.

[70] X-Z. Li, M. I. J. Probert, A. Alavi, and A. Michaelides. Quantum nature of the proton in water-hydroxyl overlayers on metal surfaces. *Phys. Rev.*

Lett., 104:066102, Feb 2010. doi: 10.1103/PhysRevLett.104.066102. URL http://link.aps.org/doi/10.1103/PhysRevLett.104.066102.

[71] A.Michaelides and P. Hu. A density functional theory study of hydroxyl and the intermediate in the water formation reaction on Pt. *The Journal of Chemical Physics*, 114:513–519, 2001.

[72] P. J. Feibelman, B. Hammer, J. K. Norskov, F. Wagner, M. Scheffler, R. Stumpf, R. Watwe, et al. The co/pt(111) puzzle. *The Journal of Physical Chemistry B*, 105(18):4018–4025, 2001. doi: 10.1021/jp002302t. URL http://dx.doi.org/10.1021/jp002302t.

[73] Víctor A. Ranea and Eduardo E. Mola. Oxygen assisted H_2O dissociation on the Pt(110)(1 $\times$ 2) surface from first principles. *Surface Science*, 627:42 – 48, 2014. ISSN 0039-6028. doi: http://dx.doi.org/10.1016/j.susc.2014.04.005. URL http://www.sciencedirect.com/science/article/pii/S0039602814000995.

[74] T. Kumagai, A. Shiotari, H. Okuyama, S. Hatta, T. Aruga, I. Hamada, T. Frederiksen, and H. Ueba. H-atom relay reactions in real space. *Nat Mater*, 11(2):167–172, 02 2012. URL http://dx.doi.org/10.1038/nmat3176.

[75] J. Carrasco, A. Michaelides, M. Forster, S. Haq, R. Raval, and A. Hodgson. A one-dimensional ice structure built from pentagons. *Nat Mater*, 8(5):427–431, 05 2009. URL http://dx.doi.org/10.1038/nmat2403.

[76] U. Bardi. The atomic structure of alloy surfaces and surface alloys. *Reports on Progress in Physics*, 57(10):939, 1994. URL http://stacks.iop.org/0034-4885/57/i=10/a=001.

[77] C. A. Lucas, N. M. Markovia, and P. N. Ross. Surface structure and relaxation at the Pt(110)/electrolyte interface. *Phys. Rev. Lett.*, 77:4922–4925, Dec 1996. doi: 10.1103/PhysRevLett.77.4922. URL http://link.aps.org/doi/10.1103/PhysRevLett.77.4922.

[78] J. Fearon and G. W. Watson. Hydrogen adsorption and diffusion on Pt (111) and PtSn (111). *J. Mater. Chem.*, 16:1989–1996, 2006. doi: 10.1039/B600250C. URL http://dx.doi.org/10.1039/B600250C.

[79] Vladimir Ponec. Alloy catalysts: the concepts. *Applied Catalysis A: General*, 222(12):31 – 45, 2001. ISSN 0926-860X. doi: http://dx.doi.org/10.1016/S0926-860X(01)00828-6. URL http://www.sciencedirect.com/science/article/pii/S0926860X01008286. Celebration Issue.

[80] M. Zhu, G. Sun, and Q. Xin. Effect of alloying degree in PtSn catalyst on the catalytic behavior for ethanol electro-oxidation. *Electrochimica Acta*, 54 (5):1511 – 1518, 2009. ISSN 0013-4686. doi: http://dx.doi.org/10.1016/j.electacta.2008.09.035. URL http://www.sciencedirect.com/science/article/pii/S0013468608011523.

[81] J. Timo and G. William. Water formation on Pt and Pt-based alloys: A theoretical description of a catalytic reaction. *ChemPhysChem*, 7(5):992–1005, 2006. ISSN 1439-7641. doi: 10.1002/cphc.200500613. URL http:

//dx.doi.org/10.1002/cphc.200500613.

[82] D. P. Woodruff and J. Robinson. Some structural issues in surface alloys and alloy surfaces: rumpling, stacking faults and disorder. *Applied Surface Science*, 219:1–10, October 2003. doi: 10.1016/S0169-4332(03)00627-5.

[83] M. J. Harrison, D. P. Woodruff, and J. Robinson. Surface alloys, surface rumpling and surface stress. *Surface Science*, 572(23):309 – 317, 2004. ISSN 0039-6028. doi: http://dx.doi.org/10.1016/j.susc.2004.09.006. URL http://www.sciencedirect.com/science/article/pii/S0039602804012117.

[84] A. Atrei, U. Bardi, J. X. Wu, E. Zanazzi, and G. Rovida. LEED crystallographic investigation of ultrathin films formed by deposition of Sn on the Pt(111) surface. *Surface Science*, 290(3):286 – 294, 1993. ISSN 0039-6028. doi: http://dx.doi.org/10.1016/0039-6028(93)90712-S. URL http://www.sciencedirect.com/science/article/pii/003960289390712S.

[85] A. K. Schmid, N. C. Bartelt, and R. Q. Hwang. Alloying at surfaces by the migration of reactive two-dimensional islands. *Science*, 290(5496):1561–1564, 2000. ISSN 0036-8075. doi: 10.1126/science.290.5496.1561. URL http://science.sciencemag.org/content/290/5496/1561.

[86] G. Contini, V. Di Castro, N. Motta, and A. Sgarlata. Formation of a two-dimensional alloy/surface phase: Auger and STM study of Cu(Sn)(111). *Surface Science*, 405(23):L509 – L513, 1998. ISSN 0039-6028. doi: http://dx.doi.org/10.1016/S0039-6028(98)00139-3. URL http://www.sciencedirect.com/science/article/pii/S0039602898001393.

[87] S. H. Overbury and Y. Ku. Formation of stable, two-dimensional alloy-surface phases: Sn on Cu(111), Ni(111), and Pt(111). *Phys. Rev. B*, 46: 7868–7872, Sep 1992. doi: 10.1103/PhysRevB.46.7868. URL http://link.aps.org/doi/10.1103/PhysRevB.46.7868.

[88] A. Rochefort, J. Andzelm, D. R. Salahub, and N. Russo. Chemisorption and diffusion of atomic hydrogen in and on cluster models of Pd, Rh, and bimetallic PdSn, RhSn, and RhZn catalysts. *Journal of the American Chemical Society; (United States)*, 112:23, Nov 1990. doi: 10.1021/ja00179a003.

[89] J. Andzelm, A. Rochefort, N. Russo, and D. R. Salahub. Interaction of atomic hydrogen with cluster models of Pd, Rh and bimetallic PdSn and RhSn catalysts. *Surface Science*, 235(2):L319 – L323, 1990. ISSN 0039-6028. doi: http://dx.doi.org/10.1016/0039-6028(90)90780-C. URL http://www.sciencedirect.com/science/article/pii/003960289090780C.

[90] D. Teschner, A. Wootsch, and Z. Paal. Preferential CO oxidation in hydrogen (PROX) on unsupported PtSn catalyst. *Applied Catalysis A: General*, 411412:31 – 34, 2012. ISSN 0926-860X. doi: http://dx.doi.org/10.1016/j.apcata.2011.10.017. URL http://www.sciencedirect.com/science/article/pii/S0926860X11006120.

[91] V. R. Stamenkovic, M. Arenz, C. A. Lucas, M. E Gallagher, P. N. Ross, and N. M. Markovic. Surface chemistry on bimetallic alloy surfaces Adsorption of anions and oxidation of CO on Pt3Sn(111). *Journal of the American Chemical Society*, 125(9):2736–2745, 2003. doi: 10.1021/ja028771l. URL http://dx.doi.org/10.1021/ja028771l. PMID: 12603163.

[92] Jan Rossmeisl, Gustav S. Karlberg, Thomas Jaramillo, and Jens K. Norskov. Steady state oxygen reduction and cyclic voltammetry. *Faraday Discuss.*, 140:337–346, 2009. doi: 10.1039/B802129E. URL http://dx.doi.org/10.1039/B802129E.

[93] B. Hammer and J. K. Norskov. Why gold is the noblest of all the metals. *Nature*, 376(6537):238–240, 07 1995. URL http://dx.doi.org/10.1038/376238a0.

[94] V. Stamenkovic, B. S. Mun, K. J. J. Mayrhofer, P. N. Ross, N. M. Markovic, J. Rossmeisl, J. Greeley, and J. K. Norskov. Changing the activity of electrocatalysts for oxygen reduction by tuning the surface electronic structure. *Angewandte Chemie International Edition*, 45(18):2897–2901, 2006. ISSN 1521-3773. doi: 10.1002/anie.200504386. URL http://dx.doi.org/10.1002/anie.200504386.

[95] S. Royer and D. Duprez. Catalytic Oxidation of Carbon Monoxide over Transition Metal Oxides. *ChemCatChem*, 3(1):24–65, December 2010. doi: 10.1002/cctc.201000378. URL https://hal.archives-ouvertes.fr/hal-00755526.

[96] A. Soon, M. Todorova, B. Delley, and C. Stampfl. Oxygen adsorption and stability of surface oxides on Cu(111): A first-principles investigation. *Phys. Rev. B*, 73:165424, Apr 2006. doi: 10.1103/PhysRevB.73.165424. URL http://link.aps.org/doi/10.1103/PhysRevB.73.165424.

[97] G. Dorenbos, M. Breeman, and D. O. Boerma. Low-energy ion-scattering study of the oxygen-induced reconstructed P(2x1) and C(6x2) surfaces of Cu(110). *Physical Review. B: Condensed Matter and Materials Physics*, 47 (3):1580–1588, 1 1993. ISSN 0163-1829.

[98] S. R. Parkin, H. C. Zeng, M. Y. Zhou, and K. A. R. Mitchell. Low-energy electron-diffraction crystallographic determination for the Cu(110)2×1-O surface structure. *Phys. Rev. B*, 41:5432–5435, Mar 1990. doi: 10.1103/PhysRevB.41.5432. URL http://link.aps.org/doi/10.1103/PhysRevB.41.5432.

[99] W. Liu, K. C. Wong, H. C. Zeng, and K. A. R. Mitchell. What determines the structures formed by oxygen at low index surfaces of copper? *Progress in Surface Science*, 50(1):247 – 257, 1995. ISSN 0079-6816. doi: http://dx.doi.org/10.1016/0079-6816(95)00059-3. URL http://www.sciencedirect.com/science/article/pii/0079681695000593.

[100] F. Frechard and R. A. van Santen. Theoretical study of the adsorption of the atomic oxygen on the Cu(110) surface. *Surface Science*, 407(1):200 – 211, 1998. ISSN 0039-6028. doi: http://dx.doi.org/10.1016/S0039-6028(98)00180-0. URL http://www.sciencedirect.com/science/article/pii/S0039602898001800.

[101] S. Vollmer, G. Witte, and C. Woll. Determination of site specific adsorption energies of CO on copper. *Catalysis Letters*, 77(1):97–101, 2001. ISSN 1572-879X. doi: 10.1023/A:1012755616064. URL http://dx.doi.org/10.1023/A:1012755616064.

[102] J. Ahner, D. Mocuta, R. D. Ramsier, and J. T. Yates Jr. Dynamics and structure of chemisorbed CO on Cu(110): An electron stimulated desorption ion angular distribution study. *Journal of Vacuum Science & Technology A: Vacuum, Surfaces, and Films*, 14(3):1583–1587, 1996. doi: 10.1116/1.580300. URL http://dx.doi.org/10.1116/1.580300.

[103] L. J. Lauhon and W. Ho. Single-molecule vibrational spectroscopy and microscopy: CO on Cu(001) and Cu(110). *Phys. Rev. B*, 60:R8525–R8528, Sep 1999. doi: 10.1103/PhysRevB.60.R8525. URL https://link.aps.org/doi/10.1103/PhysRevB.60.R8525.

[104] Z. Zuo, W. Huang, P. Han, and Z. Li. Adsorption of CO on Cu (110) and (100) surfaces using COSMO-based DFT. *Journal of Molecular Modeling*, 15(9):1079–1083, 2009. ISSN 0948-5023. doi: 10.1007/s00894-009-0471-8. URL http://dx.doi.org/10.1007/s00894-009-0471-8.

[105] M. Feng, P. Cabrera-Sanfelix, C. Lin, A. Arnau, D. Sanchez-Portall, J. Zhao, P. M. Echenique, and H. Petek. Orthogonal interactions of CO molecules on a one-dimensional substrate. *ACS Nano*, 5(11):8877–8883, 2011. doi: 10.1021/nn203041c. URL http://dx.doi.org/10.1021/nn203041c. PMID: 21980915.

[106] C. M. A. M. Mesters F. H. P. M. Habraken. The adsorption and incorporation of oxygen on Cu(100) and its reaction with carbon monoxide; comparison with Cu(111) and Cu(110). *Surface Science*, 97, February 1980. doi: 10.1016/0039-6028(80)90118-1.

[107] T. Sueyoshi, T. Sasaki, and Y. Iwasawa. Reactive oxygen atoms on Cu(110) formed at 100 K: vibrational spectra and CO oxidation. *Surface Science*, 343(1):1 – 16, 1995. ISSN 0039-6028. doi: http://dx.doi.org/10.1016/0039-6028(95)00811-X. URL http://www.sciencedirect.com/science/article/pii/003960289500811X.

[108] L. Wang, T. Maxisch, and G. Ceder. Oxidation energies of transition metal oxides within the GGA+U framework. *Phys. Rev. B*, 73:195107, May 2006. doi: 10.1103/PhysRevB.73.195107. URL http://link.aps.org/doi/10.1103/PhysRevB.73.195107.